Unraveling Mechanisms of B cell Reactivity in COVID-19, ANCA-Associated Vasculitis and Psoriatic Arthritis

Ioana Pernes Rones

Balliol College

University of Oxford

A thesis presented for the degree of

Doctor of Philosophy

Michaelmas 2025

Acknowledgements

This thesis represents the culmination of work undertaken during many transformative years of my life, including the profound transition to motherhood. There were many moments when finishing felt out of reach, but I continued because of the wonderful people who stood by me.

I am deeply grateful to my supervisors, Prof. Rachael Bashford-Rogers, Prof. Paul Bowness and Prof. John Todd for their guidance, understanding, and continuous support throughout this journey. Special thanks go to Rachael who believed in me even before I secured a DPhil position, and who supported me in shaping a project in the field of autoimmune disease that I am so passionate about. I am also grateful for her unwavering support on both a professional and personal level for her encouragement and understanding during major personal milestones. I would like to extend my thanks to Paul for his kindness, care and constant encouragement, and to John for his infectious positivity, as well as for providing laboratory resources and wise counsel whenever needed. My thanks also go to Prof Christopher Buckley whose initiative to include me in the CARTOGRAPHY project helped shape the final results chapter of my DPhil. I also wish to acknowledge all our collaborators who provided samples or expertise, as well as the patients and donors who contributed to this research. I am grateful to the Wellcome Trust for funding my DPhil and enabling me to pursue this research.

I am sincerely grateful to my postdoctoral supervisor, Dr Felicia Tucci, for her constant mentorship and friendship, and for all the wisdom-filled cappuccinos we shared. Felicia has been a pillar of comfort, a steady presence whose light has guided me throughout this journey. I would also like to thank the

past and present members of the Bashford-Rogers lab for their wonderful energy and camaraderie: for shared lunches, many snacks and timely sanity checks over a 3 p.m. cup of tea. Many thanks also go to the Diabetes and Inflammation lab for always being such a lovely and supportive group. I could not have wished for better colleagues.

I would like to express my gratitude to my closest friends, Vivi, Mercede, Klara, Diana, Elias, Ricardo and Daria, who have been like a second family, and whose unfailing love and encouragement have meant the world to me, making even the most challenging times feel lighter. I have also been privileged to share my Genomic Medicine and Statistics DPhil with a wonderful peer group, Vassi, Annie, Hrushi, Fred, Nik, and Piotr, and I thank them for our engaging chats, frisbee sessions and for being a ray of light during the darkest days of lockdown.

I am truly privileged to have received constant love and support from my extended family. I am indebted to my mum, my aunt Rodica, and my sister Daria, who travelled long distances to support us and provide childcare, making it possible for me to devote essential time to research and thesis writing. I also thank my dad for his steadfast support, and my grandmas, Mica and Buni, who always rooted for me, even from afar.

Finally, I extend my deepest thanks to my own family. To my daughter, Otilia, thank you for being such a joy and for reminding me what matters most. I am profoundly grateful to my husband, Tom, who has been a pillar of strength throughout this journey; for the many *draga-dragas*, ceaseless words of encouragement, for the early breakfasts prepared and nursery pick-ups. I could not have completed this work without him.

Tom, you are an exceptional husband and father, and I dedicate this thesis

to you and to our daughter, Otilia.

The completion of this thesis reflects the collective support of everyone who has carried me through these years. I am humbled and profoundly grateful to call them *my village*.

Declaration

I declare that the work presented in this thesis is my own, unless otherwise stated in the Methods, such as when collaborators contributed to experiments or analysis, or when previously published data was accessed. This thesis has not been submitted, either partially or in full, for another qualification of this University, or for a qualification at any other institution.

Contributions by collaborators and accessed data:

Chapter 4 and **Chapter 5:** The bioinformatic pipelines for the analysis of B cell receptor (BCR) repertoire were developed and previously published by my supervisor, Associate Professor Rachael Bashford-Rogers, as detailed in Methods.

Chapter 5: Single-cell multi-omic sequencing data of Psoriatic Arthritis and Rheumatoid Arthritis patients has been accessed from the CARTOGRAPHY collaboration between Oxford and Johnson & Johnson Innovation Medicine.

Chapter 5: The recombinant antibody production of selected B cell clones was manufactured by TWIST Biosciences, as detailed in Methods.

Chapter 5: Human Proteome (HuProt) microarray assays and related analysis was performed their manufacturer, CDI Labs, as detailed in Methods.

Ioana Pernes Rones 1^{st} December 2025

Signature *Date*

Abstract

B cells are central components of the adaptive immune system, contributing to host defence through antigen presentation, cytokine secretion and antibody production. Because of these diverse functions, B cell responses require precise regulation: insufficient activation predisposes to infection and oncogenesis, whereas excessive activity can promote autoimmunity. Central and peripheral tolerance mechanisms normally restrain autoreactive B cells, with central tolerance removing or altering self-reactive clones through receptor editing or deletion, and peripheral tolerance maintaining autoreactive mature B cells in an unresponsive state termed anergy. However, these checkpoints are not infallible. Enriched autoreactive B cell populations or autoantibody responses have been observed in contexts such as SARS-CoV-2 infection, ANCA-associated vasculitis (AAV), whereas in psoriatic arthritis (PsA) the contribution of B cells has remained comparatively unclear. A more detailed understanding of B cell tolerance, activation and differentiation, together with how these pathways are perturbed in human disease, is essential for guiding the development of targeted B cell–directed therapies.

This thesis investigates three facets of B cell biology across three disease contexts. First, it characterises markers associated with naïve B cell anergy in healthy individuals and COVID-19 patients, identifying a reproducible relationship between surface IgM expression and functional responsiveness, supporting the concept of naïve B cell anergy as a continuum rather than a binary state. Second, it examines B cell receptor (BCR) repertoire reconstitution following treatment with belimumab (anti-BAFF) combined with rituximab (anti-CD20) compared with rituximab plus placebo in AAV, analysing samples collected within the COMBIVAS clinical trial. Recovery of

specific B cell subsets, including IGHA2 and IGHG2-expressing populations, was delayed under BAFF inhibition, indicating altered selection dynamics that align with the numerically lower relapse rates reported for combination therapy. Third, this thesis investigates the contribution of B cells to PsA pathogenesis, demonstrating pronounced clonal B cell expansions within PsA synovium, comparable to those observed in rheumatoid arthritis, and showing that BCRs from expanded clones can recognise fibroblast-derived antigens. Finally, it identifies fibroblast activation protein (FAP) as a candidate extracellular autoantigen in PsA, suggesting a previously underappreciated B cell–fibroblast axis in disease.

Together, these findings refine our understanding of human B cell tolerance and reveal mechanisms by which B cells may contribute to inflammatory and autoimmune pathology, offering potential avenues for therapeutic intervention.

Keywords— B cell receptor repertoire - autoimmunity - peripheral tolerance - ANCA-vasculitis - psoriatic arthritis

Table of Contents

List of Figures

List of Tables

List of Abbreviations

A ..... Adenosine

AAV ..... ANCA-associated vasculitis

AID ..... Activation-induced cytidine deaminase

ANCA ..... Anti-neutrophil cytoplasmic autoantibody

ANOVA ..... Analysis of variance

APRIL ..... A proliferation-inducing ligand

BAFF ..... B cell activating factor

BCMA ..... B cell maturation antigen

BCR ..... B cell receptor

BLM ..... Belimumab

BH ..... Benjamini-Hochberg

bDMARD ... Biological disease-modifying anti-rheumatic drug

β**ME** ..... β-mercaptoethanol

bp ..... Basepair(s)

C ..... Cytidine

CAR ..... Chimeric antigen receptor

cDNA ..... Complementary DNA to RNA

CDR ..... Complementarity determining region

CITE-Seq .... Cellular indexing of transcriptomes and epitopes followed by sequencing

CPP ..... Cyclic citrullinated peptide

COVID-19 ... Coronavirus disease 2019

CSR ..... Class-switch recombination

DAMPS ..... Damage-associated molecular patterns

DMARDs .... Disease-modifying anti-rheumatic drugs

DMSO ..... Dimethyl sulfoxide

DNase ..... Deoxyribonuclease

dNTP ..... Deoxyribonucleoside triphosphate

ds ..... Double-stranded

DTT ..... Dithiothreitol

EF ..... Extra-follicular

EGPA ..... Eosinophilic granulomatosis with polyangiitis

ELISA ..... Enzyme-linked immunosorbent assay

FACS ..... Fluorescence-activated cell sorting

FAP ..... Fibroblast activating protein

FBS ..... Foetal bovine serum

FCS ..... Foetal calf serum

FDR ..... False discovery rate

G ..... Guanosine

GC ..... Germinal centre

GPA ..... Granulomatosis with polyangiitis

GWAS ..... Genome-wide association studies

h ..... Hour(s)

HBV ..... Hepatitis B virus

HCV ..... Hepatitis C virus

HIV ..... Human deficiency virus

HLA ..... Human leukocyte antigen

IFN ..... Interferon

Ig ..... Immunoglobulin

IGK ..... Immunoglobulin kappa light chain

IGL ..... Immunoglobulin lambda light chain

IL ..... Interleukin

IMID ..... Immune-mediated inflammatory disorder

kB ..... Kilobase(s) or 1000bp

kDa ..... Kilodalton(s)

LA ..... Least anergic

MA ..... Most anergic

mAb ..... Monoclonal antibody

MANOVA ... Multivariate analysis of variance

MHC ..... Major histocompatibility complex

MPA ..... Microscopic polyangiitis

MPO ..... Myeloperoxidase

min ..... Minute(s)

MS ..... Multiple sclerosis

NET ..... Neutrophil extracellular traps

PAMPS ..... Pathogen-associated molecular patterns

PBMC ..... Peripheral blood mononuclear cell

PBO ..... Placebo

PR3 ..... Proteinase-3

PsA ..... Psoriatic arthritis

PsO ..... Psoriasis

QC ..... Quality control

RA ..... Rheumatoid arthritis

rAb ..... Recombinant antibody

RAG ..... Recombination activating gene

RF ..... Rheumatoid factor

RM ..... Repeated measures

RNase ..... Ribonuclease

RT ..... Reverse transcriptase

RT ..... Room temperature

RTX ..... Rituximab

RSS ..... Recombination signal sequence

s ..... Second(s)

SARS-CoV-2 Severe acute respiratory syndrome coronavirus 2

scRNA-Seq .. Single cell RNA-sequencing

SjS ..... Sjögren's syndrome

SLE ..... Systemic lupus erythematosus

T ..... Thymidine

TI ..... Type 1 diabetes

TACI ..... Transmembrane activator and CAML interactor

TD ..... T cell - dependent

TGF ..... Transforming growth factor

TI ..... T cell - independent

TLR ..... Toll-like receptor

TNF ..... Tumour necrosis factor

TNFi ..... Tumour necrosis factor inhibitor

U ..... Uridine

UMI ..... Unique molecular identifier

1 | Introduction

B cells are fundamental components of the adaptive immune system, responsible for humoral immunity. Their primary function is to recognise specific foreign antigens via the B cell receptor (BCR), leading to activation, clonal expansion, differentiation into antibody-secreting plasma cells, and the generation of immunological memory. Through the production of highly specific antibodies, B cells provide long-lasting protection against pathogens.

However, B cell immunity is inextricably linked to the risk of autoimmunity. When the intricate mechanisms designed to maintain self-tolerance fail, B cells can recognise and attack the body's own tissues, contributing to the pathogenesis of numerous autoimmune and chronic inflammatory diseases. Understanding the precise mechanisms that regulate B cell activation, maintain tolerance, and dictate B cell fate is therefore paramount for both preventing infection and treating autoimmunity.

1.1 B cell biology

B cells are specialised white blood cells that, along with T cells, are crucial members of the adaptive immune system. B cell functions are tightly interwoven into the immunological network, as they can interact with antigen-presenting cells, present antigens themselves to prime and reinforce T cell responses, produce antibodies to establish long-lasting responses to pathogens, secrete cytokines to modulate cellular responses, and even exhibit cytotoxic activity. Therefore, B cell activity requires strict regulation to prevent disease. Insufficient B cell responses can lead to infection or cancer, whereas aberrant B cell activity has been involved in autoimmune diseases such as systemic

lupus erythematosus (SLE), multiple sclerosis (MS), Sjögren's syndrome (SjS), ANCA-associated vasculitis (AAV) or rheumatoid arthritis (RA). Multiple selection checkpoints during B cell development are often found to be dysregulated in disease (Rubin, Bloom, & Robinson, 2019; Merino-Vico, Frazzei, van Hamburg, & Tas, 2023; Hegoburu, Amer, Frizelle, & Purcell, 2025).

1.1.1 B cell receptor structure

Mature B cells express a membrane-bound immunoglobulin as a receptor. The B cell receptor consists of two pairs of a heavy and a light chain linked by disulphide bonds, together with two co-receptors Igα/Igβ (CD79a/b) (Figure 1.1). These co-receptors play a crucial role in transmitting activation signals through immunoreceptor tyrosine-based activation motifs (ITAMs) upon antigen-binding. Each heavy and light chain is composed of a constant and a variable region. The variable region is formed by conserved beta sheets called framework regions, connected by highly variable molecular loops called complementarity determining regions (CDR). The three CDR loops form the antigen-binding domain and are the most diverse regions of the receptor, and therefore enable recognition of a wide array of antigens. CDR3 on the heavy chain is the most variable of the CDRs due to its variable length and sequence of aminoacids (Morea, Tramontano, Rustici, Chothia, & Lesk, 1998). The receptor's structure also features a hinge that joins the two fragment antigen-binding (Fab) regions with the fragment crystallisable (Fc) receptor-binding region. In its secreted form as an antibody, the Fc region of the immunoglobulin mediates functional interactions through the Fc receptors on other immune cells, such as phagocytes. The Fab fragments contain the antigen-binding domain (Dong et al., 2022).

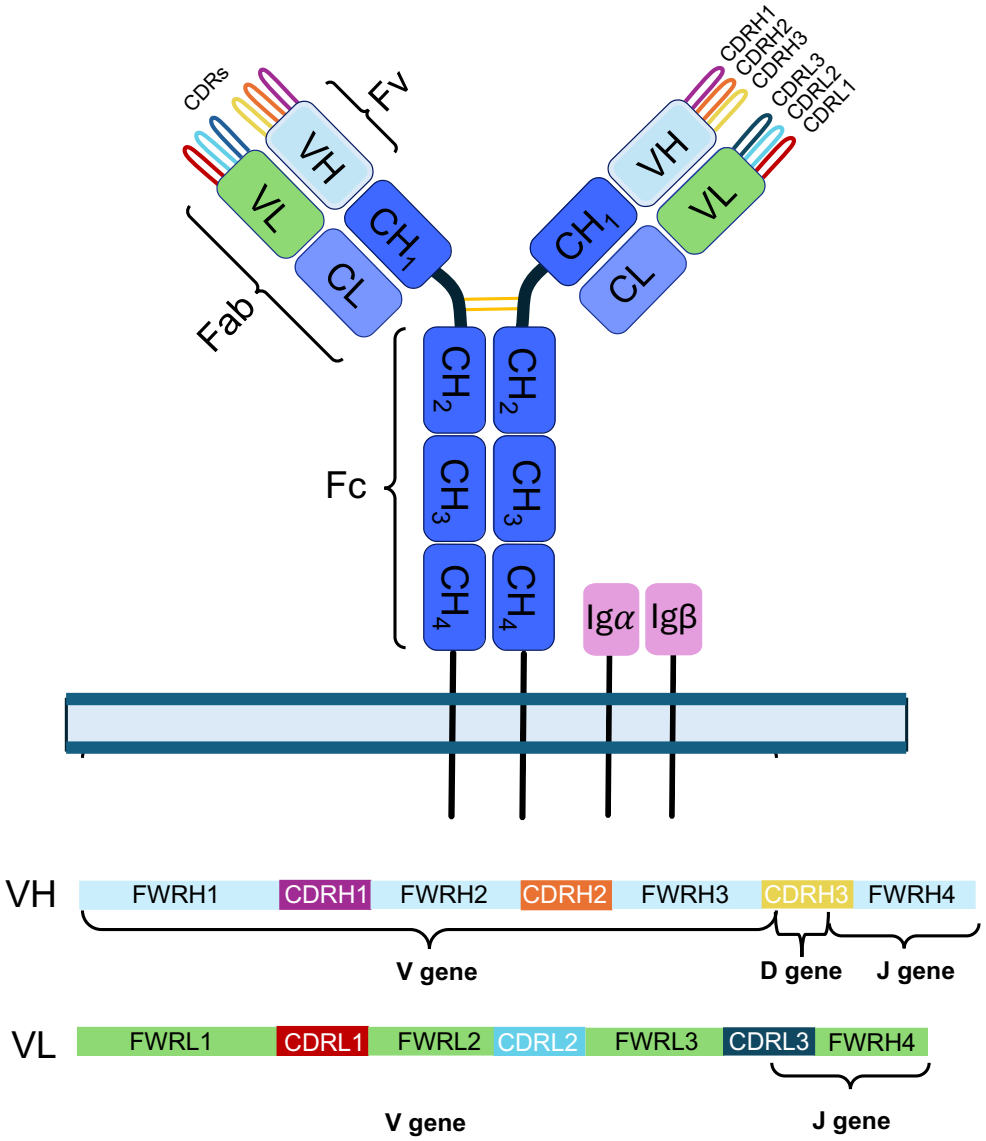

Figure 1.1: Schematic representation of an IgM B cell receptor structure with co-receptors Igα/Igβ. Complementarity determining regions (CDR) are depicted in distinct colours along with their placement within the variable region of the heavy chain gene (VH) and light chain gene (VL). Disulphide bonds are marked with yellow lines.

1.1.2 B cell repertoire diversity generation

The adaptive immune system has evolved to produce highly diverse B and T cell receptor repertoires to be able to recognise the vast and heterogeneous array of pathogenic threats. Each B cell produces a unique BCR. It is estimated that 2-4 x 10^{11} B cells reside in the human body, which only sample the potential diversity of the B cell repertoire in a healthy individual, estimated at 10^{16}–10^{18} unique BCRs (Briney, Inderbitzin, Joyce, & Burton, 2019; Sender et al., 2023). This vast diversity is possible through key processes including somatic V(D)J rearrangement, introduction of junctional diversity and somatic hypermutation.

1.1.2.1 Somatic recombination

Somatic recombination or V(D)J recombination is a process through which one variable (V), one diverse (D) and one joining (J) segment from the heavy chain (*IGH*) locus, and one V and one J segment from light chain locus (of the κ (*IGK*) or λ (*IGL*) genes) are joined in a single exon. On the *IGH* locus there are 44 V segments, 27 D segments and 6 J segments, which are known to be used productively in the somatic recombination process (Khatri et al., 2021). Somatic recombination is predominantly driven by the recombination-activating gene 1 and 2 (RAG1/RAG2) proteins and other enzymes that act on the recombination signal sequence (RSS) motifs flanking the V, (D) and J regions of the heavy and light genes. In the first instance, one D and one J segment are rearranged and joined. The DNA spanning in-between the D and J segments is removed. In the second step, one V region is rearranged to join the DJ and to form the VDJ exon of the heavy chain gene. Again, the DNA that spans the region between the V and the DJ exon is removed.

The process of V, D and J segment joining is imperfect, as the recombinant machinery may add or remove nucleotides. Additionally, further diversity is introduced in the locus through additions of N nucleotides by the enzyme terminal deoxynucleotidyl transferase (TdT) and P nucleotide additions by the DNA polymerase, a process called junctional diversity. The transcription of the recombined heavy chain includes the constant region μ (Cμ) and δ (Cδ), which leads to the production of an IgM heavy chain or an IgD heavy chain through alternative mRNA splicing. The germline light chain locus contains 43/39 V and 5/7 J productive segments on the κ, respectively, λ genes (Khatri et al., 2021). The somatic recombination of the light chain is similar to that of the heavy chain. However, as the light chain lacks D segments, the recombination occurs in one step: one V and one J segment produce a joined VJ exon of the *IGK* or the *IGL* gene.

The extensive combinatorial possibilities of the V, D, and J segments of the heavy chain multiplied by those of the V and J segments on two light chains demonstrate that the somatic recombination alone can produce a vast diversity of BCR repertoire of about 10^{12} unique BCRs. These processes illustrate the potential repertoire diversity of each individual. However, the extent of the human repertoire is even more diverse, as hundreds of alleles are known for each V(D)J segment, and more are discovered through the genome sequencing of unrepresented populations (Calonga-Solís et al., 2019; Mikocziova et al., 2020).

1.1.2.2 Somatic hypermutation

Somatic hypermutation (SHM) is a process through which point mutations are introduced in the variable regions of the heavy and light chain genes, usually occurring in the context of germinal centres (GCs). The result of SHM

is a broader range of BCR affinities, including the opportunity for the antigen specificity of the BCR to be refined. SHM occurs during the G0/G1 phase of the cell cycle, mediated by activation-induced cytidine deaminase (AID), at a stage which AID has access to cellular DNA. It occurs at an approximate rate of 1 mutation per 1000 base pairs (bp) per cell cycle, although recent models suggest that the SHM rate is dynamic and dependent on the initial BCR affinity (Merkenschlager et al., 2025). Although SHM is stochastic, mutational hotspots have been identified in the variable genes, such as WR$\underline{\text{C}}$H (W = A/T, R = A/G and H = A/C/T) motifs. (Pham, Bransteitter, Petruska, & Goodman, 2003).

1.1.2.3 Class-switch recombination

Class-switch recombination (CSR) is a process through which the heavy chain constant region of the BCR is changed from IgM and IgD to other immunoglobulin classes: IgG, IgA or IgE.

CSR is mainly driven by the AID enzyme and is mostly a directional process given by the order of constant regions in the heavy chain locus (Cμ/Cδ - Cγ3 - Cγ1 - Cα1 - Cγ2 - Cγ4 - Cε - Cα2). After a B cell switches to a downstream isotype, it cannot revert to an upstream class, as the intervening DNA is excised. However, further switching to more distal constant regions remains possible. Consequently, the isotype patterns observed within members of a clonal B cell family provide a record of their evolutionary trajectory and can be used to infer lineage relationships within the repertoire.

The heavy chain constant region gene is comprised of several constant segments (Cμ, Cδ, Cγ, Cϵ, Cα), each downstream of conserved switch region motifs. Different cytokines will initiate the transcription of specific segments of the

constant region, causing AID to target those regions, leading to a nick and cut in the DNA at those switch region motifs. The excised DNA forms a loop and is deleted from the germline, whereas the remaining DNA is rejoined through non-homologous end joining.

CSR does not alter the receptor specificity, but it specialises the function of the secreted antibody.

CSR occurs in activated B cells following interaction with T cells in secondary lymphoid organs, outside of germinal centres (Roco et al., 2019). The selection of the new isotype is modulated mainly by the synergy between T cell-dependent interactions (through CD40L) and cytokines such as IL-4, TGFβ, IL-5, IL-6, IFNγ, IL-21 or IL-10 (Table 1.1, (J.-C. Liu et al., 2024)).

T cell-independent class switching can also occur, a process preponderantly present in the mucosal sites such as the intestine. In response to pathogen-associated molecular pattern (PAMP) signals such as CpG, dendritic cells can secrete TGFβ, B cell-activating factor (BAFF), a proliferation-inducing ligand (APRIL) and present microbial peptides, which activate B cells through Toll-like receptors (TLRs) or BCR cross-linking. BAFF and APRIL act on transmembrane activator and calcium-modulating cyclophilin-ligand interactor (TACI) on B cells. TGFβ, the activation of TACI on B cells or TLR activation, can lead to AID upregulation, NF-κB pathway activation and result in class switching to IgA, mainly IgA2 (den Hartog et al., 2018; He et al., 2007; Stavnezer & Kang, 2009; Cerutti, 2008).

Isotype	Primary cytokine drivers	Role	References
IgG1	IL-4, IL-21	The most dominant IgG subtype. Role in complement activation and opsonisation. IL-10 has also been linked to IgG1 production.	(Pène et al., 2004; Avery, Bryant, Ma, de Waal Malefyt, & Tangye, 2008; Brière, Servet-Delprat, Bridon, Saint-Remy, & Banchereau, 1994; Hjelholt, Christiansen, Sørensen, & Birkelund, 2013)
IgG2	Complex	Role in encapsulated-bacterial response. IgG2 can be stimulated by IFN-γ with IL-6. IgG2 is also driven by T cell-independent (TI) responses.	(Kawano, Noma, & Yata, 1994; Weller et al., 2023)
IgG3	IL-21, IFN-γ	Strongest complement pathway activator. IL-10 has also been linked to IgG3 production. IL-4 suppresses IgG3.	(Avery et al., 2008; Brière et al., 1994; Pène et al., 2004)
IgG4	IL-4, IL-13	The least abundant IgG subtype in serum. Associated with T helper 2 (Th2) cell responses. IL-10 may also drive IgG4. Role in allergy and parasitic defence.	(Rispens & Huijbers, 2023; Aalberse, Stapel, Schuurman, & Rispens, 2009; Punnonen et al., 1993)
IgA1	TGF-β, IL-10, IL-21, IL-5	The dominant IgA subclass in serum. Primarily driven by T cell-dependent (TD) responses.	(Cerutti, 2008; J.-C. Liu et al., 2024)
IgA2	APRIL, BAFF, TGF-β	Mostly localised in the intestine. Driven by both TD and TI responses via the TACI receptor and through bacterial stimulation.	(den Hartog et al., 2018; He et al., 2007; Cerutti, 2008; Stavnezer & Kang, 2009)
IgE	IL-4, IL-13	Critical in allergic responses and parasite defence. Associated with Th2 cell responses. IgE production is antagonised by IFN-γ.	(Pène et al., 1988; Punnonen et al., 1993; J.-C. Liu et al., 2024)

Table 1.1: **Cytokine drivers of human immunoglobulin isotype switching**

1.2 B cell receptor (BCR) repertoire and immune tolerance

1.2.1 Principles of repertoire analysis

High-throughput sequencing of B cell receptors (BCR-seq) enables quantitative inference of B cell population structure and dynamics from immunoglobulin variable-region sequences. Repertoire analysis can offer insights into: (1) B cell clonality and clonal expansion (inferred from shared V(D)J usage and highly similar CDR3 sequences), (2) diversity (the distribution of clonal family sizes which arises through somatic hypermutation and forms sequence diversity), (3) somatic hypermutation which can help infer B cell lineages (typically SHM burden of naïve B cells $<$ memory B cells $\leq$ plasmablasts/plasma cells), and (4) class-switch recombination (Bashford-Rogers et al., 2019). Together, these readouts provide a framework to reconstruct clonal evolution and to compare immune states across tissues, time points, and disease contexts.

BCR repertoire features are interpreted alongside biological context. Expanded clones may reflect recent activation, persistence, or tissue residency, SHM levels can distinguish from naïve-like to GC-experienced lineages, and isotype distributions can indicate the balance of extrafollicular versus germinal-centre contributions. Importantly, BCR repertoire analysis is strongest when integrated with phenotypic and/or transcriptomic complementary analysis such as scRNA-seq, CITE-seq and where possible, functional validation.

1.2.2 Repertoire analysis as a window into autoreactivity

Autoreactive and polyreactive B cells are associated with characteristic BCR features that can be quantified from repertoire data. At the level of germline gene usage, certain heavy-chain variable genes are disproportionately represented among self-reactive antibodies. The most prominent example is VH4–34, which is intrinsically autoreactive and enriched in SLE and other autoimmune settings (Richardson et al., 2013; Bashford-Rogers et al., 2019). In VH4–34 antibodies, preservation of germline-encoded motifs (including AVY and NHS) is linked to maintenance of autoreactive potential, whereas mutation of these motifs is associated with 'redemption' away from self-reactivity (Sabouri et al., 2014; Schickel et al., 2017; Richardson et al., 2013).

The use of λ light chain usage marks multiple rounds of B cell recombinational processes during development in order to redeem an autoreactive clone, but this process is not perfect and autoreactive antibodies have been shown to be skewed towards λ light chain usage (Slot et al., 2021). Therefore, the λ light chain usage can inform about the germline autoreactive potential and track clones with higher autoreactive potential.

Beyond chain usage, CDR3 properties are also informative. Longer CDRH3 regions confer a more flexible and protruding antigen binding loop, which can aid pathogenic antigen binding, as described in HIV (McLellan et al., 2011). However, this feature can also increase the chance of binding to self-antigens and is associated with autoimmunity. The net charge of the CDR3 is also an important feature to be determined. Positively charged CDR3 regions favour binding to negatively charged nucleic acids and chromatin, a feature described in SLE (Guth, Zhang, Smith, Detanico, & Wysocki, 2003). Finally, evidence of V-gene replacement can indicate secondary recombination events

that may occur during attempts to revise potentially autoreactive receptors (Burrows et al., 2020).

Therefore, analysing the BCR repertoire provides a powerful framework to characterise B cell clonal evolution, including clonal expansion, somatic hypermutation, isotype usage or the persistence of intrinsically autoreactive specificities.

1.2.3 B cell development

B cells were first discovered in birds, in the organ called the 'bursa of Fabricius', hence named 'B' lymphocytes. In humans, B cells develop in the bone marrow, from haematopoietic stem cells. B cell development is dependent on the interaction with the bone marrow stroma. Cell-surface interactions through tyrosine kinase receptors such as FLT3 and Kit, or through cell-adhesion molecules such as VLA-4, as well as soluble factors such as interleukin 7 (IL-7) induce signals in progenitor cells that trigger the formation and rearrangement of the B cell receptor (BCR), and delineate the stages of B cell development. The formation of the BCR begins with the somatic recombination of the heavy chain locus. Once complete, the transcription of the recombined heavy chain together with the constant region μ (Cμ), leads to the production of an IgM heavy chain. The heavy chain associates with surrogate light chains to form the pre-BCR. If the heavy chain rearrangement produced a functional receptor, the pre-BCR constitutively transduces signals, independently of antigen. These tonic signals trigger allelic exclusion, and therefore the end of heavy chain rearrangement, promote cell survival and induce transient proliferation. Only about half of the cells successfully reach this pre-B cell stage. The rearrangement of the light chain locus follows. Once the B cell produces a BCR, it must pass a series of selection checkpoints before being

licensed to leave the bone marrow into the secondary lymphoid structures such as the spleen and lymph nodes (Melchers, 2015; Murphy, Weaver, Berg, Barton, & Janeway, 2022).

1.2.4 Central and peripheral tolerance of B cells

B cells are selected in the bone marrow such that the developed cells are functional, but not strongly autoreactive, in a process called central tolerance. Bone marrow cells present self-antigens to B cells within their niche, leading to the negative or positive selection of the B cells. Negative selection occurs through lack of BCR engagement (neglect), incorrect or incomplete BCR production. These scenarios prevent the transduction of downstream signals required to maintain cell survival and result in cell death. Strong interactions between the developing B cells and the presented self-antigen commonly result in two fates. Firstly, B cells attempt to resolve the autoreactivity of their BCR by entering a new round of light chain receptor editing. If unsuccessful, B cells undergo clonal deletion through apoptosis. Mouse studies have shown that the avidity of the BCR is much more important than the affinity at this selection point (Hartley et al., 1991; Goodnow et al., 1988). In addition, BCR-independent immune recognition via toll-like receptor-9 (TLR-9) and chemokines which can modulate its function such as CXCL4 are also essential in establishing central tolerance (Çakan et al., 2023). The high avidity of the antigen-bound BCR triggers receptor internalisation, and subsequent reactivation of the RAG1/2 proteins and downstream recombination enzymes. These initiate a new rearrangement of the κ light chain locus first, if V and J segments are still available to be recombined. If not, then the second *IGK* allele is used for a new VJ recombination. If the strong autoreactivity of the BCR persists, then the λ light chain locus will be recombined, until the B cell

is redeemed, or until there are no more segments left to be recombined. The latter option creates an incomplete BCR and ultimately results in cell death. B cells continue to rearrange their light chain locus for up to 3 days to resolve their BCR, before undergoing clonal deletion. The surviving B cells transduce tonic signals through their BCR leading to the downregulation of RAG proteins and therefore the end of the somatic recombination. This process marks the positive selection of immature B cells which become transitional B cells, and are now able to exit the bone marrow into secondary lymphoid organs. The central tolerance checkpoints reduce the polyreactivity of the B cell repertoire from about 50% in the early immature B cells in the bone marrow to less than 10% of the transitional B cell emigrants. The figure is even lower in mature naïve B cells, due to the apoptosis-prone transitional B cells in the periphery, as shown in murine studies. However, central tolerance is not perfect at removing autoreactive B cells. An estimated 20% of mature naïve B cells which circulate in the periphery exhibit autoreactivity (Wardemann et al., 2003). Therefore, peripheral tolerance mechanisms are necessary to prevent the development of autoimmune diseases.

Two main mechanisms of peripheral tolerance are induction of anergy and apoptosis. B cell anergy is characterised by a state of unresponsiveness to stimulation, such as reduced calcium signalling upon BCR cross-linking (Duty et al., 2008). Anergy is reversible and in mice a factor which maintains anergy includes ongoing BCR occupancy by cognate antigen (Gauld, Benschop, Merrell, & Cambier, 2005; Duty et al., 2008). Anergic B cells may also be spatially regulated, as in mice, reduced CXCR5 can bias follicular exclusion and favour extrafollicular activation pathways (Ekland, Forster, Lipp, & Cyster, 2004). However, the extent of anergy dynamics and how it can be modulated and disrupted remain incompletely defined, particularly in

humans.

1.2.5 B cell activation and differentiation

B cell activation is initiated when the B cell receptor (BCR) binds cognate antigen, triggering BCR signalling, antigen internalisation and subsequent processing for presentation in the context of MHC class II. Full activation typically requires additional inputs that can be delivered through either T cell–dependent (TD) or T cell–independent (TI) pathways, and is further tuned by co-receptors and cytokine receptors that collectively set the activation threshold of the B cell. Key modulators include innate receptors such as Toll-like receptors (TLRs), co-receptors that modulate BCR signalling (such as CD21 and CD22), survival signalling through BAFF-family receptors and input from cytokines through cytokine receptors that further modulate proliferation, differentiation and antibody secretion.

In TD responses, antigen-primed B cells present peptide–MHC II to $CD4^+$ T cells and receive co-stimulation via CD40 engagement by CD40L expressed on activated T cells. T cell-derived cytokines, including IL-2, IL-4, and IL-21, further support B cell expansion and influence class-switch recombination (CSR) and differentiation trajectories. In contrast, TI responses rely on innate sensing of pathogen- and damage-associated molecular patterns (PAMPs and DAMPs). These signals can activate B cells through endosomal TLRs such as TLR7 and TLR9, often in synergy with cytokines and BAFF-family ligands, enabling rapid antibody production in the absence of classical T cell help.

The canonical B cell activation pathway starts with mature naïve B cells localising into specialised follicular areas of the secondary lymphoid organs, called B cell zones, where they scout antigens. There, they encounter antigens

captured by follicular dendritic cells and become activated through interactions with follicular T helper cells. These interactions promote the proliferation of B cells and can lead to the initiation of germinal centres (GC). After initial episodes of cell division, activated B cells have the following fates: (1) differentiate into short-lived plasmablasts or memory B cells and exit the secondary lymphoid organ into the periphery, or (2) upon repeated antigenic challenge, B cells may class-switch and form GC (Roco et al., 2019). In GC reactions, B cells cycle between the light zone of the GC, where they re-encounter antigen, and the dark zone of the GC, where B cells continue with further cycles of proliferation, and affinity maturation through somatic recombination, and further class-switch recombination. The B cells committed to the GC reaction will result in the majority of the memory B cell pool, and in the long-lived plasma cells which will migrate to the bone marrow for antibody production.

B cells can also become activated and differentiate through extrafollicular (EF) reactions to produce both switched and unswitched memory B cells and long-lived plasma cells (Bortnick et al., 2012; Foote, Mahmoud, Vale, & Kearney, 2012; Taillardet et al., 2009). EF reactions refer to B cell proliferation and further maturation which occurs outside of the follicular B cell zone. There, B cells can become activated in both a T cell-dependent (Keller et al., 2021) or T cell independent manner, via TLR engagement of DAMPs and PAMPs, as shown in mice (Herlands, Christensen, Sweet, Hershberg, & Shlomchik, 2008; Di Niro et al., 2015).

Key differences between EF and GC reactions include their kinetics and mutational output. GC can start to involute after approximately 2 weeks post-infection, while the EF B cells and plasmablasts can continue to expand, sometimes in life-long reactions in autoimmune diseases such as SLE. EF

activation is also associated with lower SHM than GC reactions, a feature particularly prominent in expanded unswitched B cells and plasmablasts in SLE. This is consistent with the concept that GC reactions preferentially select high-affinity clones through iterative mutation and selection, whereas EF responses can support rapid expansion and differentiation with comparatively limited mutation, thereby accommodating a broader and often more polyreactive range of BCR specificities (Ota et al., 2023; Tipton et al., 2015). The EF B cell activation pathway has also been associated with critically ill coronavirus disease 2019 (COVID-19) patients (Woodruff et al., 2020). Although some B cell subsets such as T-bet$^+$ CD21^{low} have been associated with EF responses, and intracellular signalling axes including PI3K/mTOR have been implicated in supporting EF differentiation, the upstream mechanisms that sustain EF differentiation remain incompletely defined (Keller et al., 2021; Staniek & Rizzi, 2025).

1.2.6 B cell lineages

These activation routes give rise to phenotypically distinct B cell states that can be operationally resolved by surface-marker expression. Human peripheral B cell subsets are canonically classified as transitional (CD19$^+$ CD10$^+$), naïve (CD19$^+$ IgD$^+$ IgM$^+$ CD27$^-$), unswitched memory (CD19$^+$ IgD$^{-/+}$ IgM$^+$ CD27$^+$), switched memory (CD19$^+$ IgD$^-$ IgM$^-$ IgG$^+$/IgA$^+$/IgE$^+$ CD27$^+$), and antibody-secreting cells, including plasmablasts (CD19$^+$ CD27$^+$ CD38^{++}) and long-lived plasma cells (typically CD20$^-$), which can be further refined using markers such as CD24, CD38, CD21, CD22 and others, as detailed in Table 1.2 (Pinto, Benard, & Fernandes, 2025; Kaminski, Wei, Qian, Rosenberg, & Sanz, 2012; Sanz et al., 2019). Importantly, although CD27 is widely used to delineate between naïve and memory B cells, 'atypical' B cells (IgD$^-$CD27$^-$),

including subsets called double negative (DN), age-associated B cells (ABC) or tissue-like, can exhibit levels of somatic hypermutation comparable to $CD27^+$ memory subsets, supporting their classification as antigen-experienced memory B cells (Wei et al., 2007).

Recent comprehensive efforts to better characterise memory B cells highlighted markers such as CD21 to have bimodal distributions, suggesting the heterogeneity within memory B cell subsets. To distinguish between $CD27^-$ naïve and $CD27^-$ memory B cells, the use of $CD11c^+$ and $CD200^-$ was proposed, as these markers appeared to be expressed at comparable levels between classical memory $CD27^+$ isotype-switched B cells and isotype-switched $CD27^-$ memory B cells (Weisel et al., 2022).

Among the markers commonly used for B cell refinement, CD21 and CD22 are of particular interest because they directly modulate BCR signalling thresholds. CD21, also called complement receptor type 2 (CR2), can form complexes with CD19-CD81 as best characterised in mice, acting as an enhancer of BCR response. However, its function in humans has been challenged in recent studies, since recent evidence suggests that CD21 can also form complexes with CD35 (CR1) and engagement of CD21 through its natural ligand C3d, induces a diminished calcium signalling, proliferation and antibody production, consistent with an inhibitory function. This aligns with the pathogenic B cell phenotypes characterised by $CD21^{low}$ in SLE (Kovács, Mácsik-Valent, Matkó, Bajtay, & Erdei, 2021; Erdei et al., 2021). CD22 (Siglec 2) is an adhesion molecule restricted to B cells and it is an inhibitory co-receptor, as it signals through immunoreceptor tyrosine-based inhibitory motifs (ITIMs). Its vital role in B cell receptor signalling regulation has been demonstrated in mice, as mice deficient in CD22 display markedly high levels of calcium signalling upon BCR-crosslinking, coupled with decreased viability, whereas

TLR4 engagement results in increased B cell proliferative capacity; antibody secretion was also heightened in mice (Nitschke, Carsetti, Ocker, Köhler, & Lamers, 1997; Otipoby et al., 1996; N. Kawasaki, Rademacher, & Paulson, 2011). CD22 is expressed at high levels on naïve B cells and remains detectable on memory B cells, but its expression declines during differentiation into plasmablasts and is largely absent on plasma cells (Daridon et al., 2010; Clark & Giltiay, 2018).

Most studies of these receptors have been performed *ex vivo* at baseline, or under conditions of receptor engagement aimed at defining their functional roles in B cells. In contrast, the kinetics and regulation of CD21 and CD22 expression following B cell stimulation, particularly in human systems, remain poorly characterised. Given that these co-receptors modulate BCR signalling, and that pathogenic expansion of B cell populations with altered CD21 and/or CD22 expression has been reported, there is a clear need to define how their expression dynamically changes under activating conditions.

1.2.7 Human anergic B cells

Anergic B cells have been described in three contexts. First, recent emigrants from bone marrow or transitional cells have been shown to exhibit refractory responses to anti-IgM stimulation. Transitional cells are marked by an enriched autoreactive repertoire, shorter lifespan, downregulation of CD21, CD22 and upregulation of CD10 (Gross, Lyandres, Panigrahi, Prak, & DeFranco, 2009).

Second, mature naïve B cells with an enriched autoreactive or polyreactive repertoire, and characterised by increased usage of VH4-34 chain have also been described as anergic (Pugh-Bernard et al., 2001). A subset of these cells were termed B_{ND} and have been shown to comprise at least 2.5% of total

Table 1.2: **Non-exhaustive list of human peripheral B cell populations defined by core and additional markers.** Unless indicated otherwise, populations are $CD19^+$. Table adapted from (Sanz et al., 2019)

B cell population	Subset	Core markers	Additional markers	Function/properties
Transitional	T1/T2	IgD^+ $CD27^-$ $CD38^{++}$ $CD24^{++}$	$CD10^{++/+}$ IgM^{++} MTG^+; CD10/IgM: T1>T2>T3	Developmental precursor
	T2–MZP	IgD^+ $CD27^-$ $CD38^{++}$ $CD24^{++}$ $CD21^{++}$	$CD10^+$ IgM^{++}	MZ precursor
	T3	IgD^+ $CD27^-$ $CD38^+$ $CD24^+$ $CD21^+$	$CD10^{+/-}$ IgM^+ MTG^+	Developmental precursor or activated naïve
Naïve	Resting	IgD^+ $CD27^-$ $CD38^+$ $CD24^+$ $CD21^+$	IgM^+ MTG^-	Antigen-inexperienced mature cells
	Activated	IgD^+ $CD27^-$ $CD38^-$ $CD24^-$ $CD21^-$	IgM^+ MTG^+ $CD95^+$ $CD23^-$ $CD11c^+$; T-bet^+ $FcRL5^+$ $SLAMF7^+$ $CXCR5^-$	Precursor of short-lived PB and GC reactions
	Anergic	IgD^+ $CD27^-$ $CD38^{+/lo}$ $CD24^+$ $CD21^-$	$IgM^{low/-}$	Hypo-responsive; maintenance of tolerance
Memory	Unswitched	IgD^{lo} $CD27^+$ $CD38^{+/lo}$ $CD24^+$ $CD21^+$	$CD1c^+$ IgM^{++}	Natural memory; MZ equivalent
	Pre-switched	IgD^- $CD27^+$ $CD38^{+/lo}$ $CD24^+$ $CD21^+$	IgM^+	Pre-switch memory; early IgM / IgG memory precursor
	Switched resting	IgD^- $CD27^+$ $CD38^{+/lo}$ $CD24^+$ $CD21^+$	IgG/IgA^+ $CD95^-$	Pre-existing memory reservoir
	IgD^- $CD27^+$ $CD38^-$ $CD24^-$ $CD21^-$	IgG/IgA^+ $CD95^+$ $CD86^+$	Effector memory–PB/PC precursor	
	Atypical tissue-based	IgD^- $CD27^-$ $CD38^{lo}$ $CD24^{lo}$ $CD21^-$	$FcRL4^+$ $IgM/IgG/IgA^+$ $FcRL5^+$	Mucosal surveillance; exhausted/BCR-hyporesponsive memory
Double negative (DN)	DN1	IgD^- $CD27^-$ $CD38^+$ $CD24^+$ $CD21^+$	$FcRL4^-$ $IgM/IgG/IgA^+$ $FcRL5^-$; $CXCR5^+$	Memory precursors
	DN2	IgD^- $CD27^-$ $CD38^-$ $CD24^-$ $CD21^-$	$IgM/IgG/IgA^+$ T-bet^+ $CD11c^+$; $FcRL5^+$ $CXCR5^-$ $SLAMF7^+$	Extrafollicular ASC precursors
	—	IgD^- $CD27^-$ $CD38^-$ $CD24^-$ $CD21^-$	$FcRL4^+$	Atypical/tissue-based memory
Antibody secreting cells	Early PB	IgD^- $CD27^{lo/+}$ $CD38^{++}$ $CD24^-$	$CD20^{+/-}$ HLA-DR^+ $CD138^-$	Naïve- and memory-derived PB precursors
	PB	IgD^- $CD27^{++}$ $CD38^{+++}$ $CD24^-$	$CD20^-$ HLA-DR^+ $CD138^-$ $Ki67^+$	Antibody secretion
	PC	IgD^- $CD27^{++}$ $CD38^{+++}$ $CD24^-$	$CD19^{+/-}$ $CD20^-$ $CD138^+$	Antibody secretion

Abbreviations: MTG, Mitotracker Green; MZ, Marginal Zone; PB, plasmablast; PC, plasma cell; GC, germinal centre.

circulating B cells, and have been characterised by IgD^+ in conjunction with low surface IgM (Duty et al., 2008; Szodoray et al., 2016; Mouat, Goldberg, & Horwitz, 2022; Smith et al., 2019). In COVID-19, the possible reactivation of this anergic compartment was associated with downregulation of CD21 and CD22 relative to B_{ND} cells in healthy controls (Castleman et al., 2022), a population with similar characteristics with a more recently described B_{ND2} population in T1D (Stensland et al., 2023).

Finally, a memory anergic B cell population with downregulated CD27 often termed 'atypical' memory B cell (IgD^-CD27^-, sometimes $CD21^-$), is described similarly to double-negative B cells 1 (DN1, $IgD^-CD27^-CD21^+CD11c^-$), age-associated B cells (ABC) (Mouat et al., 2022), tissue-like ($FcRL4^+$) (Ehrhardt et al., 2005) or exhausted B cells (Moir et al., 2008). These cells have been variably linked to anergy-like hyporesponsiveness (e.g., reduced BCR/TLR responsiveness, proliferation, differentiation) in a strongly disease-dependent manner: in some settings they expand yet remain hyporesponsive (Sims et al., 2005), in others they exhibit an activated effector phenotype consistent with a breach of anergic restraint (Jenks et al., 2018), and in chronic infection they are often framed as displaying exhaustion-associated dysfunction (Moir et al., 2008). Of note, subsets of these cells are enriched in autoreactive BCRs but also appeared to carry higher somatic hypermutation levels and therefore be more consistent with a memory B cell rather than an early emigrant (Saadoun et al., 2013). Double negative 2 B cells (DN2 $CD11c^+$) however, were described to be the progeny of activated naïve B cells through EF responses, as DN2-resulting plasmablasts are often characterised by low SHM, and an enrichment of these cells has been linked to SLE, RA and COVID-19 (Álvarez Gómez et al., 2023; Wing et al., 2023; Woodruff et al., 2020; Jenks et al., 2018; Isnardi et al., 2010). Atypical B cells, ABCs or

tissue-like cells have been described to be enriched in several autoimmune diseases including RA (Yeo et al., 2015), SjS (Saadoun et al., 2013), common variable immunodeficiency (CVID) (Mouat et al., 2022) and malaria (Portugal et al., 2015; Portugal, Obeng-Adjei, Moir, Crompton, & Pierce, 2017; Holla, Ambegaonkar, Sohn, & Pierce, 2019). In an autoimmune context, atypical B cells are often characterised by decreased or absent IgM receptor and $CD21^{-/low}$, $CD11c^{+}$ and/or T-bet^{+}, consistent with a reactivated phenotype, whereas in the context of infection these cells are often described as refractory or exhausted (Moir et al., 2008; Moir & Fauci, 2014). Some of my DPhil work, in collaboration with other Bashford-Rogers team members and outside of the scope of this thesis, complements prior studies by providing insights into these heterogenously-defined populations. We observed that transcriptionally these various phenotypes of atypical B cells shared many features. However, the inclusion of consistent markers into assay panels across various diseases tested will significantly help in standardising the definitions of these refractory or reactivated atypical B cells (Pernes, Alsayah, Tucci, & Bashford-Rogers, 2024; Holla et al., 2021).

1.3 COVID-19

Severe acute respiratory syndrome coronavirus 2 (SARS-CoV-2) is a respiratory virus first identified in 2019 and the causal agent of coronavirus disease 2019 (COVID-19). As of November 2025, there have been over 700 million confirmed cases and 7.1 million reported deaths worldwide, based on the World Health Organisation (WHO) database. Considerable effort has been directed towards defining the immune determinants of COVID-19, both to understand pathogenesis and to inform therapeutic strategies.

1.3.1 Overview of B cell immune responses in COVID-19

SARS-CoV-2 infection is associated with major perturbations of the immune system, including profound alterations in B cell compartments. Several studies have reported reduced frequencies of circulating naïve B cells together with increased plasmablasts or antibody-secreting cells (ASCs), particularly in severe COVID-19, where these features are associated with poorer outcomes. This pattern suggests strong activation of the naïve B-cell pool followed by differentiation into ASCs. Mechanistically, such responses have been linked to extrafollicular (EF) pathways, based on evidence of broad autoreactivity, low somatic hypermutation (SHM) in expanded ASCs, and longer CDR3 regions (Ahern et al., 2022; Kuri-Cervantes et al., 2020; Woodruff et al., 2022). Together, these observations suggest that, similarly to systemic lupus erythematosus (SLE), peripheral tolerance mechanisms that normally restrain polyreactive and autoreactive naïve B cells (including anergy) may be disrupted in severe COVID-19 (Woodruff et al., 2020).

Consistent with this, expanded and reactivated anergic B cells within the B_{ND} compartment (IgD^+ IgM^-) have been described in COVID-19, characterised by downregulation of CD21 and CD22 compared to healthy donor B_{ND} (Castleman et al., 2022). In parallel, a reduction in memory B cells has been observed in COVID-19, alongside evidence for diminished germinal-centre (GC) reaction formation, linked to impaired Tfh function, associated with arrest of GC formation (Kaneko et al., 2020). Taken together, these findings point to a scenario in which EF ASC generation is prominent while GC-dependent maturation and memory formation are constrained, particularly in severe COVID-19 disease.

The most severe cases of SARS-CoV-2 infection are characterised by gen-

eralised immune hyperactivation in the context of a cytokine storm, with concomitant increases in neutralising antibody titres and an increased frequency of autoimmune manifestations (Woodruff et al., 2022). In line with the clinical relevance of cytokine-driven immunopathology, IL-6R blockade became part of recommended care for severe/critical disease with systemic inflammation, consistent with a cytokine milieu capable of perturbing peripheral tolerance (Coperchini, Chiovato, & Rotondi, 2021; Santa Cruz et al., 2021; X. Xu et al., 2020).

Beyond acute infection, recall responses may further bias output toward ASC differentiation. Highly mutated memory B cells were shown to be less likely to re-enter germinal centres following antigen re-encounter than naïve B cells, and instead preferentially differentiate into ASCs. Notably, memory B cells of low anti-spike affinity differentiated into ASCs more readily than low-affinity naïve B cells, suggesting that the low affinity alone was not the primary driver of ASC differentiation, but the level of cellular maturation appeared to be a key determinant (Li et al., 2024).

Furthermore, the magnitude and kinetics of spike-specific antibody responses have been associated with the clinical outcome, highlighting a narrow balance between effective anti-viral immunity and broader dysregulation (Legros et al., 2021).

Lastly, despite these profound disturbances, recent longitudinal studies have shown that many of these perturbations largely return to baseline, concomitant with symptom resolution. For example, the cellular frequencies including those of anergic B cells and plasmablasts recover by around 200 days post-symptom onset (Jokiranta et al., 2026). Therefore, COVID-19 is an intriguing model in which to study the determinants of breach in human B cell anergy,

as well as its modulation and recovery.

1.4 ANCA-associated vasculitis (AAV)

Anti-neutrophil cytoplasmic autoantibody (ANCA)-associated vasculitis (AAV) is an umbrella term for a group of three conditions mostly affecting the small vessels, which are called granulomatosis with polyangiitis (GPA), microscopic polyangiitis (MPA) and eosinophilic granulomatosis with polyangiitis (EGPA). These are rare diseases, with a combined prevalence in the UK of approximately 250 per million, and a peak incidence between 65-74 years of age (Watts, Mooney, Skinner, Scott, & Macgregor, 2012).

1.4.1 Clinical features

Clinical features in AAV vary greatly in severity and can manifest with sino-nasal otitis, uveitis and acute kidney dysfunction and progress to life-threatening multi-organ involvement (including pulmonary haemorrhage, interstitial lung disease, gastrointestinal perforations, pericarditis or necrotising glomerulnephritis) (Casal Moura et al., 2025).

As the name itself suggests, a common feature across ANCA-associated vasculitis conditions is the presence of circulating antibodies against neutrophil cytoplasmic antigens, most commonly against proteinase 3 (PR3) and myeloperoxidase (MPO). Over 90% of GPA and MPA are ANCA positive at diagnosis. GPA is dominated by PR3-ANCA (approximately 65% of patients) followed by MPO-ANCA (approximately 24% of patients). MPA is predominant in MPO-ANCA (approximately 58% of patients) followed by PR3-ANCA (approximately 25% of patients) (Hagen et al., 1998). EGPA patients are less frequently ANCA positive at diagnosis (approximately 40%

of patients) than GPA and MPA, and these titres are usually MPO-ANCA (Sablé-Fourtassou et al., 2005).

Clinically, PR3-ANCA has been associated with ear and nasal involvement, acute kidney injury and lung nodules, whereas MPO-ANCA with has been correlated with increased risk of chronic kidney disease and interstitial lung involvement.

Healthy individuals can display ANCA titres, but in AAV these are much higher. In non-AAV patients, other factors can induce ANCA-positivity such as infections like endocarditis (Van Gool et al., 2022; Mahr et al., 2014)

1.4.2 Pathogenesis

AAV pathogenesis is strongly linked to ANCAs, although the initiating events that lead to loss of tolerance to MPO and PR3 are not fully defined. One discussed model proposes that dysregulated formation and/or impaired clearance of neutrophil extracellular traps (NETs) increases the availability of neutrophil granule antigens such as MPO and PR3 in an immunostimulatory context. This may promote antigen presentation and a break in tolerance, supporting autoreactive T cell responses and B cell differentiation that culminates in ANCA production. Once present, ANCAs can bind to primed neutrophils and trigger their activation, leading to degranulation, oxidative burst, local tissue injury and further NET release. On the other hand, ANCA-activated neutrophils can engage the alternative complement pathway, generating C5a, which further primes and recruits neutrophils and amplifies inflammation. Together, these innate effector loops can drive ongoing vascular and tissue damage and facilitate recruitment and persistence of adaptive immune cells within inflamed tissues, sustaining chronic inflammation (Nakazawa, Masuda,

Tomaru, & Ishizu, 2019; Jennette, Falk, Hu, & Xiao, 2013).

1.4.3 Aetiology

AAV onset is thought to reflect an interplay between genetic susceptibility, epigenetic regulation, and environmental exposures. Genome-wide association studies (GWAS), largely performed in individuals of European ancestry, indicate that genetic risk segregates more strongly by ANCA specificity than by clinical syndrome. In these studies, PR3-ANCA disease (often presenting as GPA) is most strongly associated with the *HLA-DP* region, whereas MPO-ANCA disease (often presenting as MPA) predominantly associates with the *HLA-DQ* locus (Lyons et al., 2012; Xie et al., 2013). Population-specific risk alleles may also contribute to geographic differences in disease patterns. For example, *HLA-DRB1*09:01*, which is relatively frequent in Japan but uncommon in European populations, has been associated with MPA, consistent with epidemiological observations that MPO-AAV is proportionally more common in Japanese cohorts whereas PR3-AAV is more frequent in British cohorts (A. Kawasaki et al., 2016; Fujimoto et al., 2011; Nakazawa et al., 2019).

Beyond the MHC, several non-HLA loci have been implicated. These include *PTPN22* (involved in dysregulation of IL-10 pathways), as well as loci related to ANCA antigens and their regulation such as *PRTN3* (encoding PR3) and *SERPINA1* (encoding α1-antitrypsin, a PR3 inhibitor) (Lyons et al., 2012; Nakazawa et al., 2019). Epigenetic mechanisms are also implicated, as hypomethylation of *MPO* and *PRTN3* was associated with increased ANCA titre (B. E. Jones et al., 2017). Environmental factors associated with an increased AAV risk include silica exposure and farming (Nakazawa et al., 2019).

1.4.4 Therapeutic approaches and challenges

Current treatment approaches in AAV depend on the severity at diagnosis, distinguishing non–organ-threatening disease from organ- or life-threatening disease. Induction of remission therapy for non-severe, non-organ involving AAV is usually high-dose glucocorticoids with methotraxate.

For organ or life-threatening AAV, induction of remission therapy is usually with high-dose glucocorticoids in conjunction with rituximab or cyclophosphamide, which is typically administered for up to 12 months. This is followed by maintenance therapy with rituximab (GPA or MPA) or mepolizumab (EGPA) for 2-4 years, when it can be stopped if remission has been maintained (Hellmich et al., 2024).

However, these therapies are not perfect, since induction therapy does not reach remission in at least 10-12% of patients by 12 months (Stone et al., 2010; de Groot et al., 2009; R. B. Jones et al., 2010). In addition, approximately 50% of AAV cases relapse within 5 years of first treatment induction (Terrier et al., 2018). This suggests that alternative therapeutic methods are needed for the induction and maintenance of remission in AAV.

Patients with PR3-ANCA are at higher risk of relapse compared to MPO-ANCA, and patients with GPA suffer higher rates of relapse than MPA (Specks et al., 2013; Casal Moura et al., 2025; Terrier et al., 2018). In addition, GPA PR3-ANCA patients with granulomatous involvement achieved lower remission and a higher relapse rate than other GPA patients (Holle et al., 2012). Together, this suggests that PR3-ANCA, especially in GPA together with granulomatous involvement is the highest risk group of patients for relapse.

1.4.5 BAFF as a target in AAV

The frequent relapse patterns in AAV suggest that current regimens suppress inflammation effectively but may not durably maintain the autoreactive B cells which sustain disease.

Rituximab depletes $CD20^+$ B cells, sparing $CD20^-$ populations such as late plasmablasts or long lived plasma cells. Relapse rate in AAV has been associated with a few key factors including incomplete depletion of $CD20^+$ cells, re-emergence of circulating ANCAs and a more rapid recovery of the repertoire. These observations have led to the hypothesis that controlling the survival signals that shape B cell re-emergence may improve long-term outcomes in high-risk PR3-AAV.

BAFF is a TNF-family cytokine, homologous to APRIL with roles in B cell survival, including plasmablast viability (Avery et al., 2003). BAFF signals through three receptors [BAFFR, B cell maturation protein A (BCMA) and transmembrane activator and CAML interactor (TACI)], while APRIL only through TACI and BCMA. BAFFR is expressed on all B cell lineages, including peripheral but excluding bone marrow plasma cells (Darce, Arendt, Wu, & Jelinek, 2007). BAFFR is broadly expressed across peripheral B cell stages and is particularly important for transitional-to-naïve B cell survival, while TACI and BCMA are enriched in activated and antibody-secreting compartments; BCMA is expressed on plasmablasts and plasma cells, and it supports their survival (Ettinger et al., 2007; Darce et al., 2007). Downstream, BAFF signalling through BAFFR triggers alternative NF-κB signalling pathway for survival, whereas signalling through TACI or BCMA induces the canonical NF-κB pathway (Gardam & Brink, 2014).

This axis is relevant to AAV because elevated BAFF can relax peripheral selection, disproportionately supporting autoreactive B cell clones compared with non-autoreactive counterparts (Thien et al., 2004; Lesley et al., 2004). In AAV, circulating BAFF levels are increased compared with healthy controls (Sanders, Huitma, Kallenberg, & Stegeman, 2006; Krumbholz et al., 2005), supporting the rationale that BAFF blockade might (1) constrain BAFF-dependent transitional/naïve B cell survival during repopulation after depletion and (2) indirectly reduce the re-generation of pathogenic antibody-secreting responses by limiting plasmablast survival (Avery et al., 2003).

Belimumab, a monoclonal antibody that neutralises soluble BAFF, has demonstrated clinical efficacy in SLE and produces predictable immunological effects, including preferential reduction of transitional and naïve B cell compartments, with delayed effects on memory and plasmablast subsets in a longitudinal study (Jacobi et al., 2010; Ramsköld et al., 2019). Belimumab has shown promising results in primary Sjögren's syndrome (Mariette et al., n.d.). These considerations motivated the COMBIVAS trial, a randomised, double-blind, placebo-controlled mechanistic study evaluating sequential rituximab plus belimumab versus rituximab plus placebo in active PR3-AAV (McClure et al., 2023).

1.5 Psoriatic arthritis (PsA)

Psoriatic arthritis is a chronic immune-mediated disease that commonly affects the skin and joints. Up to 30% of patients with psoriasis (PsO) develop pathologic joint involvement within an average of 10 years after the PsO diagnosis. PsA is considered to be of multifactorial aetiology, both genetic and environmental factors contributing to the disease. The genetic component

is highlighted through the prevalence of PsA across various ethnicities. PsA is higher in European (175 per 100,000 people) than in Asian - Taiwanese (40 per 100,000) or South American (17 per 100,000) populations. Moreover, a family history of PsA increases the risk of PsA development (Lembke, Macfarlane, & Jones, 2024). Genome-wide association studies have determined several genetic variants strongly associated with PsA including related to antigen presentation (histocompatibility complex class I molecules PsA: *HLA-B27*, PsO: *HLA-C06*), interleukin (IL)-12, IL-23 and IL-17 signalling pathways (*IL12B*, *IL23R*, *TRAF3IP2*), NF-κB modulators (TNIP1 (*TNFAIP3*), REL (*REL*)), cytokine signalling transduction (tyrosine kinase 2 (*TYK2*)), and interferon-induced or receptor molecules (*IFIH1*, interferon lambda receptor-1 (*IFNLR1*)) (Stuart et al., 2015). However, monozygotic twin studies found psoriasis to be 66% concordant, but PsA only 10%, showcasing the importance of environmental triggers within susceptible individuals (Lønnberg et al., 2013; Pedersen, Svendsen, Ejstrup, Skytthe, & Junker, 2008). Indeed, the heterogeneity of PsA is also hinted by its equal prevalence among women and men, like axial spondyloarthritis (AxSpA), but unlike other autoimmune diseases where women are considerably disproportionately more affected such as systemic lupus erythematosus (SLE), Sjögren's syndrome (SjS), multiple sclerosis (MS), systemic sclerosis, RA or Hashimoto's (Pollard, 2012; van Vollenhoven, 2009). Environmental factors identified to adversely impact PsA development or progression include infections, trauma, obesity and stress (Kumthekar & Ogdie, 2020).

1.5.1 Clinical overview of PsA

Psoriasis precedes the arthritic pathology in approximately 80% of the cases (Tan et al., 2023). The clinical features of PsA include painful, swollen and stiff

joints, often accompanied by nail pitting (Sobolewski, Walecka, & Dopytalska, 2017)), and other extra-articular features such as uveitis (Abbouda et al., 2017; Deligeorgakis, Skouvaklidou, Skepastianos, Tsafis, & Kougkas, 2025) and metabolic disturbance (Ottas, Fishman, Okas, Kingo, & Soomets, 2017). Both small joints (including distal interphalangeal joints) and large joints (including hip, knee and wrist) are commonly affected. The pathology is underlined by inflammatory processes at multiple sites including the synovium, entheses (area of tendon attachment to bone), nail bed or entire digits (Kishimoto et al., 2021).

1.5.2 Pathogenesis of PsA

The pivotal inflammatory pathway in PsA pathogenesis is driven by the IL-17/IL-23 axis, which leads to the observed enrichment of IL-17$^+$ cytotoxic T cells (T_c) in the PsA synovium. The exact cellular processes that trigger the initial IL-17 polarisation are still unclear. A model of pathogenesis places innate immune cells (monocytes, macrophages, dendritic cells and neutrophils) as early inflammatory mediators. Disruption of angiogenesis and of endothelial cells could trigger IL-1 and granulocyte-macrophage stimulating factor (GM-CSF), which in turn would promote the innate immune cells to secrete IL-17, IL-22 and TNF. These cytokines would polarise the T cell repertoire towards an IL-17$^+$ T_c and helper T (T_h) 17 cell population in the joints. IL-17 would also promote neutrophil function through NF-κB activation. The proinflammatory cytokines would then create a positive feedback loop and ultimately lead to the clinically observed entheseal and synovial inflammation and to bone remodelling (Vecellio et al., 2021; Steel et al., 2020; Blauvelt & Chiricozzi, 2018).

1.5.3 Therapeutic approaches and challenges

Current management of psoriatic arthritis (PsA) includes low-key treatments such as non-steroidal anti-inflammatory drugs (NSAIDs) may be used for short-term symptomatic relief, but are recommended as monotherapy only in mild disease and for limited durations.

For patients with active peripheral arthritis, rapid initiation of conventional synthetic DMARDs (csDMARDs) is recommended, with methotrexate commonly preferred. If treatment targets are not achieved with csDMARDs, escalation to biologic DMARDs (bDMARDs) is recommended. Options include TNF inhibitors (TNFi) and IL-17 or IL-23 pathway-inhibitors, with selection guided by the patient's disease domains and co-morbidities (e.g. inflammatory bowel disease or uveitis). Targeted synthetic DMARDs (tsDMARDs), including JAK inhibitors provide additional options, particularly after refractory disease (Gossec et al., 2024).

Even with contemporary therapies, a substantial proportion of patients do not achieve the treatment target. In a systematic review and meta-analysis of minimal disease activity in PsA (45 studies; 12,469 patients), the overall prevalence of MDA in cross-sectional studies was 35% (95% CI 30–41%), and even among patients receiving biologic DMARDs it was 57% (95% CI 41–71%) (Zardin-Moraes et al., 2020). These data highlight an ongoing unmet need for improved therapeutic strategies and better approaches to matching patients to effective treatments.

PsA is also clinically heterogeneous and lacks validated diagnostic and predictive biomarkers. The identification of robust biomarkers could enable earlier and more accurate diagnosis, support patient stratification for personalised

medicine, and help identify individuals with PsO at increased risk of progression to PsA prior to clinically apparent joint pathology manifestation (FitzGerald et al., 2021).

1.5.4 B cells and autoantibodies in PsA

PsA has traditionally been classified as a seronegative arthritis because most patients do not exhibit circulating autoantibodies typically associated with rheumatoid arthritis (RA), such as rheumatoid factor (RF) or anti-cyclic citrullinated peptide (anti-CCP) antibodies (Merola, Espinoza, & Fleischmann, 2018). However, there has been increasing appreciation of the patient subsets who have circulating antibodies and their links to PsA pathogenicity and potential refractory disease. For instance, anti-CCP antibodies have been found in 5-13% of PsA patients and these have been linked to a more erosive form of disease (Behrens et al., 2016; Perez-Alamino, Garcia-Valladares, Cuchacovich, Iglesias-Gamarra, & Espinoza, 2014). In addition RF can also present and anti-nuclear-antibodies (ANA), though mechanistic links to PsA pathology are limited (Zhu, Shi, & Chu, 2020). Additional autoantibodies such as anti-LL37 and anti-ADAMTSL5 have also been described (Frasca, Palazzo, Chimenti, Alivernini, et al., 2018; Yuan et al., 2019).

B cells and plasma cells have been reported not only to infiltrate the inflamed synovium in PsA (Floudas et al., 2022), but also to form tertiary lymphoid structures (TLS) with micro-anatomical structures which are suggestive of active *in situ* reactions (Cañete et al., 2007; Cuervo et al., 2021). This suggests that their presence in the PsA synovium may be more than bystander activation and be driven through GC-like reactions *in situ*. Therefore, in spite of a low prevalence of circulating antibodies in PsA, the synovium contains organised niches that form to support B cell selection, differentiation and local

effector functions, and therefore B cell infiltration is unlikely to be incidental. Additionally, a recent study described B cell infiltrates in the synovial fluid to be 4 times more abundant in PsA compared to osteoarthritis (OA), further suggesting a role in this disease (Tzemach et al., 2025).

Tissue infiltrating B cells could be contributing to the synovial or entheseal inflammation not only through local secretion of autoantibodies, but also through autoantibody-independent roles, such as cytokine release or antigen presentation.

1.6 Research Gaps and Aims of the Thesis

While B cells are central to both infectious and autoimmune processes, significant mechanistic gaps remain in understanding their dynamic regulation and functional failure. This thesis investigates dysregulated B cell responses across three distinct clinical areas, chosen for their unique impacts on the immune system, thus offering complementary perspectives on B cell resilience and breakdown.

Key gaps in the field:

1. Peripheral tolerance dynamics: The model of naïve B cell anergy in humans lacks refinement, particularly regarding its functional markers and plasticity. It is unclear how this crucial mechanism of peripheral tolerance is dynamically impacted by acute systemic inflammation, such as in COVID-19, to temper or exacerbate the immune response. It is still unknown whether mechanisms like anergy suppress the inflammatory surge, and how the naïve B cell population changes with hyperactivation.
2. Repertoire steering: In AAV, the molecular impact of combining B

cell depletion (rituximab) with BAFF inhibition (belimumab) on the quality and autoreactivity profile of the recovering B cell repertoire is unknown. This limits the rationale for optimal maintenance therapy and the understanding of how therapeutic strategies can be used to steer B cell recovery towards a less autoreactive state.

3. The role of tissue-infiltrating B cells in PsA: In PsA, the role of B cells is often dismissed due to its 'seronegative' classification. The extent of B cell involvement, whether it is localised to the inflamed joint synovium and expanded in an antigen-driven manner, and the identity of any local autoantigens driving the pathology remain critical unresolved questions.

This thesis utilised a combination of flow cytometry, functional *in vitro* assays, and advanced B cell receptor repertoire sequencing to unravel the mechanisms of B cell reactivity across these three disease models. The specific aims were:

Chapter 3 — To investigate the relationship between surface IgM expression and functional responsiveness of human naïve B cells, and to characterise how this peripheral tolerance mechanism is re-modelled in the context of acute infection (COVID-19).

Chapter 4 — To dissect the impact of dual B cell targeting therapy (rituximab plus belimumab) on B cell repertoire reconstitution dynamics and quality in AAV, focusing on clonal characteristics and isotype usage.

Chapter 5 — To characterise the B cell repertoire within the inflamed synovium of PsA patients and to identify novel, disease-relevant autoantigens associated with local clonal B cell expansion.

Collectively, this work seeks to move beyond viewing B cells merely as antibody-producing cells, focusing instead on their dynamic regulation, their

capacity for functional failure and their localised contribution to inflammatory pathology. The findings aim to refine the fundamental models of B cell tolerance and provide the mechanistic rationale for targeted therapeutic intervention in the context of infection and autoimmune diseases.

2 | Materials and Methods

2.1 Human donors and samples

All healthy volunteers and patient donors were recruited under ethical approval granted by the University of Oxford, University of Cambridge, or the University of Birmingham (UK). Written informed consent was obtained from all participants prior to sample collection.

Human samples were collected under the following ethical approvals:

- Chapter 3: healthy donor PBMC samples (REC 06/Q1605/55); COVID-19 convalescent PBMC samples and matched healthy control PBMC samples (REC 21/YH/0206).
- Chapter 4: COMBIVAS clinical trial whole blood samples (REC 18/EE/0275).
- Chapter 5: CARTOGRAPHY study PBMC and synovial biopsy samples from PsA and RA patients (REC 07/H0706/81; REC 06/Q1606/139).

2.1.1 Healthy blood donors and sample collection

Healthy donor volunteers were recruited at the University of Oxford under ethical approval (REC 06/Q1605/55). Whole blood was collected in EDTA tubes (BD, #367525) by Patrick MacLean and Andrew Kwok. Buffy coats were received from healthy donors of the NHS Oxford Blood Donor Centre. The samples were stored on rollers at room temperature (RT) up to PBMC isolation for a minimum of one hour. PBMC extractions were carried out on the same day. These are used in Chapter 3.

2.1.2 Convalescent COVID-19 and matched control samples

Frozen convalescent COVID-19 PBMCs and gender-matched healthy control PBMCs were received courtesy of Alexandra Deeks from Dunachie Group, Oxford, UK, under ethical approval (REC 21/YH/0206). The samples were obtained from mild cases of COVID-19 in the community, sampled 10-15 days after the onset of the COVID-19 symptoms. These are used in Chapter 3.

2.1.3 COMBIVAS trial samples

Frozen whole blood in PAXgene RNA tubes and frozen PBMCs were received from the University of Cambridge, as part of the COMBIVAS clinical trial (IRAS ID: 229033, REC: 18/EE/0275). COMBIVAS aimed to determine the effect of sequential therapy of belimumab and rituximab in patients with active ANCA-associated vasculitis (AAV). Peripheral blood samples were taken on three timepoints: Day 1 (before treatment), Month 12 (Week 52) and Month 24. Alternatively, unscheduled samples were also taken at other timepoints upon disease relapse, as detailed in Table 2.1. These are used in Chapter 4.

2.1.4 CARTOGRAPHY study cases

The CARTOGRAPHY project is an Oxford-Janssen collaboration aimed at creating a cellular and molecular atlas of various immune-mediated inflammatory disorders (IMIDs). The ethics approval is covered by REC 07/H0706/81 and REC 06/Q1606/139. Chapter 5 of this thesis uses the single-cell multiomic data from the synovium and PBMC from RA and PsA patients, which originates from the CARTOGRAPHY project. The treatment history of

		Timepoint						
Patient	**Treatment**	D1	M10	M12	M16	M18	M22	M24
P1	BLM	1	0	1	0	0	0	1
P2	BLM	1	0	1	0	1	0	0
P3	PBO	0	0	1	0	1	0	0
P4	PBO	1	0	1	0	0	1	0
P5	BLM	1	0	1	0	0	0	1
P6	BLM	1	0	0	0	0	0	1
P7	PBO	1	0	1	0	0	0	1
P8	BLM	1	0	1	0	0	0	1
P9	PBO	1	0	2	0	0	0	0
P10	PBO	1	0	1	0	1	0	0
P11	BLM	1	0	1	0	0	0	1
P12	BLM	1	0	1	0	0	0	1
P13	BLM	1	1	0	0	0	0	0
P14	PBO	1	0	1	0	0	0	1
P15	BLM	1	0	0	0	0	0	1
P16	BLM	1	0	0	1	0	0	0
P17	BLM	1	1	0	0	0	0	0
P18	BLM	1	0	1	0	1	0	0
P19	PBO	1	1	0	0	0	0	0
P20	PBO	1	0	1	1	0	0	0
P21	PBO	1	0	1	0	0	0	1
P22	PBO	1	0	1	0	0	0	1
P23	BLM	1	0	0	0	0	0	1
P24	PBO	1	0	1	0	0	0	1
P25	PBO	1	0	1	0	0	0	1
P26	PBO	1	0	1	0	0	0	1
P27	PBO	1	0	0	0	0	0	0
Total (BLM)		13	2	7	1	2	0	8
Total (PBO)		13	1	13	1	2	1	7

Table 2.1: **Longitudinal sampling timepoints for patients in the COMBIVAS trial used in Chapter 4**. Treatment groups are indicated as BLM (belimumab) and PBO (placebo). D - day; M - month. Samples collected due to disease relapse at unscheduled timepoints (M10, M16, M18, and M22), along with the second sample from Patient 9 at M12, were excluded from the main BCR repertoire analysis.

these patients is as follows: 1) patients have had chronic disease, were TNF inhibitor (TNFi) treated, and were refractory at the point of sampling; 2) patients were treatment-naïve, and were sampled both before and after TNFi

therapy.

A detailed table with patient codes, numbers of samples and sample types is detailed in Table 2.2.

2.2 Human PBMC isolation

Whole peripheral blood collected in EDTA tubes was diluted 1:1 in PBS (Gibco, #10010056). PBMCs were isolated using lymphoprep (STEMCELL, #07851) density gradient centrifugation, at 800 g for 20 minutes with no brake. PBMCs were washed in PBS at 300 g. For long-term storage, the cells were resuspended in 90% foetal bovine serum (FBS) and 10% dimethyl sulfoxide (DMSO), seeded at 7.5×10^6 cells/mL and frozen at -80°C for one day, before being transferred into liquid nitrogen until use.

2.3 Human PBMC thawing

The frozen PBMC samples were thawed in a 37°C water bath. Pre-warmed RPMI media (Sigma-Aldrich, #R8758) at 37°C was added dropwise with a Pasteur pippete in each sample tube. The samples were mixed by gently pipetting and transferred to a 15 mL or 5 mL tube and topped up with 4 mL pre-warmed RPMI media.

Patient	Diagnosis	Stage	Synovial tissue	PBMC
P1	PsA	Chronic	Yes	Yes
P2	PsA	Chronic	Yes	Yes
P3	PsA	Chronic	Yes	Yes
P4	PsA	Chronic	Yes	Yes
P5	PsA	Chronic	Yes	Yes
P6	PsA	Chronic	Yes	Yes
P7	PsA	Chronic	Yes	No
P8	PsA	Chronic	Yes	No
P9	PsA	Chronic	Yes	No
P10	PsA	Pre/Post-TNFi	Yes	Yes
P11	PsA	Pre/Post-TNFi	Yes	Yes
P12	PsA	Pre/Post-TNFi	Yes	Yes
P13	PsA	Pre/Post-TNFi	Yes	Yes
P14	PsA	Pre/Post-TNFi	Yes	Yes
P15	PsA	Chronic	Yes	No
P16	RA	Pre/Post-TNFi	Yes	Yes
P17	RA	Chronic	Yes	Yes
P18	RA	Pre/Post-TNFi	Yes	Yes
P19	RA	Pre/Post-TNFi	Yes	Yes
P20	RA	Chronic	Yes	Yes
P21	RA	Chronic	Yes	Yes
P22	RA	Chronic	Yes	No
P23	RA	Chronic	Yes	No
P24	RA	Pre/Post-TNFi	Yes	Yes
P25	RA	Pre/Post-TNFi	Yes	Yes
P26	RA	Chronic	Yes	No
P27	RA	Chronic	Yes	No
P28	RA	Chronic	Yes	No
P29	RA	Chronic	Yes	No
P30	RA	Chronic	Yes	No

Table 2.2: **Patient clinical characteristics and sample availability from the CARTOGRAPHY study.** This table summarises diagnosis, disease stage and availability of synovial tissue and/or PBMCs for each patient included in Chapter 5. Patients comprise those with established treatment at baseline (chronic) and treatment-naïve individuals resampled following anti-TNF therapy. Disease stage abbreviations are: -I, pre-TNFi; -II, post-TNFi; -C, chronic. PsA - Psoriatic arthritis; RA - Rheumatoid arthritis

2.4 Anergic B cells in COVID-19 methods

2.4.1 B cell enrichment and isolation

2.4.1.1 Magnetic B cell enrichment

Frozen human PBMCs were thawed as described in section 2.3 and enriched for either total B cells using B cell Isolation Kit II (Miltenyi, #130-091-151) or for naïve B cells initially using the Naïve B Cell Isolation Kit II (Miltenyi, #130-091-150) for optimisations. Naïve B cells were later enriched using EasySep Human Naïve B Cell Enrichment kit (STEMCELL, #19254). Cell-of-interest enrichment purity was routinely achieved over 80%, confirmed by flow cytometry (data not shown).

2.4.1.2 Fluorescence-activated cell sorting (FACS) for proliferation assay

Human naïve B cells previously magnetically enriched using EasySep Human Naïve B Cell Enrichment kit (STEMCELL, #19254) were FACS-sorted based on their IgM expression intensity, as determined for each sample. Prior to the cell sort, the cells were stained with cell proliferation dye eFluor450 (eBioscience, #65-0842-85) and for viability (ThermoFisher, LIVE/DEAD Fixable Near IR dead cell stain kit, #L34975) as per manufacturer's instructions. The cells were resuspended in 100 µL and stained with the cell-sorting antibody panel detailed below at a concentration of 1 µL per 2×10^5 cells in the dark, on ice. The cell-sorting antibody panel is detailed in Table 2.3. The cells were sorted directly into 1.5 mL DNA LoBind tubes (Eppendorf) containing 300 µL of pre-chilled *B cell media* (RPMI 1640 + L-glut media (Gibco, #21875034) supplemented with 10% FBS, 1% Pen-Strep, 10 mM HEPES, 1 mM sodium

pyruvate, 1% MEM (Gibco, #11140050) and 55 mM βME).

Table 2.3: **FACS-sorting antibody panel used for isolation of human B cell subsets.**

Marker	Fluorochrome	Clone	Supplier	Catalogue #
IgM	BUV395	G20-127	BD Horizon	563903
CD19	SB600	HIB19	eBioscience	63-0199-42
CD3	PerCP-Cy5.5	OKT3	eBioscience	45-0037-42
CD27	PE-Cy7	0323	eBioscience	25-0279-42
CD10	PerCP-Cy5.5	Hi10a	BioLegend	312215

All antibodies were used at a concentration of 1 μL per 2×10^5 cells in 100 μL staining volume, in the dark and on ice.

For FACS-sorting, the cells were gated based on: Lymphocyte gate (FSC-A vs SSC-A), Singlets (FSC-A vs FSC-W), Live cells (Near-IR$^-$ vs SSC-A), CD19$^+$ and CD3/CD10$^-$, IgD$^+$ and CD27$^-$ (Figure 2.1). Then, the population expressing the bottom 33% of IgM intensity was sorted as 'IgM Low/Lo', the middle 33% was sorted as 'IgM Mid' and the top 33% was sorted as 'IgM High/Hi'. The sorted cell numbers varied with each experiment, ranging between 15,000 - 40,000 cells for each IgM subset. Comparable numbers of cells were FACS-sorted for each IgM-defined subset between COVID-19 and healthy matched donors per experiment. The cells were resuspended in *B cell media* and plated for the proliferation assay.

2.4.2 Proliferation assay and flow cytometry

Frozen human PBMC were thawed as described in section 2.3 and enriched for total B cells or for naïve B cells as described in section 2.4.1.1. The cells were stained with cell proliferation dye eFluor450 (eBioscience, #65-0842-85), as per standard protocol. The cells were resuspended in *B cell media* (RPMI 1640 + L-glut media (Gibco, #21875034) supplemented with 10% FBS, 1% Pen-

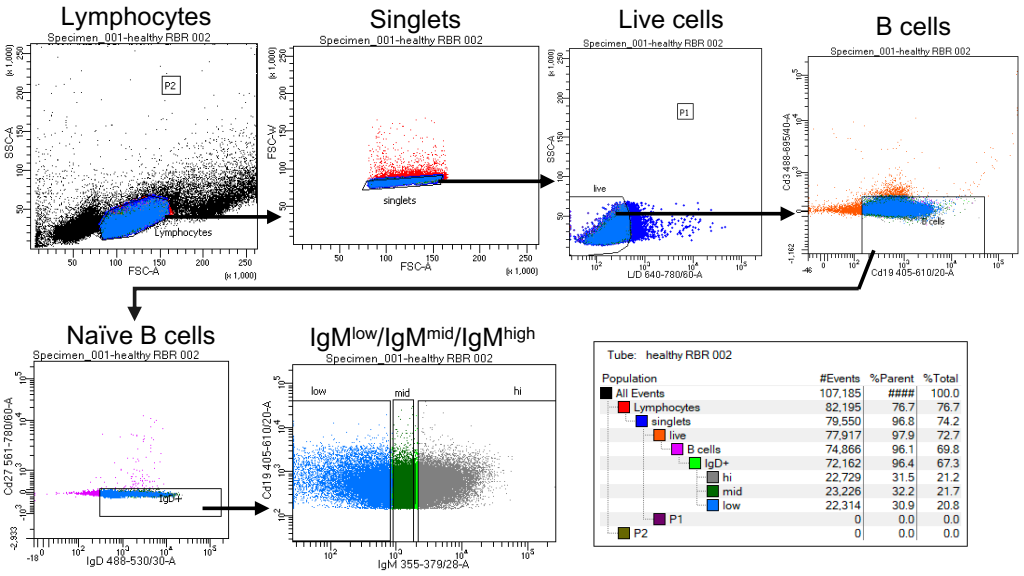

Figure 2.1: Gating strategy for FACS-sorting of IgM^{hi}, IgM^{mid} and IgM^{low} naïve B cell subsets. Flow cytometry plots with the gating strategy used for FACS-sorting of one representative example.

Strep, 10 mM HEPES, 1 mM sodium pyruvate, 1% MEM (Gibco, #11140050) and 55 mM βME). Cell concentration was calculated using a 1:1 trypan blue solution with a haemocytometer, or with an automated cell counter (Countess II, Invitrogen). Seeded cells at a concentration of 1×10^5 cells/well in round-bottom 24-well plates were stimulated with the stated concentrations of CpG (ODN 2006, Invivogen, #tlrl-2006), IL-2 (Peprotech, #200-02), CD40L (Enzo Life Science, #ALX-522-015-2010) or BAFF (Peprotech, #30-13-5uG). The cells were placed in cell culture for up to 5 days at 37°C and 5% CO_2. Proliferation was assessed by flow cytometry on day 0 and on day 3, day 4 or day 5 of cell culture. Cells were harvested in 5 mL polystyrene tubes, washed with PBS and stained with viability dye (ThermoFisher, LIVE/DEAD Fixable Near IR dead cell stain kit, #L34975) based on the manufacturer's protocol. Fc block (2 µL/1×10^6 cells, BD, #564219) was added 5 min prior to the 30 min antibody staining in 100 µL staining buffer (PBS with 1% FBS).

The flow cytometry staining antibody panel is detailed in Table 2.4. The flow cytometer used to acquire the samples was LSR FORTESSA X20 (BD).

Table 2.4: **Flow cytometry antibody panel used for phenotypic characterisation of human B cells.**

Marker	Fluorochrome	Clone	Supplier	Catalogue #
IgM	BUV395	G20-127	BD Horizon	563903
CD19	SB600	HIB19	eBioscience	63-0199-42
CD38	BV711	HIT2	BioLegend	303528
IgD	FITC	IA6-2	BD	555778
CD3	PerCP-Cy5.5	OKT3	eBioscience	45-0037-42
CD21	PE	HB5	eBioscience	12-0219-42
CD14	PE-Texas Red	TuK4	eBioscience	MHCD1417
CD27	PE-Cy7	0323	eBioscience	25-0279-42
CD22	APC	RFB-4	eBioscience	MHCD2205
CD10	PerCP-Cy5.5	Hi10a	BioLegend	312215
CD24	AF700	eBioSN3	eBioscience	56-0247-41

All antibodies were used at a concentration of 1 μL per 2×10^5 cells in 100 μL staining volume, unless otherwise stated.

2.5 BCR repertoire in COMBIVAS methods

2.5.1 RNA extractions

2.5.1.1 Healthy PBMC samples

Frozen PBMC samples in CryoStor buffer (STEMCELL, #07930) were received, and were thawed as described in section 2.3. The samples were centrifuged at 300 g and the pellet resuspended in RLT Plus buffer+ 1% βME (Qiagen, RNeasy Plus Mini kit, #74134). The RNA extractions were performed using the RNeasy Plus Mini kit, according to manufacturer's protocol. The RNA was stored at -80°C until use.

2.5.1.2 COMBIVAS PAXgene RNA tube samples

Frozen whole blood stored in PAXgene RNA tubes (BD Biosciences, #762165) were received. The tubes were thawed at 4°C overnight and left to equilibrate at room temperature (*RT*) for 4 h, before proceeding with the standard PAXgene RNA extraction kit protocol (Qiagen, #762174). RNA was eluted in BR5 elution buffer from the aforementioned kit, and RNA concentration was quantified with the Qubit high sensitivity RNA kit (Invitrogen, #Q32852).

2.5.2 Reverse transcription

The reverse transcription (RT) reaction was performed using the SuperScript IV Reverse Transcriptase kit (Invitrogen, #18090050), RNaseOUT(Invitrogen, #10777019) and an in-house primer RT primer mix detailed in appendix table A.1 (Bashford-Rogers et al., 2019). The RNA quantity used per reaction varied according to the type of sample, as follows: whole blood in PAXgene tubes - 800 ng RNA; PBMC control sample - 150 ng RNA. Depending on the volume of RNA used, the samples were prepared in single RT reactions (RNA volume $\leq$ 11 µL), or double RT reactions (RNA volume between 11 - 22.7 µL). The RNA was diluted with ddH_2O to the required volume per single/double reaction, as needed, and added to each well. For a single reaction, 1 µL of in-house primer-mix (2 µM) and 1 µL of deoxyribonucleotide triphosphates (dNTP, 10 mM) was added to each reaction well. For a double RT reaction 2 µL of in-house primer-mix (2 µM) and 2 µL of dNTP (10 mM) was added to each reaction well. The wells containing RNA, dNTP and in-house primer mix was incubated at 65°C for 5 min and 1 min on ice. The reverse transcription mix was prepared for each (single/double) reaction, as follows: 8 µL for single / µL double of 5X SuperScript IV buffer; 2 µL single/ µL for double DTT

(0.1 M), 2 µL single/ µL double RnaseOUT (40 U/mL) and 1 µL single/ µL double SuperScript IV enzyme (200 U/µL). The reverse transcription mix (7 µL per single reaction / 13.3 µL for double reaction) was added to each annealed sample, to a final volume of 20 µL per single reaction/ 40 µL per double reaction. The samples were placed in the ThermoCycler at the program 1 cycle (55°C, 50 min), 1 cycle (80°C, 10 min), 1 cycle (4°C, ∞). For residual mRNA degradation post-reaction, 1 µL of RNaseH (New England Biolabs, M0297S) was added to each well, and the samples were incubated at 37°C for 20 min.

2.5.3 cDNA bead clean-up

cDNA was cleaned using standard AMPure XP beads (Beckman Coulter, #A63880). A standard bead concentration of 1.8 x ratio of the original well volume was added, mixed and incubated for 8 min. The wells were placed on the magnet for 5 min. The supernatant was removed. The plate was taken off the magnet and 25-45 µL of nuclease-free water was added, and left for 10 min incubation. The wells were placed on the magnet for 5 min and the supernatant containing the cDNA transferred into fresh tubes/plate. Cleaned-up cDNA product was routinely eluted in 40 µL nuclease-free water for the reactions where 100 ng RNA input was added, and 25 µL nuclease-free water where RNA input was lower than 100 ng or 'too low to be detected'.

2.5.4 BCR amplifications

KAPA HiFi HotStart ReadyMix (Roche, #KK2601) was used for BCR amplifications. The indexed forward primer probe and reverse primer CNUS sequences are detailed in appendix table A.2. A total of 100 µL reaction mix was prepared, per reaction: 20 µL of cDNA, 50 µL KAPA HiFi HotStart

ReadyMix buffer, 2.6 µL indexed forward primer (10 µM), 2.6 µL reverse primer CNUS (10 µM), 24.8 µL nuclease-free water. The amplification was carried out in the ThermoCycler using the following program: 1 cycle (95°C, 3 min), 30 cycles (98°C, 20 s; 62°C, 30 s; 72°C, 1 min), 1 cycle (72°C, 7 min).

2.5.5 BCR gel electrophoresis

BCR amplification and amplicon size was verified by running 10 µL of the product with 3 µL loading buffer on a 2 % agarose gel for 40 min at 110 V, alongside 5 µL of 100 bp DNA ladder. The intensity of the bands was labelled as 'bright', 'intermediate' and 'low' as an approximation for the PCR product quantity.

2.5.6 Library preparation

The sequencing library was prepared using the KAPA HyperPrep Kit (Roche) in combination with the KAPA Unique Dual-Indexed Adapter Kit (Roche), based on the manufacturer's protocol with the batch-particularities detailed in the sections below.

2.5.6.1 Sample pooling

BCR amplification sample products were pooled according to their unique indexes in a stoichiometrically balanced mixture based on the intensity of the bands displayed on the electrophoresis gel ('bright'/'intermediate'/'low'), run as described in Section 2.5.5. To achieve a balanced mixture within each pool, samples of similar band intensity were grouped to be pooled (i.e. 'bright' with 'bright' samples, etc). To achieve comparable quantities between sample pools, the following relation of proportionality was established: 1 part of a

'bright' sample was equivalent to 2 parts of an 'intermediate' sample or of 4 parts a 'low' sample.

2.5.6.2 Pooled-sample bead clean-up

Bead clean-up of sample pools was carried out using 0.7x AMPure XP beads (Beckman Coulter, #A63880). Sample pools were left to incubate with beads at *RT* for 10 min, then placed on the magnet for 5 min. The supernatant was removed. The tubes were removed from the magnet and the beads were resuspended in 100 µL of freshly prepared 70% EtOH. The samples were placed back on the magnet for 1 min. Then, the ethanol was discarded. The beads were left to dry on the magnet for 3 min. The beads were resuspended in 55 µL of ddH_2O, incubated for 10 min and the samples were eluted. 5 µL of each cleaned pool was run on a 2 % agarose gel for 40 min at 110 V, along with 5 µL of a 100 bp DNA ladder. Here is an example of a bead-cleaned sample pool (Figure 2.2). The bands were quantified in nanograms with the ladder as reference using the BioRad gel reader software.

2.5.6.3 Calculations for end-tail repair and adapter ligation

The final total quantity of PCR product in each sample pool was determined based on the electrophoresis gel run in Section 2.5.6.2. If the total amount of product in one sample pool was above 1 ng, then half the volume of that sample pool (25 µL was taken forward and topped up with 25 µL of ddH_2O, to a final volume of 50 µL for end-tail ligation. Otherwise, if the total amount of product in one sample pool was below 1 ng, the entire volume of the sample pool was used (50 µL). Sample pools containing less than 1 ng of product after dilution were assigned a 20:1 adapter-insert ratio; whereas sample pools containing more than 1 ng of product were assigned a 10:1 adapter-insert

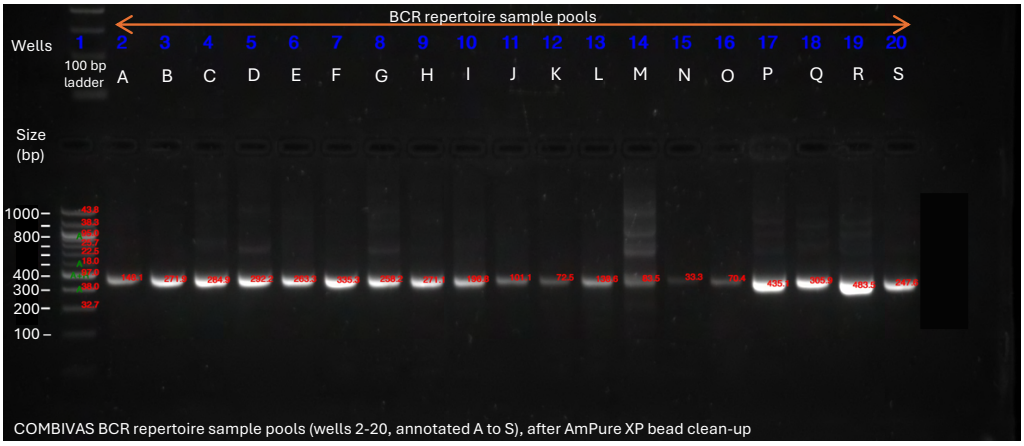

Figure 2.2: Amplified COMBIVAS BCR repertoire sample pools after bead clean-up. Each sample pool is annotated with a letter from A to S (wells 2-20) and is comprised of up to 12 uniquely indexed amplified COMBIVAS BCR repertoire samples). The bands were quantified in nanograms using the ladder as reference and are here annotated in red, as calculated by the BioRad software.

ratio.

2.5.6.4 End-tail repair and extension

A mixture containing 7 µL of End Repair and A-Tailing Buffer and 5 µL End Repair and A-Tailing Enzyme Mix was added to each 50 µL diluted sample pool. The tubes were placed in the PCR machine to incubate at 20°C for 30 min, with no heated lid. Subsequently, the tubes were incubated at 65°C for 30 min with heated lid (85°C), followed by 4°C.

2.5.6.5 Adapter ligation

The chosen unique adapters from stock (15 µM) were diluted in separate tubes with ddH_2O based on the calculations described in Section 2.5.6.3, in a 10 µL volume. Then, 30 µL ligation buffer and 10 µL DNA ligase were added to each 10 µL diluted unique adapter solution. Once the End repair

and A-tailing reaction finished, the full 60 µL reaction volume was added in each relevant well containing the 40 µL ligation with 10 µL diluted unique adapter solution. The ligation reaction was carried out for 2 h at 20°C in the ThermoCycler.

2.5.6.6 Post-ligation bead clean-up

The adaptor-ligated sample pools were cleaned with 0.7X AMPure XP beads (Beckman Coulter, #A63880) as described in Section 2.5.6.2. 5 µL of the sample pools prior and after ligation were run on a 2% agarose gel as described in Section 2.5.6.2.

2.5.6.7 Quantification of sample pools, library pooling and sequencing

The sequencing libraries were quantified based on the intensity of the bands displayed on the electrophoresis gel run in section 2.5.6.6. These were pooled in a stoichiometrically balanced mixture and sent for paired-end 300 bp sequencing on the Illumina MiSeq platform by Azenta Life Sciences.

2.5.7 BCR repertoire analysis

The code used to perform the BCR repertoire analysis was developed and published by Rachael Bashford-Rogers and is available at $github.com/Bashford-Rogers-lab/Bulk\_Repertoire\_Analysis$ (Bashford-Rogers et al., 2019). Briefly, the raw reads were filtered for a base determination accuracy of over 99.9% (median Phred quality score > 32). Forward and reverse reads which overlapped a minimum of 50 bp were merged and split by sample barcodes. Sequences which shared the same barcode and contained at least 5 members were collapsed. Isotypes were assigned based on IMGT/HighV-QUEST

(Brochet, Lefranc, & Giudicelli, 2008).

For the BCR network analysis, heavy chain sequences were segmented into overlapping subsequences of 10 bp for comparative analysis. A unique ID was assigned to a cluster of heavy chain sequences in which any two members differ by at most one point mutation. Clustering ended when no additional sequences could be incorporated within the one mutation threshold of any existing member.

To enable comparison across samples with differing read depths, the samples were downsampled to the read count of the lowest-depth sample of the cohort. Metrics were then recalculated across 1000 independent subsampling iterations, and the mean value across iterations was reported unless stated otherwise.

Outputs of the BCR repertoire analysis include: Sequence overlap (clonal sharing) between samples (Jaccard index, detailed below), proportion of the repertoire represented by the largest 5 expanded clones (D5), cluster and Vertex Gini index, frequency of isotype usage, frequency of IGHV4-34 with unmutated NHS/AVY motifs usage per isotype, frequency of variable gene replacement in the repertoire.

The frequency of variable gene replacement in the repertoire was calculated as follows: Stem regions of the BCR were defined as the N–IgHD–N–IgHJ region beginning 3 bp downstream of the IgHV gene boundary. At each timepoint, all BCRs containing the identified stem regions were retrieved, and the same stem regions were also searched for in repertoires from unrelated healthy controls. Stem regions were grouped into similarity clusters such that every stem within a cluster was within a single base-pair difference of at least one other member of that cluster. For each stem-cluster, the relative frequencies

of IgHV genes were calculated based on the sequences containing stems from that group.

Samples were excluded from BCR repertoire metric analyses if the number of productive BCR sequences fell below predefined thresholds, which were set to ensure robustness of each metric. Specifically, analyses of somatic hypermutation (SHM) frequency and IGHV4-34 usage required a minimum of 10 BCR sequences per sample. Analyses of secondary rearrangements required at least 50 BCR sequences per sample.

For metrics sensitive to sampling depth, including clonal expansion, clonal diversification and the proportion of the repertoire occupied by the top 5 clones (D5), samples were subsampled to fixed numbers of BCR sequences per isotype. Samples not meeting these minimum counts were excluded from the respective analysis. Subsampling thresholds were as follows: total repertoire (2500 sequences), IGHM (1500), IGHA1 (120), IGHA2 (120), IGHD (120), IGHG1 (10), IGHG2 (10), IGHG3 (10), IGHG4 (10) and IGHE (10).

Equations used in the BCR repertoire analysis are detailed below.

Jaccard index The Jaccard index was used to represent the overlap of the BCR repertoire across samples. The formula of the Jaccard index between two samples A and B is given by:

$$J(A, B) = \frac{|A \cap B|}{|A \cup B|}$$

Gini index The Gini index represents the relative inequality of B cell clones within one sample and is given by:

$$G = \sum_{i=1}^{N} \frac{\left(r_i - \frac{i}{N}\right)}{N}$$

A sample of identical clone sizes represents perfect equality (G = 0). Inequal clone representation results in a Gini index value closer to 1.

Shannon index The Shannon index quantifies the diversity of B cell clones within a sample and is defined as:

$$H = -\sum_{i=1}^{S} p_i \ln(p_i)$$

where p_i is the relative frequency of clone i, and S is the total number of unique clones. A sample dominated by a single clone yields a Shannon index close to 0, whereas greater clonal diversity results in higher values of H.

2.6 B cells in PsA methods

2.6.1 Single-cell multi-omic sequencing analysis

2.6.1.1 Pre-processing and QC

The accessed CARTOGRAPHY dataset had already undergone quality control filtering by Devika Agarwal and Calliope Dendrou (part of the CARTOGRAPHY Consortium), as follows. For RNA-derived data, cells were retained if they contained between $500 \leq n_{\text{genes}} \leq 55{,}000$ detected genes and a mitochondrial gene fraction of $\leq 15\%$. For protein-specific filtering, cells were excluded if they had $n_{\text{proteins}} > 18{,}000$ or if the proportion of isotype counts exceeded 7.5%. The B cells were subsetted from the whole cell pool prior to them be

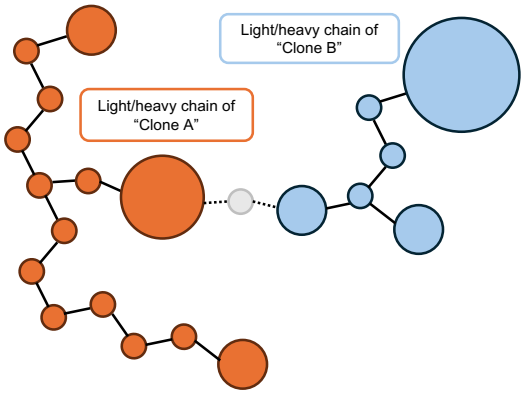

Figure 2.3: Schematic example of light/heavy chain ID assignment. Each node represents a unique light chain sequence, with node size proportional to the number of identical sequences observed. The edge indicates that two sequences differ by a single point mutation. Sequences that are connected through one mutation differences are grouped under the same ID. The sequences of Clone A (orange) and Clone B (blue) are closely related, but the absence of the intermediate gray sequence prevents them from being assigned the same ID. The clone ID is defined as the pairing of a light chain ID with a heavy chain ID.

made accessible to me by Devika Agarwal and Calliope Dendrou (part of the CARTOGRAPHY Consortium), as follows. Cells were clustered at a PCA resolution of 0.6. Clusters which were formed were manually annotated. The cluster which had the highest transcriptomic expression level of MZB1, SDC1, IGHG1, MS4A1 and TCF4 was annotated as "B cells and Plasma cells". This is the object I used and analysed in Chapter 5.

2.6.1.2 Core analysis

The single-cell data was analysed in `R` (version 4.2.0) using the Seurat package (version 5.0). The RNA-sequencing, CITE-sequencing and BCR V(D)J data was scaled, normalised before being integrated in one object. Genes which can skew dimensionality reduction (cell cyle genes, mitochondrial and ribosomal genes, immunoglobulin heavy and light chain genes) were regressed

from the transcriptomic analysis prior to variable gene determination and cell clustering. Dimensionality reduction was carried out through principal component analysis (PCA) followed by Uniform Manifold Approximation and Projection for Dimension Reduction (UMAP). Sample integration was performed with Harmony. Cell annotation was based on the integrated analysis of features derived from RNA-sequencing, CITE-sequencing and BCR V(D)J sequencing. The BCR network analysis generation (here adapted for V(D)J object generation, see 'VDJ Sequencing' in Figure 2.4) was carried out using code written by Rachael Bashford-Rogers, as previously described in Section 2.5.7. For the BCR network generation, a unique ID was assigned to each cluster of heavy chain or light chain sequences in which any two members differ by at most one point mutation. The clone ID was defined as the pairing of a light chain ID with a heavy chain ID (Figure 2.3).

The scripts used for the analysis are available on my personal Github page, accessible at: $https://github.com/janep24/DPhil-Thesis-Scripts$. An overview of the pipeline is depicted in Figure 2.4.

2.7 Recombinant antibody production

Frozen human primary cells from the joint of an osteoarthritis patient (passage 4, received as a courtesy of Professor Christopher Buckley, University of Oxford) or human healthy dermal fibroblasts (Sigma, #C-12302) were thawed and cultured in Dulbecco's Modified Eagle Medium (DMEM, low glucose, with GlutaMAX and pyruvate supplement, Gibco, #10567014) supplemented with 10% FBS and 1% Pen-Strep. Cells were expanded in T-75 flasks for a minimum of 14 days and up to 9 passages prior to immunofluorescence (IF) staining. Cells were detached using TrypLE (Gibco, #12604013), washed and

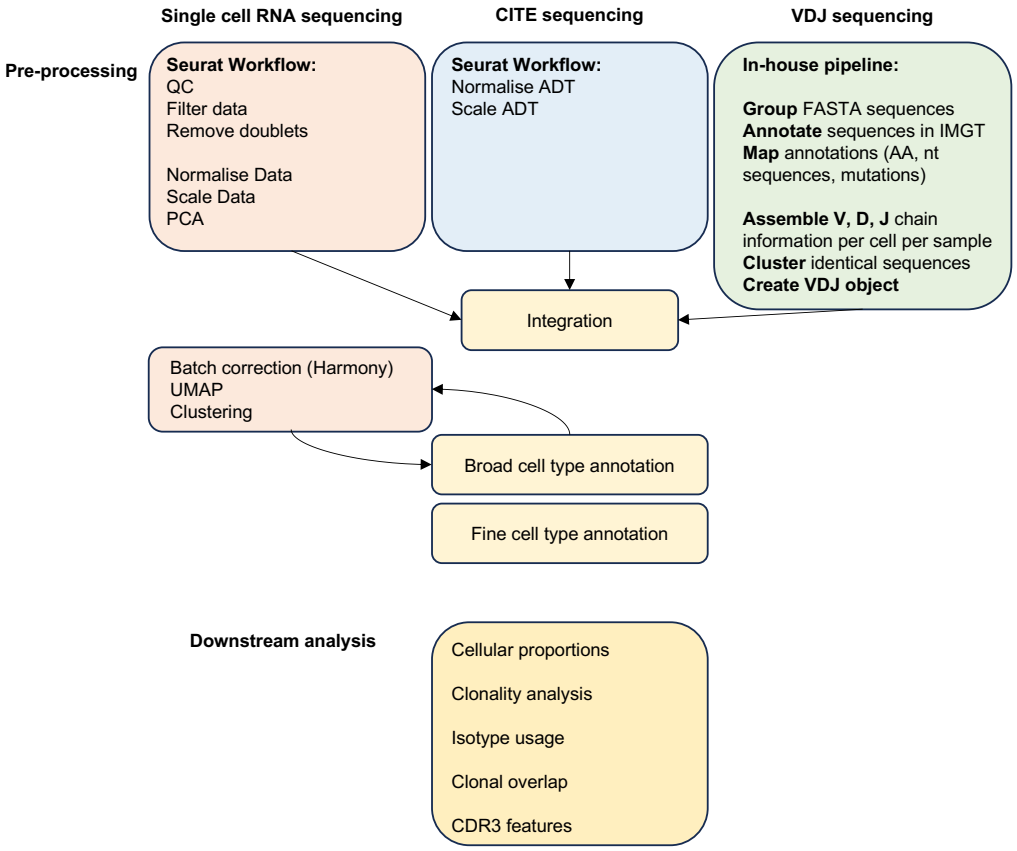

Figure 2.4: Workflow schematic of the CARTOGRAPHY data analysis pipeline QC - Quality control; PCA - Principal component analysis; ADT - antibody derived tag; UMAP - Uniform Manifold Approximation and Projection for Dimension Reduction; AA - aminoacid; nt - nucleotide; V - variable; D - diverse; J - joining; CDR3 - complementarity determining region 3.

seeded in 96-well flat-bottom plates (ibidi, #89627) at a density of 2×10^4 cells per well. After 24 h incubation at 37°C and 5% CO_2, cells were washed three times with PBS and fixed either with 4% paraformaldehyde (PFA) in PBS for 10 min at room temperature or with pre-chilled methanol for 10 min at -20°C for simultaneous fixation and permeabilisation.

Following fixation, cells were washed three times with PBS and blocked for 1 h at *RT* in PBS supplemented with 5% Ig-free BSA and 0.2% Tween20. Primary

and secondary antibody incubations, including concentrations and staining conditions are detailed in Table 2.5. Vimentin staining was performed only in methanol-fixed samples, whereas PFA-fixed samples were not incubated with anti-vimentin antibodies. Secondary antibodies were applied according to the host species of the primary antibodies. For PFA-fixed samples, additional membrane staining with wheat germ agglutinin (WGA) was performed prior to nuclear counterstaining.

Primary antibody staining was carried out overnight at 4°C, followed by washing and incubation with secondary antibodies for 45 min at 37°C. After final washes, cells were counterstained with DAPI (NucBlue Fixed Cell ReadyProbes, Invitrogen) prior to microscopic acquisition.

Table 2.5: **Primary and secondary antibodies used for immunofluorescence staining.**

Target	**Clone**	**Supplier**	**Cat.#**	**Conc.**
Primary antibodies				
Rabbit anti-vimentin	EPR3776	Abcam	ab92547	1:200
Custom mouse IgG2a rAb	–	TWIST enceBiosci	–	20 μg/mL
Mouse IgG2a isotype	E5Y6Q	Cell Signaling	61656	20 μg/mL
Secondary antibodies				
Goat anti-rabbit IgG-AF647	–	Invitrogen	A32733	1:1000
Goat anti-mouse IgG-AF488	–	Invitrogen	A32723	1:1000
Other stains				
WGA-AF488	–	Invitrogen	W6748	1:1000
WGA-AF647	–	Invitrogen	W32466	1:1000
DAPI	–	Invitrogen	R37606	70:1000

Vimentin staining was performed only in methanol-fixed samples. Secondary antibodies were selected according to the host species of the primary antibody. WGA staining was performed only in PFA-fixed samples.

2.8 Confocal microscopy analysis

Cells were acquired on an Olympus 4000 LSM confocal microscope with a 10x objective. The initial image analysis was performed using Arrivis Vision4D (Version 4.1.2). The first two batches of image acquisition and the development of the Arrivis analysis pipeline were carried out in collaboration with the Imaging Facility at the Centre for Human Genetics, University of Oxford.

In experiments with methanol-fixation (intracellular and extracellular staining experiments), the cells were first segmented based on nuclei using Cellpose (nucleus diameter 12 µm), Cellpose model Cyto2, quality threshold 0.4), then filtered based on nucleus size (nuclei with VoxelCount >200 were removed). The cells were segmented using the 'region growing' method based on the channel with vimentin staining (Watershed method, Threshld 200, Max distance between cells 158 µm). Lastly, incomplete cells were removed from analysis with a Touching Edge Filter (based on the cell Region Growing, on all 4 edges (Top, Bottom, Right, Left).

The experiments with PFA-fixation (extracellular staining experiments) were run on a distinct pipeline. To achieve cell segmentation, the cell surface area was firstly improved by 'Denoising' based on the WGA channel with 'Discrete Gaussian' method based on an average cell diameter of 50 µm). Then the nuclei were segmented using Cellpose (nucleus diameter 14 µm), Cellpose model Cyto2, quality threshold 0.4).

The nuclei were filtered by size (nuclei with VoxelCount >200 were removed). Then, the cell surface area was identified by 'region growing' from the denoised cell surface area previously identified (Threshold = 62, Max cell distance =

158 µm)). The incomplete cells were removed from analysis with a 'Touching Edge Filter' (based on the cell Region Growing, on all 4 edges (Top, Bottom, Right, Left).

The data was exported per nucleus and cell area and further analysed using `R` (version 4.2.0). The scripts used for analysis are available on my personal Github page, accessible at: $https://github.com/janep24/DPhil-Thesis-Scripts$.

2.9 HuProt microarrays

Each recombinant antibody was run on an individual HuProt microarray, by the manufacturer facility, CDI Labs. CDI Labs run the arrays, quality control and provided the experimental read metrics including raw median fluorescence intensity (MFI) reads, $\log_2$ MFI reads and Z-scores. The transformation $\log_2$ was used to normalise variance across samples. Spots were classified as false positives and removed if their signal in the secondary-only antibody stain exceeded $\log_2 > 2$, relative to the median signal of the secondary-only antibody array. The Z-scores were then calculated based on the filtered log2 normalised data for each protein per individual array. In each array, a target was considered a hit if all three criteria below were met: (1) raw MFI > 100, (2) Z-score > 3 and (3) the normalised $\log_2$ signal was 2-fold higher than the median value of secondary-only array for that spot (i.e. all hits exhibited at least 4-fold increase in signal relative to the raw secondary-only readings for that specific spot).

2.10 Exploring existing associations of the FAP antibody target in PsA

The GWAS associations regarding the single nucleotide polymorphisms in proximity to FAP (Figure 5.21a) were obtained from the GWAS Catalog (Cerezo et al., 2025) and from the Open Targets platform (Buniello et al., 2025).

The eQTL and sQTL data regarding FAP (Figure 5.21b) were obtained from the GTEx v8 Portal on 05/08/25.

The bulk-RNA and spatial transcriptomic data regarding FAP in PsA and RA (Figure 5.21c-e) was accessed from a publicly available dataset (Rauber et al., 2024) and further analysed using `R` (version 4.2.0).

2.11 Statistical analyses

Statistical analyses are detailed in text, or in each figure legend in the results section. The statistical analysis in the first results chapter was carried out using GraphPad Prism (version 10) and for the rest of the thesis this was run in `R` (version 4.2.0).

3 | Investigating the molecular and BCR-dependent determinants of B cell anergy

3.1 Introduction

The process of generating the B cell receptor (BCR) repertoire inherently produces a diverse array of receptors, a significant portion of which are autoreactive and capable of antagonising self-antigens. To prevent autoimmunity, the immune system employs stringent tolerance checkpoints. Central and peripheral tolerance mechanisms are in place to clonally delete, redeem or silence autoreactive B cell clones (Nemazee & Bürki, 1989; Gay, Saunders, Camper, & Weigert, 1993; Goodnow et al., 1988). Failure of either mechanisms have been associated with development of autoimmune disease. Defects in central tolerance are suggested by the accumulation of immature/transitional B cells in the periphery, while peripheral tolerance dysregulation is marked by an enrichment of autoreactive or polyreactive mature naïve B cells (Wardemann et al., 2003). Multiple autoimmune diseases including systemic lupus erythematosus (SLE), rheumatoid arthritis (RA), type 1 diabetes (T1D), Sjöngren syndrome (SjS) were found to have enriched autoreactive mature naïve B cell populations in the periphery (Meffre & O'Connor, 2019). B cell anergy is one of the main peripheral tolerance mechanisms in B cells (Pike, Abrams, & Nossal, 1983; Goodnow et al., 1988).

3.1.1 B cell anergy

B cell anergy refers traditionally to a state of functional unresponsiveness to BCR stimulation. These cells are characterised by reduced proximal activation

(low calcium mobilisation) and decreased proliferation, differentiation and antibody secretion (Duty et al., 2008; Quách et al., 2011). Low levels of BCR signalling through cognate antigen have been shown to be necessary for the maintenance of B cell anergy (Gauld et al., 2005). The abrogation of anergic state has been demonstrated through either removal of self-antigen or through stimulation with sufficient mitogen of either anti-BCR or through co-receptor stimulation (CD40L), toll-like receptor engagers (CpG) and cytokines (IL-2, IL-4, IL-21, BAFF) (Quách et al., 2011; Szodoray et al., 2016; Pugh-Bernard et al., 2001). Cell signalling pathways demonstrated to be involved in human B cell anergy include the SHIP-1-PTEN-SHP-1 axis, with PTEN inversely correlated with BCR levels and calcium mobilisation in anergic B cells (Smith et al., 2019; Getahun, Beavers, Larson, Shlomchik, & Cambier, 2016).

3.1.2 Current gaps in understanding human anergic B cells

Most of the knowledge about B cell anergy stems from murine models, where transgenic models with controlled BCR specificities like anti-HEL allowed their characterisation. These approaches allowed for the identification of many anergy features such as sustained low-level antigen engagement, IgM downregulation, elevated SHP-1 activity and impaired Ca^{2+} flux (Gauld et al., 2005; Zikherman, Parameswaran, & Weiss, 2012; Getahun et al., 2016; Goodnow et al., 1988). However, translating murine findings to humans is often challenging, because human anergic-like populations must be inferred from naturally occurring phenotypes rather than transgenic models, and the phenotype and functions often differ between species. For example, B1 B cells are murine cells characterised by an autoimmune repertoire without clear equivalence in humans (Descatoire, Weill, Reynaud, & Weller, 2011;

Mattos, Vandendriessche, Waisman, & Marques, 2024). Secondly, LPS is a potent B cell mitogen in murine models recognised by TLR4 and has been used in the context of investigating B cell anergy in mice, however human B cells do not express TLR4 (Venkataraman, Shankar, Sen, & Bondada, 1999; Caro-Maldonado et al., 2014; Pike et al., 1983; Chiron, Bekeredjian-Ding, Pellat-Deceunynck, Bataille, & Jego, 2008). Therefore, human studies are needed to underpin the molecular pathways contributing to tolerance mechanisms, including B cell anergy.

A further limitation is conceptual. In mice, anergy can be studied in systems where antigen engagement history is defined and hyporesponsiveness can be interpreted in that causal context (Cambier, Gauld, Merrell, & Vilen, 2007). In humans, functional hyporesponsiveness can be measured directly, but putative anergic populations are commonly identified as discrete, fixed populations defined by arbitrary baseline thresholds (e.g. B_{ND} anergic cells IgD^{+} IgM^{low}(Duty et al., 2008)) in circulation. Here it is proposed that this binary classification is insufficient and that anergy is, conceptually, a spectrum reflecting a continuum of not only signalling but also BCR expression thresholds and subsequent proliferative potential. While IgM expression correlates with proximal BCR signalling responsiveness across the naïve pool, it remains unclear how this continuous IgM axis maps onto downstream functional potential. To address this, this study moves beyond binary definitions, adopting a framework using IgM^{Low}, IgM^{Mid}, and IgM^{Hi} populations to dissect how IgM expression intrinsically correlates with other functional correlates of anergy, including proliferation, differentiation and the expression of key co-receptors.

A related challenge in human B cell tolerance is the role of key regulatory co-receptors: the inhibitory receptor CD22 and the complement receptor

CD21 (which inhibits and enhances signalling in different contexts). These molecules are crucial modulators of the BCR signalling threshold, and their downregulation is frequently included in the phenotypic definition of anergy. However, previous work treats CD21 and CD22 expression as a static, fixed baseline phenotype. A critical mechanistic unknown is whether the low expression of these co-receptors is an ingrained feature of the anergic clone or a dynamic output of its activation history and environment. This study hypothesises whether B cell co-receptor expression is a dynamic read-out of activation status. Specifically, it aims to determine if the dynamic change in IgM expression during B cell activation, rather than IgM baseline alone, is the primary driver linking IgM status to the subsequent expression of CD21 and CD22. Understanding the conditions that drive this dynamic linkage is vital, as manipulating the B cell's activation threshold via CD21 and CD22 provides a potential lever for either rescuing protective immune responses or preventing the escape of pathogenic IgM^{low} cells from functional anergy.

3.1.3 Naïve anergic-like B cell population enriched in patients with COVID-19

The investigation of anergy dynamics requires not only homeostasis, but also a model of acute systemic inflammation. Acute SARS-CoV-2 infection induces profound remodelling of the B cell compartment, including the enrichment of atypical B cells and plasmablasts linked to clinically poorer outcomes (Ahern et al., 2022; Woodruff et al., 2020, 2022). Previous work in the Bashford-Rogers team using single-cell multi-omics analysis from a large-scale single-cell atlas (Ahern et al., 2022) showed that multiple proteins and transcripts associated with B cell anergy (IgM, IgD, CD21, CD22 and FCGR2B) were significantly correlated. B cells with the lowest cellular surface

expression of IgM, CD19, CD21 and CD22 had reduced proliferation rates, enhanced features of anergy ('anergy score', including reduced BCR - HIF1α and CD40-signalling pathways), but an increased interferon type I signature compared to cells with higher expression levels of these markers. These cells were not enriched in VH4-34 usage, but showed an increase usage of λ light chain (data not shown), suggesting an enrichment of 'rescued' B cells after autoreactive or non-functional BCR rearrangements. This analysis suggested that B cells sit within a spectrum of anergy. Furthermore, this most anergic naïve B cell population enriched in COVID-19 patients, raising the possibility that infection perturbs anergy-related pathways (Figure 3.1).

This finding prompts the determination of whether human naïve anergic-like B cells represent a stable unresponsive subset or a transient state disrupted by stimulation. COVID-19 therefore provides a model in which to investigate how immune perturbation influences naïve B cell responsiveness and anergy.

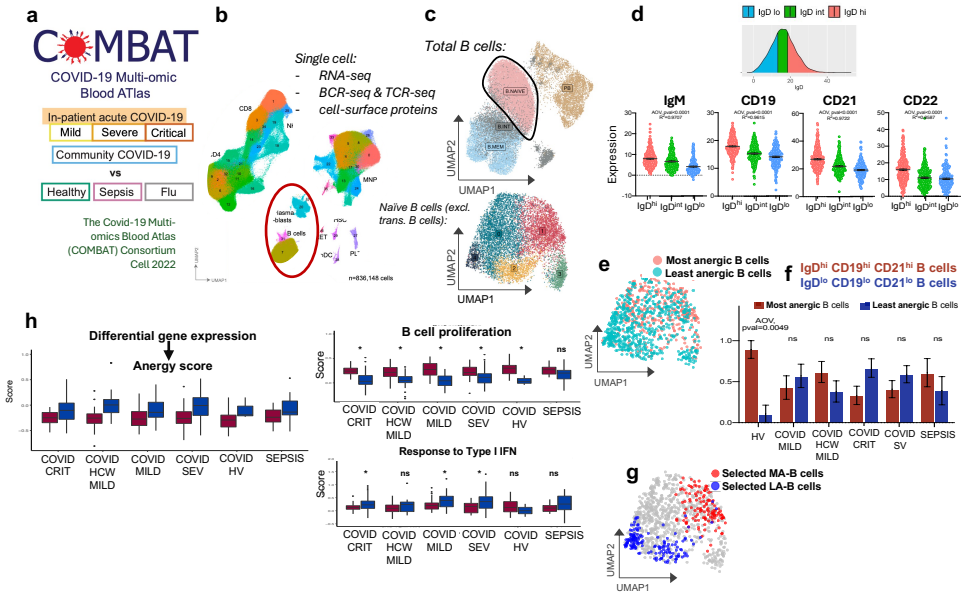

Figure 3.1: Bioinformatic analysis reveal an enrichment of putative anergic naïve B cells in COVID-19 Bioinformatic analysis was performed by Wan Ting Kong from Bashford-Rogers group on **a** The Covid-19 Multi-omics Blood Atlas (COMBAT) Consortium dataset (Ahern et al., 2022) which included single cell multi-omic data from mild, severe and critical COVID-19 patients, as well as sepsis, flu patients and healthy controls. **b** B cells were identified and selected based on the integration of RNA-seq, BCR-seq and CITE-seq data **c** Total naïve B cells were selected for analysis, after excluding transitional B cells. **d** Naïve B cells were binned in 3 groups based on their IgD expression (IgD low, IgD int and IgD high) and it was observed that IgM, CD19, CD21 and CD22 correlated with the levels of IgD expression on these cells. **e** Projection UMAP of $IgD^{low}CD19^{low}CD21^{low}$ and $IgD^{hi}CD19^{hi}CD21^{hi}$ populations formed divergent groups, termed 'Most anergic' (MA) B cells and 'Least anergic'(LA) B cells **f** Most anergic B cells are enriched in COVID-19 patients compared to healthy donors **g** Selected MA and LA B cells as extremes **h** Differential gene expression on MA and LA B cells computed an 'Anergy score' which was reduced in MA cells; pathway analysis revealed that MA B cells also showed reduced B cell proliferation but increased interferon type I signatures compared to LA B cells.

3.2 Chapter aims

Substantial gaps in our understanding remain of how human naïve B cell anergy is defined, how stable is the state of anergy, what are the determinants of B cell anergy and how it is perturbed during inflammatory responses such as SARS-CoV-2 infection. Building on the need for a spectral conceptual framework and the bioinformatic exploration of dynamic co-receptor regulation, this chapter aims to advance the fundamental understanding of human peripheral tolerance:

1. To experimentally validate the cell-surface markers of anergic B cells by defining the IgM continuum (IgM^{low} to IgM^{hi}) as the primary determinant of B cell functional potential;
2. To determine if COVID-19 infection results in an altered naïve B cell distribution or function, consistent with the perturbation of tolerance mechanisms;
3. To investigate the dynamic linkage between IgM status and the expression of co-receptors CD21 and CD22 and to determine if BCR-independent stimulation can overcome the anergic state.

3.3 Results

3.3.1 CpG and IL-2 as T cell-independent stimulation of naïve B cells

The initial objective of this study was to experimentally validate the cell-surface markers of anergic B cells within the naïve B cell compartment.

This population had been characterised from both single cell multi-omics analysis and across the literature as IgM^{low}, $CD21^{low}$ and $CD22^{low}$ expression. Naïve B cells are canonically defined by the lack of CD27 expression and the upregulation of IgD on their cell surface, whereas a low IgM expression has been linked to B cell anergy (Duty et al., 2008). Importantly, anergy should be considered as a continuum rather than a set of discrete cellular states, and the foundation of this work therefore relies on defining the cellular markers that correlate with different positions along this anergy spectrum. By identifying and comparing the phenotypic extremes of this spectrum, I aimed to dissect the molecular patterns through which anergy operates. To most accurately capture the previously described putative-anergic B cell population by flow cytometry, I stratified the naïve B cells based on IgM expression levels (IgM^{-}, $IgM^{+/low}$ and IgM^{+}), and defined the population-of-interest ('anergic-like B cells') as $IgM^{+/low}CD21^{-}CD22^{-}$.

Anergic B cells are typically associated with reduced proliferation (Quách et al., 2011). To test whether the previously identified naïve anergic-like B cells retained this unresponsive phenotype, I aimed to assess their proliferative capacity following stimulation.

B cell proliferation can be induced in a T cell-dependent (TD) or independent (TI) manner, with engagement of the B cell receptor providing the most robust proliferative signal typically using anti-IgM/anti-BCR stimulation. The putative anergic subset was defined based on low IgM expression. However, using an anti-IgM (anti-BCR) stimulation could introduce several confounding effects: it might preferentially activate cells according to their IgM abundance, trigger feedback loops that alter IgM expression, or create artefacts during flow cytometric staining should the stimulating and staining antibodies interfere with one another. To avoid these issues, B cells were instead stimulated in a

BCR-independent manner.

Toll-like receptor 9 (TLR9) engagement by CpG oligonucleotides is known to directly induce proliferation in human naïve B cells, even in the absence of BCR stimulation (Jiang et al., 2007; Huggins et al., 2007). Furthermore, the addition of IL-2 can enhance CpG-induced proliferation while limiting plasmablast differentiation. I therefore aimed to establish the optimal BCR-independent stimulation conditions (CpG + IL-2) to induce human naïve B cell proliferation *in vitro*.

A titration of CpG (0, 0.175, 0.35, 0.7, 1.4 μM) and IL-2 (100 international units (IU)/mL) was tested on magnetically-enriched total B cells from 3 healthy donors, over a period of 3, 4 or 5 days (Figure 3.2**a**). After 5 days in culture, 0.35 μM CpG induced the highest percentage of proliferation in the naïve B cell compartment (0.35 μM CpG vs 0.7 μM CpG $p = 0.046$, repeated measures ANOVA on logit-transformed data, followed by Tukey's post-hoc test) (Figure 3.2b). A titration of IL-2 was also tested, but higher doses of IL-2 did not increase the proliferation rate within the naïve B cell compartment (Supplementary Figure B.1**b**i). The duration of cell culture strongly correlated with the proliferation rates ($R^2 = 0.73$, p=0.0033, linear regression), with maximal proliferation observed after 5 days in culture (Figure 3.2**b**ii). This time point was therefore chosen for subsequent experiments. The inclusion of additional stimulating factors such as CD40L and BAFF did not enhance proliferation in the naïve B cell compartment in this experimental set-up (Supplementary Figure B.1b), and instead showed a trend towards accentuated cell death (Supplementary Figure B.1c).

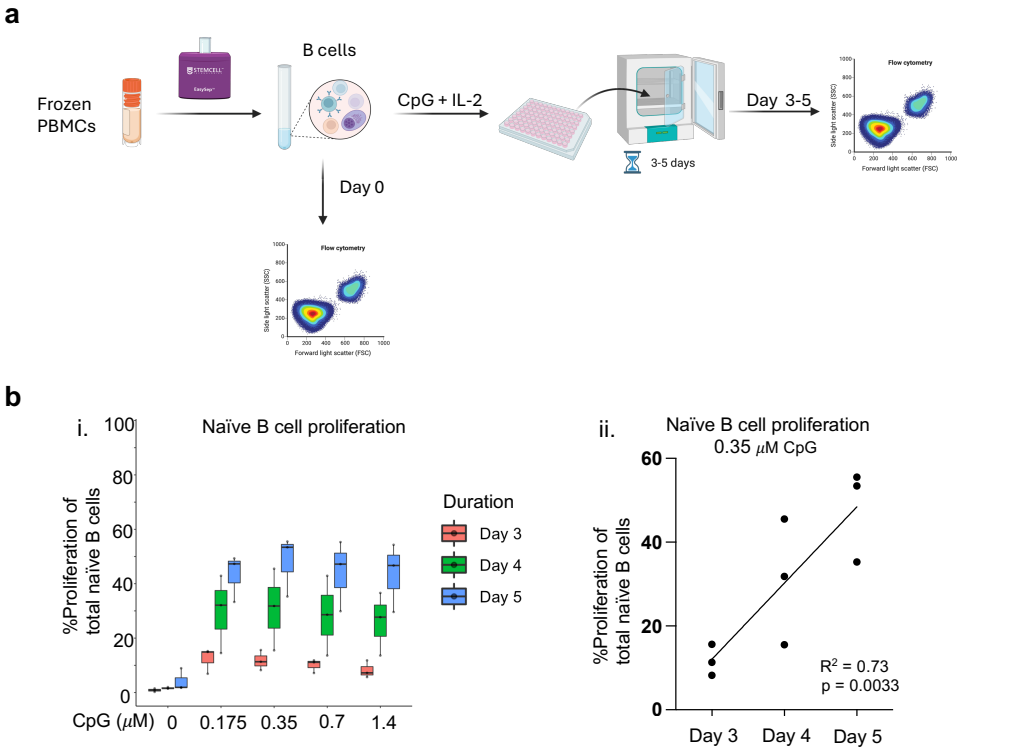

Figure 3.2: Optimisation of stimulation conditions for naïve B cell proliferation. **a** Overview of experimental methodology for B cell stimulation. Total B cells were enriched from peripheral blood mononuclear cells and stimulated with titration of CpG and IL-2 to induce proliferation. Naïve B cell proliferation was assessed after days 3, 4 or 5 days of culture. **b i.** Bar plot showing the percentage of naïve B cell proliferation levels after stimulation with fixed IL-2 (100 IU/mL) and a titration of CpG after 3, 4 or 5 days in culture; bars represent mean with interquartile range (IQR); **ii.** Plot represents the percentage of naïve B cell proliferation levels after stimulation with IL-2 (100 IU/mL) and 0.35 µM CpG, across the duration of cell culture. Statistics were tested using a linear regression. Each dot represents data from one donor, produced after $n = 3$ independent experiments.

3.3.2 Enrichment of putative-anergic naïve B cells after 5 day *in vitro* stimulation

Next, I aimed to experimentally validate the cell-surface markers of anergic B cells. This was applied to a patient cohort consisting of healthy donors($n = 5$) and individuals with recent COVID-19 ($n = 5$; 10-15 days post-symptom onset), the latter included to determine whether recent SARS-CoV-2 infection alters the function or proportional abundance of anergic B cells. Magnetically-enriched naïve B cells of each individual were stimulated for 5 days with IL-2 and CpG as previously established (Figure 3.3a). The putative anergic naïve B cell subset ($IgM^{+/low}CD21^{-}CD22^{-}$) was gated from total naïve B cells both at baseline (day 0) and after five days of stimulation (Figure 3.3b).

I first assessed whether the baseline enrichment of the putative-anergic naïve B cells observed *in silico* in COVID-19 patients was reproduced in this experimental cohort. At baseline, the frequency of the putative-anergic naïve B cell phenotype ($IgM^{+/low}CD21^{-}CD22^{-}$, Figure 3.3b), calculated as a percentage of the $IgM^{+/low}$ compartment, was low in both groups (healthy 1.62%; COVID-19 0.98%; Figure 3.3c). After five days of stimulation with IL-2 and CpG these populations expanded substantially but to comparable levels between donor groups (healthy 8.04%; COVID-19 10.02%; Figure 3.3cii).

These findings indicated that any functional differences induced by COVID-19 infection might become apparent only after *in vitro* activation of naïve B cells. I therefore proceeded to compare the functional responsiveness of the putative-anergic compartment across donor groups following stimulation.

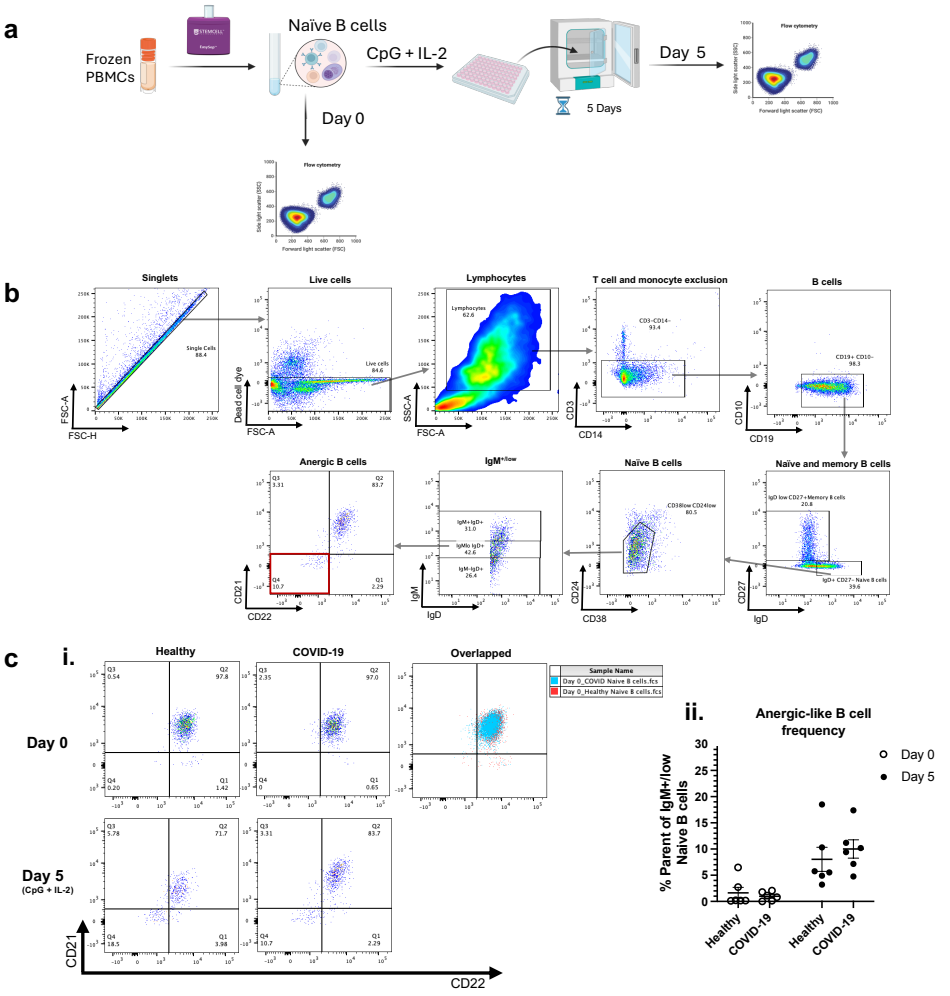

Figure 3.3: Proportions of putative-anergic B cells in health vs COVID-19. **a** Schematic of experimental design; naïve B cells were magnetically-enriched prior to CpG+IL-2 stimulation for 5 days; flow cytometry acquisition was performed at baseline (Day 0) and 5 days after incubation (Day 5). **b** Gating strategy for the putative-anergic B cells by flow cytometry; the putative-anergic phenotype inquired is marked in red ($CD19^{+}CD10^{-}IgD^{+}CD27^{-}CD24^{low}CD38^{low}IgM^{+/low}CD21^{low}CD22^{low}$). **c** Frequencies of putative-anergic B cells out of the IgM^{low} naïve B cells at baseline (Day 0) and following 5 days of stimulation with CpG+IL-2; **i.** Representative flow cytometry plots of $n = 1$ experiment; **ii.** Summary plot of 3 independent experiments, each dot represents one sample (COVID-19 $n = 6$; healthy $n = 6$); bars depict the mean with standard error of the mean (SEM)

3.3.3 Proliferation correlates with IgM expression in health and COVID-19

I assessed the proliferation induced by the 5 day stimulation across the naïve B cell populations defined by IgM, CD21 and CD22 status (Figure 3.3a).

After 5 days, IL-2 stimulation without CpG maintained reduced IgM levels (Figure 3.4b) and resulted in limited proliferation compared to IL-2 + CpG stimulation (Figure 3.4c), and was therefore used as a negative control.

Naïve B cells were divided into IgM^{++}, $IgM^{+/low}$ and IgM^{-}. The negative threshold was set by IgM fluorescence minus one (FMO) control, and the positive signal was divided into two equal-intensity bins to separate $IgM^{+/low}$ and IgM^{++} signal based on the IgM MFI. Remarkably, a significant effect of IgM status was identified on the naïve B cell proliferation ($p < 0.001$, two-way mixed-effects ANOVA, Figure 3.4c). Within both COVID-19 and healthy donors, reduced proliferation frequencies correlated with a declining IgM expression ($IgM^{++} > IgM^{+/low}$: COVID-19 $p = 0.047$, healthy $p = 0.019$; $IgM^{+/low} > IgM^{-}$ $p < 0.0001$ both groups), resulting in the pattern of proliferation from highest proliferation $IgM^{++} > IgM^{+/-} > IgM^{-}$ to lowest proliferative rates (Figure 3.4c).

Next, I determined if CD21 and CD22 expression was associated with differences in proliferation. Indeed, the putative-anergic naïve B cell subset ($IgM^{+/low}CD21^{-}CD22^{-}$, gated from the CD22 vs CD21 plot represented in Figure 3.4a) showed a lower proliferation trend in COVID-19, although this difference did not reach statistical significance compared to health ($p > 0.05$, two-way repeated measures (RM) ANOVA on logit-transformed data with Tukey's post-hoc, Figure 3.4d). However, a difference in the proliferation rates

was observed between IgM^{++} and IgM$^{+/low}$ CD21CD22^{Hi} populations, both within COVID-19 ($p = 0.004$) and health ($p = 0.008$). These observations suggested that IgM expression, more than CD21 and CD22 status, may be a stronger determinant of the proliferative potential of naïve B cells (Figure 3.4d).

3.3.4 COVID-19 patients exhibited differential proportions of IgM^{Hi} naïve proliferative B cells

By day 5 post-stimulation, naïve B cells from COVID-19 donors displayed a non-significant trend towards reduced median IgM intensity fluorescence (MFI) compared to healthy donors ($p > 0.05$, two-way RM-ANOVA with Tukey's post-hoc, Figure 3.4b). Proliferation frequencies within each IgM-defined subset similarly showed no significant COVID-19–associated differences (all COVID-19-health comparisons $p > 0.05$, two-way RM-ANOVA on logit-transformed data with Tukey's post-hoc, Figure 3.4e). However, when considering the frequency of proliferating cells as a proportion of the total naïve B cell compartment, COVID-19 samples exhibited a significantly reduced proportion of IgM^{++} proliferating cells ($p = 0.021$, two-way RM-ANOVA on logit-transformed data with Tukey's post-hoc, Figure 3.4c). This suggests that COVID-19 might alter naïve B cell compartment's response to stimulation, resulting in a shifted cellular composition.

Supporting this, COVID-19 samples displayed a significantly different distribution of IgM-stratified naïve B cell subsets following *in vitro* stimulation ($p = 0.029$, MANOVA with patient and IgM group as factors and experiment as covariate on centre-log-ratio-transformed data, Figure 3.4f). Follow-up univariate ANOVA tests revealed that COVID-19 samples had a lower proportion

of IgM^{++} and higher proportion of IgM^{-} naïve B cells than in healthy donors (both comparisons $p = 0.012$, false discovery rate (FDR) - adjusted). Together, these analyses demonstrate that COVID-19 infection is associated with a shift in the IgM distribution of the naïve B cell pool following activation, potentially contributing to altered proliferative responses.

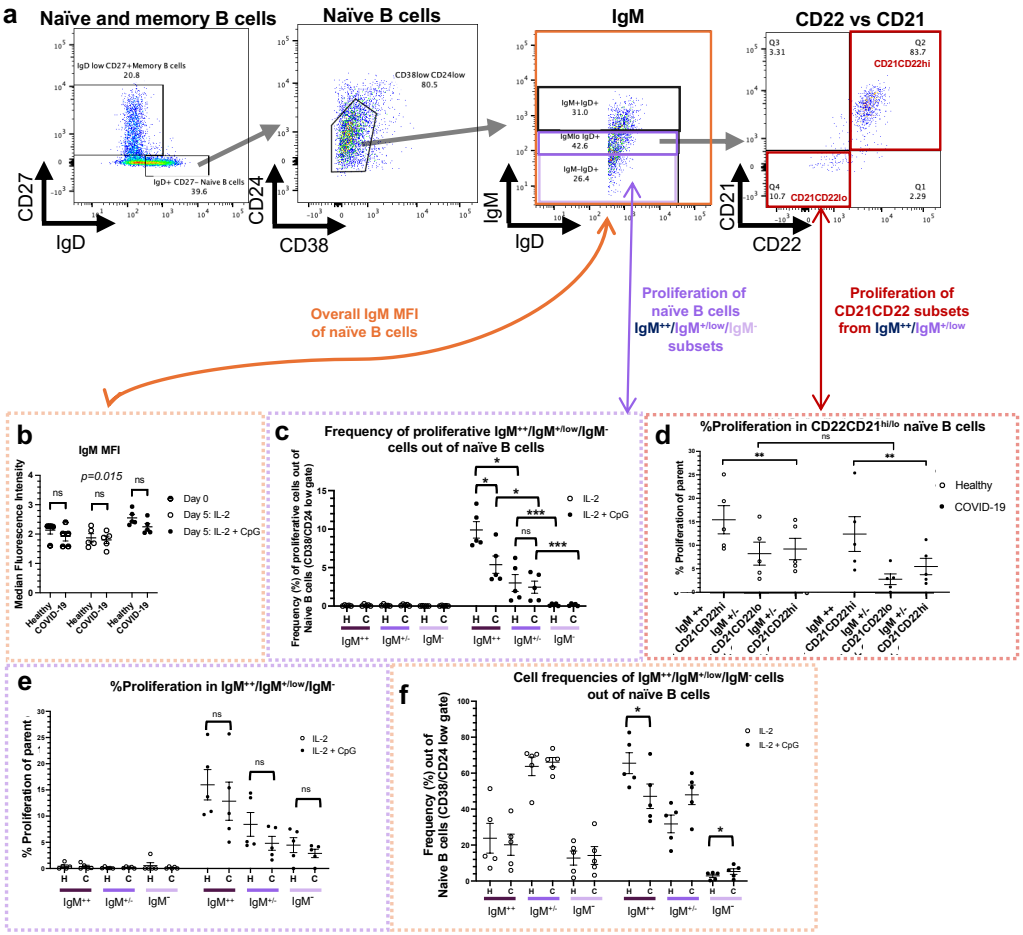

Figure 3.4: Proliferation of naïve B cell subsets in health and COVID-19 after *in vitro* CpG and IL-2 stimulations (see next page)

Figure 3.4 ***(previous page)*****: Proliferation of naïve B cell subsets in health and COVID-19 after *in vitro* CpG and IL-2 stimulations.** **a** Partial gating strategy of a putative-anergic B cell phenotype ($IgM^{+/low}CD21^{-}CD22^{-}$). **b** Plot showing the median intensity fluorescence (MFI) of the overall IgM on naïve B cells (orange gate in **a**); data were logicle-transformed and plotted on a linear scale for visualisation; $p - value = 0.015$ for the main effect of stimulation (baseline vs IL-2 vs IL-2 + CpG). **c** Plot showing the frequencies of proliferative cells within IgM subsets, calculated as proportions of the naïve B cells. **d** Proliferation of $CD21CD22^{high}$ or $CD21CD22^{low}$ (red gates in **a**) within IgM^{++} or $IgM^{+/low}$ populations, calculated as a proportion of the total number of cells in the respective subset. **e** Plot showing the frequencies of proliferative cells across IgM subsets, calculated as proportions of the total number of cells in the respective subset. **f** Plot displaying the cellular frequencies based on IgM expression within the naïve B cell compartment. Each dot represents one sample. Bars indicate mean with standard error of the mean (SEM). Each dot represents one donor; $n = 5$ healthy donors and $n = 5$ COVID-19 donors were analysed. Bars indicate mean with standard error of the mean (SEM). Data were generated from $n = 5$ independent experiments. Statistical significance was tested on logit-transformed data (**b,c,e**) or raw data (**d**) using two-way repeated measures ANOVA with Tukey's post-hoc test; (**f**) MANOVA followed by univariate ANOVA on centre-log-ratio transformed data with FDR correction; H – healthy; C – COVID-19; MFI – median intensity fluorescence; *p<0.05; $^{**}p \leq 0.01$; $^{***}p \leq 0.001$; ns - not significant.

3.3.5 Enhanced proliferation associated with IgM^{Hi}-FACS-sorted naïve B cells after stimulation

Next, I aimed to determine if IgM expression on naïve B cells had an impact on cell differentiation potential. Given that B cell anergy is defined as a lower sensitivity to stimulation, I hypothesised that IgM lo B cells would have a lower propensity to differentiate into memory B cells or plasmablasts, and that this regulation may be different in post SARS-CoV-2 infection. Specifically, this experiment aimed to determine whether IgM determines the differentiation state of a B cell and whether COVID-19 leads to: (1) the

induction of differential proliferation; (2) distinct patterns of IgM, CD21 and CD22 expression or cell frequencies and (3) variations in B cell differentiation proportions. To investigate this, magnetically-enriched naïve B cells were additionally sorted using fluorescence-activated cell sorting (FACS), based on their baseline IgM MFI levels (IgM^{Hi}, IgM^{Mid} and IgM^{Low}), prior to 5 day CpG+IL-2 stimulation (Figure 3.5a). To ensure comparable cell numbers across groups and enable statistical analyses, IgM expression thresholds were divided into three sections per donor (brightest 33% - IgM^{Hi}, middle 33% - IgM^{Mid} and lowest 33% - IgM^{Low}, Methods Figure 2.1). FACS-sorted populations exceeded a purity of 90% (Supplementary Figure B.2a).

After 5 days of CpG+IL-2 stimulation, the characteristics of live B cells were investigated (Figure 3.5b). Of note, IgM^{Hi}-sorted samples showed a trend toward higher viability relative to IgM^{Low} following stimulation, but this difference did not reach statistical significance (Supplementary Figure B.4). The proliferation rates were not statistically significant between COVID-19 and healthy donors within either of the IgM-sorted samples ($p > 0.05$, Figure 3.5c). However, proliferation varied between IgM-defined subsets. IgM^{Hi}-sorted cells had the highest rate of proliferation, reaching statistical significance in COVID-19 samples ($p = 0.009$ COVID-19 IgM^{Low} vs. IgM^{Hi}; $p = 0.019$ IgM^{Mid} vs. IgM^{Hi}, two-way RM-ANOVA on logit-transformed data with Tukey's post-hoc test, Figure 3.5c). The healthy donors displayed a similar, albeit non-statistically significant proliferation trend. Within the live B cell population, the IgM MFI maintained its differences significantly across the IgM^{Hi}, IgM^{Mid} and IgM^{Low} samples, consistent with the original sorting strategy ($p = 0.0039$, two-way RM-ANOVA, Figure 3.5d), but did not differ between healthy and COVID-19 donors ($p > 0.05$, two-way RM-ANOVA, Figure 3.5d). Taken together, these results reinforce the earlier findings

that lower baseline (prior to stimulation) IgM expression is associated with increased anergy, whereas higher IgM levels correspond to more responsive cells.

3.3.6 Baseline IgM expression of IgM-FACS-sorted samples does not correlate with CD21 and CD22 expression following stimulation

The baseline IgM expression level used to define the IgM^{Low} IgM^{Mid} and IgM^{Hi} FACS-sorted populations did not have a significant effect on the CD21 or CD22 MFI after 5 days of stimulation ($p > 0.05$, two-way RM-ANOVA). Similarly, no differences were observed between healthy and COVID-19 donors ($p > 0.05$, two-way RM-ANOVA, Figure 3.5d). This finding is consistent with the comparable levels of cell frequencies observed within the 'Q2:CD21-CD22hi' compartment across the IgM^{Low}, IgM^{Mid} and IgM^{Hi} samples, in both healthy and COVID-19 donors (Figure 3.5e). Because the sorting panel did not include CD21 or CD22, baseline expression of these markers could not be directly assessed in this experiment. To address this, I retrospectively analysed day 0 data from the first cohort using an equivalent gating strategy to the one applied for FACS. This analysis showed that at baseline the MFI of CD21, but not CD22, varied in accordance with the IgM^{Low} IgM^{Mid} and IgM^{Hi} populations in healthy donors, and to a lower extent in COVID-19 (healthy CD21 IgM^{Low} vs CD21 IgM^{Hi}: $p = 0.01$; COVID-19 CD21 IgM^{Low} vs CD21 IgM^{Mid} $p = 0.0035$, COVID-19 CD21 IgM^{Low} vs CD21 IgM^{Hi} $p > 0.05$; all CD22 groups $p > 0.05$; two-way RM-ANOVA, Supplementary Figure B.3). Together, these results suggest that stimulation may drive B cell differentiation, generating a heterogeneous population with variable levels of

CD21 and CD22 expression, largely independent of their starting IgM level.

3.3.7 Enhanced memory B cell and plasmablast differentiation associated with IgM^{Hi}-FACS-sorted samples in health and COVID-19

The levels of B cell differentiation were next determined. Overall, the major B cell subset frequencies did not differ between healthy and COVID-19 donors across any of the IgM-sorted samples [atypical B cells (CD27^{-}IgD^{-}), naïve B cells (CD27^{-}IgD^{-}), memory(CD27^{+} IgD^{-}) Figure 3.5f; plasmablasts (CD27^{+}IgD^{-}CD24^{-}CD38^{++}), Figure 3.5g]. Despite the lack of disease-related differences, distinct patterns emerged between the IgM-sorted populations. IgM^{Low} samples showed an enrichment trend of atypical B cell phenotype in both healthy and COVID-19 donors, whereas IgM^{Hi} samples had a higher proportion of memory B cells, in both healthy and COVID-19 (Figure 3.5f).

Plasmablast frequencies were also IgM-dependent. In both healthy and COVID-19 donors, plasmablasts were most abundant in IgM^{Hi} samples. IgM^{Low} and IgM^{Mid} subsets showed significantly lower plasmablast frequencies in both healthy (IgM^{Low} vs IgM^{Hi}: $p = 0.006$; IgM^{Mid} vs IgM^{Hi}: $p = 0.02$, two-way RM-ANOVA on logit-transformed data with Tukey's post-hoc; Figure 3.5g) and COVID-19 donors (IgM^{Low} vs IgM^{Hi}: $p = 0.001$; IgM^{Mid} vs IgM^{Hi}: $p = 0.011$, two-way RM-ANOVA on logit-transformed data with Tukey's post-hoc; Figure 3.5g).

Together, these results indicate that higher baseline IgM expression promotes greater proliferative and differentiation potential, whereas IgM^{Low} subsets display features consistent with reduced activation capacity and increased anergy, in both healthy donors and individuals recovering from COVID-19.

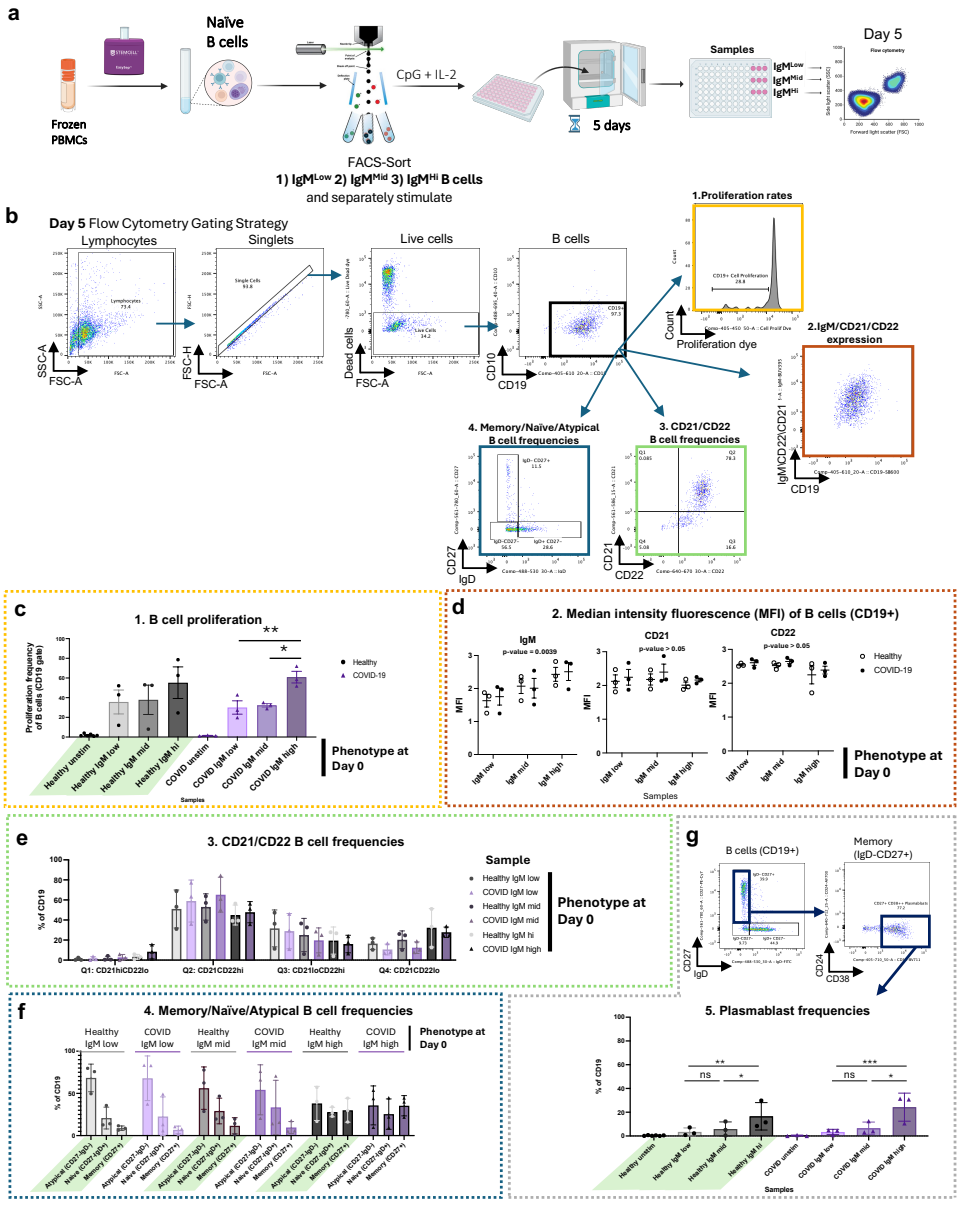

Figure 3.5: Features of FACS-sorted IgM^{Hi}, IgM^{Mid} and IgM^{Low} naïve B cell samples after *in vitro* CpG and IL-2 stimulations *(see next page)*

Figure 3.5 ***(previous page)*****: Features of FACS-sorted IgM^{Hi}, IgM^{Mid} and IgM^{Low} naïve B cells after *in vitro* CpG and IL-2 stimulations a** Overview of the experimental set-up; Naïve B cells were magnetically-enriched from peripheral blood mononuclear cells (PBMC) of 6 donors ($n = 3$ healthy; $n = 3$ COVID-19) and processed across 3 independent experiments. The naïve B cells (CD27$^-$; IgD$^+$) were further FACS-sorted based on their IgM expression level (IgM^{Low}, IgM^{Mid}, IgM^{Hi}); the naïve B cell IgM^{Low}, IgM^{Mid}, IgM^{Hi} populations were separately stimulated with CpG+IL-2 for 5 days and acquired as separate samples on day 5 via flow cytometry. **a** Gating strategy for flow cytometric analysis on 'Day 5'; The core analysis in this figure was carried out on the live B cells ('B cells' gate CD19$^+$ bolded in black), within each IgM-FACS-sorted sample (IgM^{Low}, IgM^{Mid} or IgM^{Hi}) at day 0. **c** Bar plot showing the proliferation of live B cells (CD19$^+$ gate). **d** Plots showing the median intensity fluorescence of IgM, CD21 and CD22 of live B cells (CD19$^+$ gate). **e** Bar plots showing the percentage of B cells relative to CD21 and CD22 expression out of the total live B cell pool, as defined by the quadrants depicted in the CD22 vs CD21 plot in gating strategy (**a**3., green plot). **f** Bar plots display cell type frequencies measured as a percentage of live B cells (CD19$^+$ gate); the proportions were derived from the IgD vs CD27 plot in the gating strategy (**a**4. blue plot).**g** Bar plots display plasmablast frequencies (IgD$^-$CD27$^+$CD38^{++}), measured as a percentage of live B cells (CD19$^+$ gate). Each dot represents an IgM-defined sample as sorted on day 0 (IgM^{Low}, IgM^{Mid} or IgM^{Hi}); statistical differences were tested on logit-transformed data using a two-way repeated-measures (RM) ANOVA (**d**) with Tukey's post-hoc and p-value adjustment (**c and g**); MFI – median intensity fluorescence; *$p < 0.05$; **$p \leq 0.01$; ***$p \leq 0.001$; ns - not significant.

3.3.8 IgM expression is transient after stimulation in both health and COVID-19

To assess the effect of stimulation on IgM expression, IgM^{Low}, IgM^{Mid} and IgM^{Hi} naïve B cells were sorted and stimulated as before for 5 days, after which FACS analysis was performed (Figure 3.6a). A mean of approximately 20% of the IgM^{Low} B cells from both healthy and COVID-19 donors shifted to IgM^{Mid} and IgM^{Hi} intensities. A mean of approximately 55% cells in both

healthy and COVID-19 donors shifted from an initial IgM^{Hi} phenotype after FACS-sorting, to a IgM^{Mid} and IgM^{Low} phenotype at day 5 post stimulation (Figure 3.6a). These findings are consistent with the heterogeneous phenotype observed after CpG + IL-2 stimulation and demonstrate substantial plasticity in IgM expression across naïve B cells.

Therefore, I wondered if a shift in the IgM expression has also occurred within the B cells which have not yet differentiated into memory B cells. Subsetting the live B cells into CD27^{-} B cells, I further stratified again based on the IgM expression levels using the original gates for FACS-sorting at day 0 (Figure 3.6b). Interestingly, in spite of the increased homogeneity of the CD27^{-} population, the proportions of IgM^{Low}, IgM^{Mid} and IgM^{Hi} expressing cells at day 5, closely resembled the frequencies observed before in the total live B cells (Figure 3.6b). This indicates that all IgM-sorted naïve B cell subsets mount a measurable response to CpG + IL-2, regardless of their initial IgM status.

To further investigate the response to stimulation of the CD27^{-} B cell populations which upregulated or downregulated their IgM expression between day 0 and day 5, the proliferation rates were calculated within each stratified IgM subset, as determined on day 5, across all samples.

To evaluate how proliferative responses relate to IgM shifts, proliferation was assessed within each day 5-IgM-defined subset across all original day 0-IgM FACS-sorted samples. Interestingly, all IgM-sorted samples had a minimum of 10% mean proliferation rate in both healthy and COVID-19 donors across all day 5-IgM-defined compartments. Strikingly, in both COVID-19 and healthy donors, day 5-defined IgM^{Hi} populations proliferated within Day 0-sorted IgM^{Low} cells, whereas day 5-defined IgM^{Low} populations proliferated in IgM^{Low}

and also in the IgM^{Hi} samples (Figure 3.6c). These results demonstrate that naïve B cells across the IgM spectrum are capable of responding to stimulation and that IgM levels undergo significant redistribution during activation, reflecting dynamic regulation rather than fixed anergic status of a B cell.

3.3.9 Post-stimulation IgM status defines CD21 and CD22 expression

To determine whether CD21 and CD22 expression is driven by a B cell's baseline IgM level or by its activation-induced IgM state, correlations with pre-stimulation IgM expression were first assessed. Pre-stimulation IgM levels showed no clear relationship with CD21 or CD22 MFI (Figure 3.5d). However, because IgM expression shifted substantially between day 0 and day 5 post-stimulation, the subsets were re-defined as IgM^{Low}, IgM^{Mid} and IgM^{Hi} based on the day 5 IgM MFI distribution. To standardise classification across samples, IgM gates were normalised using a batch-control healthy donor (bottom 33% - IgM^{Low}, middle 33% - IgM^{Mid} and brightest 33% - IgM^{Hi}). Using this post-stimulation stratification, IgM, CD21 and CD22 MFI remained comparable between healthy and COVID-19 donors ($p > 0.05$). However, clear IgM-associated patterns emerged. CD21 and CD22 MFI were highest in the IgM^{Hi} populations and lowest in the IgM^{Low} populations defined at day 5 (Both CD21 and CD22 $p < 0.05$, 2-way RM-ANOVA, Figure 3.7). This indicates that the IgM state acquired during activation can predict CD21 and CD22 expression following stimulation.

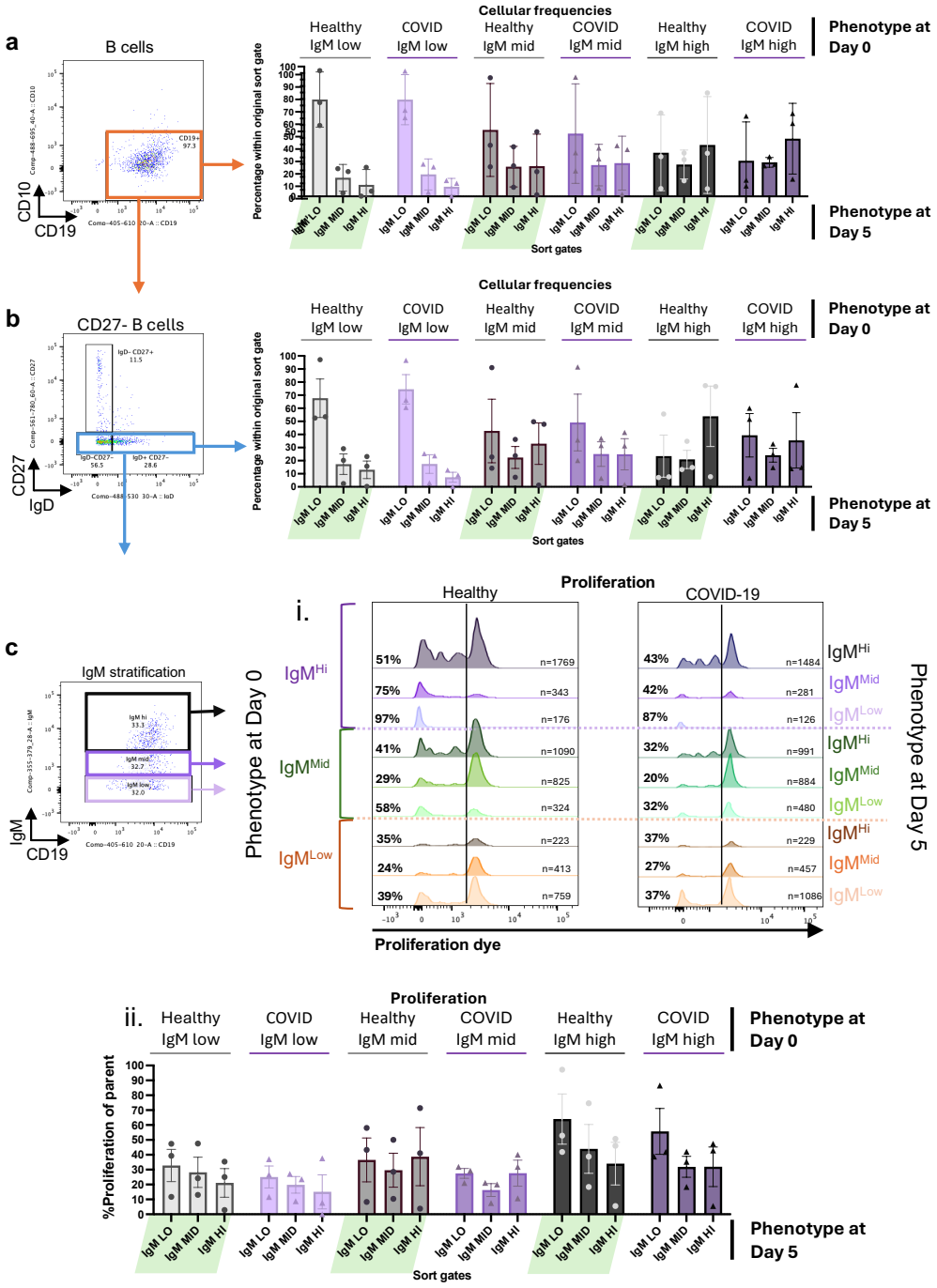

Figure 3.6: IgM redistribution and proliferation of IgM-sorted naïve B cell samples after CpG and IL-2 stimulation *(see next page)*

Figure 3.6 ***(previous page)*****: IgM redistribution and proliferation of IgM-sorted naïve B cell samples after CpG and IL-2 stimulation** The data presented in this figure represents the FACS-sorted IgM^{Hi}, IgM^{Mid} and IgM^{Low} naïve B cells after *in vitro* CpG+IL-2 stimulations for 5 days from the experiment described in Figure 3.5, of 6 donors ($n = 3$ healthy; $n = 3$ COVID-19). The live B cells (CD19^{+} gate) were further stratified based on the levels of IgM expression within each FACS-sorted sample; the thresholds for IgM^{Low}, IgM^{Mid}, and IgM^{Hi}, at 'Day 5' were set based on the original FACS-sorting gates used on 'Day 0', per sample. **a** Bar plots show the cellular proportions of Day 5-defined IgM^{Low}, IgM^{Mid} and IgM^{Hi} populations as a frequency of live B cells (CD19^{+} orange gate), per original FACS-sorted sample. **b** Bar plots show the cellular proportions of Day 5-defined IgM^{Low}, IgM^{Mid} and IgM^{Hi} cells, as a frequency of the CD27^{-} B cell compartment (blue gate), per original FACS-sorted sample. **c** Proliferation of CD27^{-} B cells was calculated within each Day 5-defined IgM^{Low}, IgM^{Mid} and IgM^{Hi} populations, as the proportion of proliferating cells out of the total cells within the respective Day 5-defined IgM subset (%Parent); **i.** representative flow plots illustrating the proliferation frequency from one experiment which included the IgM^{Low}, IgM^{Mid} and IgM^{Hi} samples from $n = 1$ healthy donor and $n = 1$ COVID-19 donor; **i.** bar plot shows the proliferation rates of Day 5-defined IgM^{Low}, IgM^{Mid} and IgM^{Hi} populations across the 3 FACS-sorted samples per donor (IgM^{Low}, IgM^{Mid} and IgM^{Hi}) of $n = 3$ healthy and $n = 3$ COVID-19 donors; each dot represents one IgM^{Low}, IgM^{Mid} or IgM^{Hi}-sorted sample of each donor; bars depict the mean with SEM; statistical testing between COVID-19 and healthy control was not significant ($p > 0.05$, two-way repeated-measures ANOVA on logit-transformed data).

3.4 Discussion

The mechanisms governing B cell anergy, a critical peripheral tolerance checkpoint, remain incompletely understood, particularly in humans. Drawing from *in silico* data identifying a putative-anergic naïve B cell population enriched during SARS-CoV-2 infection, this study aimed to experimentally validate the phenotypic markers of anergic B cells and to investigate the dynamic nature and determinants of this state in both healthy individuals

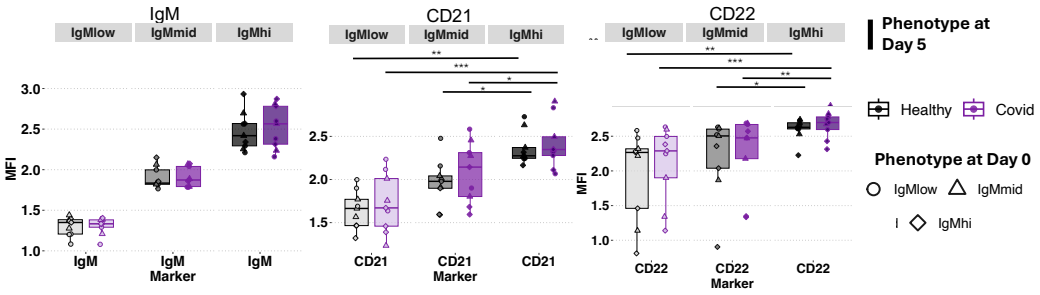

Figure 3.7: Median fluorescence intensity of CD21 and CD22 after CpG and IL-2 stimulation of the IgM^{Low}, IgM^{Mid} and IgM^{Hi}-sorted naïve B cells. Box plots display the median intensity fluorescence (MFI) of IgM, CD21 and CD22, measured in the IgM^{Low}, IgM^{Mid} and IgM^{Hi} gates of CD19^{+} B cells. IgM thresholds were defined using the upper, middle, and lower 33% of IgM expression in the batch-effect control (healthy donor stimulated with IL-2 only); statistical differences were assessed using a two-way repeated-measures ANOVA with Tukey's post-hoc; each dot is one day-5-IgM-defined gate belonging to one day-0-FACS-sorted sample ($n = 3$ healthy donors; $n = 3$ COVID-19 donors); box-plots show the mean with interquartile range (IQR). $^{*}p < 0.05$; $^{**}p \leq 0.01$, $^{***}p \leq 0.001$.

and patients recovering from COVID-19. The findings in this chapter establish IgM surface expression as a primary determinant of B cell responsiveness and differentiation potential, suggesting that the anergic state is less a stable tolerance mechanism and more a modifiable, activation-induced status.

This chapter demonstrated a clear relationship between IgM expression levels and the proliferative and differentiation capacity of naïve B cells following CpG and IL-2 stimulation *in vitro*. Specifically, B cells with lower surface IgM proliferated less, consistent with a more anergic or functionally unresponsive state. Secondly, this chapter has shown that even in populations enriched for the most anergic B cell subtypes (IgM^{Low} naïve B cells), CpG can induce proliferation and upregulation of IgM. This is consistent with the concept that anergy as a continuum, as samples with baseline higher IgM populations exhibited trends of increased proliferation compared to the

lower ones. Critically, the IgM^{Low}-sorted cells, which exhibited anergic-like features (low proliferation, reduced differentiation) at the population level, were still capable of a measurable proliferative response and differentiation into plasmablasts and memory cells, albeit less efficiently than IgM^{Hi} cells. This suggests that human naïve B cell anergy is not an irreversible state of permanent silencing, but rather a transient state of hyporesponsiveness that can be overcome by sufficient, here BCR-independent mitogenic signals. This aligns with observations that anergic B cells can be rescued from unresponsiveness *in vitro* by high levels of mitogen or co-receptor stimulation (Quách et al., 2011; Szodoray et al., 2016; Pugh-Bernard et al., 2001). Lastly, COVID-19 was found to mildly impair proliferation and to enrich for lower expressing levels of IgM populations compared to health. Together, these data suggest that naïve B cell 'anergy' could be viewed as a dynamic, BCR receptor-dependent state rather than a fixed subset defined by static surface markers.

3.4.1 B cell anergy as a continuum

Chronic low-level BCR engagement is known to maintain B cell anergy and is associated with a reduced surface IgM, lowered calcium signalling, limited proliferation and antibody production (Quách et al., 2011; Duty et al., 2008). Both sufficiently strong BCR and BCR-independent signals are able to override anergy in B cells. Consistent with this framework, the present data support a model in which naïve B cell responsiveness exists on a continuum that aligns with their baseline IgM density. Using a BCR-independent stimulation (CpG+IL-2) two experimental approaches demonstrated that naïve B cells expressing higher levels of IgM showed greater capacity for proliferation and a higher propensity to differentiate, whereas naïve B cells expressing lower

levels of IgM exhibited features typical of reduced sensitivity to activation.

In the bulk-naïve B cell stimulation experiments the highest rate of proliferation was observed in IgM^{++} populations, followed by $IgM^{+/low}$ and then IgM^{-}. The FACS-sorted experiment provided further evidence that naïve B cells expressing the highest levels of IgM are the most responsive subset. IgM^{Hi} samples proliferated more robustly than IgM^{Low} samples, reaching statistical significance in COVID-19 donors, with the same pattern present, though not significant, in healthy individuals. Differentiation outcomes likewise followed an IgM-dependent gradient. IgM^{Hi} samples displayed higher frequencies of memory B cells and plasmablasts, while IgM^{Low} cells appeared to be enriched for atypical-like phenotypes. While limited statistical power prevented formal comparisons across all differentiation subsets, the trends were reproducible and aligned between healthy and COVID-19 donors, offering some credibility in the observations despite the small sample size. Together, these findings indicate that naïve B cells with low IgM expression exhibit characteristics aligned with a more anergic state, whereas IgM^{Hi} cells retain stronger proliferative and differentiation potential. Importantly, these relationships were observed in both healthy and post–COVID-19 donors, suggesting that baseline IgM density may be an important determinant of naïve B cell responsiveness irrespective of recent viral infection. These findings are consistent with the observations reported by Quách et al. (Quách et al., 2011), who showed that IgM^{low}-sorted naïve B cells exhibited reduced proliferation compared with IgM^{int} cells. Notably, their experiments employed a stimulation cocktail containing anti-IgM in addition to CpG and IL-2. This chapter extends these observations by demonstrating that the association between IgM expression and proliferative capacity persists even in the absence of anti-IgM stimulation. Moreover, I show that IgM expression also correlates with the differentiation

potential of naïve B cells, providing additional functional insight into the continuum of B cell anergy.

The FACS-sorting experiments have also shown that the level of IgM expression may be transient after stimulation, as IgM levels shifted after stimulation from IgM^{Low} to IgM^{Mid} and IgM^{Hi}. This is in agreement with (Quách et al., 2011), where it was described that surface IgM can be upregulated on IgM^{Low} cells after *in vitro* cultures even in the absence of stimulation. Conversely, about half of the IgM^{Hi} cells appeared to downregulate their IgM levels after stimulation. Since these cells showed proliferative history, the downregulation of IgM might be due to class-switching and differentiation into memory B cells. Additional experiments using a panel which includes activation markers and IgG/A is necessary to determine this. However, remarkably after stimulation all IgM-sorted samples (low mid or high) displayed proliferative capacity even within the CD27^{-} compartment, with a trend of higher proliferation in the IgM^{Hi}-sorted samples. Because IgM^{Low} cells can both increase their IgM levels and proliferate after stimulation, their phenotype is more consistent with a plastic identity that responds to stimulus.

Taken together, these findings suggest that functional potential within the naïve B cell pool may be stratified at baseline yet remain highly plastic during activation, supporting a dynamic model of anergy in which responsiveness is shaped by the evolving cellular phenotype rather than fixed by a static IgM level. In this framework, low IgM expression reflects a transient position along an anergy continuum rather than a stable anergic identity. This concept is also supported by a study where PTEN signalling was shown to be inversely proportional with the level of IgM expression on B_{ND} cells (Smith et al., 2019).

3.4.2 Putative-anergic naïve B cells can be activated by BCR-independent stimuli

This study sought to validate a previously identified putative-anergic naïve B cell population characterised by $IgM^{+/low}CD21^{low}CD22^{low}$ expression. At baseline, the expected proportion of $CD21^{low}$ naïve B cells was detectable and comparable with previous reports (approximately 10% of naïve B cell pool, data not shown; (Isnardi et al., 2010)). In contrast, the more stringently defined $IgM^{+/low}CD21^{low}CD22^{low}$ subset was rare in both healthy donors and convalescent COVID-19 patients.

Instead, this phenotype became enriched following CpG+IL-2 stimulation. One interpretation is that the *in silico* anergic-like signature reflects a transient population induced during acute SARS-CoV-2 infection, which may no longer be present 10–15 days after symptom onset in our cohort. This is plausible given that a recent longitudinal study showed that anergic B cells (defined as $IgD^{+}IgM^{-}CD27^{-}$) decline rapidly after 5-12 days post-symptom onset in COVID-19 patients (Jokiranta et al., 2026).

An alternative explanation relates to how the *in silico* population was defined. Given that the putative-anergic phenotype in COVID-19 was calculated out of the naïve B cell pool, its apparent enrichment could reflect a contraction of non-anergic naïve B cells, as they differentiate into memory subsets. Such a shift would increase the relative proportion of phenotypes that are otherwise low-frequency in health.

The observation that CpG + IL-2 stimulation increased the $IgM^{+/low}CD21^{low}$ $CD22^{low}$ phenotype compared to baseline, suggests either that these conditions preferentially activate residual anergic-like cells or that they induce

downregulation of CD22 during activation. CD22 is an inhibitory receptor, and reduced CD22 expression following activation or differentiation aligns with previous studies reporting lower CD22 protein and mRNA levels in $CD27^{+}$ memory B cells compared with $CD27^{-}$ naïve B cells (Daridon et al., 2010).

3.4.3 Dynamics of CD21 and CD22 and their relationship with IgM

CD21 and CD22 are key co-receptors that modulate BCR signalling, and both have been shown to be involved in the regulation of B cell function (Erdei et al., 2021; Clark & Giltiay, 2018). CD22 is considered a negative regulator of BCR signalling, maintaining unresponsiveness by increasing the activation threshold (Sieger et al., 2013). Its functional relevance is supported by mouse models in which CD22 deficiency leads to heightened B cell activation and the accumulation of autoreactive IgG antibodies (O'Keefe, Williams, Batista, & Neuberger, 1999). CD21 also modulates BCR signalling through complement-mediated co-ligation of the BCR, although recent studies in humans indicate that its function is more complex than the classical murine model of CD21 as a straightforward co-activator (Kovács et al., 2021; Erdei et al., 2021).

At baseline (day 0), CD21 but not CD22 correlated with IgM expression, consistent with CD21 marking mature naïve cells with higher surface IgM, whereas CD22 was more uniformly expressed across the naïve compartment.

After 5 days of CpG + IL-2 stimulation, this simple relationship between baseline IgM and CD21/CD22 co-receptor expression was lost when the original IgM^{Low}, IgM^{Mid} and IgM^{Hi} FACS-sorted samples were analysed as whole populations. Neither CD21 nor CD22 MFI correlated with the original

IgM-sorting gate, and in some cases there was even a tendency towards lower CD22 in the IgM^{Hi}-sorted samples. This likely reflects the increased heterogeneity of the post-stimulation pool, as each original IgM-defined sample developed into a mixture containing different proportions of naïve, memory, plasmablast and atypical-like B cells. The day-0-IgM^{Hi}-sorted samples resulted in the highest proportions of CD27^{+} memory B cells and plasmablasts by day 5, whereas IgM^{Low} samples were relatively enriched in IgD^{-}CD27^{-} cells.

Because memory B cells and plasmablasts are known to downregulate CD22 compared to naïve B cells (Daridon et al., 2010), the modest reduction in CD22 MFI observed in IgM^{Hi}-sorted compared to IgM^{Low}-sorted samples is consistent with the greater representation of these differentiated subsets. Similarly, CD21 is expressed on naïve and classical memory B cells, but activated memory B cells and a group of atypical memory B cells (CD27^{-}CD21^{Low}) and plasmablasts downregulate CD21 (Holla et al., 2021; Kremlitzka et al., 2013). Therefore, the lower trend of CD21 expression in IgM^{Hi}-sorted samples is in line with the complex representation of memory B cells or atypical-like B cells which are expected to show a reduced level of CD21 compared to naïve B cells.

To disentangle the impact of baseline IgM from that of differentiation, cells were subsequently re-stratified at day 5 according to their current IgM expression (IgM^{Low}, IgM^{Mid}, IgM^{Hi}), pooling cells across all original IgM-sorted samples. When analysed in this way, an IgM-associated pattern re-emerged. CD21 and CD22 MFI were highest in the day 5 IgM^{Hi} populations and lowest in the day 5 IgM^{Low} populations. Thus, although the day 5 IgM gates encompass heterogeneous mixtures of naïve, memory, plasmablast and atypical B cells, stratifying on current IgM expression is sufficient to recover subsets that share co-receptor characteristics. These data suggest that, following

stimulation, CD21 and CD22 expression are more tightly coupled to their current IgM level than to the original baseline IgM status. Further stratification based on cell subtypes is therefore necessary to disentangle the clear relationships between each cell group, activation level and IgM.

An important potential confounder is the developmental stage of the B cells. Both CD21 and CD22 are expressed at low levels on transitional B cells and are upregulated as cells mature into naïve B cells (Gross et al., 2009), while CD10 marks human transitional B cells (Sims et al., 2005). To minimise the contribution of transitional cells to these analyses, $CD10^+$ B cells were excluded in both the bulk proliferation experiments and the FACS-sorting strategy.

Taken together, these findings indicate that CD21 and CD22 expression after CpG + IL-2 stimulation is shaped principally by the differentiation trajectories that naïve B cells undergo, and by their contemporaneous IgM levels, rather than by their original IgM-defined state. In this dynamic context, IgM expression at day 5 acts as an effective organiser of phenotypically coherent B cell subsets, capturing co-regulated changes in CD21 and CD22 that could reflect shared activation pathways.

3.4.4 COVID-19 and the naïve B cell compartment

The original *in silico* analysis suggested an enrichment of a putative-anergic naïve B cell state in COVID-19 patients. In the present cohort, a significant baseline expansion of the stringent $IgM^{+/low}CD21^{low}CD22^{low}$ phenotype was not detected. Instead, the most consistent COVID-19–associated difference observed in this chapter emerged after *in vitro* activation: following CpG+IL-2 stimulation, the overall IgM distribution within the naïve B cell

pool was shifted in COVID-19 samples compared to healthy controls, with a lower proportion of IgM^{++} cells and a higher proportion of IgM^{-} cells. Functionally, this altered composition contributed to a reduced proportion of IgM^{++} proliferating cells at the population level in COVID-19 samples, despite the IgM^{++} subset itself proliferating comparably between groups. These data therefore suggest that recent SARS-CoV-2 infection is associated with a naïve compartment that is, on average, skewed toward lower IgM states and consequently exhibits reduced maximal responsiveness upon stimulation.

One interpretation is that this compositional skew reflects a transient remodelling of the naïve B cell compartment during and shortly after infection. One possibility is that the most activation-prone naïve B cells are preferentially recruited into responses during acute SARS-CoV-2 infection, leaving a residual pool enriched for lower IgM levels, less responsive states until the compartment is replenished. Alternatively, systemic inflammation during infection may bias naïve B cells toward an anergy-like state, consistent with interferon-associated immune activation signatures reported in COVID-19 (Ahern et al., 2022). In addition, such transient reductions in maximal responsiveness could contribute to short-term vulnerability to subsequent infections, although this link is not directly tested here (Murray et al., 2024). However, these interpretations remain hypotheses, as the present data demonstrate altered composition and reduced aggregate responsiveness after stimulation, but do not directly identify the *in vivo* drivers of these changes.

Placing these findings in context, they appear compatible with the bioinformatic description of an anergy-enriched naïve compartment in COVID-19, yet they contrast with reports that acute SARS-CoV-2 infection can be associated with restoration or enhancement of BCR signalling capacity in phenotypes overlapping anergy-enriched B cell states (B_{ND} $IgD^{+}IgM^{low}CD21^{low}CD22^{low}$)

(Castleman et al., 2022). Differences in cohort composition and sampling time could be a plausible explanation for this discrepancy. This chapter's study included mild convalescent donor samples, whereas acute/severe disease cohorts may capture distinct inflammatory environments and activation histories that remodel signalling differently. Incorporating activation markers such as CD69, CD80 and CD86 would strengthen the comparability of these phenotypes across studies.

Consistent with a time-dependent model, longitudinal profiling has indicated that SARS-CoV-2–associated changes in B cell composition, including anergy-associated phenotypes, can become undetectable 200 days post-symptom onset (Jokiranta et al., 2026). Together, these observations support the view that SARS-CoV-2 drives a transient modulation of naïve and anergic-like B cell states rather than stable long-term reprogramming, emphasising the importance of time-resolved sampling to identify transitional states and infer mechanisms underlying disruption and restoration of B cell tolerance.

Finally, COVID-19 is characterised by prominent extrafollicular-like B cell responses, including plasmablast expansion, which has been linked both to neutralising antibody production and to poor clinical outcomes (Kuri-Cervantes et al., 2020; Woodruff et al., 2020). In SLE, activated naïve-like DN populations marked by CD11c can feed into extrafollicular differentiation trajectories (Jenks et al., 2018). By analogy, enrichment of $IgD^{-}CD27^{-}CD11c^{+}$ populations observed in COVID-19 has been hypothesised to arise through similar pathways (Woodruff et al., 2020). The relationship between these extrafollicular-associated populations and the anergic-like states described here remains unresolved. The phenotype enriched after CpG stimulation could, in principle, intersect with extrafollicular-biased differentiation or autoreactive outputs reported in severe COVID-19, but this cannot be assessed

in the present study because CD11c and key activation features of extrafollicular responses were not included in the phenotypic panel. Future work incorporating CD11c together with activation markers and switched isotype phenotyping will be required to determine whether the anergic-like population described here contributes to extrafollicular-driven B cell responses in COVID-19 or represents a distinct functional state.

3.4.5 Limitations

Firstly, the experiments performed here were conducted *in vitro* and may not fully reflect *in vivo* B cell physiology. Only a single set of stimulation conditions was tested, which does not reflect the complexity of cues encountered in a physiological context. Additional stimulation cocktails, co-culture systems, or *ex-vivo* organoid systems could further refine our understanding of naïve B cell responses to diverse stimuli.

Secondly, the CpG with IL-2 stimulation strategy used in this chapter was originally selected as to activate B cells without directly engaging the BCR, thereby allowing IgM levels to be interpreted without confounding effects from anti-IgM stimulation. However, our data indicate that CpG itself can modulate IgM expression, complicating this assumption. CpG signals through TLR9, which is expressed on all human B cells but at lower levels in naïve subsets. Previous work has shown that BCR engagement can upregulate TLR9 expression on naïve B cells, enhancing their responsiveness to CpG. Although here the TLR9 expression in the IgM-defined naïve B cells was not assessed experimentally, *in silico* healthy naïve B cell TLR9 expression did not correlate with IgM ($\rho = 0.04$, $p > 0.05$, Spearman's Rank correlation). In addition, a previous study examining a comparable B cell phenotype reported no difference in the levels of surface TLR9 or cell frequency between

IgM^{Low} (dimmest 20% of naïve B cells) and IgM^{Int} subsets (Quách et al., 2011). Conversely, CpG upregulates the IL-2 receptor CD25 on peripheral B cells, but whether IL-2 in turn affects CpG responsiveness remains unclear (Inaba et al., 2023). Further investigations will be required to disentangle these mechanisms and determine the extent of receptor contribution to the unresponsiveness of IgM^{Low} naïve B cells.

Thirdly, the FACS-sorting of IgM^{Low} populations for stimulations might have concentrated the cell pool towards an 'anergic' phenotype as defined in previous studies (Quách et al., 2011), however, this approach is still likely to capture a heterogeneous B cell population as we have previously shown (Pernes et al., 2024). This heterogeneity might be masking the subtleties of discrete subpopulations and their cell surface marker dynamics post-stimulation. Future work should aim to isolate sufficient cell numbers from phenotypes that closely match previously characterised anergic populations and then examine their co-receptor regulation following stimulation. Additional markers that would enable a more granular characterisation include CD11c, early activation markers such as CD69, CD25 and switched isotype markers.

Finally, whilst the purity of sorted populations was verified for selected samples and shown to be minimum 90% pure, it was not verified for every sample after FACS, meaning that the true redistribution frequency of IgM expression after five days of stimulation can only be approximated from the subset of samples for which purity was assessed. Moreover, for accurate comparison, a post-sort purity should also be checked on the same cytometer used for the day 5 readout. In this study, purity checks were only performed on the sorter itself.

3.4.6 Future work

A detailed characterisation of the phenotypic and functional spectrum of human B cell anergy may ultimately enable us to modulate these states in a context and disease-specific manner. Recent work has identified CD73 as a strongly associated marker of B_{ND} anergic B cells in humans (Dizon, Holla, Mutic, Schaughency, & Pierce, 2025). Systematic investigation of this alongside recurrent anergy markers, assessed dynamically following stimulation, would help clarify how these markers behave across different activation states. Such studies could be complemented by functional readouts of B cell responsiveness, including calcium mobilisation assays or measurement of PTEN abundance (Smith et al., 2019). In addition to characterising anergy, an important next step would be to explore whether anergy can be deliberately induced. Mouse B_{ND} cells also exhibit high CD73 expression, a key enzyme in purinergic metabolism, and recent findings show that inosine expands the B_{ND} population while preventing differentiation into antibody-secreting cells, an effect associated with amelioration of autoimmune hepatitis in a mouse model (Cui et al., 2025). These observations raise the possibility that metabolic pathways could be leveraged to therapeutically modulate B cell anergy in human disease.

3.4.7 Conclusions

This work provides experimental validation for IgM surface density as a critical functional determinant of B cell anergy/responsiveness in humans. Naïve B cells vary in responsiveness along an IgM-defined axis at baseline, yet can move along this axis during activation. This behaviour aligns with a continuum model of anergy in which cellular responsiveness is not fixed, but

evolves according to current IgM and co-receptor expression. Furthermore, this study suggests that COVID-19 is associated with a remodelling of the naïve B cell compartment towards lower IgM expression following activation, potentially representing a peripheral tolerance mechanism to temper hyper-inflammation. This research contributes to a deeper understanding of human peripheral tolerance and its perturbation in systemic diseases.

Combined with further bioinformatic analysis of single cell multi-omics data, these observations provide a basis for further investigation into the molecular features associated with human B cell anergy and activation, paving the way for the development of novel immunomodulatory therapeutic design.

4 | B cell receptor repertoire in COMBIVAS clinical trial

4.1 Introduction

Anti-neutrophil cytoplasmic antibody (ANCA)-associated vasculitis (AAV) is a group of small vessel vasculitides that although rare, can be fatal if left untreated. B cells play a fundamental role in the pathology of AAV, as demonstrated by the effectiveness of B cell-depletion therapies with rituximab in inducing remission, first described more than 20 years ago (Specks, Fervenza, McDonald, & Hogan, 2001). Rituximab, a monoclonal antibody targeting CD20 on B cells, remains one of the main remission induction therapeutic agents in AAV. However, approximately 10-12% of AAV patients fail to achieve remission within 12 months, and up to 50% relapse within 5 years, despite ongoing maintenance therapy (Machet et al., 2023; Stone et al., 2010; de Groot et al., 2009; R. B. Jones et al., 2010; Terrier et al., 2018). Relapses are particularly common in patients who are PR-3–ANCA positive, compared to MPO-ANCA positive patients (Specks et al., 2013; Terrier et al., 2018). This highlights the need for improved therapeutic strategies to reduce both the rate and frequency of relapse, particularly in PR3-AAV.

Given the pivotal contribution of B cells in AAV, strategies that improve the depth and durability of B cell-targeting therapies are of great interest. Importantly, studies have shown that incomplete peripheral B cell depletion and earlier B cell repopulation after rituximab are associated with increased relapse risk, particularly in PR3-AAV (van Dam et al., 2021; Alberici et al., 2015). These observations support therapeutic strategies aimed at prolong-

ing effective suppression of pathogenic B cell compartments. One rational approach is to target B cell survival pathways that may prevent complete B cell depletion and may promote increased autoreactive reconstitution after depletion.

B cell activating factor (BAFF, also termed BLyS/TNFSF13B) is a TNF-family cytokine that supports peripheral B cell survival and maturation. Importantly, autoreactive B cells appear to be disproportionately dependent on BAFF for persistence, as elevated BAFF can relax competitive tolerance checkpoints and rescue self-reactive clones that would otherwise be eliminated (Lesley et al., 2004). In AAV, several lines of evidence support a role for BAFF in sustaining pathogenic B cells. Circulating BAFF levels are increased in PR3-AAV compared with healthy controls (Sanders et al., 2006). Moreover, ANCAs may amplify BAFF availability, as stimulation of neutrophils with ANCA-IgG induces BAFF surface expression and release, and neutrophil supernatants can promote B cell survival *in vitro* (Holden et al., 2011). Consistent with the idea that inflamed tissues can provide survival niches, in AAV granulomatous upper-airway mucosa from GPA patients has been shown to contain chronically activated and proliferating B cells in close proximity to PR3-expressing cells and the B cell survival factors BAFF and APRIL (Y. Zhao et al., 2012).

A further consideration is that B cell depletion can be followed by a compensatory rise in BAFF, reported in other autoimmune diseases such as SLE and RA (Vallerskog et al., 2006; Cambridge et al., 2006).

In PR3-AAV, PR3-ANCA titres often decline after rituximab and a subset of patients was shown to achieve PR3-ANCA negativity (McClure et al., 2019). Because rituximab targets $CD20^{+}$ B cells rather than $CD20^{-}$

plasmablasts/plasma cells, these serological responses are most consistent with a model in which ANCA production is, at least in a proportion of patients, maintained largely by short-lived antibody-secreting cells that depend on continual reconstitution from $CD20^+$ precursors. Conversely, persistent ANCA in some patients is compatible with ongoing contribution from long-lived plasma cells that are not removed by anti-CD20 therapy. Since BAFF promotes survival of newly emerging B cells and can enhance the survival of plasmablasts, a post-depletion, high-BAFF environment could plausibly favour the re-emergence of autoreactive clones during B cell repopulation and support renewed generation of pathogenic short-lived antibody-secreting cells (Lesley et al., 2004; Avery et al., 2003; Karnell & Ettinger, 2012).

Taken together, these observations provide a mechanistic rationale to test whether BAFF blockade can improve the depth and durability of B cell targeting strategies in PR3-AAV. The COMBIVAS clinical trial was therefore designed as a randomised, double-blind, placebo-controlled mechanistic study to evaluate sequential rituximab plus belimumab versus rituximab plus placebo in active PR3-ANCA–positive AAV (McClure et al., 2023).

4.1.1 Chapter aims

This chapter examines the BCR repertoire features from the peripheral blood samples collected at three therapeutic timepoints (day 1 - D1, month 12 - M12 and month 24 - M24) from participants in the COMBIVAS trial. The following questions are explored:

1. What is the effect of belimumab plus rituximab therapy on the B cell repertoire reconstitution, compared to rituximab plus placebo?
2. Is there evidence of differential B cell reconstitution between belimumab

plus rituximab, and rituximab plus placebo?

4.2 Study and experimental design

Patients recruited in COMBIVAS were randomised to receive rituximab and belimumab or rituximab and placebo. Patients were treated with belimumab at D1, followed by a dose of RTX at weeks 2 and 4. Further weekly belimumab or placebo treatment was administered until M12. Patients were then followed-up to M24 without further therapy administration. The patients were also sampled in case of disease relapse, resulting in an unscheduled sample.

The bulk B cell receptor (BCR) repertoire of patients participating in the COMBIVAS trials was sequenced. Sequencing of the samples was performed from peripheral whole blood. The BCR repertoire sequencing analysis was performed using the pipeline developed by Rachael Bashford-Rogers (Bashford-Rogers et al., 2019).

4.3 Results

4.3.1 Summary of COMBIVAS clinical trial results

I attach below a summary extract from the COMBIVAS clinical trial report (not yet published), to provide clinical context to the BCR repertoire results described later. '*In this randomised controlled trial of 35 patients with ANCA-associated vasculitis, 34 were evaluable for analysis. In the per-protocol cohort (n=32), PR3-ANCA negativity was observed more frequently with rituximab–belimumab (29.4%) than with rituximab–placebo (13.3%, HR 4.70, 95% CI 0.65–33.8, $p = 0.12$), and median ANCA titres at 52 weeks*

were lower in the combination group (3.4 iU (IQR 2.5-12.4) versus 12.0 iU (IQR 6.2-29.5)). Both groups achieved B cell depletion by week 12, however, belimumab delayed B cell reconstitution, maintaining reduced total and naïve B cell counts at 12–18 months. In the intention-to-treat analysis, no patients on rituximab–belimumab experienced progressive disease prior to remission, compared with three on rituximab–placebo. Time to remission was significantly faster with combination therapy (42 vs. 91 days; HR 2.29, 90% CI 1.08–4.85; $p = 0.031$), and relapse rates were lower (35% vs. 53%, HR 0.64; 95% CI 0.23–1.80; $p = 0.40$), although not statistically significant. ANCA re-emergence occurred following belimumab withdrawal in 4/5 relapsing patients, and no relapses occurred during ANCA negativity. Serious adverse event rates were similar between groups. Overall, rituximab–belimumab therapy was associated with delayed B cell recovery, enhanced PR3-ANCA suppression, faster remission, and a trend toward reduced relapse risk.'

4.3.2 Overview of the data

The combination therapy of rituximab and belimumab is hereafter referred to as 'belimumab' (BLM), whilst rituximab and placebo is referred to as 'placebo' (PBO). Samples from 27 patients with AAV randomised to receive either BLM or PBO were received from the COMBIVAS clinical trial. Of these, 15 patients (BLM $n = 8$, PBO $n = 7$) completed the full treatment course without experiencing disease relapse and were sampled at the baseline (D1) and the final timepoint (M24). In addition, 12 of these 15 patients (BLM $n = 5$, PBO $n = 7$) were also sampled at month 12 (M12). Samples taken at unscheduled time points due to disease relapse (e.g. month 10, 14 or 16) were excluded from the downstream analysis. A table of the sampling timepoints per patient is detailed in Chapter 2.

The BLM group comprised of 6 males and 2 females (mean age 53.8 ± 18.5 years), and the PBO group 4 males and 3 females (mean age 54.9 ± 13.5 years). Two patients in the BLM group and one in the PBO group had received prior cyclophosphamide treatment.

4.3.3 COMBIVAS cellular context

Although the cellular counts post-therapy were not analysed as part of this chapter, it is valuable to consider the cellular context following the trial, as the BCR repertoire metrics are relative measures, and do not inform about the cellular count change, due to the constraints of bulk BCR sequencing.

Both treatment arms achieved B cell depletion by month 3. Total and naïve B cell counts were lower in the belimumab group than in the placebo group at M12 and M18.

4.3.4 High-quality BCR repertoire capture from COMBIVAS PBMC samples

The BCR repertoire sequencing was successful in all of the submitted samples, with all 74 of these yielding over 1000 reads (Figure 4.1a). The number of unique sequences per sample closely matched the total number of sequence reads, indicating a diverse representation of the BCR repertoire (Figure 4.1b).

Overall, the clonal overlap across samples was low. Positive control samples showed the greatest pairwise sharing (∼1% of the repertoire), while clinical samples from the same donor shared a maximum average of ∼0.25% of total reads. In contrast, overlap between unrelated samples was negligible (<0.03% of total reads), suggesting low levels of contamination (Figure 4.2).

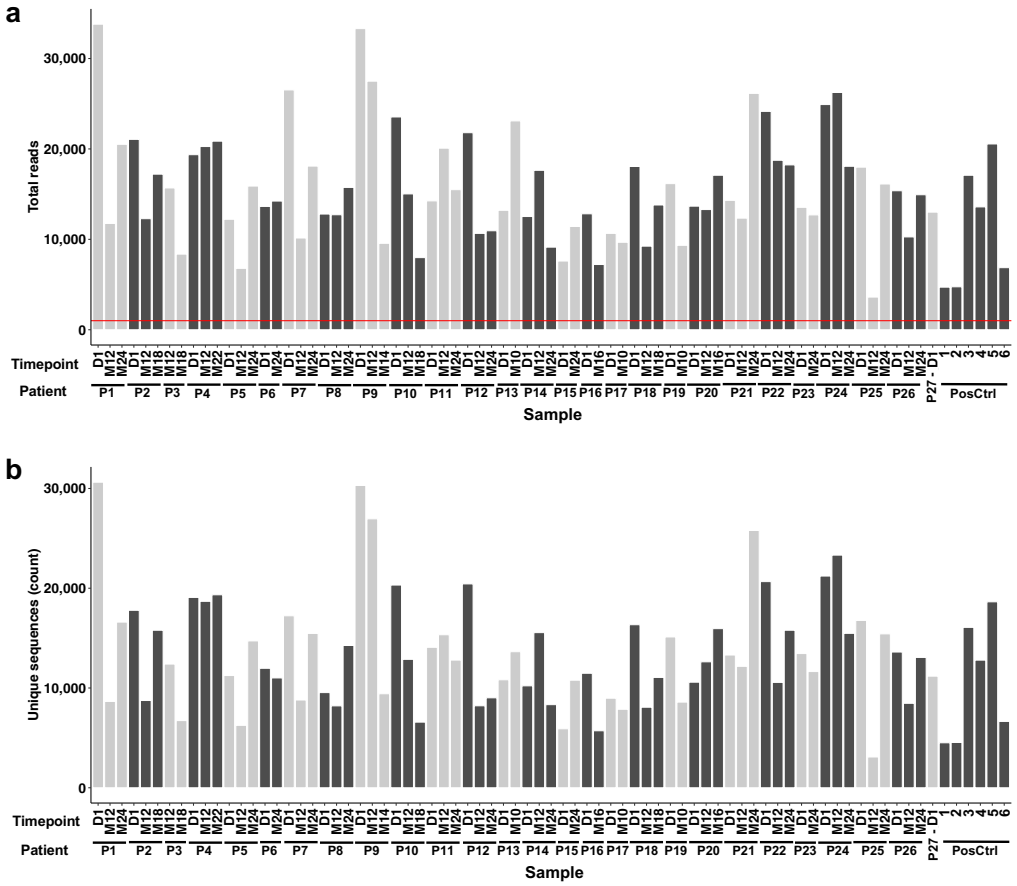

Figure 4.1: Overview of total and unique reads per sample. a Bar plot showing the total read depth for each sample; the red horizontal line indicates the threshold of 1000 reads. **b** Bar plot showing the number of unique B cell receptor (BCR) sequences detected per sample. Each bar represents one sample. D – day; M – month; PosCtrl – positive control.

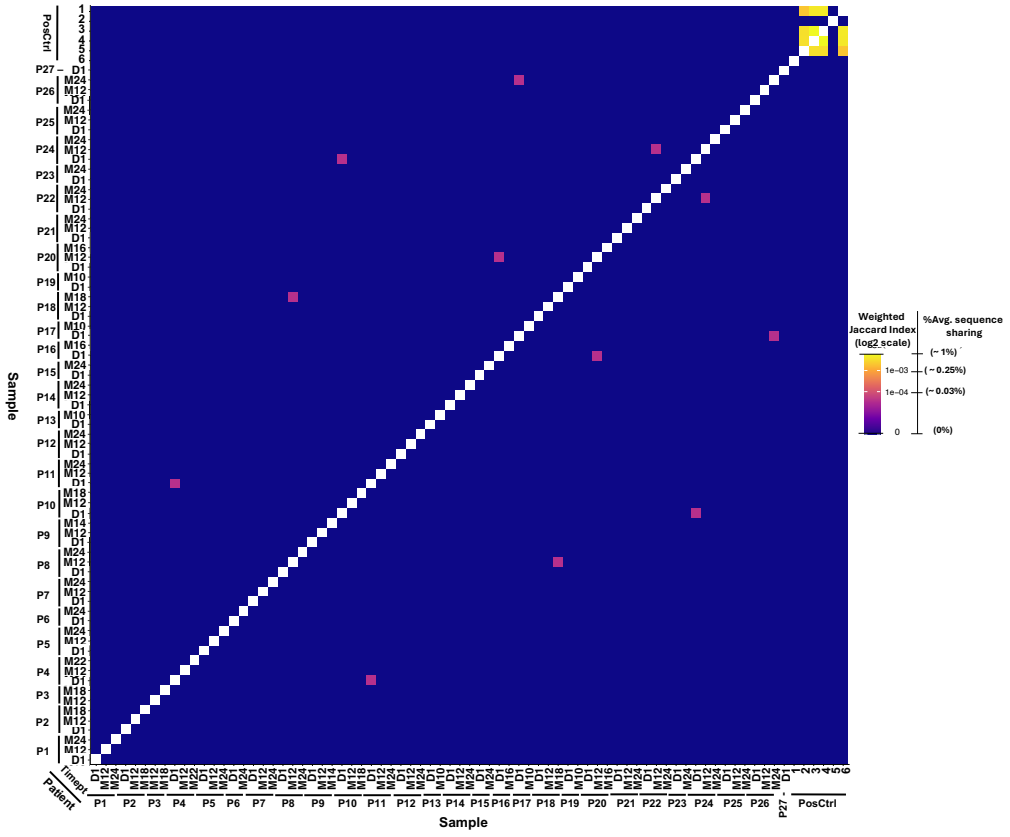

Figure 4.2: Heatmap of BCR repertoire overlap across all COMBIVAS samples. Each cell shows the $\log_2$-transformed weighted Jaccard index between pairs of repertoires, which reflects the abundance-weighted similarity of B cell receptor sequence composition per sample. Elevated values may indicate sample cross-contamination or biological repertoire sharing. D - day; M - month; PosCtrl - positive control; Timept - timepoint.

4.3.5 Belimumab showed a tendency to maintain low IGHA2 and IGHG2 while appearing to increase IGHA1 and IGHG1 usage

A non-significant trend toward altered isotype-usage distribution was observed between the treatment arms (Figure 4.3). IGHA1 usage was higher after belimumab at M12 (BLM 7.9% vs. PBO 4.5%) and remained higher at M24 (BLM 11.3% vs. PBO 8.4%). IGHA2 was maintained at lower levels at M24 in the belimumab group (BLM 4.8% vs. PBO 8.3%). Belimumab was also associated with slightly lower IGHD percentages at M24 (BLM 14.4% vs. PBO 18.1%) and a trend toward increased IGHE levels at M24 (BLM 0.08% vs. PBO 0.05%). A slightly elevated trend of IGHG1 usage was observed after belimumab at M24 (BLM 4.2% vs. PBO 1.4%). IGHG2 levels tended to be higher at M12 after belimumab compared to placebo (BLM 1.5% vs. PBO 0.6%). At M24, IGHG2 levels remained relatively stable in the belimumab group, whereas an increase was observed in the placebo group (BLM 1.6% vs. PBO 2.6%). IGHG3, IGHG4 and IGHM showed broadly overlapping distributions between treatment arms at M24 (see Table 4.1 for 95% confidence intervals, and Supplementary Table C.1 for complete summary data).

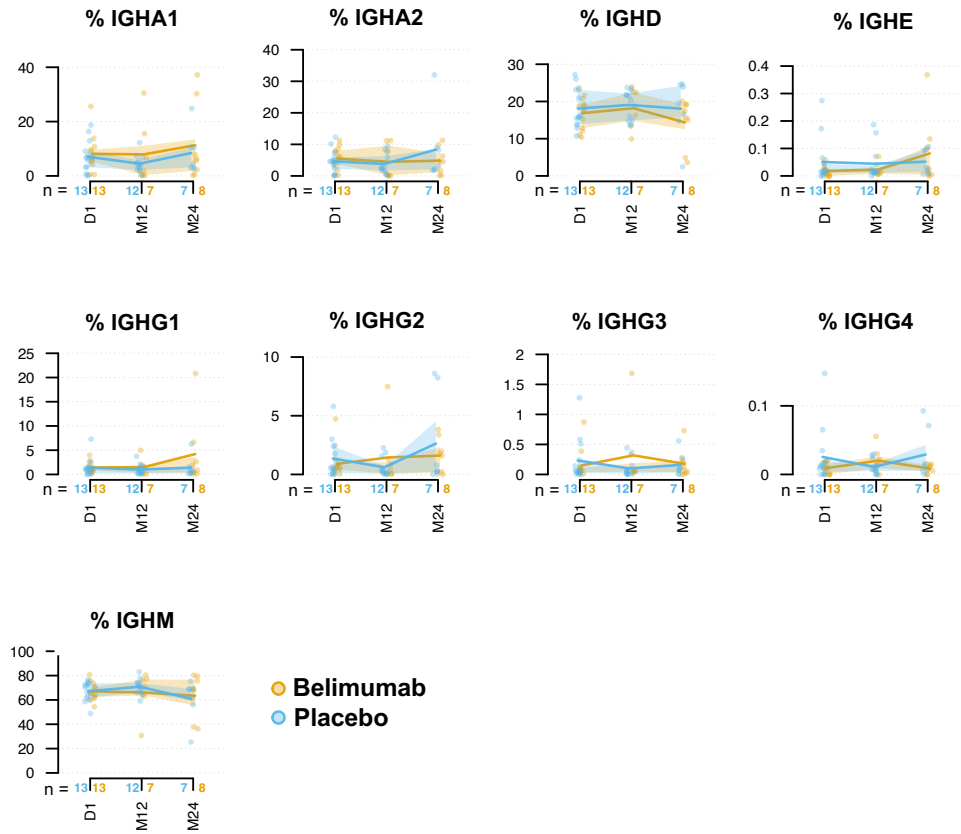

Figure 4.3: B cell repertoire isotype composition between treatment groups. Each panel shows the B cell isotype usage as a percentage of the total repertoire, split by treatment arm across timepoints. No statistical significant value has been recorded at any timepoint between the treatment arms, after adjustment for age, sex, prior cyclophosphamide treatment ± baseline ($p > 0.05$, likelihood ratio test after beta regression ± covariates with multiple testing correction). Statistical differences between treatment arm per timepoint were tested on centre-log-ratio transformed data with an ANCOVA (covariates age, sex and prior cyclophosphamide treatment), with p-value permutations and FDR correction for multiple testing (p>0.05, all comparisons). Each point represents one patient. The solid lines represent the group mean for each treatment arm. The shaded bands indicate the inter-quartile range (IQR). n - number of patients per treatment arm at each timepoint (placebo in blue; belimumab in orange); D1 – day 1; M12 – month 12; M24 – month 24.

Isotype	Timepoint	BLM mean (95% CI)	PBO mean (95% CI)
IGHA1	M12	7.9 (0.0, 18.5)	4.5 (2.4, 6.5)
	M24	11.3 (0.0, 23.2)	8.4 (1.0, 15.8)
IGHA2	M24	4.8 (1.3, 8.3)	8.3 (0.0, 18.4)
IGHD	M24	14.4 (8.9, 19.8)	18.1 (10.7, 25.4)
IGHE	M24	0.08 (0.00, 0.19)	0.05 (0.01, 0.09)
IGHG1	M24	4.2 (0.0, 10.1)	1.4 (0.0, 3.4)
IGHG2	M12	1.5 (0.0, 4.0)	0.6 (0.1, 1.1)
	M24	1.6 (0.4, 2.8)	2.6 (0.0, 6.3)
IGHG3	M24	0.2 (0.00, 0.4)	0.2 (0.00, 0.3)
IGHG4	M24	0.01 (0.00, 0.01)	0.03 (0.00, 0.06)
IGHM	M24	63.4 (48.8, 78.1)	60.9 (45.4, 76.4)

Table 4.1: **Mean percentage of BCR isotypes by treatment group (95% confidence intervals).** BLM - Belimumab; PBO - Placebo.

4.3.6 Belimumab showed trends of higher clonal expansion and diversification by M24 in IGHA1, IGHA2 and IGHG2

B cell clonality metrics were calculated in two ways. The Vertex Gini index (GI) is used as a measure of clonal expansion of B cells with unique BCRs, whereas the cluster Gini index is a measure for the expansion of the entire clonal family, accounting for related sequences arising from somatic hypermutation within the same clone.

The Vertex Gini index (Figure 4.4a) and cluster Gini index (Figure 4.4b) displayed comparable trends across the isotypes and the overall B cell clonality ('all'). By M24 the overall ('all') Vertex and cluster Gini indices were similar between the treatment arms (Vertex GI BLM 0.07 vs. PBO 0.06, cluster

GI BLM 0.15 vs. PBO 0.14), slightly increased compared to baseline levels (Vertex GI BLM 0.05 vs. PBO 0.03, cluster GI BLM 0.10 vs. PBO 0.08).

At isotype level by M12, the Vertex Gini index was comparable between treatment arms across isotypes with the exception of IGHG2 which showed a slight increased GI compared to placebo (Vertex GI BLM 0.03 vs. PBO 0.009, cluster GI BLM 0.08 vs. PBO 0.03). However, at M24 several isotypes displayed higher Vertex and cluster trends compared to placebo including IGHA1 (Vertex GI BLM 0.08 vs. PBO 0.05, cluster GI BLM 0.20 vs. PBO 0.12), IGHA2 (Vertex GI BLM 0.12 vs. PBO 0.08, cluster GI BLM 0.24 vs. PBO 0.21) and IGHG2 (Vertex GI BLM 0.02 vs. PBO 0.005, cluster GI BLM 0.04 vs. PBO 0.03), whereas IGHG1 (Vertex GI BLM 0.009 vs. PBO 0.02, cluster GI BLM 0.02 vs. PBO 0.05) and IGHM (Vertex GI BLM 0.06 vs. PBO 0.07, cluster GI BLM 0.11 vs. PBO 0.13) showed lower trends compared to placebo. A table with the 95% CI is detailed in Table 4.2 and complete summary table is in Supplementary Table C.2)

The observed trends in clonality metrics suggest that belimumab may delay the reconstitution of the overall BCR repertoire by month 12 compared with placebo. By month 24, belimumab's delaying effect on reconstitution appears restricted to selected memory B cell isotypes (IGHA1, IGHA2 and IGHG2), whereas the recovery of the IGHG1 isotype seems to be supported.

Statistical differences between treatment arms at each time point were assessed using centre-log-ratio (CLR)–transformed data in an ANCOVA model, with age, sex, and prior cyclophosphamide treatment included as covariates. P-values were obtained by permutation testing and adjusted for multiple comparisons using FDR correction (all comparisons $p > 0.05$).

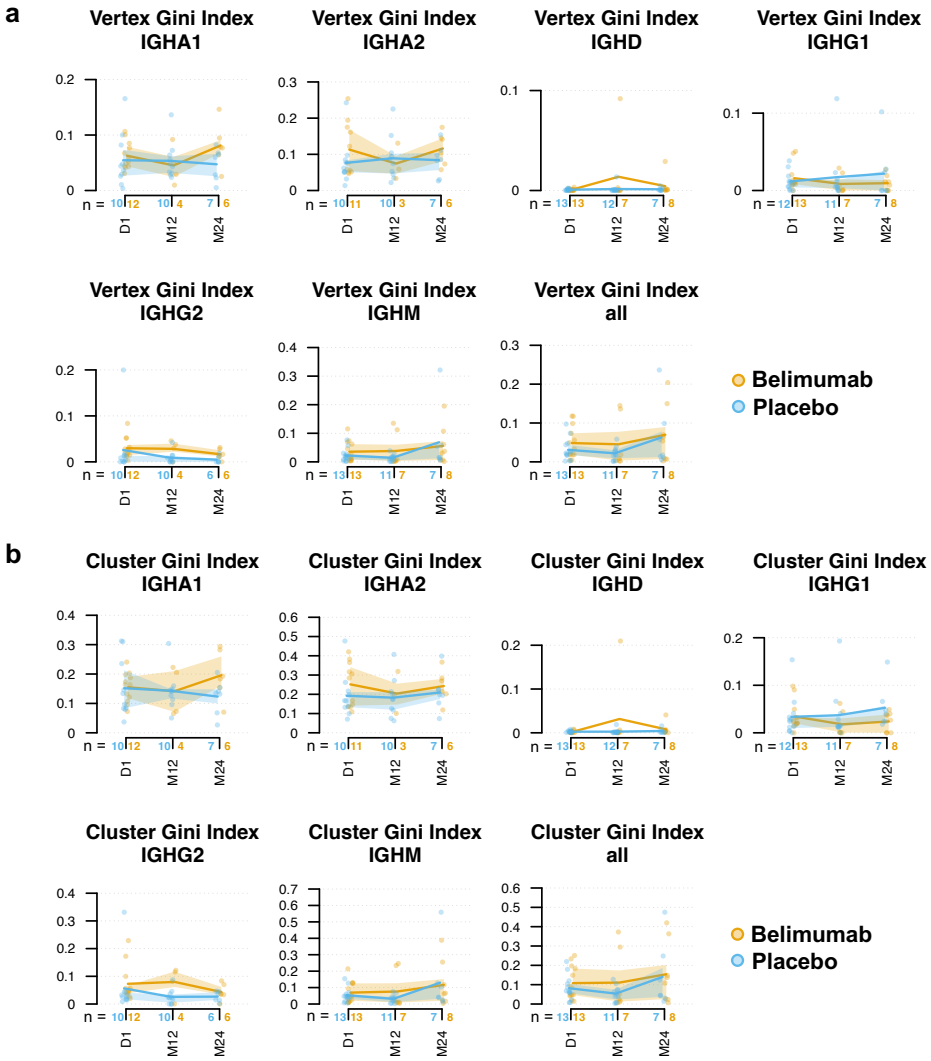

Figure 4.4: B cell clonal expansion between treatment groups. Each plot shows B cell clonality features across timepoints, split by isotype. **a** Vertex Gini index, as a measure of clonal expansion of B cells with identical receptors. **b** cluster Gini index as a measure of B cell clonal family expansion, accounting for related sequences arising from somatic hypermutation within the same clone. Logit-transformed data was analysed by ANCOVA (covariates: age, sex, prior cyclophosphamide), with permutation-derived p-values and FDR correction (all $p > 0.05$). Each point represents one patient. The solid lines represent the group mean for each treatment arm. The shaded bands indicate the inter-quartile range (IQR). n - number of patients per treatment arm at each timepoint (placebo in blue; belimumab in orange); D1 – day 1; M12 – month 12; M24 – month 24.

Index	Isotype	Timepoint	BLM mean (95% CI)	PBO mean (95% CI)
Vertex	all	D1	0.05 (0.02, 0.07)	0.03 (0.01, 0.05)
Vertex	all	M24	0.07 (0.01, 0.13)	0.06 (0.00, 0.14)
Vertex	IGHG2	M12	0.03 (0.00, 0.06)	0.009 (0.00, 0.02)
Vertex	IGHA1	M24	0.08 (0.04, 0.12)	0.05 (0.02, 0.07)
Vertex	IGHA2	M24	0.12 (0.07, 0.16)	0.08 (0.04, 0.13)
Vertex	IGHG1	M24	0.009 (0.001, 0.02)	0.02 (0.00, 0.06)
Vertex	IGHG2	M24	0.02 (0.00, 0.03)	0.005 (0.00, 0.01)
Vertex	IGHM	M24	0.06 (0.00, 0.11)	0.07 (0.00, 0.17)
Cluster	all	D1	0.11 (0.06, 0.16)	0.08 (0.04, 0.12)
Cluster	all	M24	0.15 (0.02, 0.29)	0.14 (0.00, 0.30)
Cluster	IGHG2	M12	0.08 (0.00, 0.17)	0.03 (0.01, 0.04)
Cluster	IGHA1	M24	0.20 (0.11, 0.28)	0.12 (0.07, 0.18)
Cluster	IGHA2	M24	0.24 (0.15, 0.33)	0.21 (0.12, 0.30)
Cluster	IGHG2	M24	0.04 (0.01, 0.07)	0.03 (0.01, 0.05)
Cluster	IGHG1	M24	0.02 (0.01, 0.04)	0.05 (0.01, 0.09)
Cluster	IGHM	M24	0.12 (0.00, 0.23)	0.13 (0.00, 0.31)

Table 4.2: **Mean Vertex and cluster Gini indices by treatment group at selected timepoints.** Values represent group means with 95% confidence intervals. BLM - Belimumab; PBO - Placebo.

4.3.7 Belimumab shows trends toward lower dominant clone size at M12 for IGHA1/IGHA2 and higher clonal dominance within IGHD, IGHM and the overall repertoire at M12 and M24

To further understand the composition underlying clonality metrics such as the Vertex and cluster Gini indices, the size of the most expanded clone within each repertoire was next examined. Assessing the proportion of the largest expanded B cell cluster provides insight into whether clonal expansion is driven by a single dominant B cell within the total repertoire or within specific isotypes, while also highlighting trends of repertoire reconstitution. Therefore, the percentage of the largest expanded B cell cluster per sample (percentage max cluster size), was calculated across all isotypes (Figure 4.5a) and across the overall repertoire (Figure 4.5b). Overall, at M12 belimumab showed comparable sizes of the largest B cell clone compared to placebo (BLM 0.35% vs. PBO 0.29%), but by M24 belimumab displayed a higher trend of cluster sizes than placebo (BLM 0.82% vs. PBO 0.50%, Figure 4.5b). This is in agreement with the higher trends in the overall clonality indices in the belimumab arm at M12 presented in the section above, and supports the hypothesis that belimumab may delay the reconstitution of the overall B cell repertoire. It also nuances the previous finding whereby although the clonality index was similar to placebo at M24, the overall representation of the most dominant clone per sample tended to be higher in belimumab, consistent with a less diversified and slower-recovering repertoire.

At the isotype level (Figure 4.5a), belimumab showed trends of reduced percentage maximum cluster size at M12 within IGHA1 (BLM 1.29% vs.

PBO 2.08%) and IGHA2 (BLM 1.14% vs. PBO 2.56%). Conversely, BLM appeared to induce higher sizes of the most dominant clone at M12 and M24 within IGHD (M12 1.31% vs. PBO 0.93%; M24 BLM 1.12% vs. PBO 0.96%) and IGHM (M12 BLM 0.55% vs. PBO 0.37%; M24 BLM 0.91% vs. PBO 0.73%). The percent of maximum cluster size within IGHE also showed higher trends at M24 than placebo (BLM 8.15% vs. PBO 7.46%). The confidence intervals of these values are reported in Table 4.3, and a complete summary table is in Supplementary Table C.3.

Isotype	**Timepoint**	**BLM mean (95% CI)**	**PBO mean (95% CI)**
all	M12	0.35 (0.00, 0.77)	0.29 (0.09, 0.49)
all	M24	0.82 (0.24, 1.41)	0.50 (0.05, 0.95)
IGHA1	M12	1.29 (0.10, 2.48)	2.08 (1.38, 2.78)
IGHA2	M12	1.14 (0.00, 2.50)	2.56 (1.54, 3.59)
IGHD	M12	1.31 (0.31, 2.30)	0.93 (0.80, 1.06)
IGHD	M24	1.12 (0.62, 1.62)	0.96 (0.80, 1.12)
IGHM	M12	0.55 (0.00, 1.24)	0.37 (0.07, 0.67)
IGHM	M24	0.91 (0.18, 1.64)	0.73 (0.10, 1.37)
IGHE	M24	8.15 (0.66, 15.64)	7.46 (0.00, 16.79)

Table 4.3: **Mean percentage of maximum cluster size by treatment group at selected timepoints.** Values represent group means with 95% confidence intervals. BLM - Belimumab; PBO - Placebo.

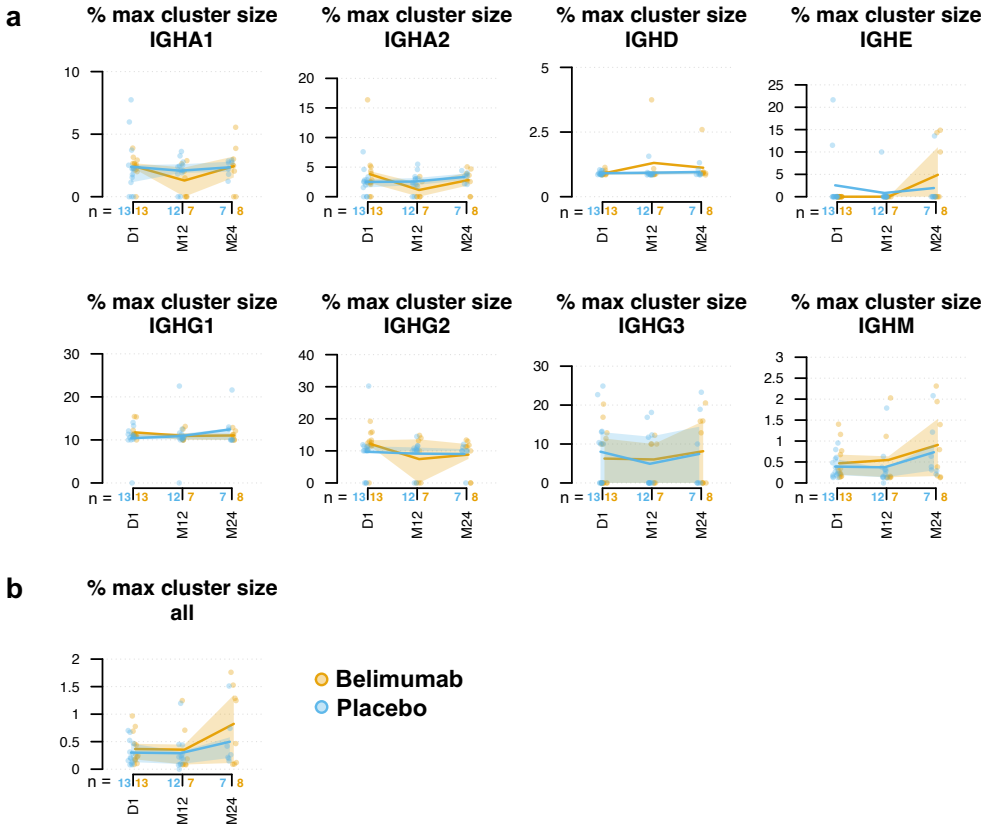

Figure 4.5: Percentage of the largest B cell clonal family (cluster) of the sample repertoire. B cell clusters account for related sequences arising from somatic hypermutation within the same clone. **a** Each plot represents the maximum B cell cluster size of each isotype as a percentage of all clones of that isotype, calculated per sample. **b** Plot illustrates the largest B cell cluster size as a percentage of the total repertoire per sample. Logit-transformed data was analysed by ANCOVA (covariates: age, sex, prior cyclophosphamide), with permutation-derived p-values and FDR correction (all $p > 0.05$). Each point represents one patient. The solid lines represent the group mean for each treatment arm. The shaded bands indicate the inter-quartile range (IQR). n - number of patients per treatment arm at each timepoint (placebo in blue; belimumab in orange); D1 – day 1; M12 – month 12; M24 – month 24

4.3.8 Belimumab showed trends toward higher top-5 clone sizes at M12 across isotypes, and at M24 within IGHA1, IGHG2, IGHM and the overall repertoire

Examining the representation of the top-5 clones (D5) per sample provides complementary insight into the dynamics of clonality and extends the analysis beyond the single most expanded clone.

By M12 in the belimumab arm, the D5 metric tended to be higher across all isotypes [IGHA1 (BLM 12.35% vs. PBO 8.94%), IGHA2 (BLM 17.32% vs. PBO 12.94%), IGHG1 (BLM 33.08% vs. PBO 20.13%), IGHG2 (BLM 36.87% vs. PBO 21.79%) and IGHM (BLM 5.04% vs. PBO 3.22%)] and the overall repertoire (BLM 3.55% vs. PBO 2.17%) (Figure 4.6). The confidence intervals of these values are reported in Table 4.4, and a complete summary table is in Supplementary Table C.4. These observations are consistent with clonality trends (Gini index and %max clone) reported earlier in this chapter, suggesting that belimumab may delay the reconstitution of the B cell repertoire compared with placebo by M12.

By M24 a higher D5 metric trend was maintained in the belimumab arm within IGHA1 (BLM 10.12% vs. PBO 7.91%), IGHG2 (BLM 31.35% vs. PBO 18.76%), IGHM (BLM 2.17% vs. PBO 1.26%) and the overall repertoire (BLM 2.87% vs. PBO 1.36%). The confidence intervals of these values are reported in Table 4.4, and a complete summary table is in Supplementary Table C.4. This is consistent with the previously described Gini index trends for the overall repertoire, IGHA1 and IGHG2 at M24, supporting the notion that belimumab may delay B cell repertoire reconstitution within these

compartments compared with placebo. However, this pattern does not extend to IGHA2, IGHG1 or IGHM, which did not mirror the Gini index clonality trends.

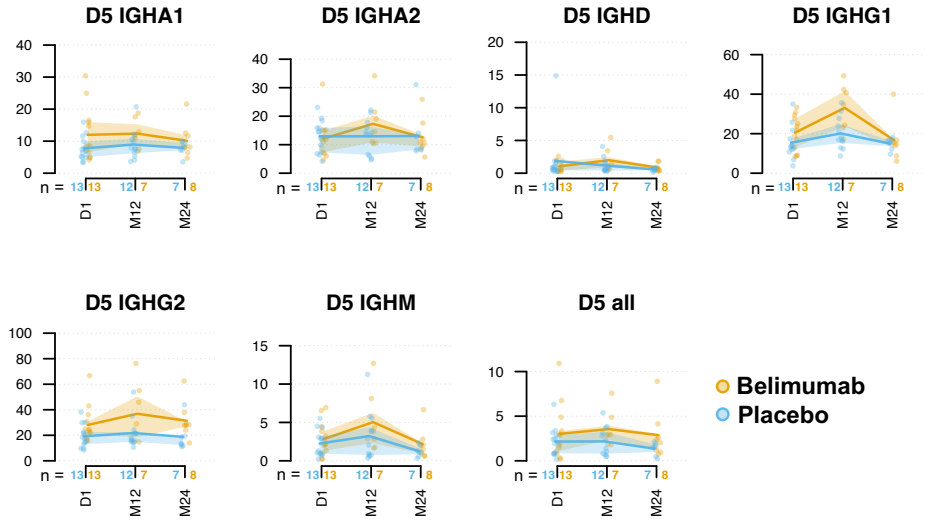

Figure 4.6: The largest 5 expanded B cell clones as a percentage of the repertoire. B cell clusters account for related sequences arising from somatic hypermutation within the same clone. Each plot depicts the fraction of the repertoire occupied by the 5 most expanded B cell clones of each isotype, expressed as the percentage of all clones of that isotype per sample, and the five largest clones across the full repertoire relative to all clones in the sample ('all'). Logit-transformed data was analysed by ANCOVA (covariates: age, sex, prior cyclophosphamide), with permutation-derived p-values and FDR correction (all $p > 0.05$). Each point represents one patient. The solid lines represent the group mean for each treatment arm. The shaded bands indicate the inter-quartile range (IQR). n - number of patients per treatment arm at each timepoint (placebo in blue; belimumab in orange); D1 – day 1; M12 – month 12; M24 – month 24

Isotype	Timepoint	BLM mean (95% CI)	PBO mean (95% CI)
IGHA1	M12	12.35 (8.14, 16.57)	8.94 (6.00, 11.88)
IGHA2	M12	17.32 (9.36, 25.28)	12.94 (9.06, 16.82)
IGHG2	M12	36.87 (15.50, 58.23)	21.79 (14.22, 29.37)
IGHM	M12	5.04 (1.32, 8.76)	3.22 (1.20, 5.25)
all	M12	3.55 (1.67, 5.44)	2.17 (1.16, 3.19)
IGHA1	M24	10.12 (5.70, 14.55)	7.91 (5.84, 9.98)
IGHG2	M24	31.35 (19.48, 43.22)	18.76 (8.08, 29.45)
IGHM	M24	2.17 (0.53, 3.81)	1.26 (0.59, 1.94)
all	M24	2.87 (0.63, 5.11)	1.36 (0.68, 2.03)

Table 4.4: **Mean of top-5 expanded clones per sample D5 metric (%) by treatment group at selected timepoints.** Values represent group means with 95% confidence intervals. BLM – Belimumab; PBO – Placebo.

4.3.9 SHM is similar between treatment arms

Next, the level of somatic hypermutation (SHM) across the B cell repertoire was calculated. Between the treatment arms, all SHM levels were similar across the timepoints in all groups (class-switched, individual isotypes, expanded and unexpanded B cells) (Figure 4.7).

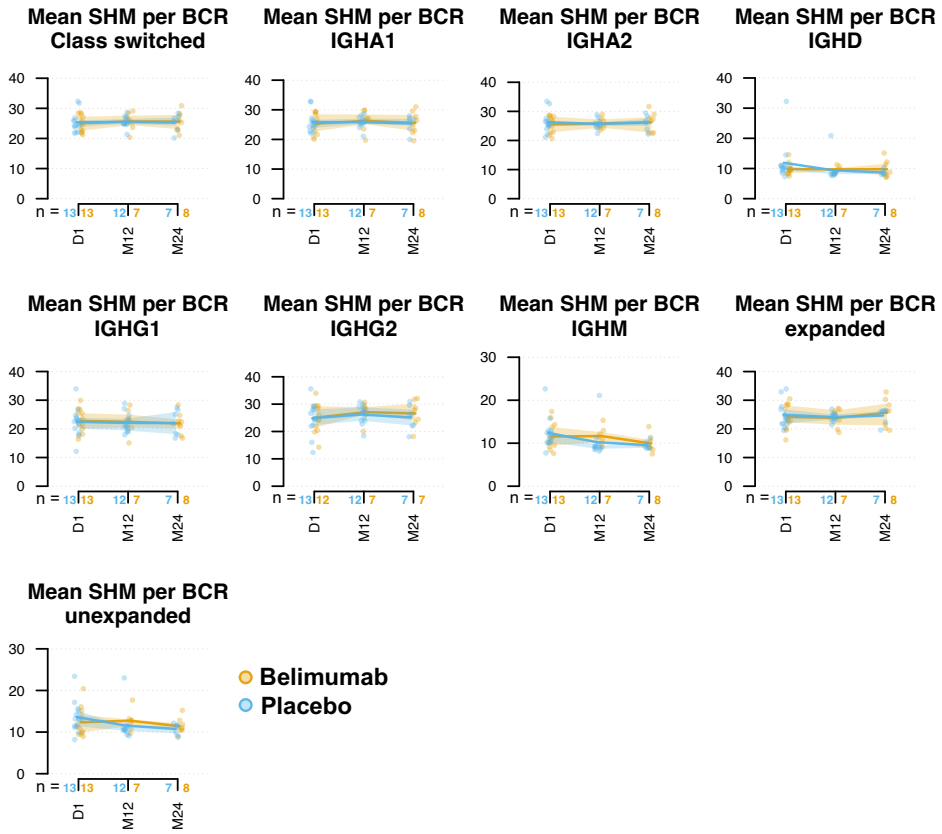

Figure 4.7: Somatic hypermutation levels of the B cell repertoire. Each plot represents the mean somatic hypermutation levels calculated per sample after grouping by isotype, class-switch status or clonal expansion status. Each point represents one patient. Data was analysed by ANCOVA (covariates: age, sex, prior cyclophosphamide), with permutation-derived p-values and FDR correction (all $p > 0.05$).The solid lines represent the group mean for each treatment arm. The shaded bands indicate the inter-quartile range (IQR). n - number of patients per treatment arm at each timepoint (placebo in blue; belimumab in orange); D1 – day 1; M12 – month 12; M24 – month 24

4.3.10 Belimumab tends to reduce IGHV gene rearrangement signatures by M24 within IGHA1, IGHA2 and IGHM

The rate of VH gene rearrangement may provide insights into the dynamics of the autoreactive repertoire, as increased VH rearrangements have been shown to correlate with the rescue of autoreactive clones (Burrows et al., 2020). Secondary rearrangements were quantified by identifying shared stem regions within BCR sequences (N-IgHD-N-IgHJ segments) within samples, clustering them by single-base similarity, and normalising their IgHV gene frequencies through repeated subsampling to enable cross-sample comparison. Belimumab showed reduced trends of VH gene replacement frequencies by M24 in IGHA1 (BLM 0.22% [95% confidence interval (CI) 0, 0.5] vs. PBO 1.73% CI[0.4, 3.05]), IGHA2 (BLM 0.86% CI[0.12, 1.6] vs. PBO 1.39% CI[0.07, 2.72]) and IGHD (BLM 0.07% CI[-0.008, 0.16] vs. PBO 0.16% CI[0.07, 0.25]).

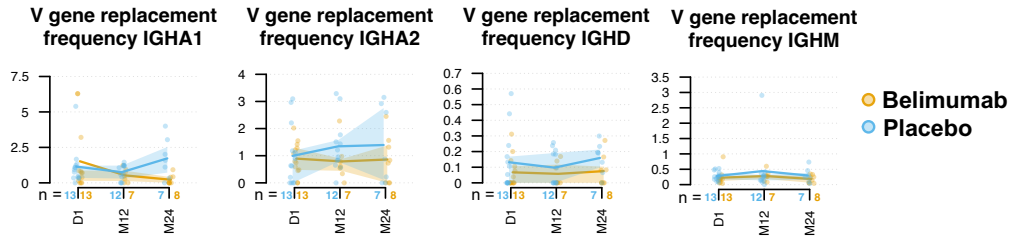

Figure 4.8: Level of secondary IGHV gene rearrangements. Logit-transformed data was analysed by ANCOVA (covariates: age, sex, prior cyclophosphamide), with permutation-derived p-values and FDR correction (all $p > 0.05$). Each point represents one patient. The solid lines represent the group mean for each treatment arm. The shaded bands indicate the inter-quartile range (IQR). n - number of patients per treatment arm at each timepoint (placebo in blue; belimumab in orange); D1 – day 1; M12 – month 12; M24 – month 24

4.3.11 Belimumab tends to reduce VH4-34 autoreactive B cells within the class-switched compartment

Given the inherent autoreactive properties of germline IGHV4-34 sequence (unmutated AVY/NHS motifs), its frequency per isotype and class-switch status was calculated (Figure 4.9). By M24, belimumab showed trends of reduction in the IGHA1 (BLM 0.88% vs. PBO 2.40%), IGHA2 (BLM 0.37% vs. PBO 1.80%), IGHG1 (BLM 0.42% vs. PBO 1.58%), IGHG2 (BLM 0.03% vs. PBO 1.74%) and overall class-switched compartment (BLM 0.62% vs. PBO 1.94%). The confidence intervals are reported in Table 4.5. This suggests that belimumab may reduce the pool of autoreactive clones within the class-switched repertoire.

Isotype	Timepoint	BLM mean (95% CI)	PBO mean (95% CI)
IGHA1	M24	0.88 (0.13, 1.63)	2.40 (0.00, 5.29)
IGHA2	M24	0.37 (0.02, 0.72)	1.80 (0.00, 4.58)
IGHG1	M24	0.42 (0.00, 0.90)	1.58 (0.05, 3.11)
IGHG2	M24	0.03 (0.00, 0.90)	1.74 (0.06, 3.24)
Class-switched	M24	0.62 (0.09, 1.14)	1.94 (0.00, 4.56)

Table 4.5: **Mean frequency (%) of IGHV4-34 by treatment group at M24.** Values represent group mean frequencies with 95% confidence intervals. BLM – Belimumab; PBO – Placebo.

4.3.12 Belimumab is comparable to placebo at levels of clonal persistence between D1 and M12 or M24

Since belimumab showed distinct trends of clonal expansion across timepoints and between isotypes, it was explored if the clonal persistence between was impacted. Therefore, the frequency of clonal overlap between baseline and later timepoints (M12 and M24) was calculated.

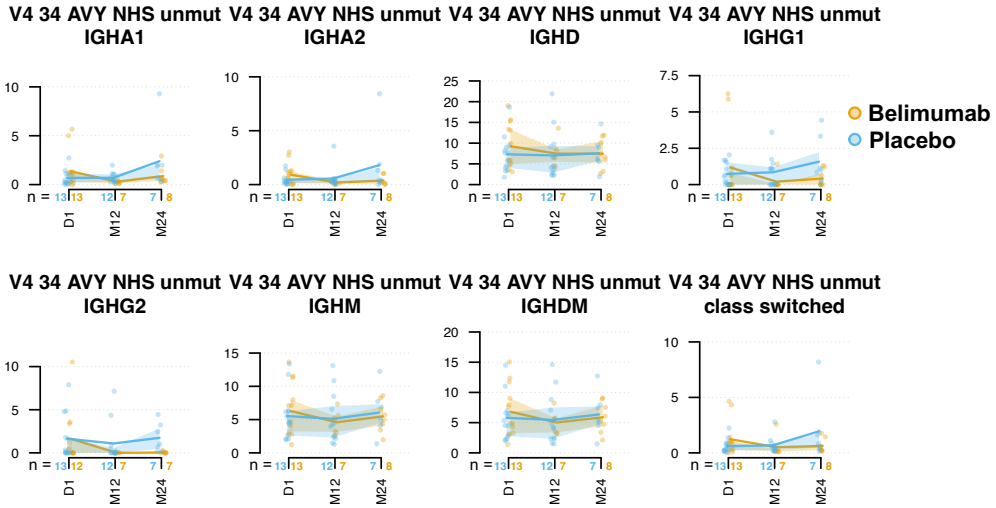

Figure 4.9: Percentage of VH4-34 AVY and NHS usage. Plots show the percentage of VH4-34 AVY and NHS gene usage within each isotype, expressed as a proportion of all VH genes for that isotype, or as the total VH4-34 usage among class-switched B cell clones per sample. Logit-transformed data was analysed by ANCOVA (covariates: age, sex, prior cyclophosphamide), with permutation-derived p-values and FDR correction (all $p > 0.05$). Each point represents one patient. The solid lines represent the group mean for each treatment arm. The shaded bands indicate the inter-quartile range (IQR). n - number of patients per treatment arm at each timepoint (placebo in blue; belimumab in orange); D1 – day 1; M12 – month 12; M24 – month 24

Belimumab had a similar degree of overlap comparable to placebo in switched and unswitched compartments, in both timepoint groups (D1-M12, D1-M24, $p > 0.05$, ANCOVA (covariates of age and sex) with FDR adjusted p-value for multiple testing, Table 4.6).

Group	**Timepoint (D1 vs.)**	**p-value (Treatment)**	**p-value (Age)**	**p-value (Sex)**
Unswitched	M12	0.447	0.097	0.156
Unswitched	M24	0.275	0.658	0.639
Switched	M12	0.767	0.145	0.318
Switched	M24	0.644	0.617	0.566
All	M12	0.846	0.044	0.920
All	M24	0.344	0.577	0.564

Table 4.6: **B cell class (unswitched/switched) clonal overlap across timepoints relative to D1 statistics.** The overlap of BCR sequences was calculated per treatment arm (BLM $n = 6$, PBO $n = 6$) between D1 - M12 and D1 - M24. The sequences were subsampled to a depth of 1000 reads per sample and the average of the overlap was calculated after 1000 iterations. ANCOVA with covariates of age and sex was calculated. Prior-cyclophospamide treated patients were removed prior to the analysis. D1 – day 1; M12 – month 12; M24 – month 24

4.4 Discussion

This chapter provides novel insights into how combined belimumab and rituximab therapy influences B cell receptor repertoire recovery in PR3-AAV. Through detailed quantitative analyses of repertoire structure, it reveals distinct patterns of repertoire reconstitution, underscoring the potential impact of BAFF modulation on the timing of recovery, isotype usage and the persistence of autoreactive B cell pools.

The BCR repertoire analysis from the COMBIVAS trial unexpectedly showed no statistically significant differences in global repertoire metrics, such as overall clonality or SHM, between the rituximab–belimumab and rituximab–placebo groups at the M12 and M24 reconstitution timepoints. This was surprising given the central hypothesis of the trial: that BAFF inhibition would selectively restrict the survival and maturation of autoreactive B cells emerging after rituximab-mediated depletion. Under this model, measurable differences in repertoire diversity, clonal structure, or mutational composition between treatment arms were anticipated.

Several factors likely account for the minimal divergence observed. Firstly, both groups received rituximab, which induces near-complete peripheral B cell depletion. This large, shared perturbation may overshadow the more subtle, longer-term modulatory influence of belimumab on reconstituting B cell subsets. However, minimal differences were seen between M0 and M12, suggesting that most repertoire reconstitution has already occurred by the time of sampling. Secondly, the small sample size (n=12–15 at each timepoint) substantially restricts statistical power.

Although not statistically significant, several trends in the repertoire data

are entirely consistent with the clinical results suggesting that belimumab delayed B cell reconstitution, contributed to deeper PR3-ANCA suppression, and trended toward reduced relapse risk. The repertoire analyses provide immunological context for these outcomes and suggest that belimumab may indeed shape the recovering B cell pool, but at a level not readily captured by bulk peripheral sequencing.

Detectable B cell recovery within 12 months after rituximab treatment has been associated with increased risk of PR3-AAV relapse (Alberici et al., 2015). Therefore, a desired outcome of the COMBIVAS trial was a delay in the B cell reconstitution after belimumab. COMBIVAS trial results confirmed B cell depletion after belimumab and placebo by month 3 and described a reduction in the detectable total B cells and naïve B cells, but not memory B cells, compared to placebo at M12 and M18 (COMBIVAS results report, data not shown). This is in agreement with previous reports in SLE where rituximab with belimumab hindered the reconstitution of naïve B cells but not that of memory or plasma cells (Kraaij et al., 2018).

Consistently, analysis of the BCR repertoire revealed a slight reduction in IGHD usage at month 24 compared with both baseline and placebo. This finding suggests that belimumab may limit the egress of BAFF-dependent naïve and potentially autoreactive B cells from the bone marrow. This observation is in agreement with known BAFF biology, as selection of naïve B cells in the periphery relies on BAFF (Rowland, Leahy, Halverson, Torres, & Pelanda, 2010), and with previous studies reporting reductions in the naïve B cell compartment following belimumab treatment in SLE (Jacobi et al., 2010; Stohl et al., 2012; Ramsköld et al., 2019).

Enrichment of PR3-reactive plasmablasts has been linked to an increased

risk of AAV relapse (Berti et al., 2023). It was hypothesised that belimumab might reduce the development of short-lived plasmablasts and therefore delay the memory repertoire recovery. Interestingly, by M12, class-switched isotype usage in the belimumab arm was largely comparable to that in the placebo arm, even with trends toward higher levels of IGHA1, IGHG2 and IGHG3 than placebo. However, except for IGHG2, these isotypes appeared to be less expanded than placebo, suggesting that belimumab may be associated with a faster early recovery of the switched B cell repertoire. Nevertheless, the current data do not allow direct conclusions about the plasmablast compartment.

At the repertoire level, belimumab compared to placebo produced higher trends in the overall B cell clonality at M12 (Vertex and cluster Gini index). In corroboration with the reduced counts of total B cells compared to placebo at M12 described above, it suggests that belimumab may contribute to a delay in the total B cell repertoire recovery. Although belimumab then showed comparable levels of overall B cell clonality at M24 between groups, trends toward slightly higher proportions in dominant clones (higher trend of percentage maximum clone and D5 after belimumab) support that belimumab might be superior to placebo in reducing the B cell repertoire reconstitution. However, persistence of dominant clones might not be a desirable effect if these are autoreactive. Encouragingly, belimumab showed trends of reduction in the autoreactive BCRs (reduced VH4-34 AVY-NHS usage in class-switched B cell compartment), suggesting a potential qualitative benefit in the repertoire composition.

Belimumab was associated with trends of altered isotype usage within the class-switched B cell compartment, with patterns of reduced proportions of IGHA2, IGHG2 and IGHG4 by M24, compared to placebo. These trends may reflect BAFF-dependent mechanisms of class switch recombination or a

skew in isotype-specific cellular survival.

Consistent with this pattern in SLE, clinical trials of combined rituximab and belimumab have also reported reductions in IGHA2 B cells and circulating IgA2 levels. Further mechanistic insights revealed that greater post-treatment reduction in IgA2 is suggested by higher BAFFR expression on IGHA2 plasmablasts compared to IGHA1, which may render IgA2-biased responses more vulnerable to BAFF blockade during reconstitution (McCluskey et al., 2025).

These observations fit with established biology in which T cell-independent (TI) pathways can drive switching in extrafollicular B cells (Litinskiy et al., 2002). Notably, IgA2 switching is particularly linked to TACI-mediated BAFF signalling and bacterial antigens in mucosal sites (Cerutti, 2008), while IgG2 is classically associated with responses to encapsulated bacteria, a canonical TI response (Vidarsson, Dekkers, & Rispens, 2014). In line with a selective impact on these compartments, clonality metrics further suggest a slower recovery of IGHA2 and IGHG2 after belimumab, as indicated by higher Vertex and cluster Gini indices at M12 and M24. These trends would be a favourable outcome, by preventing a rapid expansion of B cell clones. However, as mentioned before, the persistent expanded clones may be problematic if they are pathogenic. These findings align with prior observations which reported increased clonality metrics of IGHA B cells after rituximab treatment in AAV (Bashford-Rogers et al., 2019). Interestingly, the COMBIVAS cohort exhibited lower IGHA proportions both at baseline (∼14% vs. ∼30%) and after rituximab treatment (∼17% vs. ∼60%) compared with their study. Patient variability in the small sample size in our study (8 vs. 42 patients) could be attributed to the difference in IGHA percentage baseline. The difference in IGHA proportions post-rituximab could stem from the difference

in sampling timing (M12 and M24 vs. M3), as the AAV repertoires in their study may not have had sufficient time for a broader reconstitution, leading to a transient skew toward the IGHA1 isotype.

By M24, belimumab-treated patients exhibited higher proportions of hallmark memory isotypes IGHG1 and IGHA1 compared to placebo. The higher usage of IGHG1 appeared to be represented by a trend of more diverse clonal members compared to placebo, reflected by lower trends of B cell clonality (Vertex and cluster Gini index) at M24 in belimumab and similar representation of B cell clones in the highest expanded B cell compartments (%max clone and D5 is similar between belimumab and placebo). These findings suggest that IGHG1 compartment has recovered more rapidly and balanced after belimumab by M24. In addition, belimumab appeared to be superior at removal of VH4-34 autoreactive clones within the IGHG1 compartment (lower VH4-34 NHS AVY IGHG1 frequencies) than placebo. Conversely, IGHA1 clones appeared not only to be represented more after belimumab but also to be more clonally expanded (higher Vertex Gini index, D5) and with higher intra-clonal diversity (higher cluster Gini index). This suggests that belimumab could delay the recovery of IGHA1, but that persistent IGHA1 clones may remain after the treatment. V gene replacement has been associated with the 'redemption' of autoimmune B cell clones (Burrows et al., 2020). Belimumab showed lower trends in autoimmune 'redemption' (reduced V gene replacement frequency) of IGHA1 compared to placebo by M24, suggesting it might achieve a smaller initial autoreactive B cell pool. This aligns with the observed reduction trend of VH4-34 autoreactive IGHA1 clones in the belimumab arm.

Taken together, trends suggest that belimumab could influence long-term repertoire reconstitution in an isotype-specific manner, potentially limiting the

recovery of isotypes which might be more BAFF-dependent (IGHA2, IGHG2 and IGHG4). Conversely, belimumab might be sustaining the reconstitution or persistence of the most prominent memory isotypes in peripheral blood (IGHG1 and IGHA1). While a quicker IGHG1 repertoire recovery could drive the re-emergence of ANCA-positivity, it could also be advantageous in maintaining antimicrobial immunity and limit infections. The persistence of expanded IGHA1 clones could also pose pathogenic risk. Nevertheless, analysis of clonal sharing between baseline and M12/M24 was comparable between the treatment arms, suggesting that belimumab is not inferior at suppressing persistent clones.

The pathogenic circulating anti-PR3 antibodies are usually of the IgG isotype. Interestingly, clonality of IgG at baseline in this study appeared lower than other subtypes such as IgA, consistent with the dominance of IgA at M24. This suggests that clonal expansion in the pathogenic compartment may not be necessary to trigger disease. This is in agreement with a previous report where the clonal metrics at baseline in AAV were in fact not different than health, suggesting that AAV may be a polyclonal rather than strongly expanded B cell-driven response (Bashford-Rogers et al., 2019). Additionally, the data presented here are metrics of the peripheral blood B cell compartment, which may not mirror the circulating antibodies or recapitulate the cellular proportions within granulomatous lesions, where tissue-resident plasma cells and tertiary lymphoid structures are known to persist.

4.4.1 Statistical considerations

The statistical analysis of the BCR repertoire was inherently complex. The analysis pipeline generated multiple groups of metrics containing variables that could be correlated, independent, or interdependent (for example, com-

positional data where the sum of all rows equals 100%). This complexity was compounded by the clinical study design, which included sampling at three timepoints (D1, M12, and M24) across two treatment arms (BLM and PBO). The primary null hypothesis tested was that no difference existed between treatment arms at M24 across all metrics, after adjusting for age, sex, and prior cyclophosphamide treatment.

To address this, we conducted multivariate linear regressions for each group of related metrics, accounting for covariates at each individual timepoint. These models tested whether treatment had any effect on each group of metrics after adjustment for age, sex, and prior cyclophosphamide use. To examine treatment effects on individual metrics, we applied univariate linear models with permutation-based p-value testing.

To evaluate treatment effects over time (D1, M12, M24) while considering baseline values as covariates, I attempted a repeated-measures multivariate linear regression model. However, this approach required complete data across all metrics and timepoints for each participant. Missing data in any metric led to the exclusion of that participant or required data imputation. Imputation was not appropriate in cases where no prior patient data were available to inform missing values (e.g. absence of an entire isotype such as IGHG4 at baseline). Excluding participants with incomplete data substantially reduced statistical power (BLM $n = 2$, PBO $n = 2$). Consequently, I transitioned from multivariate analysis to a univariate linear mixed-effects model to better accommodate incomplete datasets. Nevertheless, the results were statistically non-significant across the metrics between the treatment arms.

Baseline differences between treatment arms were observed in several BCR repertoire metrics and were validated by flow cytometric analysis from the

COMBIVAS trial data (data not shown). This raised the question of whether subsequent timepoints should be statistically adjusted for baseline differences. However, because rituximab induced profound B cell depletion by month 3 in both treatment arms, the main factor influencing subsequent B cell repertoire reconstitution may actually be the individual response to rituximab rather than the repertoire composition at baseline. Nevertheless, in my analyses the baseline values were included as covariates in the statistical models to account for potential confounding, but the resulting p-values remained similarly non-significant. These findings suggest that although baseline variability existed, it was unlikely to explain the absence of statistically significant differences between treatment groups at M12 or M24 in the BCR repertoire metrics.

4.4.2 Limitations

The principal limitation of this study is its small sample size, which substantially reduced statistical power. A power calculation based on the observed relapse rates between treatment arms indicated that approximately 103 participants per arm would be required to achieve adequate statistical power (alpha = 0.05). In contrast, our study included a maximum of 8 longitudinal participants in the BLM arm and 7 in the PBO arm.

The absence of statistically significant differences between treatment arms should therefore be interpreted with caution, as the small sample size and incomplete longitudinal data limited the power of the analysis and prevented the use of full multivariate longitudinal models.

4.4.3 Future work

The integration of BCR repertoire with single-cell transcriptomic data could provide a more comprehensive understanding of how the B cell repertoire is reconstituted following rituximab and belimumab therapy. It would be particularly informative if matched tissue would be available for analysis. The interrogation of the BCR repertoire in tissue could address the dynamics of cellular migration between the blood and tissue, and could potentially resolve the questions regarding the selective recovery of specific isotypes in peripheral blood.

Further aims could include the correlation of clinical outcomes with the BCR repertoire features including relapse rates and clinical biomarkers. Furthermore, including light-chain sequencing in BCR analyses could enable further insights into the quality of immune reconstitution. These approaches would be particularly valuable for patient stratification, which could improve the timing of B cell–targeted therapies in AAV.

4.4.4 Conclusions

In summary, belimumab was associated with trends toward delayed overall B cell repertoire reconstitution compared with placebo, with more pronounced and selective effects across isotypes. Specifically, belimumab appeared to favour the recovery of IGHG1 and IGHA1 while limiting the reconstitution of IGHG2, IGHA2, IGHG4 and naïve B cell repertoires by M24. This pattern is consistent with belimumab's known role in modulating early B cell maturation and its dependence on T cell–independent pathways involved in class switching to IgA2 and IgG2. Furthermore, the observed trend toward a reduction in VH4-34–encoded autoreactive BCRs suggests a potential

qualitative improvement in repertoire composition, indicative of diminished autoreactivity. Although these findings did not reach statistical significance, they align with the proposed mechanism of belimumab in selectively depleting autoreactive and naïve B cells. Validation in larger longitudinal cohorts will be essential to confirm these effects and to clarify their implications for sustained immune tolerance and disease control in PR3-AAV.

5 | Pathogenesis of B cells in Psoriatic Arthritis

5.1 Introduction

Psoriatic arthritis (PsA) is a chronic inflammatory disease that affects both the skin and joints. PsA is mainly diagnosed through observation of joint pathology after a confirmed psoriasis (PsO) diagnosis, but clinical biomarkers remain largely limited. Critically, it is still poorly understood why only a subset of psoriasis patients progress to arthritis, and the molecular pathways that link the pathologies across the skin, joint, eye and other extra-articular sites (FitzGerald et al., 2021).

One promising avenue is the study of autoantibodies against joint antigens as potential connectors between the skin and synovial pathology. In rheumatoid arthritis (RA), B cells and plasma cells contribute to inflammation through autoantibodies (anti-cyclic citrullinated peptides (CCP) and rheumatoid factor (RF)) and these have been associated with disease progression (Sokolova, Schett, & Steffen, 2022; Smolen et al., 2018).

Although PsA has traditionally been considered 'seronegative' compared to RA, building evidence nuances that view. Up to 13% of PsA patients were found to be positive for RF and up to 21% for anti-CCP antibodies (Punzi et al., 2007; Ghazzali, Harch, Akasbi, Mezouar, & Harzy, 2022; Gruber et al., 2020; Eker, Pamuk, Pamuk, Dönmez, & Çakır, 2014; Rotondo, Corrado, Cici, Berardi, & Cantatore, 2021). PsA patients have also tested positive for autoantibodies against novel antigens such as LL-37 (including citrullinated or carbamylated forms) or ADAMTS-L5 (Ghazzali et al., 2022; Frasca, Palazzo,

Chimenti, Alivernini, et al., 2018; Wu, Yuan, & Tyring, 2019; Pouw et al., 2022). Anti-LL-37 antibodies correlate with disease activity in PsA but not in PsO. In addition, anti-LL-37 antibodies are elevated in both synovial fluid and plasma of PsA patients, but not in osteoarthritis (OA) or healthy controls (Frasca, Palazzo, Chimenti, Alivernini, et al., 2018; Frasca, Palazzo, Chimenti, Botti, et al., 2018). These data illustrate the heterogeneity of PsA, and motivate exploration of additional autoantibodies, their antigenic targets and functional roles in PsA pathogenesis.

Beyond serostatus, multiple lines of evidence suggest that B cell biology is active locally in PsA joints. Tertiary lymphoid structure formation is a feature prevalent in chronic inflammation, such as malignancy, infection or autoimmune diseases (L. Zhao et al., 2024). TLS have also been shown to form in PsA, and can display organised T-B segregation, $PNAd^{+}$ high endothelial venules and lymphoid chemokines such as CXCL13 and CCL21, providing the micro-anatomical prerequisites for germinal-centre-like reactions *in situ*. Importantly, regression of these lymphoid features with effective TNF blockade argues against pure bystander infiltration and supports potential pathogenic relevance (Cañete et al., 2007).

Consistent with this, single-cell profiling of PsA synovial tissue identifies B cell and plasma cell populations expression patterns indicative of an *in situ* infiltrating humoral compartment (Floudas et al., 2022).

Recent synovial-fluid multi-omics further reports increased B cell abundance in PsA compared with osteoarthritis, suggesting the inflammatory milieu in PsA and motivating a deeper characterisation of the infiltrating B cells (Tzemach et al., 2025).

Taken together, this evidence argues that PsA synovium can support organised,

potentially antigen-driven B cell responses even in the absence of classical circulating serological markers. This motivates a focused investigation of synovial B cells at the level of the B cell receptor (BCR) repertoire, where features such as clonal expansion, class switching and somatic hypermutation provide quantitative evidence of antigen experience and selection *in situ*. Resolving whether expanded synovial clones are autoreactive, and defining their cognate targets, will be critical to establish whether B cells contribute mechanistically to PsA pathology and to identify candidate biomarkers and therapeutic opportunities.

5.1.1 Chapter aims

PsA remains a debilitating and heterogeneous inflammatory disorder, yet the underlying cellular mechanisms driving its characteristic synovitis, particularly the contribution of B cells, are poorly understood. This lack of mechanistic clarity stands in sharp contrast to the established autoantibody-driven pathology of RA, leaving a critical gap in our ability to develop PsA-specific, B cell-targeted therapies. This chapter directly addresses this challenge by undertaking a high-resolution characterisation of the BCR repertoire within the PsA synovial tissue, the definitive site of pathology. By comparing the PsA BCR repertoire features with that of RA and evaluating the repertoire's modulation following anti-TNF treatment, this study seeks to fundamentally determine if B cells initiate or sustain pathogenic autoimmunity in PsA. Ultimately, this work is designed to identify the specific, clonally expanded, autoreactive B cell populations and their cognate protein targets, providing essential translational data for novel therapeutic development. To achieve this, this chapter investigates the following critical objectives:

1. Do the features of the BCR repertoire exhibit distinct characteristics

between PsA and RA?

2. Is the synovial BCR repertoire in PsA patients responsive to modulation by anti-TNF therapy?
3. Is there evidence of B cell clonal expansion within the PsA synovium?
4. Are clonally expanded B cells identified in the PsA synovium characterised by autoreactivity?
5. What are the specific protein targets recognised by these expanded B cell clones in the synovial tissue?

5.1.2 Experimental design

The CARTOGRAPHY study is a collaboration between the University of Oxford and Johnson & Johnson Innovation Medicine, which aimed to create a multi-omic atlas of blood and tissue across immune-mediated inflammatory disorders (IMIDs). For the purposes of the work presented in this thesis, I was granted access to a restricted subset of B cells within the CARTOGRAPHY dataset. The parent study generated multi-omic single-cell profiles through single-cell RNA sequencing (scRNA-seq), cellular indexing of transcriptomes and epitopes by sequencing (CITE-seq) and BCR V(D)J-sequencing across all cellular populations of peripheral blood mononuclear cells (PBMC) and synovial tissue across multiple IMIDs. The data made available to me encompassed only the B cell and plasma cell populations from the peripheral blood and synovial tissue of patients with PsA and RA.

Using the received subset of the CARTOGRAPHY study, the samples were integrated and the cell clusters were annotated. The features of the BCR V(D)J data were annotated and integrated into the single-cell object. Syn-

ovium B cell clones from patients with PsA were selected on the basis of (a) clonal expansion, (b) sharing between patients (public), (c) size of the clone, (d) λ light chain usage from which recombinant antibodies (rAbs) were generated.

The autoreactivity of the rAbs was assessed through screening on primary synovial cells derived from a patient with osteoarthritis and on healthy human dermal fibroblasts. To identify their protein targets, reactive rAbs were subsequently screened using human proteome microarrays (HuProt), which contain a library of more than 21,000 three-dimensionally folded human proteins.

5.2 Results

5.2.1 Bioinformatic integration and annotation of the B cell clusters from the joint-derived B cell samples of patients with RA and PsA

The CARTOGRAPHY dataset accessed contained B cell single cell multi-omic data from 14 patients with PsA and 14 patients with RA. Within each disease group, patients were further classified into those with a history of use of multiple disease modifying antirheumatic drugs (DMARDs), referred to as 'chronic' (n = 9 PsA, n = 10 RA), and those sampled at earlier stages of disease who were treatment-naïve and subsequently sampled again after tumour necrosis factor-inhibitor (TNFi) therapy (n = 5 PsA, n = 5 RA) (Figure 5.1a). Samples were collected from the synovium (joint-derived tissue) and peripheral blood mononuclear cells (PBMCs). However, not all patients had complete matched sets of tissue and PBMC data.

Overall, synovial samples contained higher numbers of B cells compared to the PBMC samples in both PsA (synovial mean: 527.9 cells/sample vs PBMC mean: 432.6 cells/sample) and RA (synovial mean: 590.9 cells/sample vs PBMC mean: 377.8 cells/sample). Of these, 14 PsA and 11 RA synovium samples contained $>$ 50 B cells, enabling statistical comparison (Figure 5.2). As a quality control measure, samples with fewer than 50 B cells were excluded from further analysis.

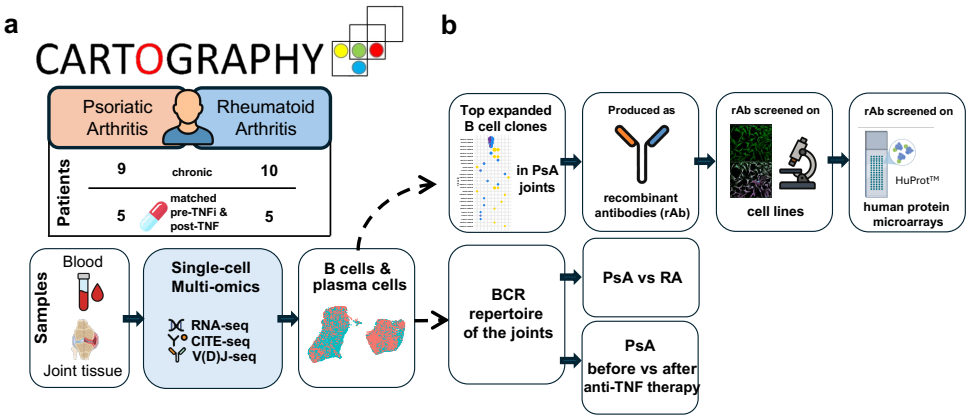

Figure 5.1: Schematic overview of the dataset used and methodology. **a** A subset of the CARTOGRAPHY project dataset of the University of Oxford in collaboration with Johnson & Johnson Innovative Medicine was accessed. This included single-cell multi-omic data (RNA-seq, CITE-seq and V(D)J-seq) of B cells and plasma cells from peripheral blood and joint tissue (synovium) of patients with psoriatic arthritis (PsA) and rheumatoid arthritis (RA). A subset of patients had a history of established treatments at baseline ($n = 9$ PsA, $n = 10$ RA), while the reminder were treatment-naïve and subsequently resampled following tumour necrosis-inhibitor (TNFi) therapy ($n = 5$ PsA, $n = 5$ RA). **b** Schematic overview of the data analysis and experimental approach included in this chapter; the B cell receptor (BCR) repertoire from the joints of patients with PsA and RA was contrasted; then, to address the role of the B cells in the pathogenesis of PsA, the top expanded B cell clones in the joints of the patients with PsA were identified; the BCRs of these top expanded clones were produced by a third-party company as recombinant antibodies (rAb); the rAb were screened for autoreactivity on cell lines using immunofluorescence microscopy; to characterise the targets of the expanded B cell clones in PsA, a few selected rAb were sent to be screened on HuProt microarrays comprised of a library of over 21,000 full-length, 3D human proteins. Diagram created with illustrations from NIAID NIH BioArt Source and Biorender.

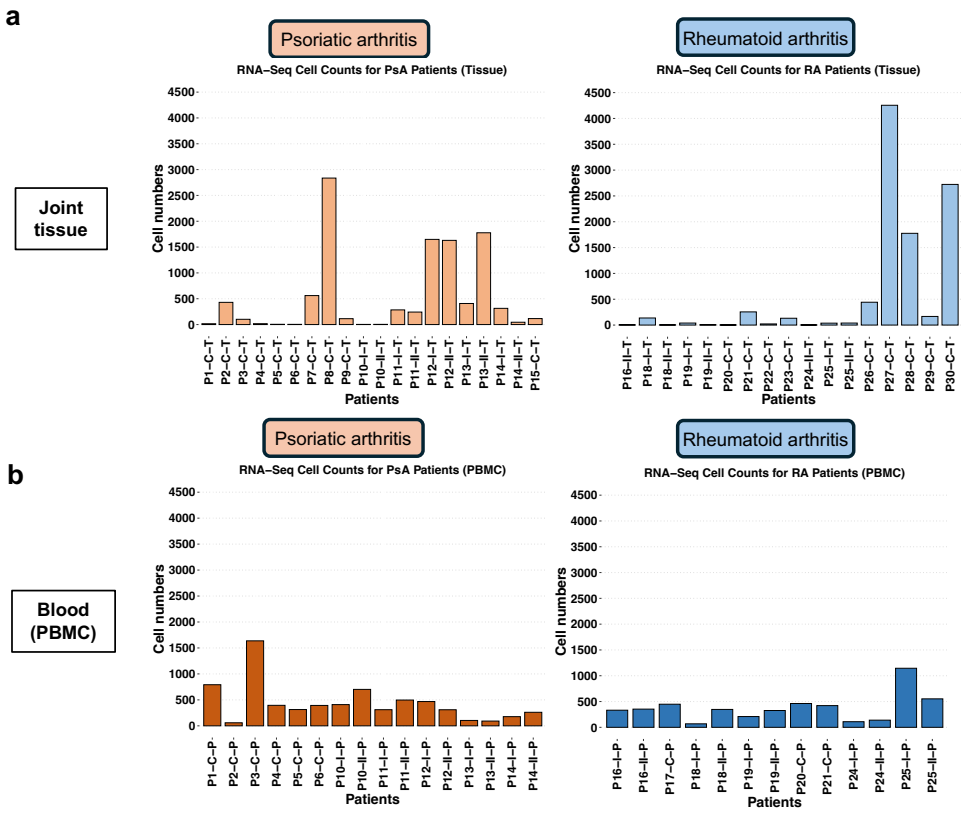

Figure 5.2: Overview of B cell numbers per patient based on the scRNA-seq data, stratified by sample origin and diagnosis. a Number of B cells from the joint-derived tissue of patients with psoriatic arthritis (PsA) and rheumatoid arthritis (RA) per sample. **b** Number of B cells from the peripheral blood mononuclear cells (PBMC) of PsA patients and RA patients per sample. Each bar represents one sample. Patient codes indicate treatment and disease stage ('-I' – pre-TNFi; '-II' – post-TNFi; '-C' – chronic) and sample type ('-P' – PBMC; '-T' – synovial tissue).

The joint-derived B cell samples were integrated and clustered

The primary objective of this study was to elucidate the role of infiltrating B cells in the synovium of patients with PsA. Therefore, the bioinformatic analysis focused on the integration and annotation of joint-derived samples, using RA as a disease control. Single-cell B cell RNA sequencing data were scaled and normalised, followed by sample integration using the Harmony

algorithm, using sample identifiers as a batch key. This approach achieved effective batch correction and integration as demonstrated by the Uniform Manifold Approximation and Projection (UMAP) visualisation plots coloured by Diagnosis and Sample ID (Figure 5.3a). The integrated dataset revealed two major B cell populations, which were further subdivided into six transcriptionally distinct clusters based on the variable features identified from the RNA-seq data (Figure 5.3b).

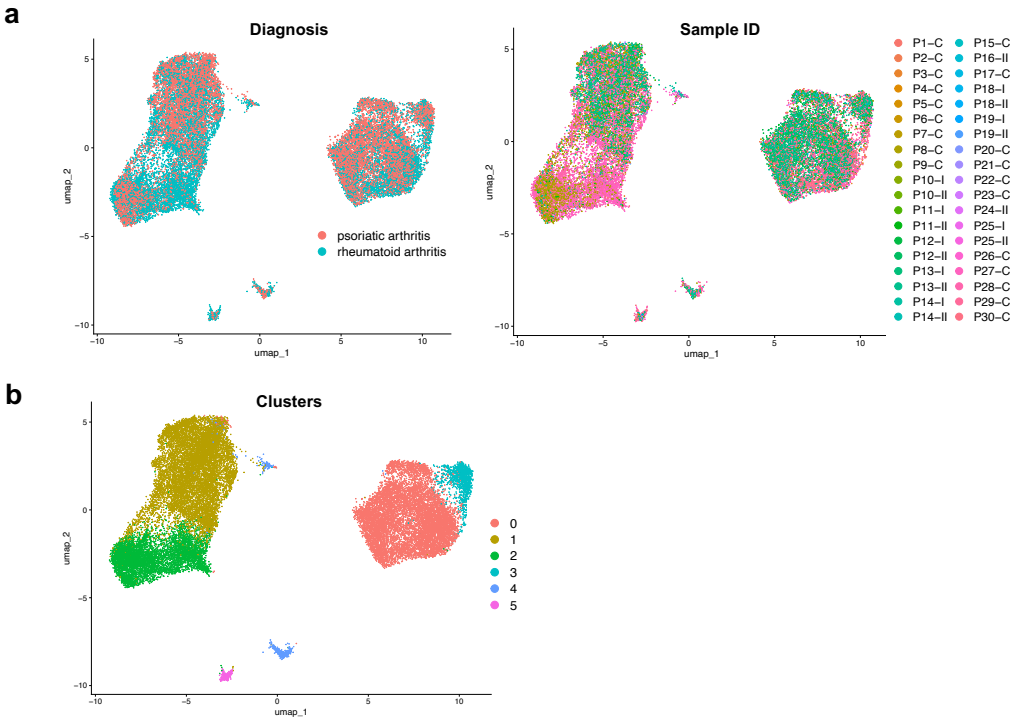

Figure 5.3: Integration and clustering of the B cell dataset from joint tissue only of psoriatic arthritis (PsA) and rheumatoid arthritis (RA) patients. a Uniform Manifold Approximation and Projection (UMAP) visualisation of B cells from the joint-derived tissue, coloured by diagnosis (PsA and RA) and by sample ID, after sample integration with Harmony algorithm; sample codes indicate disease stage: '-I' – pre-TNFi samples, '-II' – post-TNFi samples, '-C' – chronic patients. **b** UMAP cell cluster visualisation of $n = 21,670$ cells ($n = 11,249$ PsA, 14 patients; $n = 10,421$ RA, 15 patients) following sample integration. Each dot represents one cell.

B cell annotation delineates memory, naïve and plasma cells

The B cell clusters were annotated based on a combination of gene expression, cell surface protein levels and BCR V(D)J-seq signatures.

The large clusters (1 and 2) on the UMAP plot in Figure 5.3b displayed higher levels of somatic hypermutation (>15 mutations / BCR sequence, Figure 5.4a) and the highest expression of VDJ RNA sequences (>75th percentile of the VDJ unique molecular identifier (UMI), Figure 5.4b). These features suggest that clusters 1 and 2 predominantly contained plasma cells that express and secrete the largest volumes of antibodies, rather than non-antibody secreting B cell subsets. In support of this, the plasma cell clusters showed elevated gene expression of classical plasma cell marker *SDC1* (CD138), which distinguishes plasma cells from plasmablasts (Figure 5.4c), higher protein levels of CD38 and lower protein levels of CD20 (Figure 5.4d), compared with the other B cell clusters. The plasma cell clusters 1 and 2 were transcriptionally diverse and the differences between these clusters were determined. The top differential features in the plasma cell cluster 1 relative to the plasma cell cluster 2 were the following: increased levels of adhesion molecules VCAM-1 and CD99, tissue-homing and migration molecule β7-integrin and activation marker SLAMF7. Therefore, plasma cell cluster 1 was annotated as 'Activated/Homing Plasma cells' whereas cluster 2 was annotated as 'Plasma cells', indicating a lower activation and antibody secretion state (Figure 5.4f). Both of these plasma cell clusters contained preponderantly class-switched isotypes IGHG and IGHA (Figure 5.4e).

Cluster 3 was classified as 'Naïve B cells', marked by low levels of somatic hypermutation (predominantly 0-3 mutations per sequence, Figure 5.4a), low VDJ UMI abundance (<75%th percentile, Figure 5.4b), concentrated usage of IGHD/M isotypes (Figure 5.4e). In addition, cluster 3 was consistent

with naïve B cell gene expression and protein level profile as, in contrast to the other clusters, it showed increased levels of *IGHD*/IgD, *ABCB1*, *IL4R*, *TCL1A*, *FOXP1*, but lower levels of *CD27*/CD27, alongside lower levels of activation markers *CD80*, *CD86*/CD86, CD69 (Figure 5.4c-d).

The largest cluster (cluster 0) was annotated as 'Memory B cells', based higher CD20 and HLA-DR protein levels, reduced levels of CD38 (Figure 5.4d) and higher gene expression of *MS4A1* (CD20) and *CD27* (Figure 5.4c), compared to the other clusters.

The smaller cluster (cluster 5) had high expression of proliferation-associated genes, including *MKI67*, *PCNA*, and *CDK1* (Figure 5.4c), and was therefore annotated as 'Cycling B cells'. Finally, a small doublet cluster (cluster 4) containing both B cell and T cell signatures was observed and annotated as 'T cells - doublets'. This assignment was based on high expression of T cell receptor genes (*CD3D*, *CD3G*, *CD3E*, *TRAV16*, Figure 5.4c), together with T cell co-receptor genes (*CD4*, *CD8A*, *CD8B*) and elevated protein levels of CD28, CD4, and CD8 (Figure 5.4d), compared to the other clusters. The 'Cycling cells' and 'T cells - doublets' clusters were excluded from downstream analyses. The annotated clusters are shown in Figure 5.4f.

The memory B cell cluster was divided into 'switched' and 'unswitched' B cells

The annotation of the 'Memory B cells' cluster was refined and made more granular by distinguishing the 'switched' and 'unswitched' subtypes. The original memory B cell cluster (Figure 5.5a) was subsetted and re-clustered (Figure 5.5b), yielding two clear subclusters. The cluster with elevated expression of switched isotype genes (*IGHG1*, *IGHG2*, *IGHG3*, *IGHG4*, *IGHGA1*, *IGHA2* and *IGHE*) was labelled as 'Switched B cells', and the remaining

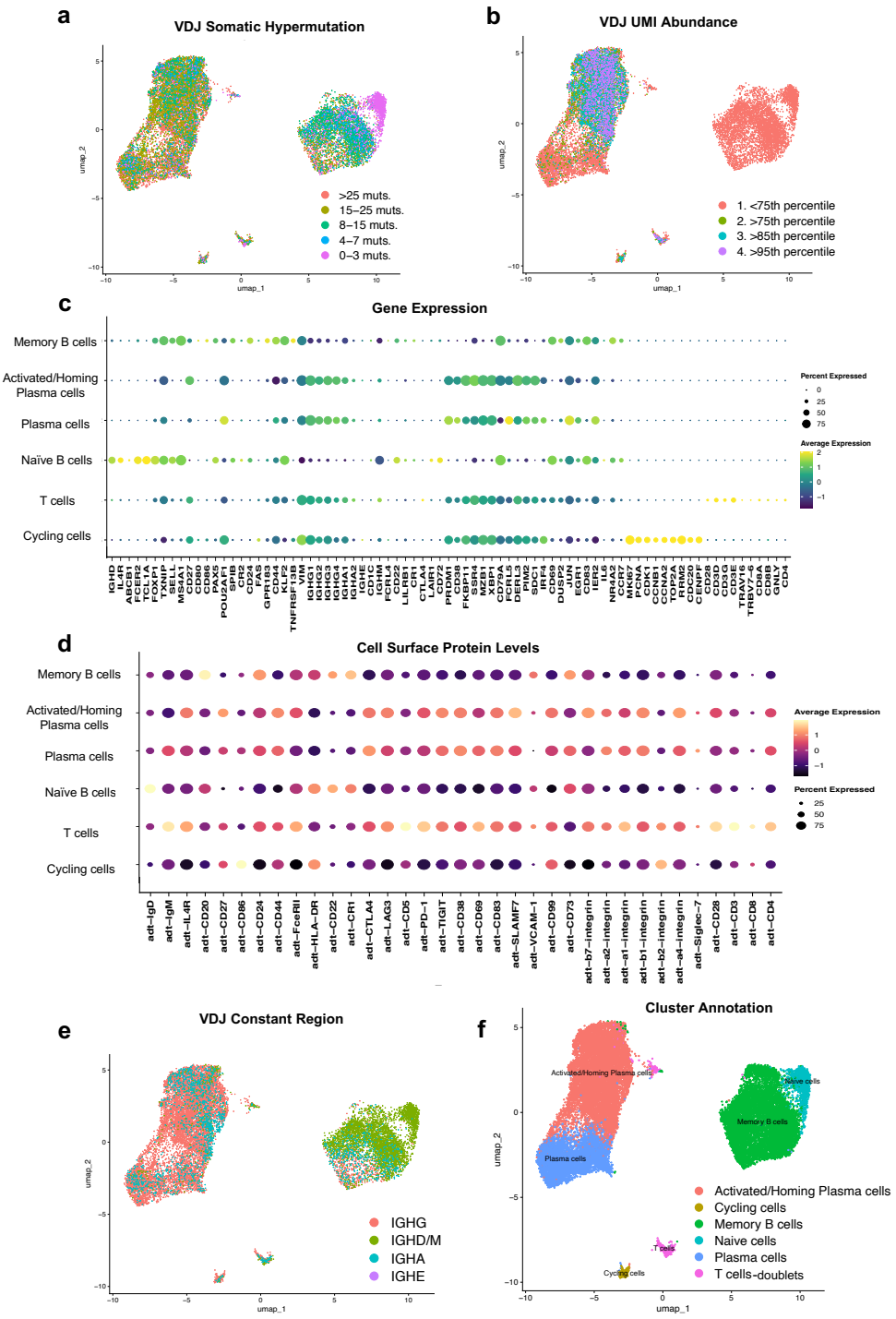

Figure 5.4: Memory B cell and plasma cell annotation from joint tissue only of psoriatic arthritis and rheumatoid arthritis patients *(see next page)*

Figure 5.4 ***(previous page)*****: Memory B cell and plasma cell annotation from joint tissue only of psoriatic arthritis (PsA) and rheumatoid arthritis (RA) patients.** Bioinformatic analysis on B cell clusters from joint- derived tissue comprised of $n = 21,670$ cells ($n = 11,249$ PsA, 14 patients; $n = 10,421$ RA, 14 patients). **a,b,e** UMAP plots coloured by the scV(D)J-seq data based on the following features: **a** the number of somatic hypermutations per V(D)J sequence; **b** percentile rank based on the total counts of V(D)J Unique Molecular Identifiers (UMIs) per cell;**e** the constant region of the main immunoglobulin isotype classes; each dot represents one cell. **c** Dot-plot of the gene expression features across B cell clusters; dot size is proportional to the gene expression frequency. **d** Dot-plot of the antibody-derived tag (ADT) features representing the cell surface protein levels across B cell clusters; dot size is proportional to the protein levels. **f** UMAP plot of the annotated cell clusters.

cluster as 'Unswitched B cells' (Figure 5.5c). The annotation was further refined at single cell-level using the scV(D)J-seq data. Memory B cells which expressed *IGHM* or *IGHD* were labelled as 'Unswitched B cells', whereas those expressing any other known isotypes were labelled as 'Switched B cells' (Figure 5.5d)

5.2.2 Exploratory comparison of the BCR repertoire features

PsA and RA share similar B cell repertoire features in the joint

To ensure comparability, the treatment-naïve samples were excluded from this analysis. The cellular composition and BCR repertoire features in the joint between psoriatic arthritis ($n = 10$) and rheumatoid arthritis ($n = 8$) were explored. No statistically significant differences in cell type composition, isotype usages, and SHM were observed between the two diseases in any cellular compartment ($p > 0.05$ for all comparisons, Wilcoxon rank-sum test with Benjamini–Hochberg (BH) correction, Figure 5.6a-c). However, a

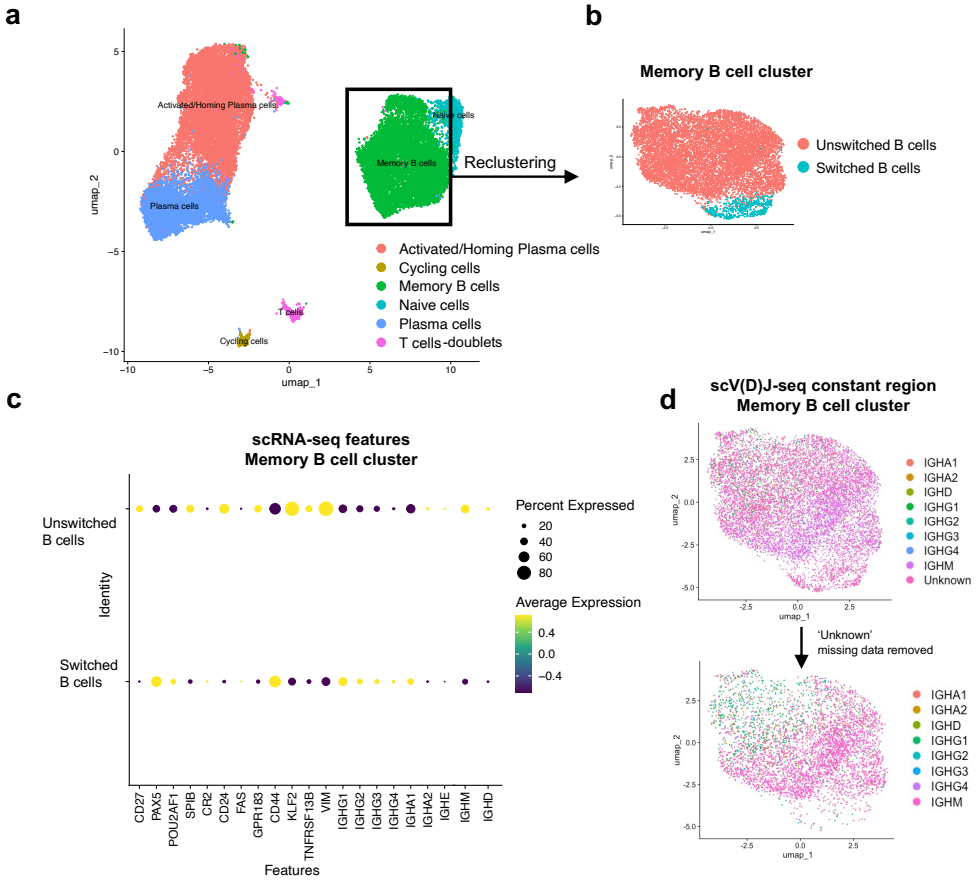

Figure 5.5: Annotation of the 'Switched' and 'Unswitched' memory B cell populations from joint tissue only of psoriatic arthritis (PsA) and rheumatoid arthritis (RA) patients. a Uniform Manifold Approximation and Projection (UMAP) of the annotated B cell clusters in the joint-derived tissue of PsA and RA patients. **b** UMAP of the reclustered memory B cell population. **c** Dot-plot representing the gene expression features of the memory B cell cluster; dot size is proportional to the gene expression frequency. **d** UMAP of the memory B cell cluster coloured by the scV(D)J-seq constant region of the immunoglobulin isotypes; each dot represents one cell.

trend was noted in PsA, with reduced plasma cell populations and increased unswitched memory B cell populations (Figure 5.6a). A trend towards increased IgM and decreased IgG isotype usage was observed in PsA (Figure 5.6b). The length and charge of the CDR3 did not differ significantly between RA and PsA ($p > 0.05$ for all comparisons, Wilcoxon rank-sum test with BH correction). However, IgA1 and IgM-expressing B cells in RA showed a trend towards longer CDR3 (Figure 5.6d) and more negatively charged CDR3 (Figure 5.6e).

To better understand the clonal expansion dynamics between PsA and RA, B cells were assigned clone IDs. Clone IDs were generated by assigning numeric codes to each unique heavy and light-chain CDR3 sequence and pairing them for each B cell. For each sample, the B cell clone with the highest number of members was calculated (maximum clone size) and expressed as a percentage of the total repertoire. RA samples displayed a trend toward larger maximum clone sizes compared with PsA, but the difference was not statistically significant ($p > 0.05$; Welch's two-tailed t test; Figure 5.6f).

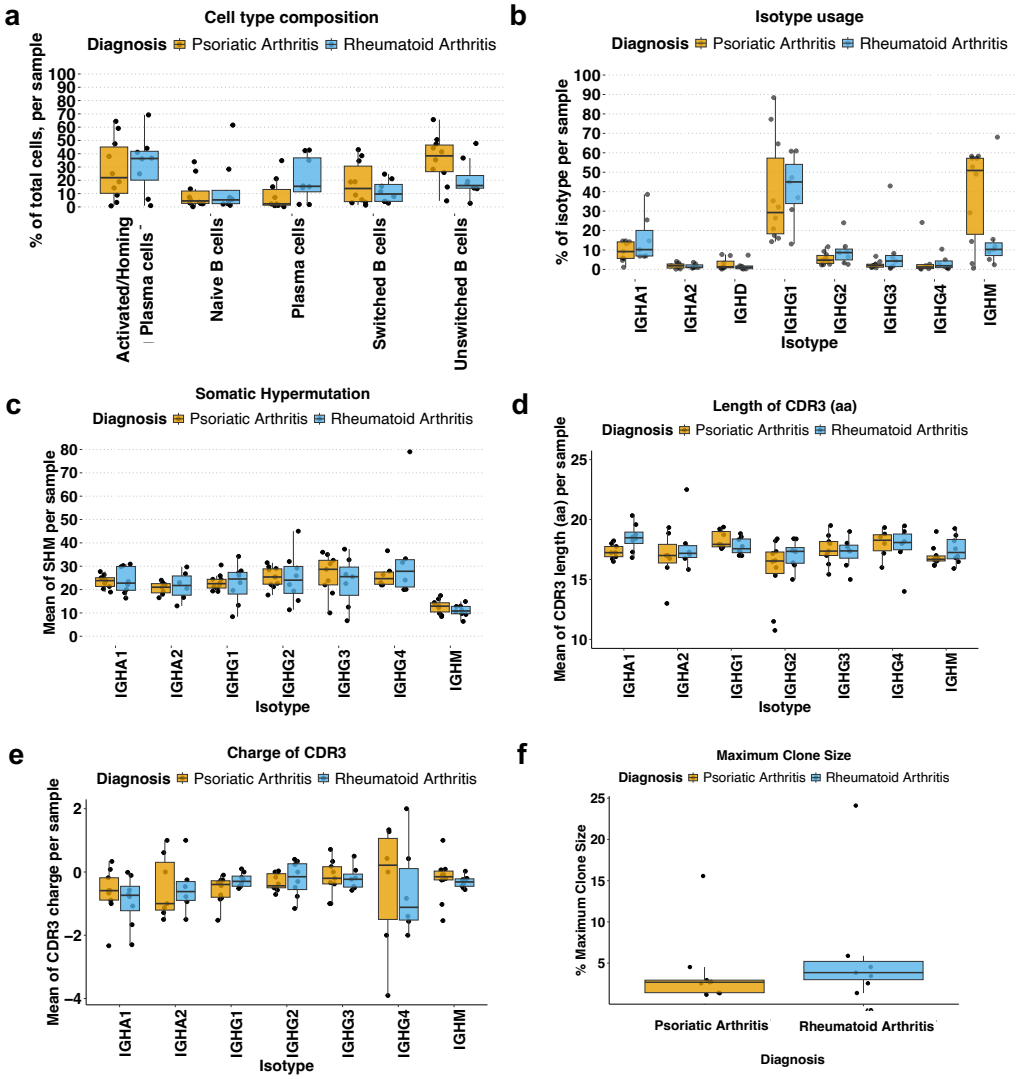

Figure 5.6: Comparison of the B cell repertoire features from joint-derived tissue samples of patients with psoriatic arthritis and rheumatoid arthritis *(see next page)*

Figure 5.6 ***(previous page)*****: Comparison of the B cell repertoire features from joint-derived tissue samples of patients with psoriatic arthritis ($n = 10$) and rheumatoid arthritis ($n = 8$). a** Box-plot of the B cell subtype composition as a percentage of total cells, per sample; each dot represents one sample; percentages were centre log-ratio (CLR) transformed prior to statistical testing; statistical comparisons between diagnoses were performed using the Wilcoxon rank-sum test with Benjamini- Hochberg (HC) correction for false discovery rate (FDR), ($p > 0.05$ for all comparisons, not significant). **b** Box-plot of the proportions of each isotype relative to the total isotype usage per sample; each dot represents one sample; values were centre log-ratio (CLR) transformed prior to statistical testing; global differences were assessed using multivariate analysis of variance (MANOVA) ($p > 0.05$, not significant), and isotype-specific comparisons between diagnoses were performed using the Wilcoxon rank-sum test ($p > 0.05$ for all comparisons, not significant). **c** Box-plot of the mean of somatic hypermutations per sample, stratified by immunoglobulin isotype of non-naïve B cells; each dot represents one sample; statistical differences between diagnoses were tested with Wilcoxon rank-sum test with BH correction for FDR ($p > 0.05$ for all comparisons, not significant). **d** Box-plot of the maximum clone size as a percentage of all clones, per sample; each dot represents one sample; percentages were logit-transformed before statistical analysis; differences between the diagnoses were assessed with Welch's two-tailed t test ($p > 0.05$, not significant). **e** Box-plot of the mean amino-acid (aa) length of mean complementarity-determining region 3 (CDR3) per sample and stratified by isotype of non-naïve B cells; global differences were assessed using MANOVA ($p > 0.05$, not significant); isotype-specific comparisons between diagnoses were assessed with a Wilcoxon rank-sum test with BH correction for FDR, ($p > 0.05$ for all comparisons, not significant). **f** Box-plot of the CDR3 charge per sample and stratified by isotype of non-naïve B cells; global differences were assessed using MANOVA ($p > 0.05$, not significant); isotype-specific comparisons between diagnoses were performed using the Wilcoxon rank-sum test with BH correction for FDR, ($p > 0.05$ for all comparisons, not significant). All patients included in this figure have previously received anti-rheumatic treatments. Box plots show the median with the interquartile range (IQR).

B cell clonal expansion and diversification are similar in PsA and RA

Gini and Shannon indices are metrics which can be applied to quantify BCR repertoire diversity. The Gini index measures inequality, with values close to 0 indicating an even distribution of clones, and values near 1 reflecting skewing, as a measure of clonal expansion. The Shannon index captures both diversity and distribution. Higher Shannon index values represent a repertoire with many unique B cells and balanced clone representation, whereas lower values indicate reduced diversity, dominated by one or a few expanded clones. B cell clonal expansion was observed in the synovium of both PsA and RA. The largest clones reached up to 120 members in PsA (∼16% of the repertoire; Gini index 0.15; Shannon index 3.64) and 500 members in RA (∼25% of the repertoire; Gini index 0.39; Shannon index 2.76) (Figure 5.7a). In contrast, B cells in the PBMC (blood) compartment were not highly expanded, with maximum clone sizes of 6 in PsA (Gini index 0.002; Shannon index 3.93) and 3 in RA (Gini index 0.008; Shannon index 3.92) (Figure 5.7b). No significant differences were detected in diversity indices between PsA and RA within either synovial or blood repertoires. However, both diseases showed significantly higher Gini indices and lower Shannon indices in the synovium compared with blood (PsA: $p = 0.001$ for both; RA: $p = 0.0003$ for both; Wilcoxon rank-sum test; Figure 5.7c).

Little clonal overlap across PsA or RA samples

Clonal overlap across PsA and RA synovial samples was assessed using the Jaccard index. The highest degree of overlap was observed between samples obtained from the same patient before and after TNFi therapy (Figure 5.8a). To further evaluate repertoire sharing in PsA synovium, samples with at least

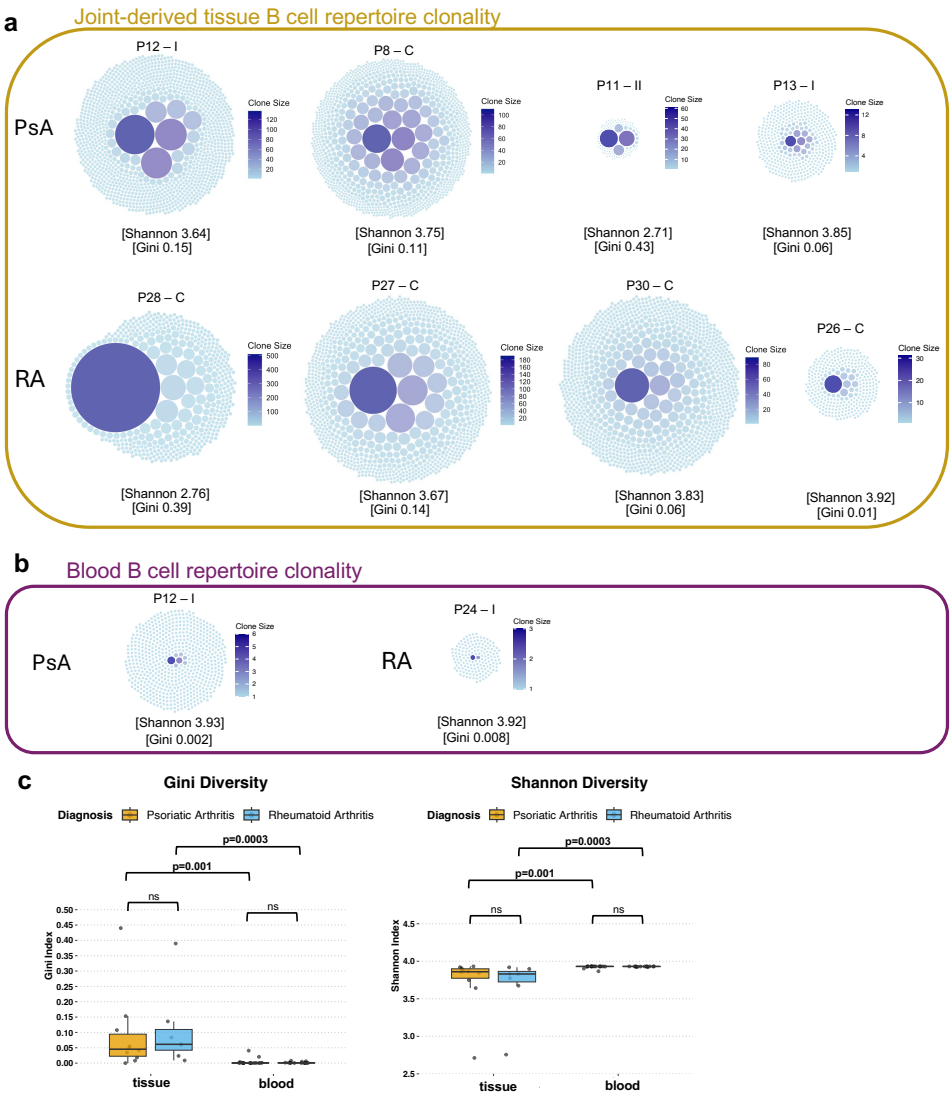

Figure 5.7: Comparison of the B cell repertoire clonality from joint-derived tissue and peripheral blood samples of patients with psoriatic arthritis (PsA) and rheumatoid arthritis (RA). a, b Bubble plots of selected patients showing B cell clonal expansion of patients with PsA and RA in a joint-derived tissue, and **b** peripheral blood, with bubble size proportional to clone size. Shannon and Gini diversity indices were averaged over 100 iterations of cell subsampling to the smallest cell count per patient. **c** Box-plots of the Shannon and Gini diversity indices of the B cell repertoires of patients with PsA ($n = 10$) and RA ($n = 8$) all previously treated with anti-rheumatic therapies. Statistical differences were tested using Wilcoxon rank-sum test. Box plots show the median with the interquartile range (IQR)

one B cell clone shared with a distinct sample were subsetted. Although clonal sharing was detectable, it remained very limited (Max Jaccard index <0.04 between any two samples; Figure 5.8b).

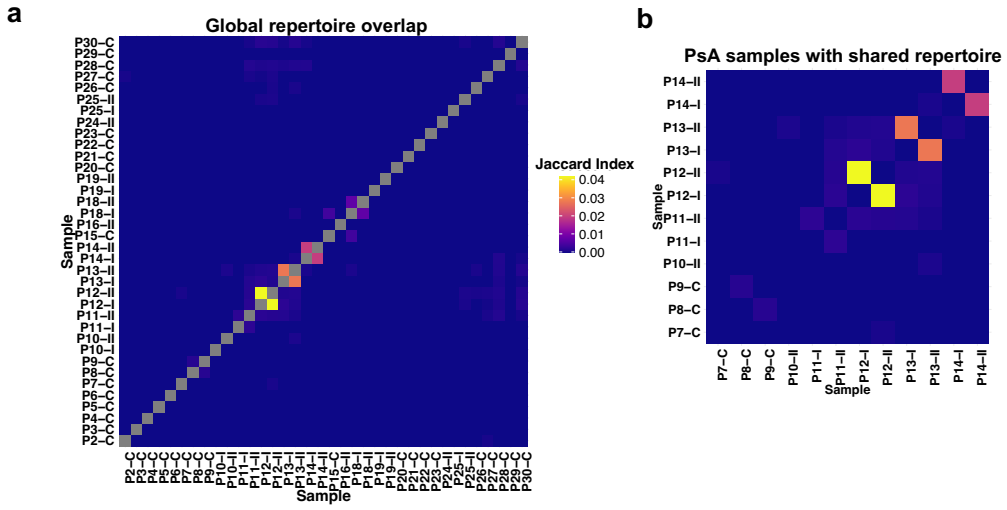

Figure 5.8: B cell clonal overlap across joint-derived tissue samples in patients with psoriatic arthritis (PsA) and rheumatoid arthritis (RA). a Jaccard index of the B cell repertoire overlap across all joint-derived tissue samples. PsA samples correspond to patients P2–P15; RA samples to P16–P30. **b** Jaccard index of B cell repertoire overlap between joint-derived samples from PsA patients with at least one shared clone. Sample codes indicate treatment and disease stage: '-I' – pre-TNFi, '-II' – post-TNFi, '-C' – chronic.

Anti-TNF therapy does not alter the cellular composition or B cell repertoire features in PsA

Since matched data were available from treatment naïve and post-TNFi therapy samples in the PsA synovium, the effects of the TNFi-therapy on the BCR repertoire were assessed. There was no significant difference recorded before and after TNFi-therapy in any of the metrics tested including cellular composition (Figure 5.9a), isotype usage (Figure 5.9b), somatic hypermutation levels on non-naïve B cells (Figure 5.9c), or clonality (Figure 5.9d) ($p > 0.05$

for all comparisons, Wilcoxon signed-rank test).

5.2.3 Investigating the pathogenesis of B cells in the joints of patients with PsA

5.2.3.1 Selection of putative-pathogenic B cell clones for recombinant antibody production

So far this chapter has shown that B cells not only infiltrate the synovium of patients with PsA, but are also clonally expanded, and include a substantial plasma cell compartment. To better understand the role of these B cells in the pathogenesis of PsA, I wanted to investigate whether the expanded B cells are autoreactive. To achieve this, I first selected B cell clones from clonal expansions, thus representing activated B cells and thus hypothesised to be enriched for pathogenic clones, to be then produced as recombinant antibodies. The selection criteria for B cell clones for downstream antibody expression and testing was (a) clonal expansion, (b) clonal sharing (public) of expanded clones between distinct individuals or between samples, (c) highest levels of clonal expansion, (d) clonal expansions using λ light chain, from which recombinant antibodies (rAbs) were generated.

B cell clones which had at least 2 members and represented over 1.5% of the total repertoire were denoted as 'top-expanded'. Since a limited number of PsA samples shared B cell clones (Figure 5.8b), the first strategy of selection of potentially pathogenic B cell clone was to identify the clones shared across multiple samples. The majority of the clones were either shared by the samples originating from the same patient, or they were not classed as 'top-expanded' (Figure 5.10a). However, one B cell clone (Clone ID 9428||all - 10283||all) was identified to be 'top-expanded' in two samples originating from the same

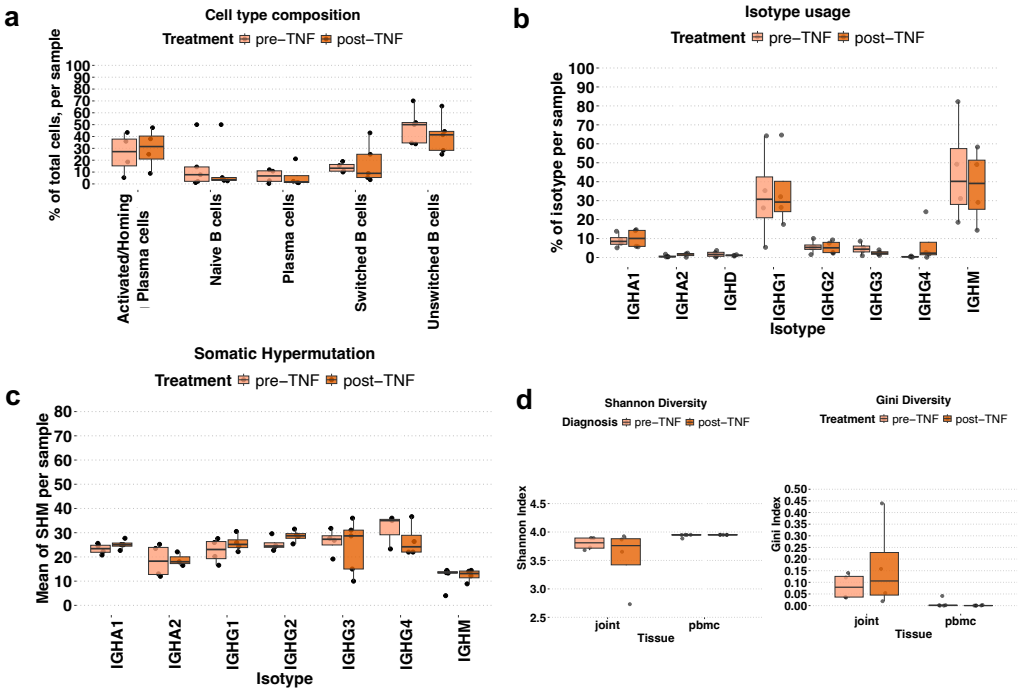

Figure 5.9: Comparison of the B cell repertoire features from joint-derived tissue samples of patients with psoriatic arthritis before ($n = 4$) and after TNF-inhibitor treatment ($n = 4$). **a** Box-plot of the B cell subtype composition as a percentage of total cells, per sample; each dot represents one sample; percentages were center log-ratio (CLR) transformed prior to statistical testing; statistical comparisons between treatment-status were performed using the Wilcoxon signed-rank test with Benjamini-Hochberg (HC) correction for false discovery rate (FDR), ($p > 0.05$ for all comparisons). **b** Box-plot of the proportions of each isotype relative to the total isotype usage per sample; each dot represents one sample; values were CLR transformed prior to statistical testing; isotype-specific comparisons between diagnoses were performed using the Wilcoxon signed-rank test ($p > 0.05$ for all comparisons, not significant). **c** Box-plot of the mean of somatic hypermutations per sample, stratified per isotype of non-naïve B cells; each dot represents one sample; percentages were CLR transformed prior to statistical testing; statistical differences were tested with a Wilcoxon signed-rank test with BH correction for FDR ($p > 0.05$ for all comparisons, not significant). **d** Box-plots of the Shannon and Gini diversity indices of the B cell repertoires; statistical differences were tested with a Wilcoxon signed-rank test ($p > 0.05$ for all comparisons, not significant). All box plots show the median with the interquartile range (IQR)

patient, and also present, but not expanded, in a sample from a distinct patient (Figure 5.10b,c). Clone 9428||all - 10283||all was therefore selected for recombinant antibody production.

Next, the largest expanded B cell clone of each sample was selected, followed by B cell clones which used λ light chains, given their association with autoreactivity (Figure 5.11). In total, 13 of the 26 top-expanded B cell clones identified in the synovium of patients with PsA were chosen for recombinant antibody production (rAb). These included 7 plasma cell–derived clones (Figure 5.12), representing a range of isotypes (1 × IgG4, 2 × IgA1, and 4 × IgG1; Figure 5.13), and 6 unswitched memory B cell clones (Figure 5.13). All selected clones exhibited mutations, consistent with a memory B cell subset, with average SHM ranging between 8 to 25 mutations (Figure 5.14). Notably, the members of the largest 2 clones (clone 9437||all-10283||all and clone 9428||all-10283||all) from patient P12 were closely related (Supplementary figure D.1), and therefore the germline revertant sequence (the predicted BCR sequence of its naïve B cell counterpart without SHM) of these clones was also selected for recombinant antibody production (rAb3). 4/13 selected B cell clones (rAb2, rAb5, rAb7 and rAb13) were also identified in peripheral blood (Supplementary Figure D.2).

5.2.3.2 Screening of rAbs derived from expanded B cell clones on human primary cells for autoreactivity

5/14 rAbs are reactive against fibroblasts

To test the autoreactivity of the rAbs, they were screened against primary cells from the synovium of an osteoarthritis (OA) patient and against healthy dermal fibroblasts. These fibrotic cells represented the approximate antigenic landscape experienced by synovial B cells. Of the 14 antibodies tested,

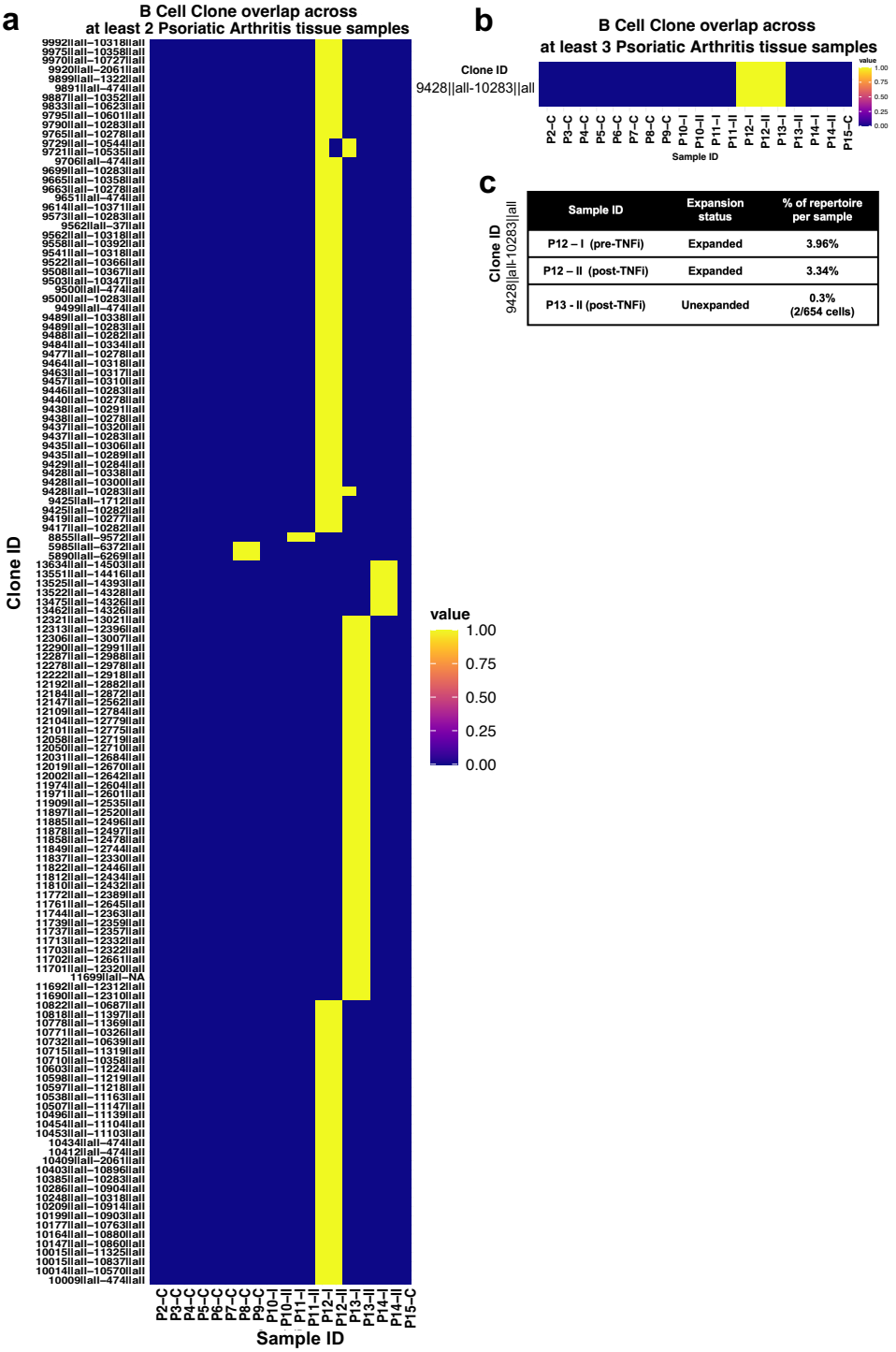

Figure 5.10: B cell clonal overlap across joint-derived samples from patients with psoriatic arthritis (see next page)

Figure 5.10 ***(previous page)*****: B cell clonal overlap across joint-derived samples from patients with psoriatic arthritis (PsA). a, b** Presence (yellow) or absence (blue) of B cell clones detected **a** in at least two PsA joint-derived samples or **b** in at least three PsA joint-derived samples. **c** Table summarising the expansion status and the clone percentage of total clones per sample of the clone detected across all three samples in **b**. Sample codes indicate treatment and disease stage: '-I' – pre-TNFi, '-II' – post-TNFi, '-C' – chronic.

8 antibodies (rAb1, rAb2, rAb3, rAb5, rAb9, rAb10, rAb11 and rAb13) displayed visual fluorescent signal against the OA-derived synovial cells. Among these, rAb1, rAb9 and rAb11 exhibited no visible signal on healthy dermal fibroblasts (Figure 5.15a). Statistical analysis revealed that the median values of normalised mean intensity of five rAbs (rAb2, rAb3, rAb5, rAb10, and rAb13) against the dermal fibroblasts, and three rAbs (rAb2, rAb3, rAb5) against OA primary cells, were significantly higher than those of the isotype control ($p < 0.012$, Kruskal–Wallis test with Dunn's post hoc and Bonferroni correction; Figure 5.16b). In surface-staining experiments, only rAb10 displayed a visible signal (Figure 5.15b). Statistical analysis showed that the mean normalised signal of rAb10 was not significantly different from the isotype control ($p = 0.06$, Kruskal–Wallis test with Dunn's post hoc and Bonferroni correction; Figure 5.17b). However, the antibody binding pattern was not uniform and was observed in a restricted cell number across the well. To better capture the sparse signal distribution, the percentage of cells that were positively stained was also calculated providing a more representative measure than median values. A positive signal was defined as any value exceeding the highest raw signal detected in the isotype control. An average of 17% of cells positively stained by rAb10 (Figure 5.17b). This data indicates that rAb1, rAb2, rAb3, rAb5, rAb9, rAb10, rAb11 and rAb13 are reactive to

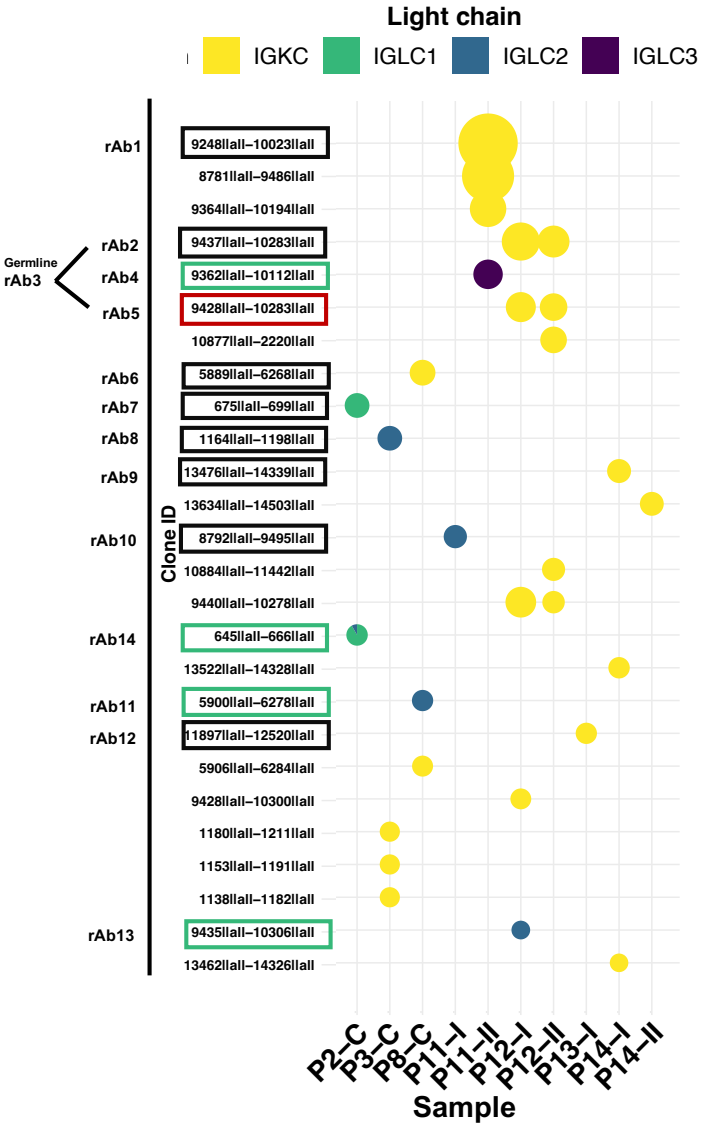

Figure 5.11: Light chain usage of the top-expanded B cell clones in joint-derived tissue from patients with psoriatic arthritis. Clones with ≥2 members and >1.5% repertoire representation per sample were defined as 'top-expanded'. Pie plots are coloured by light chain usage; pie size corresponds to clone size, and clones are ordered per patient from largest (top) to smallest (bottom). The clones highlighted with a box outline were selected for recombinant antibody (rAb) production. Clone selection was based on presence across multiple patients (red), the largest expanded clone per sample (black) and λ light chain usage (green). The rAb codes are shown in the far-left column. Sample codes indicate treatment and disease stage: '-I' – pre-TNFi, '-II' – post-TNFi, '-C' – chronic.

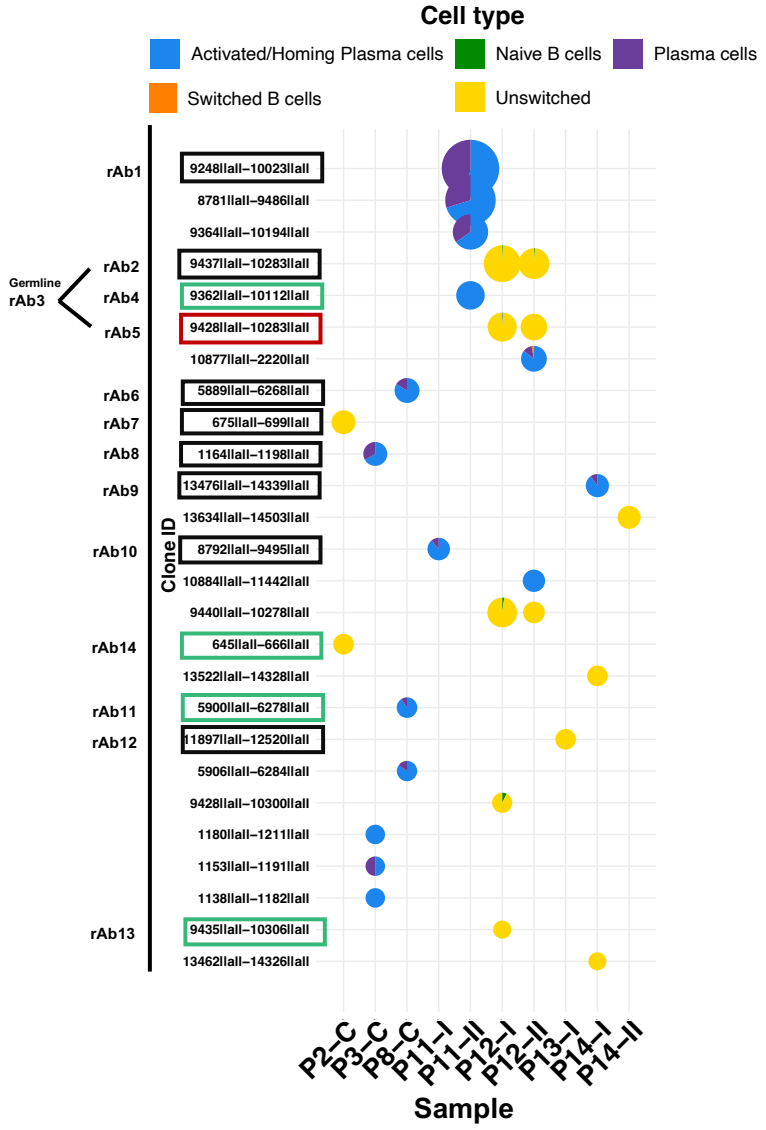

Figure 5.12: Cell types of the top-expanded B cell clones in joint-derived tissue from patients with psoriatic arthritis. Clones with ≥2 members and >1.5% repertoire representation per sample were defined as 'top-expanded'. Pie plots are coloured by cell type; pie size corresponds to clone size, and clones are ordered per patient from largest (top) to smallest (bottom). The clones highlighted with a box outline were selected for recombinant antibody (rAb) production. Clone selection was based on presence across multiple patients (red), the largest expanded clone per sample (black) and λ light chain usage (green). The rAb codes are shown in the far-left column. Sample codes indicate treatment and disease stage: '-I' – pre-TNFi, '-II' – post-TNFi, '-C' – chronic.

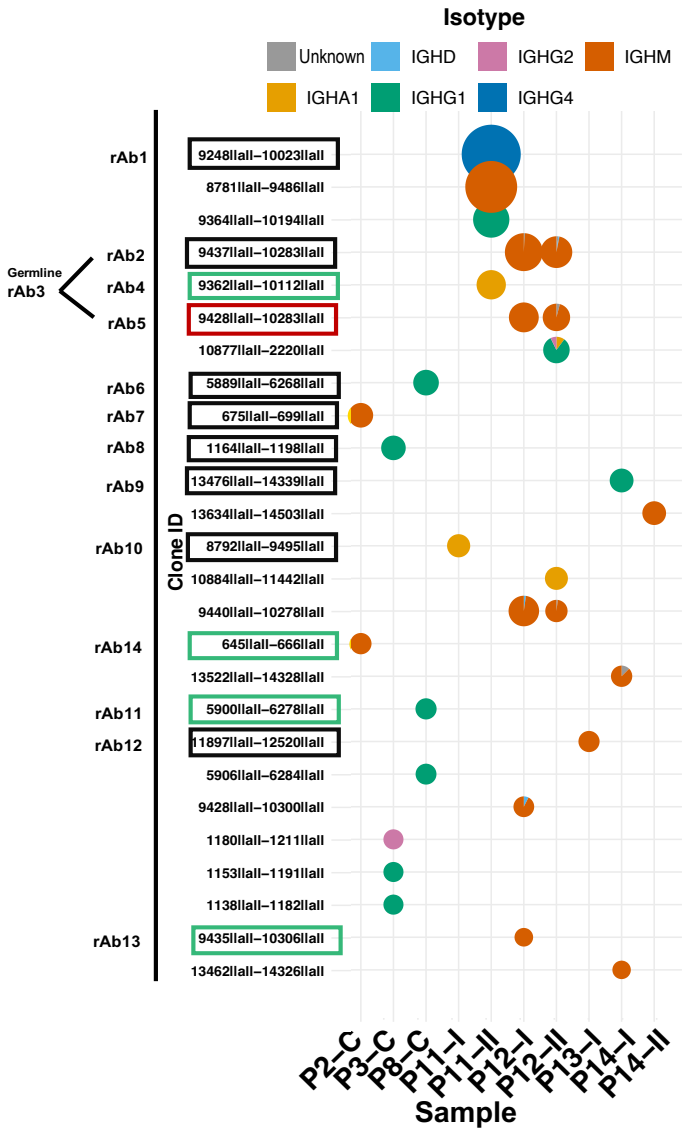

Figure 5.13: Isotypes of the top-expanded B cell clones in joint-derived tissue from patients with psoriatic arthritis. Clones with ≥2 members and >1.5% repertoire representation per sample were defined as 'top-expanded'. Pie plots are coloured by isotype usage; pie size corresponds to clone size, and clones are ordered per patient from largest (top) to smallest (bottom). The clones highlighted with a box outline were selected for recombinant antibody (rAb) production. Clone selection was based on presence across multiple patients (red), the largest expanded clone per sample (black) and λ light chain usage (green). The rAb codes are shown in the far-left column. Sample codes indicate treatment and disease stage: '-I' – pre-TNFi, '-II' – post-TNFi, '-C' – chronic.

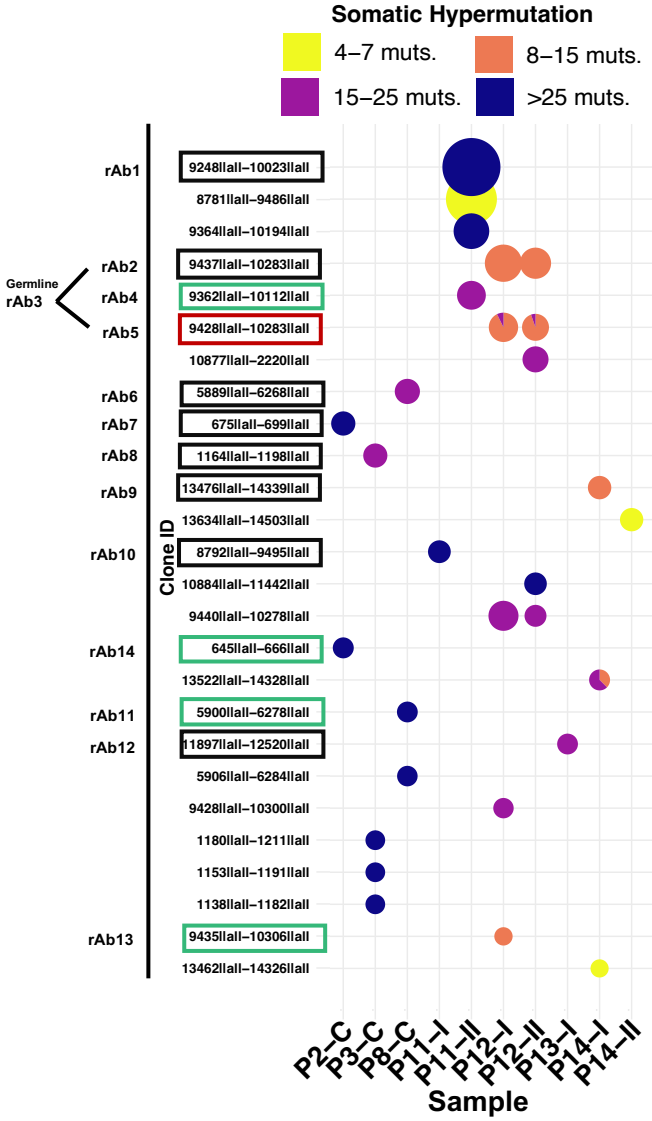

Figure 5.14: Somatic hypermutation of the top-expanded B cell clones in joint-derived tissue from patients with psoriatic arthritis. Clones with ≥2 members and >1.5% repertoire representation per sample were defined as 'top-expanded'. Pie plots are coloured by somatic hypermutation; pie size corresponds to clone size, and clones are ordered per patient from largest (top) to smallest (bottom). The clones highlighted with a box outline were selected for recombinant antibody (rAb) production. Clone selection was based on presence across multiple patients (red), the largest expanded clone per sample (black) and λ light chain usage (green). The rAb codes are shown in the far-left column. Sample codes indicate treatment and disease stage: '-I' – pre-TNFi, '-II' – post-TNFi, '-C' – chronic.

skin or synovium-derived fibroblast proteins, suggesting their autoreactive potential and warranting further investigation.

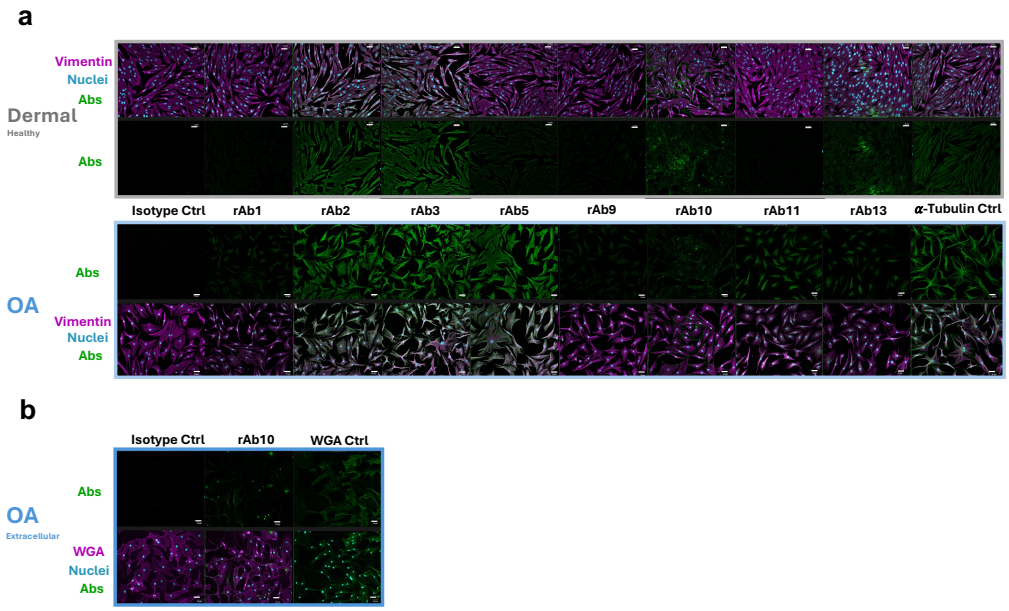

Figure 5.15: Immunofluorescence microscopy of recombinant antibodies (rAb) derived from psoriatic arthritis patients. The antibodies (Abs) were screened on primary cells derived from the joint of an osteoarthritic (OA) patient and on healthy dermal fibroblasts. The images were acquired with a 10x objective on a confocal microscope; scale bar is 50 µm. Only the rAbs which visually showed positive signal in at least one cell line are shown. A mouse IgG2 isotype was used as negative control (Ctrl). **a** Images representative of intracellular and extracellular staining experiments. The cells were fixed and permeabilised with methanol to allow for both intra- and extracellular staining with the rAbs and vimentin. A mouse alpha-tubulin primary antibody was used a positive control in the green channel. **b** Images representative of extracellular only staining experiments. The cells were fixed with 4% paraformaldehyde prior to their extracellular staining with the rAbs and wheat germ agglutinin (WGA). Single WGA - AF488 staining was used as a positive control in the green channel. rAb – recombinant antibodies derived from psoriatic arthritis patients; Abs – antibodies; Ctrl – control; WGA - wheat germ agglutinin.

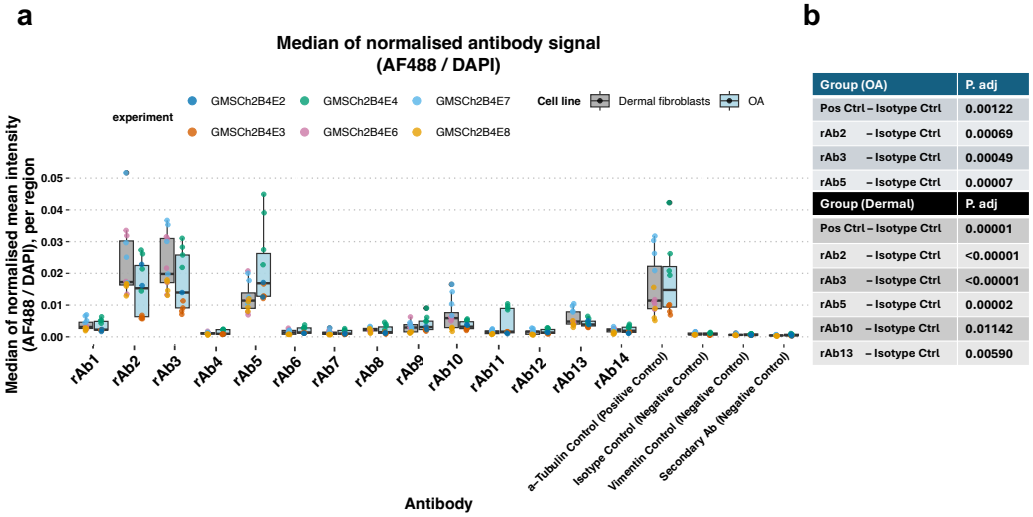

Figure 5.16: Intracellular and extracellular mean intensity fluorescence of recombinant antibodies (rAb) derived from psoriatic arthritis patients. The antibodies (Abs) were screened on primary cells derived from the joint of an osteoarthritic (OA) patient and on healthy dermal fibroblasts. The cells were fixed and permeabilised with methanol to allow for both intra- and extracellular staining with the rAbs and vimentin. A mouse IgG2 isotype was used as negative control (Ctrl). **a** Data shown is representative of three independent experiments for each cell line; each dot represents the median of normalised mean intensities of one area acquired microscopically as part of an independent experiment; the normalised mean intensity was calculated as the mean intensity of rAb / mean intensity of nucleus per cell. **b** Statistically significant adjusted p-values are shown for the comparisons in the adjacent plot; a Kruskal– Wallis test, followed by Dunn's post-hoc test with Bonferroni correction, was used to assess differences between the rAb signal and the isotype control, including the cell line as a covariate; no significant differences were observed between cell lines within any rAb group ($p > 0.05$, all rAb groups). Box plot shows the median with the interquartile range (IQR)

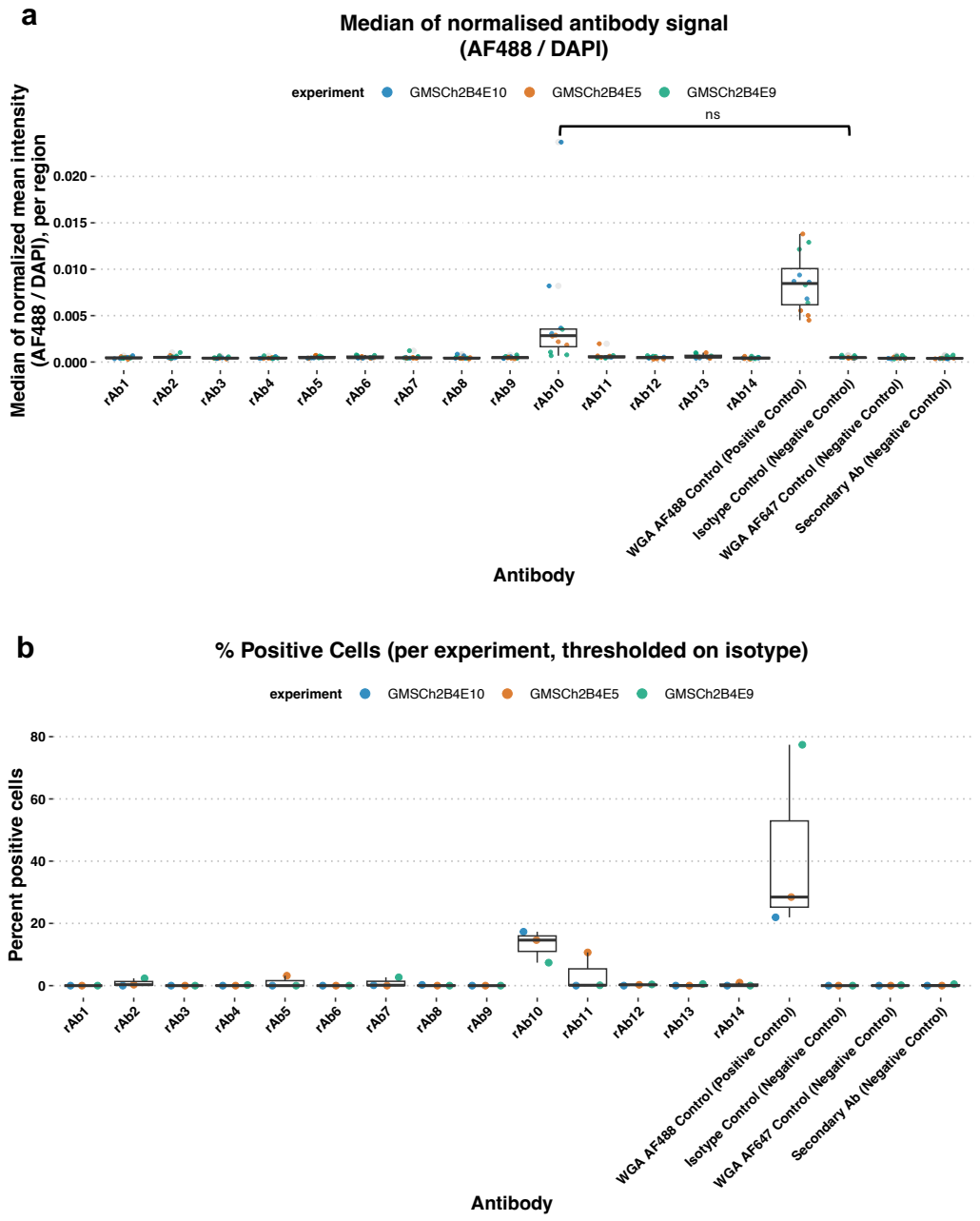

Figure 5.17: Extracellular signal of mouse anti-human IgG2 recombinant antibodies derived from psoriatic arthritis patients *(see next page)*

Figure 5.17 ***(previous page)*****: Extracellular signal of recombinant antibodies (rAb) derived from psoriatic arthritis patients.** The antibodies were screened on primary cells derived from the joint of an osteoarthritic (OA) patient. The cells were fixed with 4% paraformaldehyde prior to their extracellular staining with the rAbs and wheat germ agglutinin (WGA). Single WGA - AF488 staining was used as a positive control in the green channel. A mouse IgG2 isotype was used as negative control (Ctrl). **a** Data shown is representative of three independent experiments; each dot represents the median of normalised mean intensities of one area acquired microscopically as part of an experiment; the normalised mean intensity was calculated as the mean intensity of rAb divided by the mean intensity of nucleus per cell; differences were assessed with a Kruskal-Wallis test followed by Dunn's post-hoc test with Bonferroni correction for multiple testing (rAb10-isotype control $p > 0.05$, not significant) **b** The positive signal threshold was established as the maximum mean intensity fluorescence value of the isotype control per experiment; the percentage of positive cells was calculated per experiment. Box plots show the median with the interquartile range (IQR). rAb – recombinant antibodies derived from psoriatic arthritis patients; Abs – antibodies; Ctrl – control; WGA - wheat germ agglutinin.

5.2.3.3 Screening of fibroblast-reactive synovial-derived recombinant antibodies on HuProt microarrays

Several rAbs derived from PsA synovial tissue B cell clones displayed reactivity against one or both fibroblast cell lines tested, suggesting potential targeting of fibroblast-associated antigens. Understanding what proteins these antibodies bind to would provide information on the nature of inflammation and B cell involvement in the synovial environment in PsA.

A subset of 7 rAbs was selected for screening on unbiased, human protein microarrays (HuProt). HuProt microarrays contain a library of over 21,000 three-dimensionally folded full-length human proteins and isoforms. The selection of rAbs was based on statistical significance using the Kruskal–Wallis test with Dunn's post hoc analysis (Figure 5.16b). Additionally, rAbs that

displayed visible binding signal (Figure 5.15) and were significantly different from isotype controls as determined by pairwise Wilcoxon rank-sum tests FDR-adjusted, were also included (rAb1: $p = 0.001$; rAb9: $p = 0.001$; rAb11: $p = 0.007$). Because rAb2 and rAb5 derive from closely related clones and share the same germline revertant sequence (rAb3; Supplementary Figure D.1), only rAb3 (the germline revertant) and rAb5 (the most divergent from germline) were advanced for microarray-based protein-binding profiling.

High-throughput identification of rAb-specificities via HuProt microarray screening

Following the HuProt microarray, the proteins which had log2 Z-score > 5 and raw mean fluorescence intensity (MFI) > 100 was considered a hit. The raw MFI was represented as relative affinity categories as follows: 1 - weak, MFI < 1000; 2 - moderate, $1000 \leq$ MFI $< 10{,}000$; and 3 - high, MFI $\geq$ 10,000. The top 2 hits across each of the rAbs were as follows: rAb1 [**PIBF1** (Z-score: 13.9, MFI: 185), **FBXO2** (Z-score: 11.5, MFI: 131)]; rAb3 [**IGHG1** (Z-score: 28.1, MFI: 5677), **HEL-214** (Z-score: 20.27, MFI: 1297)]; rAb5 [**IGHG1** (Z-score: 28.7, MFI: 5037), **HEL-214** (Z-score: 19.27, MFI: 908)]; rAb9 [**NECAB3** (Z-score: 20.7, MFI: 1093), **GAMT** (Z-score: 14.7, MFI: 383)]; rAb10 [**FBXO2** (Z-score: 19, MFI: 2046), **CASQ1** (Z-score: 11.3, MFI: 356)]; rAb11 [**CTNNA2** (Z-score: 25, MFI: 828), **FAF1** (Z-score: 18.7, MFI: 349)]; rAb13 [**COPE** (Z-score: 31, MFI: 11347), **FAP** (Z-score: 30.7, MFI: 10739)]. The rest of the hits are reported in Figure 5.18. The reactivity profile of rAb5 was almost identical to its germline revertant rAb3. Protein hits which appeared across different rAbs are: **COPE** (rAb13 and rAb9 (Z-score: 9.7, MFI: 158), **FAP** [rAb13 (Z-score: 30.7, MFI: 10739) and rAb9 (Z-score: 8.3, MFI: 124)], **FBXO2** [rAb10 (Z-score: 19, MFI: 2045), rAb1

(Z-score: 11.5, MFI: 131)] and **ACVR1** [rAb13 (Z-score: 7.9, MFI: 137), rAb10 (Z-score: 6.8, MFI: 135)].

Common targeted proteins are cytosolic and involved in cell migration or amino acid metabolism

Among the 7 rAbs, a higher number of targets were intracellular, compared to extracellular (61 intracellular proteins; 12 extracellular proteins). However, the intracellular targets were not significantly enriched in any rAbs ($p > 0.05$; two-sided Fisher's exact test). rAb3 ($p = 0.007$; two-sided Fisher's exact test) and rAb5 ($p = 0.03$; two-sided Fisher's exact test) were significantly enriched in extracellular targets (Figure 5.19b). STRINGdb cellular component analysis showed that more than half of the targets (34/61) are significantly enriched in the cytosol ($p = 0.025$, FDR-adjusted), while 9/61 of the targets are enriched in the actin cytoskeleton ($p = 0.025$, FDR-adjusted; Figure 5.19a). This data suggests that B cell clones in the synovium of PsA patients display reactivities against both extracellular and intracellular targets.

Next, I wanted to test if there is any shared pathways between the emerged protein hits. STRINGdb protein network analyses per patient revealed that the observed protein-protein interaction (PPI) were not significant for 3/4 patients (PPI $p > 0.05$, Figure 5.20a), but was significant in one patient (PPI $p = 0.017$, Figure 5.20b). The PPI was also significant when all the protein hits were aggregated across patients, and they grouped in 8 clusters, out of which the largest groups were involved in metabolism (glycine, serine, threonine), cellular migration (actin nucleation regulation) and ubiquitination ($p<0.05$; Figure 5.20c). Perturbations in the glycine, serine and threonine pathways have been previously documented in psoriasis and are linked to extracellular matrix remodelling and keratinocyte hyperproliferation (Kamleh

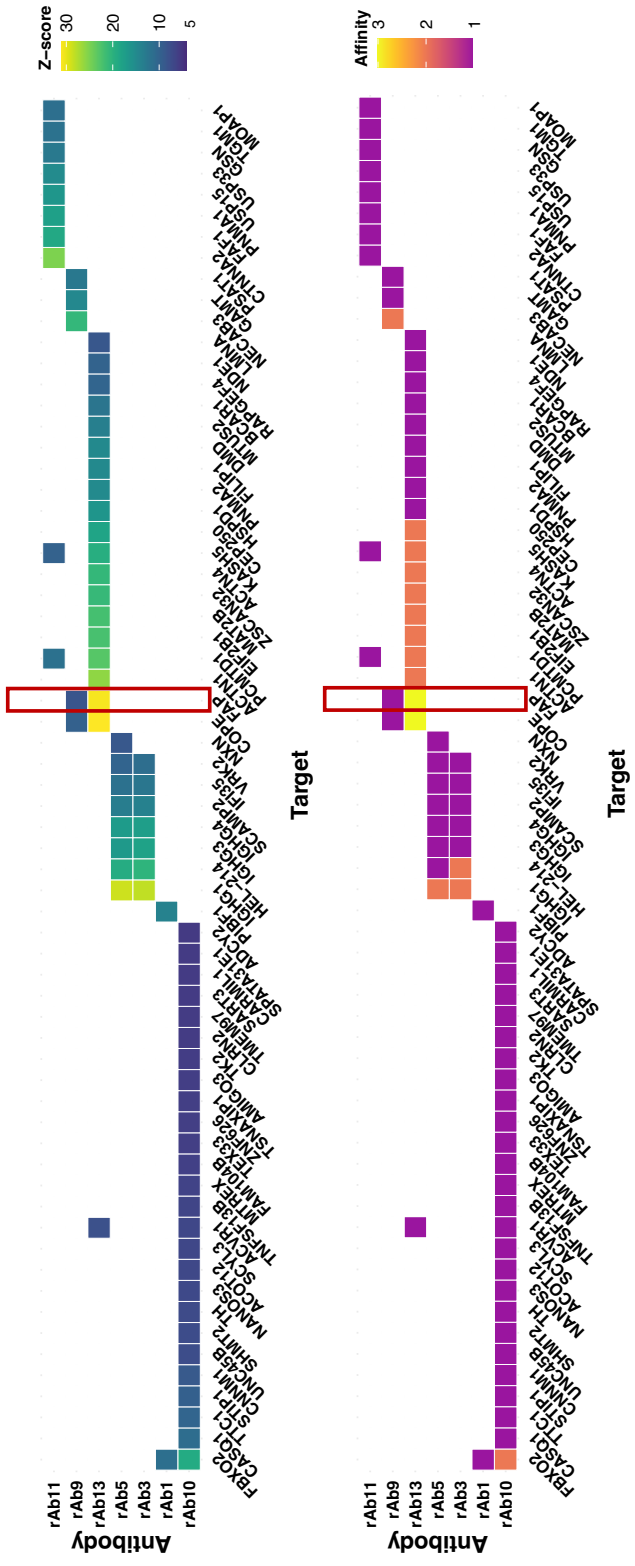

Figure 5.18: Heatmap of human protein targets recognised by recombinant antibodies (rAb) generated from expanded B cell clones isolated from joints of patients with PsA. *(see next page)*The top panel shows the Z-score for each protein target calculated per antibody. The bottom panel indicates antibody binding intensity, represented as relative affinity categories based on raw mean fluorescence intensity (MFI): (1) weak, MFI $<$ 1000; (2) moderate, 1000 $\leq$ MFI $<$ 10,000; and (3) high, MFI $\geq$ 10,000.

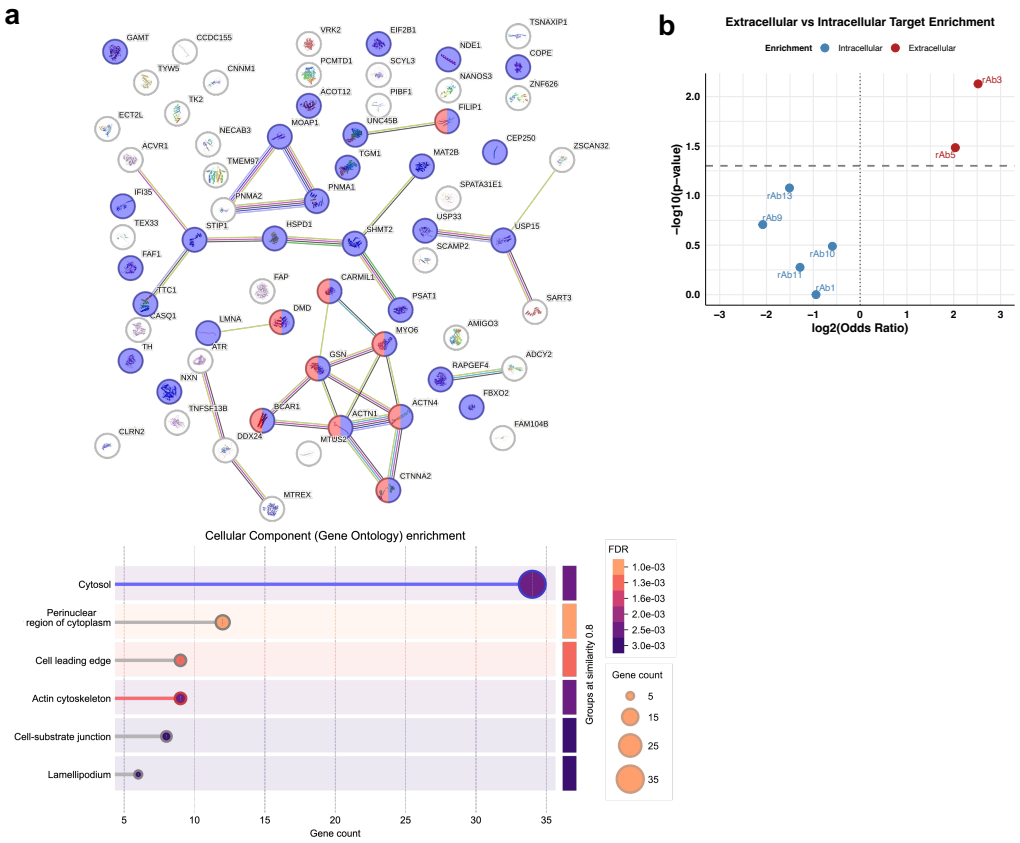

Figure 5.19: Cellular localisation and enrichment of protein targets recognised by recombinant antibodies (rAb) derived from joints of patients with psoriatic arthritis. a STRING-db network representation of rAb protein targets showing cellular localisation; proteins localised to the cytosol are highlighted in purple, while actin cytoskeleton–associated proteins are in red; figure produced with string-db.org (version 12.0). **b** Fisher's exact test of the enrichment of extracellular versus intracellular rAb targets with Haldane-Anscombe correction for odds ratio; the dashed line represents the significance threshold, shown as –log10(p) for $p = 0.05$.

et al., 2015). Disruption of the cytoskeletal and actin-remodelling pathways has also been documented in inflammatory arthritis, particularly in activated synovial fibroblasts and immune cells, providing context for the presence of these proteins among the identified rAb targets (Vasilopoulos, Gkretsi, Armaka, Aidinis, & Kollias, 2007). This data suggests that there is an enrichment of targets belonging to proteins that are cytosolic and belonging to pathways that are relevant to PsA. Collectively, these findings show that PsA synovial B cell clones preferentially target cytosolic proteins involved in metabolic and migratory processes.

FAP is a relevant target in the context of psoriatic arthritis

Extracellular proteins are more likely than intracellular ones to serve as autoantigens because they are readily accessible to immune recognition. I therefore examined which extracellular proteins, beyond IgG1, were detected among the antigen hits. Fibroblast activation protein (FAP) was identified as the joint highest hit in rAb13, and also a hit in rAb9. Notably, rAb13 and rAb9 derive from different patients, indicating that FAP reactivity is not restricted to a single B cell clone or individual 5.18. To determine whether FAP could represent a relevant extracellular target, I further examined its association with PsA. To assess whether FAP represents a biologically plausible and disease-relevant target, its genetic and transcriptomic context in PsA was further investigated.

Screening variants in GWAS catalogue (*GWAS Catalog - Study accession: GCST90243956*, n.d.; Soomro et al., 2022; Cerezo et al., 2025) revealed single nucleotide polymorphisms (SNP) (*rs73971815, rs1990760, rs2111485* in proximity to FAP that were associated with PsA (Figure 5.21a). Using the GTEx Portal database, it was observed the variant *rs73971815* was

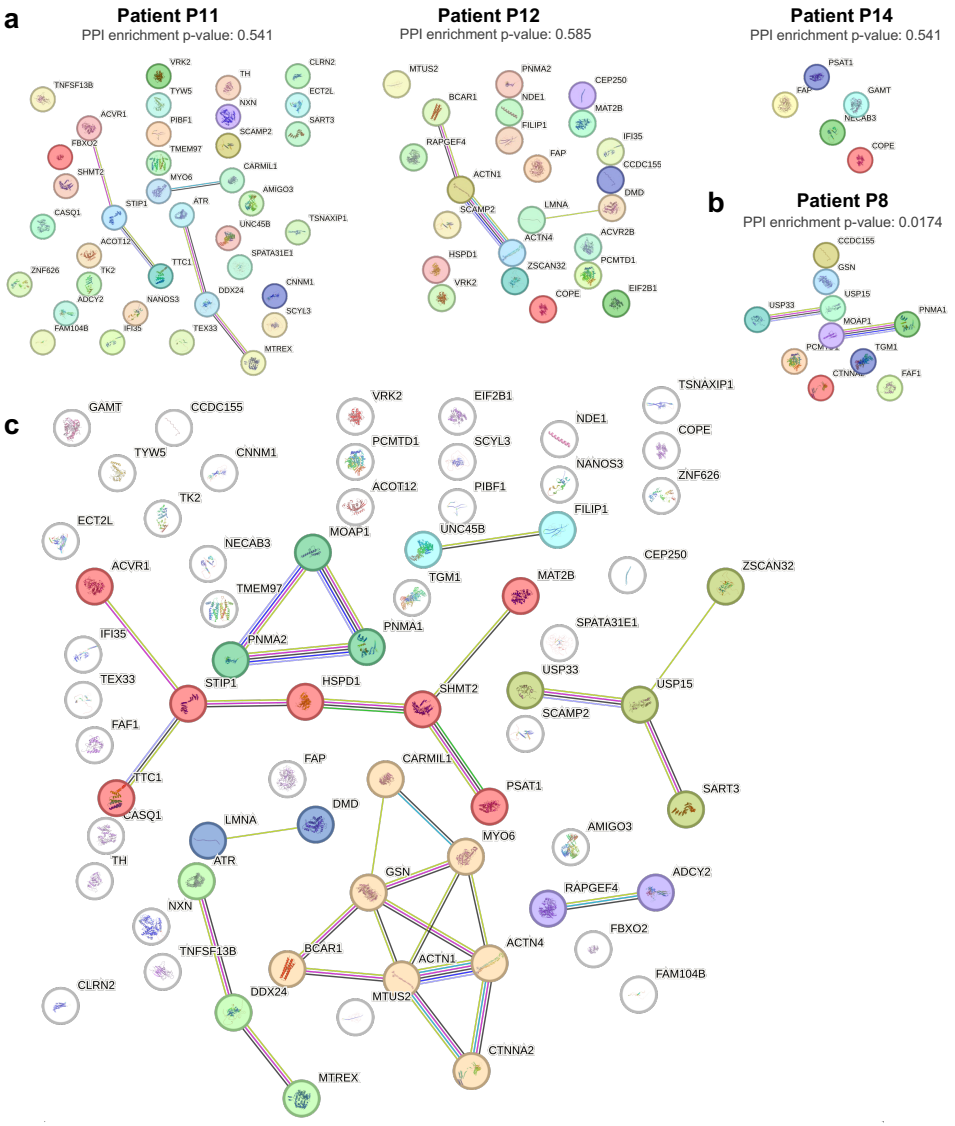

Figure 5.20: STRING-db protein network analysis *(see next page)*

Figure 5.20 ***(previous page)*****: STRING-db protein network analysis of recombinant antibody (rAb) targets derived from joints of patients with psoriatic arthritis.** **a** Network plots of rAb targets per patient, showing no significant pathway enrichment. **b** Example of a single patient with significant network enrichment. **c** Combined STRING-db network of all rAb targets, revealing clustered enrichment of protein pathways.

also found to be an expression quantitative trait locus (eQTL) and splicing quantitative trait locus (sQTL) across multiple cell types, including cell types relevant to PsA pathogensis (skin and fibroblasts, Figure 5.21b). The other two variants (*rs1990760* and *rs2111485*) are also sQTLs in fibroblasts (Figure D.3). Publicly available datasets (Rauber et al., 2024) were used to investigate the presence of FAP in the context of PsA and RA. Bulk RNA-seq revealed that *FAP* had significantly higher expression in PsA synovial tissue compared to RA ($p = 0.006$, Wilcoxon rank-sum test, Figure 5.21c). A Visium spatial transcriptomic slide revealed abundant *FAP* expression in the PsA synovium compared to health ($p = 0.006$, Wilcoxon rank-sum test across spots between $n = 1$ PsA and $n = 1$ healthy slide, Figure 5.21d). The close spatial association of anti-FAP B cells or plasma cells with FAP-enriched regions may facilitate direct cell–cell interactions. To evaluate this possibility, I analysed the co-localisation of plasma cells with *FAP*. In the PsA synovial tissue slide ($n = 1$), *FAP* exhibited a weak yet statistically significant correlation with *SDC1* (CD138, a plasma cell marker) ($\rho = 0.157$; $p < 0.001$; Spearman's Rank correlation; Figure 5.21d).

5.3 Discussion

This chapter offers novel, single-cell insights into the localised and clonally driven nature of B cell activation within the PsA synovium, firmly establishing

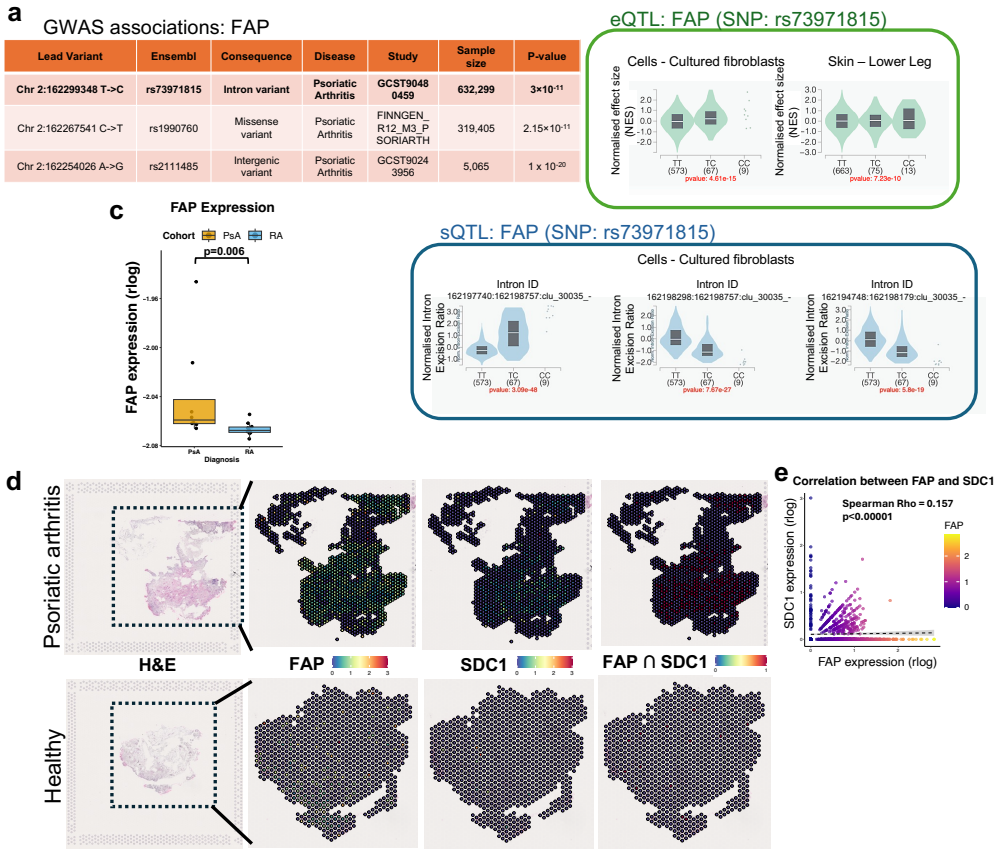

Figure 5.21: FAP is associated with PsA and may be linked to plasma cell activity in synovial tissue. **a** Table with the GWAS of three independent PsA-associated variants within proximity of the *FAP* locus (from Open Targets Genetics (Buniello et al., 2025) and GWAS Catalog (Cerezo et al., 2025)). **b** Violin plots of the expression quantitative trait locus (eQTL) and splicing quantitative trait locus analysis (sQTL) of the lead variant *rs73971815*; eQTLs are shown only for PsA-relevant tissues, and sQTLs correspond to the top three introns; figures adapted from GTEx v8 portal. **c** Box-plot of *FAP* expression in bulk RNA-seq from synovial tissue of patients with rheumatoid arthritis (RA, $n = 10$) and PsA ($n = 8$) (public dataset, (Rauber et al., 2024)); statistical differences were assessed with a Wilcoxon rank-sum test ($p = 0.006$). **d** Spatial transcriptomics (Visium) of PsA and healthy synovium (public dataset, (Rauber et al., 2024)) showing *FAP*, *SDC1* (CD138, a plasma cell marker) and their co-localisation. **e** Scatter plot of *FAP* vs *SDC1* (CD138) expression across all spots from the adjacent PsA tissue slide ($n = 1$), with fitted regression line (dashed); Spearman's Rank correlation ($\rho = 0.157$, $p < 0.001$). SNP – single nucleotide polymorphism.

the presence of an active, adaptive immune compartment that warrants further investigation as a key driver of pathogenesis. This work moves beyond previous histological observations by providing quantitative metrics on the repertoire's structure, offering a molecular view of the B cell contribution to PsA compared to RA.

B cell repertoire in PsA compared to RA

The exploratory comparison between PsA and RA synovium revealed a high degree of similarity in the local B cell repertoire. No statistically significant differences were found in key metrics such as cellular composition, isotype usage, SHM levels or overall clonality between the two diseases. However, several of the observed trends are in accordance with previous reports.

PsA synovial samples showed a tendency towards reduced plasma cell infiltration, increased IgM usage and decreased IgG usage in contrast to RA. Lower levels of plasma cells have previously been reported in PsA (van Kuijk, Reinders-Blankert, Smeets, Dijkmans, & Tak, 2006). The slight increase in IgM levels in PsA is in disagreement to historical papers where IgG or IgA are reported to be predominant (Fyrand, Mellbye, & Natvig, 1977; ALONSO et al., 1991), but in agreement with studies which reported enrichment of IgG usage in RA (Aterido et al., 2024; Elliott et al., 2020; Wing et al., 2023). These findings suggest that RA may represent a more strongly antigen-driven disease compared with PsA.

At the repertoire level, IgM-expressing B cells in PsA displayed a trend toward shorter CDR3 regions, but mildly positively charged CDR3s relative to RA. Longer CDR3 lengths have been associated with autoimmunity and have been previously reported in RA, SLE and Crohn's Disease (Meffre et al., 2001; Bashford-Rogers et al., 2019; Samuels, Ng, Coupillaud, Paget, & Meffre, 2005).

Whilst PsA may not share this characteristic, the trend towards positively charged CDR3 in IgM B cells from PsA synovium align with findings in SLE (S. Liu et al., 2017).

The clonality diversity indices were significantly different between synovial tissue and blood in both PsA and RA, but not between the two diseases. These values indicate that the synovial B cell repertoire is less diverse and more clonally expanded in both RA and PsA, compared to blood. Tertiary lymphoid structure (TLS) formation in the RA synovium, characterised by extensive B cell and plasma cell infiltration and production of class-switched antibodies is well established (Humby et al., 2009; Bombardieri, Lewis, & Pitzalis, 2017; Weyand & Goronzy, 2003; Rivellese et al., 2020), and TLS in PsA has also been described (Tenazinha, Barros, Fonseca, & Vieira-Sousa, 2022; Cañete et al., 2007). Although PsA synovium typically contains fewer infiltrating B cells than RA (data not shown), the comparable clonality metrics between the two diseases indicate that when B cells are present in PsA, they undergo substantial clonal expansion, reaching patterns similar to those observed in RA. This suggests that synovial B cells in PsA may participate in pathogenic processes despite their lower overall abundance. In addition, the low frequency of clonal sharing between synovial and blood repertoires in PsA supports the possibility that at least some B cell expansion occurs *in situ*, consistent with observations previously made in RA (Doorenspleet et al., 2011). Together, these findings indicate that infiltrating B cells in PsA synovium are not merely present but participate in local clonal dynamics, reinforcing their potential contribution to PsA pathogenesis.

Analysis of clonal overlap across PsA and RA synovial samples showed very limited sharing of B cell clones. Although this low overlap may partly reflect the relatively shallow sequencing depth per sample, it is also compatible with

a model in which synovial B cell responses in PsA are largely patient-specific, rather than dominated by convergent or shared autoreactive clones. This aligns with the recognised clinical and molecular heterogeneity of PsA and supports the broader concept that B cell–driven processes in PsA may vary between individuals, reinforcing the relevance of personalised therapeutic approaches.

BCR repertoire in PsA before and after TNFi therapy

The synovial BCR repertoire in PsA did not exhibit significant changes in isotype distribution or clonal architecture following TNF inhibition. This suggests that TNF blockade alone may not substantially reshape synovial B cell repertoires, although the absence of statistical significance should be interpreted cautiously given the limited sample size. Larger studies will be essential to determine whether TNF inhibition truly leaves B cell repertoire features largely unchanged.

If confirmed, this emerging pattern could have important clinical implications. It could indicate that PsA patients who harbour putative pathogenic B cell expansions in the synovium might benefit from adjunctive or alternative therapies aimed directly at B cell–mediated pathways. Such findings would support a more stratified, personalised approach to PsA treatment. In particular, characterising the synovial cellular landscape including the presence or absence of expanded B cell populations may help identify patients whose disease biology is less likely to be fully suppressed by TNF blockade alone.

Extracellular antigens highlight a potential B cell–fibroblast axis in PsA

Five recombinant antibodies derived from top-expanded BCR clones in the

PsA synovium significantly showed binding signal against primary cells derived from OA patients and/or healthy human fibroblasts, supporting their autoreactive potential.

Screening seven rAbs against human protein microarrays revealed mostly intracellular targets, and a few notable extracellular proteins. This reinforces the idea that expanded synovial B cells in PsA have autoreactive potential. To my knowledge, the extent of B cell reactivities within the synovium has not been documented before in PsA.

Extracellular proteins are of particular importance in the context of establishing autoimmune responses, due to their accessibility to immune recognition and therefore higher pathogenic potential.

Fibroblast activation protein (FAP), activin receptor type-1 (ACVR1) protein and IgG(1-4) were among the strongest extracellular hits identified in this study.

Two rAbs (rAb13 and rAb9) originating from distinct patients were reactive against FAP. To date, there are no published studies of anti-FAP autoantibodies or expanded B cell clones in PsA, making this finding novel. FAP is a transmembrane serine protease upregulated on fibroblasts involved in pathogenic tissue-remodelling such as fibrosis, arthritis and tumour progression (Fitzgerald & Weiner, 2020). Strikingly, neither rAb13 nor rAb9 displayed extracellular binding on the tested fibroblast cell lines. This may reflect absent or low FAP expression in these cells, or alternatively, conformational changes induced by fixation that impaired antibody recognition. Additional validation of FAP expression and antibody binding is therefore warranted. As access to matched FAP-expression data from the CARTOGRAPHY cohort was not possible, publicly available data was used to test the plausibility of this finding.

Bulk RNA-seq analysis indicated that synovial FAP expression is higher in PsA than in RA. One spatial transcriptomic slide also confirmed synovial FAP expression but not in healthy tissue, with weak but significant correlation to a plasma cell marker. These findings are in accord with previous reports which used PET/CT imaging studies and FAP-inhibitor (FAPI) radiotracers to confirm the presence of FAP in the synovium, as a marker of chondrocytes and fibroblasts in patients with PsA, OA and RA (X. Zhao et al., 2024; Yang et al., 2025; Luo et al., 2023). Moreover, FAP production was correlated with disease activity in PsA and RA (Yang et al., 2025; Luo et al., 2023).

Genetic evidence further supports FAP as a candidate. GWAS revealed three SNPs recorded in the proximity of FAP in the context of PsA (*GWAS Catalog - Study accession: GCST90243956*, n.d.; Soomro et al., 2022; Cerezo et al., 2025). One of the SNPs was also identified as an eQTL and sQTL in multiple cell types, including fibroblasts. These findings indicate that allelic variation could influence the gene expression and splicing of FAP, which may impact PsA susceptibility and progression. Taken together, the presence of anti-FAP B cell clones opens a B cell–fibroblast axis hypothesis in PsA worthy of mechanistic follow-up. Notably, the detection of one anti-FAP expanded B cell clone (original clone of rAb13) in peripheral blood suggests that corresponding antibodies could be measurable in plasma, raising the possibility of anti-FAP reactivity as a biomarker in PsA.

The main reactivities of rAb5, rAb3 (its germline revertant) and rAb2 (inferred through clonal relatedness), were directed against IgG, alternatively called rheumatoid factor. Interestingly, the germline revertant (rAb3) displayed almost identical target and affinity levels to rAb5, suggesting a minimal effect of affinity maturation in protein binding. Should the anti-RF B cell clones secrete antibodies, this finding is in agreement with other reports where RF

was present in patients with PsA (Punzi et al., 2007; Ghazzali et al., 2022). Although the RF does not target synovial proteins specifically, it can form immune complexes, activate complement pathways and amplify inflammation. The presence of RF clones in PsA synovium is potentially relevant in the context of personalised therapeutic avenues.

Activin A receptor type 1 (ACVR1) is the only predominantly extracellular target identified by rAb10. ACVR1 is a protein receptor for bone morphogenetic proteins with roles in normal bone development. Mutations in its glycine-serine domain result in abhorrent bone formation in soft tissues causing fibrodysplasia ossificans progressiva (Towler, Peck, Kaplan, & Shore, 2021). Antibodies against ACVR1 in arthropathies have not previously been reported. However, due to its role in bone formation, ACVR1 and anti-ACVR1 antibodies could be interesting targets to follow up in the context of PsA.

Intracellular antigens may reflect inflammation-driven antigen exposure

Interestingly, the majority of the identified targets were intracellular. Intracellular proteins can localise on the cell surface in conditions of cellular stress, damage or infection (De Maio, 2011). They can also become exposed following inflammatory cell death, such as necroptosis, or by defective clearance of dying cells, processes relevant in psoriasis and in cartilage degradation (Khaleque, Kim, Tanvir, Park, & Kim, 2024; Muñoz, Lauber, Schiller, Manfredi, & Herrmann, 2010; Duan et al., 2020).

Several intracellular targets identified here have been previously linked to PsA or other arthropathies (FBXO2, STIP1, HSPD1/HSPD60, PSAT1, GSN, LMNA, TNFSF13B), as detailed below, while others have not (COPE, PIBF1, NECAB3, CTNNA2).

rAb10 displayed reactivities against FBXO2, STIP1 and BAFF/TNFSF13B. FBXO2 was also a target of rAb1. F-box only protein 2 (FBXO2) is a unit of the E3 ubiquitin-protein ligase complex and has been observed in some synovial RA lesions, but not in OA (Mizutani et al., 2013). Interestingly, FBXO2 plays a role in the recognition of bacterial surface glycans and their ubiquitination for antibacterial selective autophagy (Yamada, Hikichi, Nozawa, & Nakagawa, 2021). This raises the intriguing possibility that bacterial exposure could induce FBXO2 expression or modification, enhancing its immunogenic potential within the inflamed synovium. Stress-induced phosphoprotein 1 (STIP1) is a co-chaperone for heat shock protein 70 and 90 (Hsp70, Hsp90). Autoantibodies against STIP1 have previously been reported in sera of patients with PsA and PsO compared to controls, with highest levels in PsA (Maejima et al., 2014). These findings suggest that STIP1 might also be a relevant target for deeper investigation in the synovium of PsA, as a putative functional or diagnostic marker.

Antibodies against heat shock protein 60 (HSPD1/HSPD60) have been identified to be elevated in RA and axial spondyloarthritis compared to health, though not to correlate with disease activity (Mantej, Polasik, Piotrowska, & Tukaj, 2019; Carlsen et al., 2013). Phosphoserine-aminotransferase-1 (PSAT1) was identified as a target of rAb9, and is an enzyme involved in the serine/glycine metabolism. A study found its expression increased in RA synovium compared to healthy controls, and its inhibition to reduce the TNF-mediated pathways and improve RA severity in mice, suggesting a mechanistic role in RA (F. Xu et al., 2024). Therefore, additional studies of PSAT1 in the context of PsA could be relevant to be investigated.

One of the identified targets of rAb11 was gelsolin (GSN), which is a protein involved in actin depolymerisation. GSN has an extracellular circulat-

ing isoform (plasma GSN) which has been long-studied as a biomarker of autoimmunity and inflammatory disease due to its anti-inflammatory and immuno-modulatory properties (Piktel, Levental, Durnaś, Janmey, & Bucki, 2018; DiNubile, 2008). GSN has been shown to reduce IL-6, TNF and NO *in vitro* and in mice, whereas its depletion caused pro-inflammatory mediator release (Cheng et al., 2017). Another report revealed reduced levels of GSN in PsA compared PsO and health (Esawy, Makram, Albalat, & Shabana, 2020). A similar trend has been previously identified in RA (Osborn, Verdrengh, Stossel, Tarkowski, & Bokarewa, 2008). If the anti-GSN clone identified this study is functionally depleting, it would align with the observed low plasma GSN levels in PsA, and could be potentially contributing to the inflammation.

Intracellular targets of rAb13 included actin proteins (ACTN1, ACTN4) and nuclear proteins lamin A/C (LMNA). The accumulation of lamin A/C has been described to lead to joint damage in OA and in the ageing population (Figueroa et al., 2023). Antibodies against lamin A/C have been documented in patients with Sjögren's syndrome (SjS) (Zhang et al., 2016). The number reports linking these proteins to spondyloarthritis is limited. The presence of multiple low-affinity reactivities within the same antibody, directed toward proteins from related intracellular families is suggestive of epitope spreading. While these targets merit further investigation in PsA, their limited precedent in the literature and the relatively weak binding observed here indicate that they should be considered lower-priority candidates for follow-up studies.

The top-hits amongst intracellular proteins which are not yet directly linked to arthritis are: COPE (coatomer complex protein, role in protein trafficking and vesicular transport), PIBF1 (progesterone-induced blocking factor 1, main role described in pregnancy), NECAB3 (N-terminal EF-hand calcium-binding protein 3, predominantly a neuronal protein with a role in amyloid-*beta*

production; also described in skeletal muscle and glycolysis regulator in cancer (Bueno, Schäfer, Wang, Schmeisser, & Methner, 2025)) and CTNNA2 (catenin alpha-2, predominant role in neuronal cell-cell adhesion). Their synovial protein levels in PsA should be validated before functional studies.

Functional coherence of protein targets and mechanistic implications

The protein network of all targets combined revealed more interactions than a randomly selected set of proteins, suggesting that the proteins are functionally relevant to each other. Pathway analysis highlighted an enrichment in cellular migration, metabolism, domains of ubiquitin-proteases and cytoskeletal modelling. These patterns may not be random as they mirror known perturbations relevant to PsA. For example the glycine, serine and threonine metabolic pathways are heightened, linked to the disease's underlying inflammatory processes and the rapid turnover of skin cells (keratinocyte hyperproliferation), and may serve as biomarkers for disease severity and treatment response (Kamleh et al., 2015).

Several intriguing questions arise from these observations. Why would B cell clones expand after recognition of these specific intracellular proteins? Is there a causal component to why these specific pathways are enriched? Are these proteins more immunogenic than others? And secondly, what is the relevance of these specific B cell clones in the wider context of PsA? Do these clones expand as a consequence of their cognate antigens being available, or through a bystander effect? Do their potential secreted autoantibodies have a functional role? If so, are these B cell clones/autoantibodies early mediators or amplifiers of an already existing inflammation?

In the absence of functional data, putative mechanisms through which B cells

contribute to the pathology of PsA can only be speculated. However, the profile of BCR reactivities hint towards possible processes which could lead to the expanded B cell clones observed in the PsA synovium.

The generalised inflammation and cell death in the joints could trigger the activation and proliferation of bystander B cells targeting exposed intracellular antigens, through epitope spreading. Intramolecular epitope spreading could explain the reactivity pattern of one of the patients (CARTR02517), as their BCRs were reactive against multiple ubiquitin-family proteins. Interestingly, other pathways involving metabolic or cytoskeletal modelling proteins were not enriched targets within independent patients, but emerged only upon aggregating the protein target data across patients. This suggests a possibility of intermolecular epitope spreading, where reactivity patterns broaden across multiple protein-families; in this case a shared pattern is observed across patients (Cornaby et al., 2015).

Alternatively, infection and molecular mimicry of bacterial epitopes to similar human epitopes in the joints could cause B cell clonal expansion. In psoriasis, streptococcal mimicry to keratinocyte antigens have been shown in skin (Besgen, Trommler, Vollmer, & Prinz, 2010; Mcfadden, Valdimarsson, & Fry, 1991). The cross-reactivity between skin and joint epitopes is a proposed model of arthritic pathology initiation. Dysbiosis of the gut microbiome is another avenue through which bacterial species may present epitopes that cross- react with *in situ* human proteins (Crohn's disease) or further afar, such as in RA or T1D (Scher et al., 2013). Microbiome peptide transfer in distal organs could be possible through dendritic cells, such as in the thymus, where microbiome epitope presentation was able to change the emerging T cell repertoire (Zegarra-Ruiz et al., 2021). The human heat-shock protein 60 is ∼50% homologous to its bacterial counterpart, and cross-

reactive human and bacterial anti-HSP responses have been documented across autoimmune rheumatic diseases (Gelsing, Bennike, Christiansen, & Birkelund, 2013). In this dataset, one expanded B cell clone with anti-HSPD1/HSP60 reactivity is consistent with the literature and argue for deeper microbe–B cell investigations in PsA.

In this study the protein targets originating from several expanded B cell clones in the PsA synovium are presented. Based on their reported relevance in arthritis, I propose that the following proteins and putative autoantibodies be further studied in the context of PsA: FAP, STIP1, GSN, FBXO2 and HSPD1.

It remains to be discovered whether the expansion of these B cell clones is simply correlative or causal. Further functional studies are required to establish the effect of the autoreactive B cell clones on synovial cells. If functional effects are confirmed, the autoantibodies, autoreactive B cell clones or their cognate proteins could be targeted for therapy. Otherwise, these clones could be investigated as potential biomarkers, by having their presence tested in plasma or the synovial fluid of a larger PsA patient cohort.

5.3.1 Limitations

Several caveats should be acknowledged. Firstly, the limited size of the study reduced the statistical power for BCR repertoire comparisons between PsA and RA, as well as for assessing the impact of TNF-inhibitor therapy.

Secondly, the protein target screening was performed on a restricted number of rAbs, which does not reflect the true diversity of expanded B cell clones within the PsA synovium. A broader repertoire profiling across a larger patient cohort would produce a more representative picture of B cell reactivities

in PsA. Similarly, the number of B cells sequenced from peripheral blood was low, limiting analyses of clonal evolution and detailed BCR repertoire comparisons between blood and synovium.

In addition, the CARTOGRAPHY cohort included heterogenous disease stage and treatment histories, which may have introduced confounding effects. Larger, more stratified cohorts would be needed to control for these variables.

Moreover, the presence of expanded B cell clones in synovium does not necessarily imply secretion of detectable autoantibodies suitable for biomarker use. Lastly, the identification of an antibody with plausible relevance in PsA does not automatically establish its pathogenicity or disease specificity. Autoantibodies could also be triggered by non-arthritic causes, such as infection. For example, Hepatitis C virus can cause asymptomatic infection and promote the development of RF, which could happen to be produced in seronegative psoriatic arthritis patients (Palazzi, Buskila, D'Angelo, D'Amico, & Olivieri, 2012; Örge, Çefle, Yazıcı, Gürel-Polat, & Hulagu, 2010). Consequently, these findings require validation in larger cohorts, correlation with clinical disease activity and functional investigation to determine whether these autoreactive B cells are causal mediators, amplifiers, or simply bystanders in PsA pathogenesis.

5.3.2 Future work

Validation of the current HuProt findings is essential and can be performed through targeted *in vitro* assays. For example, ELISA could be used to confirm rAb reactivity against the candidate proteins, while flow cytometry could test binding to cells with confirmed expression of proteins of interest, such as FAP. Beyond validation, functional *in vitro* studies are needed to

determine whether expanded B cell clones have causal effects on synoviocytes and the enzymatic acivity of FAP. Measuring FAP substrate cleavage in the presence of anti-FAP rAbs will determine whether these antibodies alter its enzymatic activity. Co-culture experiments with FAP-expressing fibroblasts and anti-FAP antibodies would allow assessment of downstream functional consequences, including the induction of pro-inflammatory cytokines (IL-6, GM-CSF), matrix metalloproteases (MMP1, MMP3, MMP9), and chemokines (CXCL8) by these cells. Changes in fibroblast phenotype and morphology could be characterised by flow cytometry and confocal microscopy, as they could reveal whether anti-FAP antibodies alter fibroblast behaviour or promote a pathogenic stromal phenotype. In parallel, the presence of these autoantibodies or clonally related B cells in peripheral blood or in synovial fluid should be examined in larger patient cohorts and correlated with clinical features and disease progression. Such studies could help identify PsA-specific biomarkers and distinguish signatures from psoriasis without arthritis, or from RA.

Some of the rAb hits identified on the HuProt array displayed medium-to-low affinity, raising the possibility that their true cognate antigens were absent from the microarray. Given longstanding hypotheses that PsA may involve dysregulated microbial-pathogen recognition, it would be valuable to extend screening to microbial protein microarrays to test for cross-reactivity and molecular mimicry.

Finally, the potential therapeutic implications of these findings merit exploration. Among the potential therapeutic candidates highlighted in this chapter, FAP stands out as particularly attractive, given its preferential upregulation in pathogenic stromal niches. Targeting FAP-expressing fibroblasts could interrupt fibroblast–immune cell crosstalk that may contribute

to synovial inflammation and tissue remodelling. Supporting this concept, intra-articular delivery of FAP-specific siRNA in an OA rat model reduced chondrocyte senescence and cartilage degradation (X. Zhao et al., 2024), providing proof-of-principle that modulation of FAP activity can ameliorate joint pathology.

5.3.3 Conclusions

In summary, this work makes two key advances. First, it defines the PsA joint as a site of active B cell expansion. Second, by identifying novel candidate autoantigens, such as FAP, it establishes a foundation for functional follow-up studies to clarify the B cell involvement in PsA pathogenesis, refine diagnostic approaches and support development of novel B cell–directed therapies.

6 | Discussion

This thesis explored several aspects of B cell biology, investigating how B cell responses and repertoire features are shaped and perturbed across three distinct clinical contexts: COVID-19, ANCA-associated vasculitis (AAV) and psoriatic arthritis (PsA). Collectively, the findings advance the understanding of human B cell tolerance, its mechanisms of disruption, and the immunological consequences of targeted therapies, offering potential new avenues for intervention in inflammatory and autoimmune pathology.

6.1 Anergy as a transient state on a continuum

Chapter 3 provides evidence for the plasticity of naïve B cell responses following BCR-independent stimulation *in vitro*. The proliferative capacity of naïve B cells following stimulation was shown to be tightly interlinked with the IgM level, to a similar extent in health and COVID-19. Secondly, it was shown that irrespective of the initial status of IgM expression (high, mid or low) of naïve B cells before cell culture, IgM BCR levels shifted following stimulation, a finding also reflected by the heterogeneous pool of resulting cellular phenotypes. Taken together, these findings illustrate fundamentally that the naïve B cell unresponsiveness, or anergic status is not fixed but is transient, and that it sits on a spectrum tightly interlinked with IgM. The observation of similar trends in health and COVID-19 further supports the robustness of this relationship.

In addition, the levels of surface CD21 and CD22 are better aligned with the levels of the current IgM expression within a mixed B cell population, rather than the pre-stimulation levels of surface IgM. This provides insight

into the dynamic regulation of B cell co-receptors in humans, helping to bridge an important gap between murine models and human immunobiology. A clearer understanding of these co-receptor dynamics may be relevant for therapeutic strategies that aim to fine-tune B cell activation thresholds, for example through targeted blockade or agonism.

These findings lay the foundation for a more thorough and systematic characterisation of the dynamic interactions in B cell activation, and build towards developing a model for B cell anergy modulation. The activation of naïve polyreactive B cells, which are anergic in healthy contexts, is a feature of autoimmune disease, most described in systemic lupus erythematosus (SLE), where it does not self-resolve. On the other hand, although COVID-19 has also been associated with an increase in anergic B cell phenotypes, autoreactive antibodies and complications of SARS-CoV-2 included autoimmune manifestations, these have been shown to be mostly transient, consistent with the concept that immune tolerance and anergy can be restored (Castleman et al., 2022; Woodruff et al., 2022; Jokiranta et al., 2026). Elucidating the underlying mechanisms that permit recovery of tolerance in this setting may inform approaches to therapeutically redirect autoimmune responses towards homeostasis. In particular, defining pathways that can restore or reinforce anergy in expanded autoreactive B cell populations could offer more specific alternatives to broadly B cell-depleting therapies currently available.

6.2 Belimumab biases peripheral B cell repertoire reconstitution in AAV

A surprising finding in chapter 5 was that the additive therapeutic effect of belimumab to rituximab therapy in PR3-AAV was non-significant across the BCR repertoire metrics tested. However, the observed trends in the repertoire reconstitution align with the biology of BAFF, in that T cell-independent class-switching pathways, which are more dependent on BAFF, such as IgG2 and IgA2, would be perturbed (Litinskiy et al., 2002; den Hartog et al., 2018; Barrett & Ayoub, 1986). Indeed, belimumab resulted in a delayed trend in the recovery of IgA2, IgG2 and IgG4 isotypes, as identified by the higher clonality metrics compared to placebo at 24 months after treatment induction.

Belimumab was also associated with reduced reconstitution of B cells using the inherently autoreactive VH4-34 chain (Richardson et al., 2013), a change that could plausibly contribute to the observed, albeit non-significant, clinical trial results trended towards lower PR3-ANCA titres and fewer relapses. Together, these findings suggest that while the global repertoire metrics tested were not significantly altered, BAFF blockade may still exert biologically meaningful effects on specific components of repertoire reconstitution.

However, the modest result of the COMBIVAS trial prompts the idea that alternative ways of treating highly relapsing AAV patients might need to be employed. BAFF signals through multiple receptors including TACI, a receptor shared with APRIL to provide B cell survival signals. In AAV, BAFF, APRIL and TACI expression were reported to be upregulated (Shimojima et al., 2023). Therapeutic approaches that block TACI directly, or that target BAFF in combination with APRIL, may therefore produce a more substantial

effect than BAFF blockade alone in PR3-AAV. In addition, emerging cellular therapies may represent a further avenue. A recent pilot anti-CD19 chimeric antigen receptor (CAR)-T cell therapy study has suggested the potential for deep B cell depletion and sustained remission in SLE, motivating the evaluation of this approach as a potential avenue of treatment for relapsing AAV patients (Müller et al., 2024).

6.3 B cells may interact with fibroblasts in psoriatic arthritis

A central finding of chapter 5 is the dramatic difference in BCR repertoire characteristics between the local synovial tissue and the peripheral blood. The synovium of both PsA and RA patients exhibited significantly higher measures of clonal expansion (increased Gini index) and reduced diversity (decreased Shannon index) compared to the systemic circulation. This striking compartmentalisation provides molecular evidence confirming prior studies that noted B cell infiltration and the formation of TLSs in inflamed synovium (Cañete et al., 2007). The data indicate that the B cells found *in situ* are not merely transient spectators but are actively proliferating, undergoing antigen-driven selection and maturing into memory and plasma cell populations.

Despite this clear local activation, the repertoire remains highly individualised. The minimal clonal overlap observed between distinct patients suggests that, unlike the widespread shared epitopes of anti-CCP in RA (Musters et al., 2022), the dominant B cell response in PsA is primarily private and patient-specific. This heterogeneity aligns with the clinical diversity of PsA and supports the need to move towards a personalised medicine approach.

Importantly, the rAb screening experiments on fibroblast and synovial-derived primary cells together with the HuProt microarrays demonstrate that the most highly expanded synovial B cell clones in PsA can recognise proteins that are biologically relevant within the synovial environment. These data introduce a previously unrecognised putative B cell–fibroblast axis in PsA, centred on fibroblast activation protein (FAP) as a potential autoantigenic target. Synovial fibroblasts are key stromal orchestrators of inflammation and tissue remodelling in inflammatory arthritis. The identification of FAP as a candidate antigen raises the possibility that B cells may directly sense, respond to, or perpetuate fibroblast-driven pathology. Further functional validation is required to confirm this exciting finding.

These findings have two important implications. First, they strengthen the case that B cells may contribute directly to PsA pathology. Historically, PsA has been viewed as predominantly driven by T cells and stromal signals. The present data support a model in which B cells participate alongside these effectors, potentially providing new therapeutic entry points for patients with refractory disease. Second, the BCR specificity findings provide valuable leads for understanding the multisystem nature of PsA. FAP, identified here as a candidate antigen, is expressed in pathogenic stromal niches in the joint and is also present in skin fibroblasts, suggesting the potential for shared stromal targets across tissues (Zhuang et al., 2025). Beyond FAP, studies have shown that keratin-17 is expressed in both psoriatic skin and ocular-derived cells (Shi et al., 2011; K. Xu et al., 2013), illustrating how shared antigens could unify inflammatory processes across different anatomical locations. As autoantibodies against keratin-17 have not been detected to date, deeper antigen-specific profiling of BCRs across synovium, skin and other PsA-relevant tissues could determine whether B cells participate in a shared

recognition axis across organ sites, helping to resolve a longstanding question in PsA: how joint, skin and extra-articular disease become immunologically linked.

6.4 Concluding Remarks

Collectively, the data presented here advance understanding of fundamental features of human B cell biology in three key ways. First, they support a model in which naïve B cell anergy is a dynamic, IgM-linked continuum rather than a fixed state, with implications for how tolerance may be disrupted and subsequently restored. Second, they indicate that BAFF-pathway blockade can shape post-depletion repertoire recovery, with trends consistent with delayed reconstitution of specific isotypes and reduced representation of autoreactivity-associated features. Third, they provide tissue-level molecular evidence that B cells in psoriatic arthritis are not simply enriched but are locally selected and expanded, and they nominate stromal-associated antigens that motivate a testable B cell–fibroblast axis. Together, these findings help refine mechanistic hypotheses for disease pathogenesis and directly motivate more targeted therapeutic strategies that move beyond uniform B cell depletion towards selective modulation of B cell activation, survival, and antigen-specific effector function.

Bibliography

Aalberse, R. C., Stapel, S. O., Schuurman, J., & Rispens, T. (2009, April). Immunoglobulin G4: an odd antibody. *Clinical and Experimental Allergy: Journal of the British Society for Allergy and Clinical Immunology*, *39*(4), 469–477. doi: 10.1111/j.1365-2222.2009.03207.x

Abbouda, A., Abicca, I., Fabiani, C., Scappatura, N., Peña-García, P., Scrivo, R., ... Paroli, M. P. (2017). Psoriasis and Psoriatic Arthritis-Related Uveitis: Different Ophthalmological Manifestations and Ocular Inflammation Features. *Seminars in Ophthalmology*, *32*(6), 715–720. doi: 10.3109/08820538.2016.1170161

Ahern, D. J., Ai, Z., Ainsworth, M., Allan, C., Allcock, A., Angus, B., ... Zurke, Y.-X. (2022, March). A blood atlas of COVID-19 defines hallmarks of disease severity and specificity. *Cell*, *185*(5), 916–938.e58. Retrieved 2022-10-10, from https://linkinghub.elsevier.com/retrieve/pii/S0092867422000708 doi: 10.1016/j.cell.2022.01.012

Alberici, F., Smith, R. M., Jones, R. B., Roberts, D. M., Willcocks, L. C., Chaudhry, A., ... Jayne, D. R. W. (2015, July). Long-term follow-up of patients who received repeat-dose rituximab as maintenance therapy for ANCA-associated vasculitis. *Rheumatology*, *54*(7), 1153–1160. Retrieved 2026-01-27, from https://doi.org/10.1093/rheumatology/keu452 doi: 10.1093/rheumatology/keu452

ALONSO, J. C. T., PEREZ, A. R., CASTRILLO, J. M. A., GARCIA, J. B., NORIEGA, J. L. R., & LARREA, C. L. (1991, August). PSORIATIC ARTHRITIS (PA): A CLINICAL, IMMUNOLOGICAL AND RADIOLOGICAL STUDY OF 180 PATIENTS. *British Jour-*

nal of Rheumatology, *30*(4), 245–250. Retrieved 2025-09-27, from https://doi.org/10.1093/rheumatology/30.4.245 doi: 10.1093/rheumatology/30.4.245

Aterido, A., López-Lasanta, M., Blanco, F., Juan-Mas, A., García-Vivar, M. L., Erra, A., ... Julià, A. (2024, March). Seven-chain adaptive immune receptor repertoire analysis in rheumatoid arthritis reveals novel features associated with disease and clinically relevant phenotypes. *Genome Biology*, *25*(1), 68. Retrieved 2025-09-27, from https://doi.org/10.1186/s13059-024-03210-0 doi: 10.1186/s13059-024-03210-0

Avery, D. T., Bryant, V. L., Ma, C. S., de Waal Malefyt, R., & Tangye, S. G. (2008, August). IL-21-induced isotype switching to IgG and IgA by human naive B cells is differentially regulated by IL-4. *Journal of Immunology (Baltimore, Md.: 1950)*, *181*(3), 1767–1779. doi: 10.4049/jimmunol.181.3.1767

Avery, D. T., Kalled, S. L., Ellyard, J. I., Ambrose, C., Bixler, S. A., Thien, M., ... Tangye, S. G. (2003, July). BAFF selectively enhances the survival of plasmablasts generated from human memory B cells. *Journal of Clinical Investigation*, *112*(2), 286–297. Retrieved 2025-11-30, from https://pmc.ncbi.nlm.nih.gov/articles/PMC164292/ doi: 10.1172/JCI18025

Barrett, D. J., & Ayoub, E. M. (1986, January). IgG2 subclass restriction of antibody to pneumococcal polysaccharides. *Clinical and Experimental Immunology*, *63*(1), 127–134.

Bashford-Rogers, R. J. M., Bergamaschi, L., McKinney, E. F., Pombal, D. C., Mescia, F., Lee, J. C., ... Smith, K. G. C. (2019, October). Analysis of the B cell receptor repertoire in six immune-mediated diseases. *Nature*,

574(7776), 122–126. Retrieved 2022-06-09, from https://www.nature.com/articles/s41586-019-1595-3 (Number: 7776) doi: 10.1038/s41586-019-1595-3

Behrens, F., Koehm, M., Thaçi, D., Gnann, H., Greger, G., Maria Wittig, B., & Burkhardt, H. (2016, October). Anti-citrullinated protein antibodies are linked to erosive disease in an observational study of patients with psoriatic arthritis. *Rheumatology*, *55*(10), 1791–1795. Retrieved 2025-11-27, from https://doi.org/10.1093/rheumatology/kew229 doi: 10.1093/rheumatology/kew229

Berti, A., Hillion, S., Konig, M. F., Moura, M. C., Hummel, A. M., Carmona, E., ... Cornec, D. (2023, May). Autoreactive Plasmablasts After B Cell Depletion With Rituximab and Relapses in Antineutrophil Cytoplasmic Antibody-Associated Vasculitis. *Arthritis & Rheumatology (Hoboken, N.J.)*, *75*(5), 736–747. doi: 10.1002/art.42388

Besgen, P., Trommler, P., Vollmer, S., & Prinz, J. C. (2010, May). Ezrin, Maspin, Peroxiredoxin 2, and Heat Shock Protein 27: Potential Targets of a Streptococcal-Induced Autoimmune Response in Psoriasis. *The Journal of Immunology*, *184*(9), 5392–5402. Retrieved 2025-09-26, from https://doi.org/10.4049/jimmunol.0903520 doi: 10.4049/jimmunol.0903520

Blauvelt, A., & Chiricozzi, A. (2018). The Immunologic Role of IL-17 in Psoriasis and Psoriatic Arthritis Pathogenesis. *Clinical Reviews in Allergy & Immunology*, *55*(3), 379–390. Retrieved 2025-12-02, from https://pmc.ncbi.nlm.nih.gov/articles/PMC6244934/ doi: 10.1007/s12016-018-8702-3

Bombardieri, M., Lewis, M., & Pitzalis, C. (2017, March). Ectopic lymphoid neogenesis in rheumatic autoimmune diseases. *Nature Re-*

views Rheumatology, *13*(3), 141–154. Retrieved 2022-10-19, from https://www.nature.com/articles/nrrheum.2016.217 (Number: 3) doi: 10.1038/nrrheum.2016.217

Bortnick, A., Chernova, I., Quinn, W. J., III, Mugnier, M., Cancro, M. P., & Allman, D. (2012, June). Long-Lived Bone Marrow Plasma Cells Are Induced Early in Response to T Cell-Independent or T Cell-Dependent Antigens. *The Journal of Immunology*, *188*(11), 5389–5396. Retrieved 2025-05-25, from https://doi.org/10.4049/jimmunol.1102808 doi: 10.4049/jimmunol.1102808

Briney, B., Inderbitzin, A., Joyce, C., & Burton, D. R. (2019, February). Commonality despite exceptional diversity in the baseline human antibody repertoire. *Nature*, *566*(7744), 393–397. Retrieved 2025-05-08, from https://www.nature.com/articles/s41586-019-0879-y doi: 10.1038/s41586-019-0879-y

Brière, F., Servet-Delprat, C., Bridon, J. M., Saint-Remy, J. M., & Banchereau, J. (1994, February). Human interleukin 10 induces naive surface immunoglobulin D+ (sIgD+) B cells to secrete IgG1 and IgG3. *The Journal of Experimental Medicine*, *179*(2), 757–762. doi: 10.1084/jem.179.2.757

Brochet, X., Lefranc, M.-P., & Giudicelli, V. (2008, July). IMGT/V-QUEST: the highly customized and integrated system for IG and TR standardized V-J and V-D-J sequence analysis. *Nucleic Acids Research*, *36*(suppl_2), W503–W508. Retrieved 2025-10-03, from https://doi.org/10.1093/nar/gkn316 doi: 10.1093/nar/gkn316

Bueno, D., Schäfer, M. K. E., Wang, S., Schmeisser, M. J., & Methner, A. (2025, May). NECAB family of neuronal calcium-binding proteins in health and disease. *Neural Re-*

generation Research, *20*(5), 1236. Retrieved 2025-09-25, from https://journals.lww.com/nrronline/fulltext/2025/05000/necab_family_of_neuronal_calcium_binding_proteins.2.aspx doi: 10.4103/NRR.NRR-D-24-00094

Buniello, A., Suveges, D., Cruz-Castillo, C., Llinares, M., Cornu, H., Lopez, I., ... Ochoa, D. (2025, January). Open Targets Platform: facilitating therapeutic hypotheses building in drug discovery. *Nucleic Acids Research*, *53*(D1), D1467–D1475. Retrieved 2025-11-06, from https://doi.org/10.1093/nar/gkae1128 doi: 10.1093/nar/gkae1128

Burrows, N., Bashford-Rogers, R. J. M., Bhute, V. J., Peñalver, A., Ferdinand, J. R., Stewart, B. J., ... Maxwell, P. H. (2020, November). Dynamic regulation of hypoxia-inducible factor-1α activity is essential for normal B cell development. *Nature Immunology*, *21*(11), 1408–1420. Retrieved 2025-11-10, from https://www.nature.com/articles/s41590-020-0772-8 doi: 10.1038/s41590-020-0772-8

Calonga-Solís, V., Malheiros, D., Beltrame, M. H., Vargas, L. d. B., Dourado, R. M., Issler, H. C., ... Augusto, D. G. (2019, June). Unveiling the Diversity of Immunoglobulin Heavy Constant Gamma (IGHG) Gene Segments in Brazilian Populations Reveals 28 Novel Alleles and Evidence of Gene Conversion and Natural Selection. *Frontiers in Immunology*, *10*. Retrieved 2025-05-28, from https://www.frontiersin.org/journals/immunology/articles/10.3389/fimmu.2019.01161/full doi: 10.3389/fimmu.2019.01161

Cambier, J. C., Gauld, S. B., Merrell, K. T., & Vilen, B. J. (2007, August). B-cell anergy: from transgenic models to naturally occurring anergic B cells? *Nature Reviews Immunology*, *7*(8), 633–643. Retrieved 2025-11-26, from https://www.nature.com/articles/nri2133 doi: 10.1038/

nri2133

Cambridge, G., Stohl, W., Leandro, M. J., Migone, T.-S., Hilbert, D. M., & Edwards, J. C. W. (2006, March). Circulating levels of B lymphocyte stimulator in patients with rheumatoid arthritis following rituximab treatment: relationships with B cell depletion, circulating antibodies, and clinical relapse. *Arthritis and Rheumatism*, *54*(3), 723–732. doi: 10.1002/art.21650

Carlsen, T. G., Hjelholt, A., Jurik, A. G., Schiøttz-Christensen, B., Zejden, A., Christiansen, G., ... Birkelund, S. (2013). IgG subclass antibodies to human and bacterial HSP60 are not associated with disease activity and progression over time in axial spondyloarthritis. *Arthritis Research & Therapy*, *15*(3), R61. Retrieved 2025-09-24, from https://pmc.ncbi.nlm.nih.gov/articles/PMC4060232/ doi: 10.1186/ar4234

Caro-Maldonado, A., Wang, R., Nichols, A. G., Kuraoka, M., Milasta, S., Sun, L. D., ... Rathmell, J. C. (2014, April). Metabolic reprogramming is required for antibody production that is suppressed in anergic but exaggerated in chronically BAFF-exposed B cells. *Journal of Immunology (Baltimore, Md.: 1950)*, *192*(8), 3626–3636. doi: 10.4049/jimmunol.1302062

Casal Moura, M., Merkel, P. A., Jayne, D., Cid, M. C., Basu, N., Hellmich, B., ... Kronbichler, A. (2025, December). Challenges in the diagnosis, classification and prognosis of ANCA-associated vasculitis. *Nature Reviews Rheumatology*, *21*(12), 719–736. Retrieved 2025-11-30, from https://www.nature.com/articles/s41584-025-01306-w doi: 10.1038/s41584-025-01306-w

Castleman, M. J., Stumpf, M. M., Therrien, N. R., Smith, M. J., Lesteberg, K. E., Palmer, B. E., ... Torres, R. M. (2022, April). SARS-CoV-2

infection relaxes peripheral B cell tolerance. *Journal of Experimental Medicine*, *219*(6), e20212553. Retrieved 2022-06-10, from https://doi.org/10.1084/jem.20212553 doi: 10.1084/jem.20212553

Cañete, J. D., Santiago, B., Cantaert, T., Sanmartí, R., Palacin, A., Celis, R., ... Pablos, J. L. (2007, June). Ectopic lymphoid neogenesis in psoriatic arthritis. *Annals of the Rheumatic Diseases*, *66*(6), 720–726. Retrieved 2022-06-09, from https://ard.bmj.com/content/66/6/720 doi: 10.1136/ard.2006.062042

Cerezo, M., Sollis, E., Ji, Y., Lewis, E., Abid, A., Bircan, K., ... Harris, L. W. (2025, January). The NHGRI-EBI GWAS Catalog: standards for reusability, sustainability and diversity. *Nucleic Acids Research*, *53*(D1), D998–D1005. Retrieved 2025-07-25, from https://doi.org/10.1093/nar/gkae1070 doi: 10.1093/nar/gkae1070

Cerutti, A. (2008, June). The regulation of IgA class switching. *Nature Reviews Immunology*, *8*(6), 421–434. Retrieved 2025-11-03, from https://www.nature.com/articles/nri2322 doi: 10.1038/nri2322

Cheng, Y., Hu, X., Liu, C., Chen, M., Wang, J., Wang, M., ... Min, R. (2017). Gelsolin Inhibits the Inflammatory Process Induced by LPS. *Cellular Physiology and Biochemistry: International Journal of Experimental Cellular Physiology, Biochemistry, and Pharmacology*, *41*(1), 205–212. doi: 10.1159/000456043

Chiron, D., Bekeredjian-Ding, I., Pellat-Deceunynck, C., Bataille, R., & Jego, G. (2008, September). Toll-like receptors: lessons to learn from normal and malignant human B cells. *Blood*, *112*(6), 2205–2213. Retrieved 2025-11-26, from https://doi.org/10.1182/blood-2008-02-140673 doi: 10.1182/blood-2008-02-140673

Clark, E. A., & Giltiay, N. V. (2018, September). CD22: A

Regulator of Innate and Adaptive B Cell Responses and Autoimmunity. *Frontiers in Immunology*, *9*. Retrieved 2025-11-25, from https://www.frontiersin.org/journals/immunology/articles/10.3389/fimmu.2018.02235/full doi: 10.3389/fimmu.2018.02235

Coperchini, F., Chiovato, L., & Rotondi, M. (2021). Interleukin-6, CXCL10 and Infiltrating Macrophages in COVID-19-Related Cytokine Storm: Not One for All But All for One! *Frontiers in Immunology*, *12*, 668507. doi: 10.3389/fimmu.2021.668507

Cornaby, C., Gibbons, L., Mayhew, V., Sloan, C. S., Welling, A., & Poole, B. D. (2015, January). B cell epitope spreading: Mechanisms and contribution to autoimmune diseases. *Immunology Letters*, *163*(1), 56–68. Retrieved 2025-09-26, from https://www.sciencedirect.com/science/article/pii/S0165247814002557 doi: 10.1016/j.imlet.2014.11.001

Cuervo, A., Celis, R., Julià, A., Usategui, A., Faré, R., Ramírez, J., ... Cañete, J. D. (2021, April). Synovial Immunohistological Biomarkers of the Classification of Undifferentiated Arthritis Evolving to Rheumatoid or Psoriatic Arthritis. *Frontiers in Medicine*, *8*. Retrieved 2025-12-01, from https://www.frontiersin.org/journals/medicine/articles/10.3389/fmed.2021.656667/full doi: 10.3389/fmed.2021.656667

Cui, N., Qian, Q., Zhou, Y., Zhang, H., Zhang, H., Wang, B., ... Ma, X. (2025, January). Extracellular Inosine Induces Anergy in B Cells to Alleviate Autoimmune Hepatitis. *Cellular and Molecular Gastroenterology and Hepatology*, *19*(10). Retrieved 2025-11-25, from https://www.cmghjournal.org/article/S2352-345X(25)

00080-3/fulltext doi: 10.1016/j.jcmgh.2025.101539

Darce, J. R., Arendt, B. K., Wu, X., & Jelinek, D. F. (2007, December). Regulated expression of BAFF-binding receptors during human B cell differentiation. *Journal of Immunology (Baltimore, Md.: 1950)*, *179*(11), 7276–7286. doi: 10.4049/jimmunol.179.11.7276

Daridon, C., Blassfeld, D., Reiter, K., Mei, H. E., Giesecke, C., Goldenberg, D. M., ... Dörner, T. (2010). Epratuzumab targeting of CD22 affects adhesion molecule expression and migration of B-cells in systemic lupus erythematosus. *Arthritis Research & Therapy*, *12*(6), R204. doi: 10.1186/ar3179

de Groot, K., Harper, L., Jayne, D. R. W., Flores Suarez, L. F., Gregorini, G., Gross, W. L., ... EUVAS (European Vasculitis Study Group) (2009, May). Pulse versus daily oral cyclophosphamide for induction of remission in antineutrophil cytoplasmic antibody-associated vasculitis: a randomized trial. *Annals of Internal Medicine*, *150*(10), 670–680. doi: 10.7326/0003-4819-150-10-200905190-00004

Deligeorgakis, D., Skouvaklidou, E., Skepastianos, V., Tsafis, K., & Kougkas, N. (2025, July). Uveitis in Psoriatic Arthritis: A Comprehensive Review. *European Journal of Rheumatology*, *12*(2), e24078. Retrieved 2025-11-27, from https://pmc.ncbi.nlm.nih.gov/articles/PMC12277768/ doi: 10.5152/eurjrheum.2025.24078

De Maio, A. (2011, May). Extracellular heat shock proteins, cellular export vesicles, and the Stress Observation System: A form of communication during injury, infection, and cell damage. *Cell Stress and Chaperones*, *16*(3), 235–249. Retrieved 2025-09-24, from https://www.sciencedirect.com/science/article/pii/S1355814523009410 doi: 10.1007/s12192-010-0236-4

den Hartog, G., van Osch, T. L., Vos, M., Meijer, B., Savelkoul, H. F., van Neerven, R. J., & Brugman, S. (2018, February). BAFF augments IgA2 and IL-10 production by TLR7/8 stimulated total peripheral blood B cells. *European Journal of Immunology*, *48*(2), 283–292. Retrieved 2025-11-03, from https://pmc.ncbi.nlm.nih.gov/articles/PMC5836859/ doi: 10.1002/eji.201646861

Descatoire, M., Weill, J.-C., Reynaud, C.-A., & Weller, S. (2011, December). A human equivalent of mouse B-1 cells? *The Journal of Experimental Medicine*, *208*(13), 2563–2564. Retrieved 2025-11-26, from https://pmc.ncbi.nlm.nih.gov/articles/PMC3244035/ doi: 10.1084/jem.20112232

DiNubile, M. J. (2008, December). Plasma gelsolin as a biomarker of inflammation. *Arthritis Research & Therapy*, *10*(6), 124. Retrieved 2025-09-25, from https://doi.org/10.1186/ar2547 doi: 10.1186/ar2547

Dizon, B. L. P., Holla, P., Mutic, E. C., Schaughency, P., & Pierce, S. K. (2025, May). Human naïve B cells show evidence of anergy and clonal redemption following vaccination. *npj Vaccines*, *10*(1), 96. Retrieved 2025-11-25, from https://www.nature.com/articles/s41541-025-01133-w doi: 10.1038/s41541-025-01133-w

Di Niro, R., Lee, S.-J., Vander Heiden, J. A., Elsner, R. A., Trivedi, N., Bannock, J. M., ... Shlomchik, M. J. (2015, July). Salmonella Infection Drives Promiscuous B Cell Activation Followed by Extrafollicular Affinity Maturation. *Immunity*, *43*(1), 120–131. Retrieved 2025-05-25, from https://www.cell.com/immunity/abstract/S1074-7613(15)00257-5 doi: 10.1016/j.immuni.2015.06.013

Dong, Y., Pi, X., Bartels-Burgahn, F., Saltukoglu, D., Liang, Z., Yang, J., ... Wu, H. (2022, December). Structural principles of B cell antigen

receptor assembly. *Nature*, *612*(7938), 156–161. Retrieved 2025-12-02, from https://www.nature.com/articles/s41586-022-05412-7 doi: 10.1038/s41586-022-05412-7

Doorenspleet, M. E., Hair, M. J. d., Herenius, M. M., Klarenbeek, P. L., Wijbrandts, C. A., Sande, M. G. v. d., ... Vries, N. d. (2011, March). In rheumatoid arthritis highly expanded B cell clones can be found in the early synovitis stage. *Annals of the Rheumatic Diseases*, *70*(Suppl 2), A63–A63. Retrieved 2025-11-27, from https://ard.bmj.com/content/70/Suppl_2/A63.2 doi: 10.1136/ard.2010.149005.15

Duan, X., Liu, X., Liu, N., Huang, Y., Jin, Z., Zhang, S., ... Chen, H. (2020, February). Inhibition of keratinocyte necroptosis mediated by RIPK1/RIPK3/MLKL provides a protective effect against psoriatic inflammation. *Cell Death & Disease*, *11*(2), 134. Retrieved 2025-09-24, from https://www.nature.com/articles/s41419-020-2328-0 doi: 10.1038/s41419-020-2328-0

Duty, J. A., Szodoray, P., Zheng, N.-Y., Koelsch, K. A., Zhang, Q., Swiatkowski, M., ... Wilson, P. C. (2008, December). Functional anergy in a subpopulation of naive B cells from healthy humans that express autoreactive immunoglobulin receptors. *Journal of Experimental Medicine*, *206*(1), 139–151. Retrieved 2023-11-15, from https://doi.org/10.1084/jem.20080611 doi: 10.1084/jem.20080611

Ehrhardt, G. R., Hsu, J. T., Gartland, L., Leu, C.-M., Zhang, S., Davis, R. S., & Cooper, M. D. (2005, September). Expression of the immunoregulatory molecule FcRH4 defines a distinctive tissue-based population of memory B cells. *The Journal of Experimental Medicine*, *202*(6), 783–791. Retrieved 2025-12-01, from https://pmc.ncbi.nlm.nih.gov/articles/PMC2212938/ doi: 10.1084/jem.20050879

Eker, Y. O., Pamuk, O. N., Pamuk, G. E., Dönmez, S., & Çakır, N. (2014). The Frequency of anti-CCP antibodies in patients with rheumatoid arthritis and psoriatic arthritis and their relationship with clinical features and parameters of angiogenesis: A comparative study. *European Journal of Rheumatology*, *1*(2), 67–71. Retrieved 2025-09-26, from https://eurjrheumatol.org/index.php/pub/article/view/18 doi: 10.5152/eurjrheumatol.2014.022

Ekland, E. H., Forster, R., Lipp, M., & Cyster, J. G. (2004, April). Requirements for follicular exclusion and competitive elimination of autoantigen-binding B cells. *Journal of Immunology (Baltimore, Md.: 1950)*, *172*(8), 4700–4708. doi: 10.4049/jimmunol.172.8.4700

Elliott, S. E., Kongpachith, S., Lingampalli, N., Adamska, J. Z., Cannon, B. J., Blum, L. K., ... Robinson, W. H. (2020, March). B cells in rheumatoid arthritis synovial tissues encode focused antibody repertoires that include antibodies that stimulate macrophage TNF-alpha production. *Clinical Immunology*, *212*, 108360. Retrieved 2025-09-27, from https://www.sciencedirect.com/science/article/pii/S1521661619306448 doi: 10.1016/j.clim.2020.108360

Erdei, A., Kovács, K. G., Nagy-Baló, Z., Lukácsi, S., Mácsik-Valent, B., Kurucz, I., & Bajtay, Z. (2021, September). New aspects in the regulation of human B cell functions by complement receptors CR1, CR2, CR3 and CR4. *Immunology Letters*, *237*, 42–57. Retrieved 2025-11-25, from https://www.sciencedirect.com/science/article/pii/S0165247821001000 doi: 10.1016/j.imlet.2021.06.006

Esawy, M. M., Makram, W. K., Albalat, W., & Shabana, M. A. (2020, June). Plasma gelsolin levels in patients with psoriatic arthritis: a possible novel marker. *Clinical Rheumatology*, *39*(6), 1881–1888. Retrieved 2025-

09-25, from https://doi.org/10.1007/s10067-020-04959-y doi: 10.1007/s10067-020-04959-y

Ettinger, R., Sims, G. P., Robbins, R., Withers, D., Fischer, R. T., Grammer, A. C., ... Lipsky, P. E. (2007, March). IL-21 and BAFF/BLyS Synergize in Stimulating Plasma Cell Differentiation from a Unique Population of Human Splenic Memory B Cells1. *The Journal of Immunology*, *178*(5), 2872–2882. Retrieved 2025-11-30, from https://doi.org/10.4049/jimmunol.178.5.2872 doi: 10.4049/jimmunol.178.5.2872

Figueroa, P. L. d., Fafian-Labora, J., Lorenzo-Gomez, I., Calamia, V., Lotz, M., López-Otín, C., ... Carames, B. (2023, March). Lamin A/C Accumulation By Defective Autophagy Is Associated With Chondrocyte Senescence And Joint Damage. *Osteoarthritis and Cartilage*, *31*, S327. Retrieved 2025-09-25, from https://www.oarsijournal.com/article/S1063-4584%2823%2900375-8/fulltext?utm_source=chatgpt.com doi: 10.1016/j.joca.2023.01.357

Fitzgerald, A. A., & Weiner, L. M. (2020, September). The role of fibroblast activation protein in health and malignancy. *Cancer metastasis reviews*, *39*(3), 783–803. Retrieved 2025-09-25, from https://pmc.ncbi.nlm.nih.gov/articles/PMC7487063/ doi: 10.1007/s10555-020-09909-3

FitzGerald, O., Ogdie, A., Chandran, V., Coates, L. C., Kavanaugh, A., Tillett, W., ... Mease, P. J. (2021, August). Psoriatic arthritis. *Nature Reviews Disease Primers*, *7*(1), 59. Retrieved 2025-09-24, from https://www.nature.com/articles/s41572-021-00293-y doi: 10.1038/s41572-021-00293-y

Floudas, A., Smith, C. M., Tynan, O., Neto, N., Krishna, V., Wade, S. M., ... Fearon, U. (2022, September). Distinct stromal and immune cell

interactions shape the pathogenesis of rheumatoid and psoriatic arthritis. *Annals of the Rheumatic Diseases*, *81*(9), 1224–1242. Retrieved 2022-10-10, from https://ard.bmj.com/content/81/9/1224 doi: 10.1136/annrheumdis-2021-221761

Foote, J. B., Mahmoud, T. I., Vale, A. M., & Kearney, J. F. (2012, January). Long Term Maintenance of Polysaccharide-specific Antibodies by IgM Secreting Cells. *Journal of immunology (Baltimore, Md. : 1950)*, *188*(1), 57–67. Retrieved 2025-05-25, from https://www.ncbi.nlm.nih.gov/pmc/articles/PMC3244511/ doi: 10.4049/jimmunol.1100783

Frasca, L., Palazzo, R., Chimenti, M. S., Alivernini, S., Tolusso, B., Bui, L., ... Lande, R. (2018). Anti-LL37 Antibodies Are Present in Psoriatic Arthritis (PsA) Patients: New Biomarkers in PsA. *Frontiers in Immunology*, *9*. Retrieved 2022-06-09, from https://www.frontiersin.org/article/10.3389/fimmu.2018.01936

Frasca, L., Palazzo, R., Chimenti, M. S., Botti, E., Auteri, S. E., Spadaro, F., ... Lande, R. (2018, June). SAT0039 Ll37 up-regulation and anti-ll37 reactivity are shared by psoriasis and psoriatic arthritis patients. *Annals of the Rheumatic Diseases*, *77*(Suppl 2), 884–884. Retrieved 2025-09-23, from https://ard.bmj.com/content/77/Suppl_2/884.1 doi: 10.1136/annrheumdis-2018-eular.5725

Fujimoto, S., Watts, R. A., Kobayashi, S., Suzuki, K., Jayne, D. R. W., Scott, D. G. I., ... Nunoi, H. (2011, October). Comparison of the epidemiology of anti-neutrophil cytoplasmic antibody-associated vasculitis between Japan and the U.K. *Rheumatology (Oxford, England)*, *50*(10), 1916–1920. doi: 10.1093/rheumatology/ker205

Fyrand, O., Mellbye, O. J., & Natvig, J. B. (1977, September). Immunofluorescence studies for immunoglobulins and complement C3

in synovial joint membranes in psoriatic arthritis. *Clinical and Experimental Immunology*, *29*(3), 422–427. Retrieved 2025-09-27, from https://pmc.ncbi.nlm.nih.gov/articles/PMC1541064/

Gardam, S., & Brink, R. (2014, January). Non-Canonical NF-κB Signaling Initiated by BAFF Influences B Cell Biology at Multiple Junctures. *Frontiers in Immunology*, *4*, 509. Retrieved 2025-12-01, from https://pmc.ncbi.nlm.nih.gov/articles/PMC3880999/ doi: 10.3389/fimmu.2013.00509

Gauld, S. B., Benschop, R. J., Merrell, K. T., & Cambier, J. C. (2005, November). Maintenance of B cell anergy requires constant antigen receptor occupancy and signaling. *Nature Immunology*, *6*(11), 1160–1167. Retrieved 2025-11-26, from https://www.nature.com/articles/ni1256 doi: 10.1038/ni1256

Gay, D., Saunders, T., Camper, S., & Weigert, M. (1993, April). Receptor editing: an approach by autoreactive B cells to escape tolerance. *Journal of Experimental Medicine*, *177*(4), 999–1008. Retrieved 2025-11-26, from https://doi.org/10.1084/jem.177.4.999 doi: 10.1084/jem.177.4.999

Gelsing, C., Bennike, T., Christiansen, G., & Birkelund, S. (2013, July). A role for anti-HSP60 antibodies in arthritis: a critical review. *OA Arthritis*, *1*(2). Retrieved 2025-09-26, from http://www.oapublishinglondon.com/article/879 doi: 10.13172/2052-9554-1-2-879

Getahun, A., Beavers, N. A., Larson, S. R., Shlomchik, M. J., & Cambier, J. C. (2016, May). Continuous inhibitory signaling by both SHP-1 and SHIP-1 pathways is required to maintain unresponsiveness of anergic B cells. *The Journal of Experimental Medicine*, *213*(5), 751–769. doi: 10.1084/jem.20150537

Ghazzali, S., Harch, I. E., Akasbi, N., Mezouar, I. E., & Harzy, T. (2022, June). AB0964 Psoriatic arthritis (PsA) with positive rheumatoid factor (RF) versus psoriatic arthritis with negative RF. *Annals of the Rheumatic Diseases*, *81*(Suppl 1), 1609–1609. Retrieved 2025-09-23, from https://ard.bmj.com/content/81/Suppl_1/1609.2 doi: 10.1136/annrheumdis-2022-eular.5121

Goodnow, C. C., Crosbie, J., Adelstein, S., Lavoie, T. B., Smith-Gill, S. J., Brink, R. A., ... Basten, A. (1988, August). Altered immunoglobulin expression and functional silencing of self-reactive B lymphocytes in transgenic mice. *Nature*, *334*(6184), 676–682. Retrieved 2025-05-28, from https://www.nature.com/articles/334676a0 doi: 10.1038/334676a0

Gossec, L., Kerschbaumer, A., Ferreira, R. J. O., Aletaha, D., Baraliakos, X., Bertheussen, H., ... Smolen, J. S. (2024, May). EULAR recommendations for the management of psoriatic arthritis with pharmacological therapies: 2023 update. *Annals of the Rheumatic Diseases*, *83*(6), 706–719. doi: 10.1136/ard-2024-225531

Gross, A. J., Lyandres, J. R., Panigrahi, A. K., Prak, E. T. L., & DeFranco, A. L. (2009, May). Developmental Acquisition of the Lyn–CD22–SHP-1 Inhibitory Pathway Promotes B Cell Tolerance. *Journal of immunology (Baltimore, Md. : 1950)*, *182*(9), 5382–5392. Retrieved 2025-11-23, from https://pmc.ncbi.nlm.nih.gov/articles/PMC2840041/ doi: 10.4049/jimmunol.0803941

Gruber, C., Skare, T., Campos, A. P. B., Simioni, J., Maestri, V., & Nisihara, R. (2020, November). Assessment of serum levels of anti-cyclic citrullinated peptide antibodies in patients with psoriatic arthritis: A cross-sectional study in a Brazilian cohort. *Biomedical Reports*, *13*(5), 1–

1. Retrieved 2025-09-26, from https://www.spandidos-publications.com/10.3892/br.2020.1343 doi: 10.3892/br.2020.1343

Guth, A. M., Zhang, X., Smith, D., Detanico, T., & Wysocki, L. J. (2003, December). Chromatin Specificity of Anti-Double-Stranded DNA Antibodies and a Role for Arg Residues in the Third Complementarity-Determining Region of the Heavy Chain. *The Journal of Immunology*, *171*(11), 6260–6266. Retrieved 2025-11-25, from https://journals.aai.org/jimmunol/article/171/11/6260/35974/Chromatin-Specificity-of-Anti-Double-Stranded-DNA doi: 10.4049/jimmunol.171.11.6260

GWAS Catalog - Study accession: GCST90243956. (n.d.). Retrieved 2025-07-25, from https://www.ebi.ac.uk/gwas/studies/GCST90243956 (Summary statistics were downloaded from the NHGRI-EBI GWAS Catalog (Cerezo et al., 2025) on 01/02/2025 for study GCST90243956 (Soomro et al., 2022))

Hagen, E. C., Daha, M. R., Hermans, J., Andrassy, K., Csernok, E., Gaskin, G., ... for the EC/BCR Project for ANCA Assay Standardization (1998, March). Diagnostic value of standardized assays for anti-neutrophil cytoplasmic antibodies in idiopathic systemic vasculitis. *Kidney International*, *53*(3), 743–753. Retrieved 2025-11-30, from https://www.sciencedirect.com/science/article/pii/S0085253815604525 doi: 10.1046/j.1523-1755.1998.00807.x

Hartley, S. B., Crosbie, J., Brink, R., Kantor, A. B., Basten, A., & Goodnow, C. C. (1991, October). Elimination from peripheral lymphoid tissues of self-reactive B lymphocytes recognizing membrane-bound antigens. *Nature*, *353*(6346), 765–769. Retrieved 2025-05-28, from https://www.nature.com/articles/353765a0 doi: 10.1038/353765a0

He, B., Xu, W., Santini, P. A., Polydorides, A. D., Chiu, A., Estrella, J., ... Cerutti, A. (2007, June). Intestinal bacteria trigger T cell-independent immunoglobulin A(2) class switching by inducing epithelial-cell secretion of the cytokine APRIL. *Immunity*, *26*(6), 812–826. doi: 10.1016/j.immuni.2007.04.014

Hegoburu, A., Amer, M., Frizelle, F., & Purcell, R. (2025, May). B cells and tertiary lymphoid structures in cancer therapy response. *BJC Reports*, *3*(1), 40. Retrieved 2025-12-02, from https://www.nature.com/articles/s44276-025-00146-1 doi: 10.1038/s44276-025-00146-1

Hellmich, B., Sanchez-Alamo, B., Schirmer, J. H., Berti, A., Blockmans, D., Cid, M. C., ... Jayne, D. (2024, January). EULAR recommendations for the management of ANCA-associated vasculitis: 2022 update. *Annals of the Rheumatic Diseases*, *83*(1), 30–47. Retrieved 2025-11-30, from https://ard.bmj.com/content/83/1/30 doi: 10.1136/ard-2022-223764

Herlands, R. A., Christensen, S. R., Sweet, R. A., Hershberg, U., & Shlomchik, M. J. (2008, August). T Cell-Independent and Toll-like Receptor-Dependent Antigen-Driven Activation of Autoreactive B Cells. *Immunity*, *29*(2), 249–260. Retrieved 2025-05-25, from https://www.cell.com/immunity/abstract/S1074-7613(08)00323-3 doi: 10.1016/j.immuni.2008.06.009

Hjelholt, A., Christiansen, G., Sørensen, U. S., & Birkelund, S. (2013, April). IgG subclass profiles in normal human sera of antibodies specific to five kinds of microbial antigens. *Pathogens and Disease*, *67*(3), 206–213. Retrieved 2025-11-03, from https://doi.org/10.1111/2049-632X.12034 doi: 10.1111/2049-632X.12034

Holden, N. J., Williams, J. M., Morgan, M. D., Challa, A., Gordon, J., Pepper, R. J., ... Savage, C. O. S. (2011, December). ANCA-stimulated neutrophils release BLyS and promote B cell survival: a clinically relevant cellular process. *Annals of the Rheumatic Diseases*, *70*(12), 2229–2233. Retrieved 2025-11-30, from https://ard.eular.org/article/S0003-4967(24)19064-4/abstract doi: 10.1136/ard.2011.153890

Holla, P., Ambegaonkar, A., Sohn, H., & Pierce, S. K. (2019, November). Exhaustion may not be in the human B cell vocabulary, at least not in malaria. *Immunological Reviews*, *292*(1), 139–148. doi: 10.1111/imr.12809

Holla, P., Dizon, B., Ambegaonkar, A. A., Rogel, N., Goldschmidt, E., Boddapati, A. K., ... Madi, A. (2021, May). Shared transcriptional profiles of atypical B cells suggest common drivers of expansion and function in malaria, HIV, and autoimmunity. *Science Advances*, *7*(22), eabg8384. Retrieved 2025-11-25, from https://www.science.org/doi/10.1126/sciadv.abg8384 doi: 10.1126/sciadv.abg8384

Holle, J. U., Dubrau, C., Herlyn, K., Heller, M., Ambrosch, P., Noelle, B., ... Gross, W. L. (2012, March). Rituximab for refractory granulomatosis with polyangiitis (Wegener's granulomatosis): comparison of efficacy in granulomatous versus vasculitic manifestations. *Annals of the Rheumatic Diseases*, *71*(3), 327–333. doi: 10.1136/ard.2011.153601

Huggins, J., Pellegrin, T., Felgar, R. E., Wei, C., Brown, M., Zheng, B., ... Zand, M. S. (2007, February). CpG DNA activation and plasma-cell differentiation of CD27− naive human B cells. *Blood*, *109*(4), 1611–1619. Retrieved 2025-11-13, from https://pmc.ncbi.nlm.nih.gov/articles/PMC1794051/ doi: 10.1182/blood-2006-03-008441

Humby, F., Bombardieri, M., Manzo, A., Kelly, S., Blades, M. C., Kirkham, B.,

... Pitzalis, C. (2009, January). Ectopic lymphoid structures support ongoing production of class-switched autoantibodies in rheumatoid synovium. *PLoS medicine*, *6*(1), e1. doi: 10.1371/journal.pmed.0060001

Inaba, A., Tuong, Z. K., Zhao, T. X., Stewart, A. P., Mathews, R., Truman, L., ... Clatworthy, M. R. (2023, April). Low-dose IL-2 enhances the generation of IL-10-producing immunoregulatory B cells. *Nature Communications*, *14*(1), 2071. Retrieved 2025-11-22, from https://www.nature.com/articles/s41467-023-37424-w doi: 10.1038/s41467-023-37424-w

Isnardi, I., Ng, Y.-S., Menard, L., Meyers, G., Saadoun, D., Srdanovic, I., ... Meffre, E. (2010, June). Complement receptor 2/CD21− human naive B cells contain mostly autoreactive unresponsive clones. *Blood*, *115*(24), 5026–5036. Retrieved 2022-10-10, from https://doi.org/10.1182/blood-2009-09-243071 doi: 10.1182/blood-2009-09-243071

Jacobi, A. M., Huang, W., Wang, T., Freimuth, W., Sanz, I., Furie, R., ... Davidson, A. (2010, January). Effect of long-term belimumab treatment on B cells in systemic lupus erythematosus: extension of a phase II, double-blind, placebo-controlled, dose-ranging study. *Arthritis and Rheumatism*, *62*(1), 201–210. doi: 10.1002/art.27189

Jenks, S. A., Cashman, K. S., Zumaquero, E., Marigorta, U. M., Patel, A. V., Wang, X., ... Sanz, I. (2018, October). Distinct Effector B Cells Induced by Unregulated Toll-like Receptor 7 Contribute to Pathogenic Responses in Systemic Lupus Erythematosus. *Immunity*, *49*(4), 725–739.e6. Retrieved 2023-11-24, from https://linkinghub.elsevier.com/retrieve/pii/S1074761318303789 doi: 10.1016/j.immuni.2018.08.015

Jennette, J. C., Falk, R. J., Hu, P., & Xiao, H. (2013, January). Patho-

genesis of antineutrophil cytoplasmic autoantibody-associated small-vessel vasculitis. *Annual Review of Pathology*, *8*, 139–160. doi: 10.1146/annurev-pathol-011811-132453

Jiang, W., Lederman, M. M., Harding, C. V., Rodriguez, B., Mohner, R. J., & Sieg, S. F. (2007). TLR9 stimulation drives naïve B cells to proliferate and to attain enhanced antigen presenting function. *European Journal of Immunology*, *37*(8), 2205–2213. Retrieved 2025-11-13, from https://onlinelibrary.wiley.com/doi/abs/10.1002/eji.200636984 (_eprint: https://onlinelibrary.wiley.com/doi/pdf/10.1002/eji.200636984) doi: 10.1002/eji.200636984

Jokiranta, S. T., Nguyen Ngoc, A., Huang, X., Nowlan, K., Hannolainen, L., Pyöriä, L., ... Kekäläinen, E. (2026, February). B cell dysregulation during acute COVID-19 is transient. *Immunology Letters*, *277*, 107086. Retrieved 2025-11-24, from https://www.sciencedirect.com/science/article/pii/S0165247825001191 doi: 10.1016/j.imlet.2025.107086

Jones, B. E., Yang, J., Muthigi, A., Hogan, S. L., Hu, Y., Starmer, J., ... Ciavatta, D. J. (2017, April). Gene-Specific DNA Methylation Changes Predict Remission in Patients with ANCA-Associated Vasculitis. *Journal of the American Society of Nephrology: JASN*, *28*(4), 1175–1187. doi: 10.1681/ASN.2016050548

Jones, R. B., Tervaert, J. W. C., Hauser, T., Luqmani, R., Morgan, M. D., Peh, C. A., ... Jayne, D. R. W. (2010, July). Rituximab versus Cyclophosphamide in ANCA-Associated Renal Vasculitis. *New England Journal of Medicine*, *363*(3), 211–220. Retrieved 2025-11-30, from https://www.nejm.org/doi/full/10.1056/NEJMoa0909169 (_eprint: https://www.nejm.org/doi/pdf/10.1056/NEJMoa0909169) doi: 10.1056/NEJMoa0909169

Kaminski, D. A., Wei, C., Qian, Y., Rosenberg, A. F., & Sanz, I. (2012, October). Advances in Human B Cell Phenotypic Profiling. *Frontiers in Immunology*, *3*. Retrieved 2025-11-29, from https://www.frontiersin.org/journals/immunology/articles/10.3389/fimmu.2012.00302/full doi: 10.3389/fimmu.2012.00302

Kamleh, M. A., Snowden, S. G., Grapov, D., Blackburn, G. J., Watson, D. G., Xu, N., ... Wheelock, C. E. (2015, January). LC-MS metabolomics of psoriasis patients reveals disease severity-dependent increases in circulating amino acids that are ameliorated by anti-TNFα treatment. *Journal of Proteome Research*, *14*(1), 557–566. doi: 10.1021/pr500782g

Kaneko, N., Kuo, H.-H., Boucau, J., Farmer, J. R., Allard-Chamard, H., Mahajan, V. S., ... Massachusetts Consortium on Pathogen Readiness Specimen Working Group (2020, October). Loss of Bcl-6-Expressing T Follicular Helper Cells and Germinal Centers in COVID-19. *Cell*, *183*(1), 143–157.e13. doi: 10.1016/j.cell.2020.08.025

Karnell, J. L., & Ettinger, R. (2012, January). The Interplay of IL-21 and BAFF in the Formation and Maintenance of Human B Cell Memory. *Frontiers in Immunology*, *3*, 2. Retrieved 2025-11-30, from https://pmc.ncbi.nlm.nih.gov/articles/PMC3342005/ doi: 10.3389/fimmu.2012.00002

Kawano, Y., Noma, T., & Yata, J. (1994, December). Regulation of human IgG subclass production by cytokines. IFN-gamma and IL-6 act antagonistically in the induction of human IgG1 but additively in the induction of IgG2. *The Journal of Immunology*, *153*(11), 4948–4958. Retrieved 2025-11-03, from https://doi.org/10.4049/jimmunol.153.11.4948 doi: 10.4049/jimmunol.153.11.4948

Kawasaki, A., Hasebe, N., Hidaka, M., Hirano, F., Sada, K.-E., Kobayashi, S., ... Tsuchiya, N. (2016). Protective Role of HLA-DRB1*13:02 against Microscopic Polyangiitis and MPO-ANCA-Positive Vasculitides in a Japanese Population: A Case-Control Study. *PloS One*, *11*(5), e0154393. doi: 10.1371/journal.pone.0154393

Kawasaki, N., Rademacher, C., & Paulson, J. C. (2011). CD22 regulates adaptive and innate immune responses of B cells. *Journal of Innate Immunity*, *3*(4), 411–419. doi: 10.1159/000322375

Keller, B., Strohmeier, V., Harder, I., Unger, S., Payne, K. J., Andrieux, G., ... Warnatz, K. (2021, October). The expansion of human T-bethighCD21low B cells is T cell dependent. *Science Immunology*, *6*(64), eabh0891. Retrieved 2025-11-29, from https://www.science.org/doi/10.1126/sciimmunol.abh0891 doi: 10.1126/sciimmunol.abh0891

Khaleque, M. A., Kim, J.-H., Tanvir, M. A. H., Park, J.-B., & Kim, Y.-Y. (2024, September). Significance of Necroptosis in Cartilage Degeneration. *Biomolecules*, *14*(9), 1192. Retrieved 2025-09-24, from https://www.mdpi.com/2218-273X/14/9/1192 doi: 10.3390/biom14091192

Khatri, I., Berkowska, M. A., van den Akker, E. B., Teodosio, C., Reinders, M. J. T., & van Dongen, J. J. M. (2021, July). Population matched (pm) germline allelic variants of immunoglobulin (IG) loci: Relevance in infectious diseases and vaccination studies in human populations. *Genes & Immunity*, *22*(3), 172–186. Retrieved 2025-05-15, from https://www.nature.com/articles/s41435-021-00143-7 doi: 10.1038/s41435-021-00143-7

Kishimoto, M., Deshpande, G. A., Fukuoka, K., Kawakami, T., Ikegaya, N., Kawashima, S., ... Kaname, S. (2021, June). Clinical features of psori-

atic arthritis. *Best Practice & Research Clinical Rheumatology*, *35*(2), 101670. Retrieved 2025-11-27, from https://www.sciencedirect.com/science/article/pii/S1521694221000127 doi: 10.1016/j.berh.2021.101670

Kovács, K. G., Mácsik-Valent, B., Matkó, J., Bajtay, Z., & Erdei, A. (2021, April). Revisiting the Coreceptor Function of Complement Receptor Type 2 (CR2, CD21); Coengagement With the B-Cell Receptor Inhibits the Activation, Proliferation, and Antibody Production of Human B Cells. *Frontiers in Immunology*, *12*. Retrieved 2025-11-25, from https://www.frontiersin.org/journals/immunology/articles/10.3389/fimmu.2021.620427/full doi: 10.3389/fimmu.2021.620427

Kraaij, T., Kamerling, S. W. A., de Rooij, E. N. M., van Daele, P. L. A., Bredewold, O. W., Bakker, J. A., ... Teng, Y. K. O. (2018, July). The NET-effect of combining rituximab with belimumab in severe systemic lupus erythematosus. *Journal of Autoimmunity*, *91*, 45–54. doi: 10.1016/j.jaut.2018.03.003

Kremlitzka, M., Polgár, A., Fülöp, L., Kiss, E., Poór, G., & Erdei, A. (2013, January). Complement receptor type 1 (CR1, CD35) is a potent inhibitor of B-cell functions in rheumatoid arthritis patients. *International Immunology*, *25*(1), 25–33. doi: 10.1093/intimm/dxs090

Krumbholz, M., Specks, U., Wick, M., Kalled, S. L., Jenne, D., & Meinl, E. (2005, December). BAFF is elevated in serum of patients with Wegener's granulomatosis. *Journal of Autoimmunity*, *25*(4), 298–302. doi: 10.1016/j.jaut.2005.08.004

Kumthekar, A., & Ogdie, A. (2020, June). Obesity and Psoriatic Arthritis: A Narrative Review. *Rheumatology and Therapy*, *7*(3), 447–456. Re-

trieved 2025-10-02, from https://pmc.ncbi.nlm.nih.gov/articles/PMC7410935/ doi: 10.1007/s40744-020-00215-6

Kuri-Cervantes, L., Pampena, M. B., Meng, W., Rosenfeld, A. M., Ittner, C. A. G., Weisman, A. R., ... Betts, M. R. (2020, July). Comprehensive mapping of immune perturbations associated with severe COVID-19. *Science Immunology*, *5*(49), eabd7114. Retrieved 2025-11-25, from https://www.science.org/doi/10.1126/sciimmunol.abd7114 doi: 10.1126/sciimmunol.abd7114

Legros, V., Denolly, S., Vogrig, M., Boson, B., Siret, E., Rigaill, J., ... Pozzetto, B. (2021, February). A longitudinal study of SARS-CoV-2-infected patients reveals a high correlation between neutralizing antibodies and COVID-19 severity. *Cellular & Molecular Immunology*, *18*(2), 318–327. Retrieved 2025-11-30, from https://www.nature.com/articles/s41423-020-00588-2 doi: 10.1038/s41423-020-00588-2

Lembke, S., Macfarlane, G. J., & Jones, G. T. (2024, December). The worldwide prevalence of psoriatic arthritis—a systematic review and meta-analysis. *Rheumatology*, *63*(12), 3211–3220. Retrieved 2025-10-01, from https://doi.org/10.1093/rheumatology/keae198 doi: 10.1093/rheumatology/keae198

Lesley, R., Xu, Y., Kalled, S. L., Hess, D. M., Schwab, S. R., Shu, H.-B., & Cyster, J. G. (2004, April). Reduced Competitiveness of Autoantigen-Engaged B Cells due to Increased Dependence on BAFF. *Immunity*, *20*(4), 441–453. Retrieved 2025-11-03, from https://www.sciencedirect.com/science/article/pii/S1074761304000792 doi: 10.1016/S1074-7613(04)00079-2

Li, Z., Obraztsova, A., Shang, F., Oludada, O. E., Malapit, J., Busch, K., ... Wardemann, H. (2024, September). Affinity-independent

memory B cell origin of the early antibody-secreting cell response in naive individuals upon SARS-CoV-2 vaccination. *Immunity*, *57*(9), 2191–2201.e5. Retrieved 2025-11-30, from https://www.cell.com/immunity/abstract/S1074-7613(24)00372-8 doi: 10.1016/j.immuni.2024.07.023

Litinskiy, M. B., Nardelli, B., Hilbert, D. M., He, B., Schaffer, A., Casali, P., & Cerutti, A. (2002, September). DCs induce CD40-independent immunoglobulin class switching through BLyS and APRIL. *Nature Immunology*, *3*(9), 822–829. Retrieved 2025-11-10, from https://www.nature.com/articles/ni829 doi: 10.1038/ni829

Liu, J.-C., Zhang, K., Zhang, X., Guan, F., Zeng, H., Kubo, M., ... Liu, C.-H. (2024). Immunoglobulin class-switch recombination: Mechanism, regulation, and related diseases. *MedComm*, *5*(8), e662. Retrieved 2025-11-03, from https://onlinelibrary.wiley.com/doi/abs/10.1002/mco2.662 (_eprint: https://onlinelibrary.wiley.com/doi/pdf/10.1002/mco2.662) doi: 10.1002/mco2.662

Liu, S., Hou, X. L., Sui, W. G., Lu, Q. J., Hu, Y. L., & Dai, Y. (2017, January). Direct measurement of B-cell receptor repertoire's composition and variation in systemic lupus erythematosus. *Genes & Immunity*, *18*(1), 22–27. Retrieved 2025-11-27, from https://www.nature.com/articles/gene201645 doi: 10.1038/gene.2016.45

Luo, Y., Pan, Q., Zhou, Z., Li, M., Wei, Y., Jiang, X., ... Li, F. (2023, May). 68Ga-FAPI PET/CT for Rheumatoid Arthritis: A Prospective Study. *Radiology*, *307*(3), e222052. Retrieved 2025-09-26, from https://pubs.rsna.org/doi/10.1148/radiol.222052 doi: 10.1148/radiol.222052

Lyons, P. A., Rayner, T. F., Trivedi, S., Holle, J. U., Watts, R. A., Jayne,

D. R. W., ... Smith, K. G. C. (2012, July). Genetically distinct subsets within ANCA-associated vasculitis. *The New England Journal of Medicine*, *367*(3), 214–223. doi: 10.1056/NEJMoa1108735

Lønnberg, A. S., Skov, L., Skytthe, A., Kyvik, K. O., Pedersen, O. B., & Thomsen, S. F. (2013, August). Heritability of psoriasis in a large twin sample. *The British Journal of Dermatology*, *169*(2), 412–416. doi: 10.1111/bjd.12375

Machet, T., Quémeneur, T., Ledoult, E., Mesbah, R., Lebas, C., Hachulla, E., & Pokeerbux, M. R. (2023, September). Rituximab resistance at 3 months of induction therapy in newly diagnosed or relapsing ANCA-associated vasculitis: A French multicentre retrospective study in 116 patients. *Joint Bone Spine*, *90*(5), 105591. Retrieved 2025-11-30, from https://www.sciencedirect.com/science/article/pii/S1297319X23000702 doi: 10.1016/j.jbspin.2023.105591

Maejima, H., Nagashio, R., Yanagita, K., Hamada, Y., Amoh, Y., Sato, Y., & Katsuoka, K. (2014). Moesin and stress-induced phosphoprotein-1 are possible sero-diagnostic markers of psoriasis. *PloS One*, *9*(7), e101773. doi: 10.1371/journal.pone.0101773

Mahr, A., Batteux, F., Tubiana, S., Goulvestre, C., Wolff, M., Papo, T., ... IMAGE Study Group (2014, June). Brief report: prevalence of antineutrophil cytoplasmic antibodies in infective endocarditis. *Arthritis & Rheumatology (Hoboken, N.J.)*, *66*(6), 1672–1677. doi: 10.1002/art.38389

Mantej, J., Polasik, K., Piotrowska, E., & Tukaj, S. (2019, January). Autoantibodies to heat shock proteins 60, 70, and 90 in patients with rheumatoid arthritis. *Cell Stress and Chaperones*, *24*(1), 283–287. Retrieved 2025-09-24, from https://doi.org/10.1007/s12192-018-0951-9 doi:

10.1007/s12192-018-0951-9

Mariette, X., Barone, F., Baldini, C., Bootsma, H., Clark, K. L., De Vita, S., ... Tak, P. P. (n.d.). A randomized, phase II study of sequential belimumab and rituximab in primary Sjögren's syndrome. *JCI Insight*, *7*(23), e163030. Retrieved 2025-12-01, from https://pmc.ncbi.nlm.nih.gov/articles/PMC9746921/ doi: 10.1172/jci.insight.163030

Mattos, M. S., Vandendriessche, S., Waisman, A., & Marques, P. E. (2024, August). The immunology of B-1 cells: from development to aging. *Immunity & Ageing*, *21*(1), 54. Retrieved 2025-11-26, from https://doi.org/10.1186/s12979-024-00455-y doi: 10.1186/s12979-024-00455-y

McClure, M. E., Gopaluni, S., Wason, J., Henderson, R. B., Van Maurik, A., Savage, C. C., ... on behalf the COMBIVAS investigators (2023, March). A randomised study of rituximab and belimumab sequential therapy in PR3 ANCA-associated vasculitis (COMBIVAS): design of the study protocol. *Trials*, *24*(1), 180. Retrieved 2025-11-11, from https://doi.org/10.1186/s13063-023-07218-y doi: 10.1186/s13063-023-07218-y

McClure, M. E., Wason, J., Gopaluni, S., Tieu, J., Smith, R. M., Jayne, D. R., & Jones, R. B. (2019, August). Evaluation of PR3-ANCA Status After Rituximab for ANCA-Associated Vasculitis. *Journal of Clinical Rheumatology: Practical Reports on Rheumatic & Musculoskeletal Diseases*, *25*(5), 217–223. doi: 10.1097/RHU.0000000000001030

McCluskey, D., Shipa, M. R. A., Chowdhury, K., James, J. A., Cooney, L. A., & Ehrenstein, M. R. (2025, August). IgA2+ B cells and IgA2 anti-dsDNA antibodies are selectively targeted by belimumab after rituximab therapy in systemic lupus erythematosus. *Cell Reports. Medicine*, *6*(8),

102247. doi: 10.1016/j.xcrm.2025.102247

Mcfadden, J., Valdimarsson, H., & Fry, L. (1991). Cross-reactivity between streptococcal M surface antigen and human skin. *British Journal of Dermatology*, *125*(5), 443–447. Retrieved 2025-09-26, from https://onlinelibrary.wiley.com/doi/abs/10.1111/j.1365-2133.1991.tb14769.x (_eprint: https://onlinelibrary.wiley.com/doi/pdf/10.1111/j.1365-2133.1991.tb14769.x) doi: 10.1111/j.1365-2133.1991.tb14769.x

McLellan, J. S., Pancera, M., Carrico, C., Gorman, J., Julien, J.-P., Khayat, R., ... Kwong, P. D. (2011, December). Structure of HIV-1 gp120 V1/V2 domain with broadly neutralizing antibody PG9. *Nature*, *480*(7377), 336–343. Retrieved 2025-11-28, from https://www.nature.com/articles/nature10696 doi: 10.1038/nature10696

Meffre, E., Milili, M., Blanco-Betancourt, C., Antunes, H., Nussenzweig, M. C., & Schiff, C. (2001, September). Immunoglobulin heavy chain expression shapes the B cell receptor repertoire in human B cell development. *The Journal of Clinical Investigation*, *108*(6), 879–886. doi: 10.1172/JCI13051

Meffre, E., & O'Connor, K. C. (2019, November). Impaired B cell tolerance checkpoints promote the development of autoimmune diseases and pathogenic autoantibodies. *Immunological reviews*, *292*(1), 90–101. Retrieved 2025-11-24, from https://pmc.ncbi.nlm.nih.gov/articles/PMC9145185/ doi: 10.1111/imr.12821

Melchers, F. (2015, June). Checkpoints that control B cell development. *The Journal of Clinical Investigation*, *125*(6), 2203–2210. Retrieved 2022-10-19, from https://www.ncbi.nlm.nih.gov/pmc/articles/PMC4497745/ doi: 10.1172/JCI78083

Merino-Vico, A., Frazzei, G., van Hamburg, J. P., & Tas, S. W. (2023). Targeting B cells and plasma cells in autoimmune diseases: From established treatments to novel therapeutic approaches. *European Journal of Immunology*, *53*(1), 2149675. Retrieved 2025-12-02, from https://onlinelibrary.wiley.com/doi/abs/10.1002/eji.202149675 (_eprint: https://onlinelibrary.wiley.com/doi/pdf/10.1002/eji.202149675) doi: 10.1002/eji.202149675

Merkenschlager, J., Pyo, A. G. T., Silva Santos, G. S., Schaefer-Babajew, D., Cipolla, M., Hartweger, H., ... Nussenzweig, M. C. (2025, May). Regulated somatic hypermutation enhances antibody affinity maturation. *Nature*, *641*(8062), 495–502. Retrieved 2025-05-12, from https://www.nature.com/articles/s41586-025-08728-2 doi: 10.1038/s41586-025-08728-2

Merola, J. F., Espinoza, L. R., & Fleischmann, R. (2018, August). Distinguishing rheumatoid arthritis from psoriatic arthritis. *RMD Open*, *4*(2), e000656. Retrieved 2025-12-01, from https://pmc.ncbi.nlm.nih.gov/articles/PMC6109814/ doi: 10.1136/rmdopen-2018-000656

Mikocziova, I., Gidoni, M., Lindeman, I., Peres, A., Snir, O., Yaari, G., & Sollid, L. M. (2020, June). Polymorphisms in human immunoglobulin heavy chain variable genes and their upstream regions. *Nucleic Acids Research*, *48*(10), 5499–5510. Retrieved 2025-05-28, from https://www.ncbi.nlm.nih.gov/pmc/articles/PMC7261178/ doi: 10.1093/nar/gkaa310

Mizutani, Y., Matsuoka, K., Takeda, H., Shiogama, K., Inada, K.-i., Hayakawa, K., ... Tsutsumi, Y. (2013, January). Novel approach to identifying autoantibodies in rheumatoid synovitis with a biotinylated human autoantigen library and the enzyme-labeled antigen method. *Journal*

of Immunological Methods, *387*(1-2), 57–70. doi: 10.1016/j.jim.2012.09.011

Moir, S., & Fauci, A. S. (2014, September). B-cell exhaustion in HIV infection: the role of immune activation. *Current opinion in HIV and AIDS*, *9*(5), 472–477. doi: 10.1097/COH.0000000000000092

Moir, S., Ho, J., Malaspina, A., Wang, W., DiPoto, A. C., O'Shea, M. A., ... Fauci, A. S. (2008, August). Evidence for HIV-associated B cell exhaustion in a dysfunctional memory B cell compartment in HIV-infected viremic individuals. *The Journal of Experimental Medicine*, *205*(8), 1797–1805. doi: 10.1084/jem.20072683

Morea, V., Tramontano, A., Rustici, M., Chothia, C., & Lesk, A. M. (1998, January). Conformations of the third hypervariable region in the VH domain of immunoglobulins1. *Journal of Molecular Biology*, *275*(2), 269–294. Retrieved 2025-12-02, from https://www.sciencedirect.com/science/article/pii/S002228369791442X doi: 10.1006/jmbi.1997.1442

Mouat, I. C., Goldberg, E., & Horwitz, M. S. (2022, July). Age-associated B cells in autoimmune diseases. *Cellular and Molecular Life Sciences: CMLS*, *79*(8), 402. Retrieved 2025-11-25, from https://pmc.ncbi.nlm.nih.gov/articles/PMC9263041/ doi: 10.1007/s00018-022-04433-9

Murphy, K., Weaver, C., Berg, L., Barton, G., & Janeway, C. A. (2022). *Janeway's immunobiology* (Tenth edition. / Kenneth Murphy, Casey Weaver, Leslie J. Berg. ed.). New York: W.W. Norton and Company.

Murray, H. C., Muleme, M., Cooper, D., McNamara, B. J., Hussain, M. A., Bartolo, C., ... Athan, E. (2024, August). Prevalence, risk factors, and outcomes of secondary infections among hospitalized patients with COVID-19 or post-COVID-19 conditions in Victoria, 2020-2023. *In-*

ternational journal of infectious diseases: IJID: official publication of the International Society for Infectious Diseases, *145*, 107078. doi: 10.1016/j.ijid.2024.107078

Musters, A., Balzaretti, G., van Schaik, B. D. C., Jongejan, A., van der Weele, L., Tas, S. W., ... de Vries, N. (2022). In rheumatoid arthritis inflamed joints share dominant patient-specific B-cell clones. *Frontiers in Immunology*, *13*, 915687. doi: 10.3389/fimmu.2022.915687

Muñoz, L. E., Lauber, K., Schiller, M., Manfredi, A. A., & Herrmann, M. (2010, May). The role of defective clearance of apoptotic cells in systemic autoimmunity. *Nature Reviews Rheumatology*, *6*(5), 280–289. Retrieved 2025-09-24, from https://www.nature.com/articles/nrrheum.2010.46 doi: 10.1038/nrrheum.2010.46

Müller, F., Taubmann, J., Bucci, L., Wilhelm, A., Bergmann, C., Völkl, S., ... Schett, G. (2024, February). CD19 CAR T-Cell Therapy in Autoimmune Disease - A Case Series with Follow-up. *The New England Journal of Medicine*, *390*(8), 687–700. doi: 10.1056/NEJMoa2308917

Nakazawa, D., Masuda, S., Tomaru, U., & Ishizu, A. (2019, February). Pathogenesis and therapeutic interventions for ANCA-associated vasculitis. *Nature Reviews Rheumatology*, *15*(2), 91–101. Retrieved 2025-12-01, from https://www.nature.com/articles/s41584-018-0145-y doi: 10.1038/s41584-018-0145-y

Nemazee, D. A., & Bürki, K. (1989, February). Clonal deletion of B lymphocytes in a transgenic mouse bearing anti-MHC class I antibody genes. *Nature*, *337*(6207), 562–566. Retrieved 2025-11-26, from https://www.nature.com/articles/337562a0 doi: 10.1038/337562a0

Nitschke, L., Carsetti, R., Ocker, B., Köhler, G., & Lamers, M. C. (1997, February). CD22 is a negative regulator of B-cell receptor signalling.

Current biology: CB, *7*(2), 133–143. doi: 10.1016/s0960-9822(06)00057-1

O'Keefe, T. L., Williams, G. T., Batista, F. D., & Neuberger, M. S. (1999, April). Deficiency in CD22, a B cell-specific inhibitory receptor, is sufficient to predispose to development of high affinity autoantibodies. *The Journal of Experimental Medicine*, *189*(8), 1307–1313. doi: 10.1084/jem.189.8.1307

Osborn, T. M., Verdrengh, M., Stossel, T. P., Tarkowski, A., & Bokarewa, M. (2008, September). Decreased levels of the gelsolin plasma isoform in patients with rheumatoid arthritis. *Arthritis Research & Therapy*, *10*(5), R117. Retrieved 2025-09-25, from https://doi.org/10.1186/ar2520 doi: 10.1186/ar2520

Ota, M., Nakano, M., Nagafuchi, Y., Kobayashi, S., Hatano, H., Yoshida, R., ... Fujio, K. (2023, November). Multimodal repertoire analysis unveils B cell biology in immune-mediated diseases. *Annals of the Rheumatic Diseases*, *82*(11), 1455–1463. Retrieved 2025-11-29, from https://www.sciencedirect.com/science/article/pii/S0003496724102713 doi: 10.1136/ard-2023-224421

Otipoby, K. L., Andersson, K. B., Draves, K. E., Klaus, S. J., Farr, A. G., Kerner, J. D., ... Clark, E. A. (1996, December). CD22 regulates thymus-independent responses and the lifespan of B cells. *Nature*, *384*(6610), 634–637. doi: 10.1038/384634a0

Ottas, A., Fishman, D., Okas, T.-L., Kingo, K., & Soomets, U. (2017, September). The metabolic analysis of psoriasis identifies the associated metabolites while providing computational models for the monitoring of the disease. *Archives of Dermatological Research*, *309*(7), 519–528. doi: 10.1007/s00403-017-1760-1

Palazzi, C., Buskila, D., D'Angelo, S., D'Amico, E., & Olivieri, I. (2012, July). Autoantibodies in patients with chronic hepatitis C virus infection: pitfalls for the diagnosis of rheumatic diseases. *Autoimmunity Reviews*, *11*(9), 659–663. Retrieved 2025-10-02, from https://www.sciencedirect.com/science/article/pii/S1568997211002850 doi: 10.1016/j.autrev.2011.11.011

Pedersen, O. B., Svendsen, A. J., Ejstrup, L., Skytthe, A., & Junker, P. (2008, October). On the heritability of psoriatic arthritis. Disease concordance among monozygotic and dizygotic twins. *Annals of the Rheumatic Diseases*, *67*(10), 1417–1421. Retrieved 2025-10-02, from https://ard.bmj.com/content/67/10/1417 doi: 10.1136/ard.2007.078428

Perez-Alamino, R., Garcia-Valladares, I., Cuchacovich, R., Iglesias-Gamarra, A., & Espinoza, L. R. (2014, September). Are anti-CCP antibodies in psoriatic arthritis patients a biomarker of erosive disease? *Rheumatology International*, *34*(9), 1211–1216. Retrieved 2025-11-27, from https://doi.org/10.1007/s00296-014-2956-8 doi: 10.1007/s00296-014-2956-8

Pernes, J. I., Alsayah, A., Tucci, F., & Bashford-Rogers, R. J. M. (2024, April). Unravelling B cell heterogeneity: insights into flow cytometry-gated B cells from single-cell multi-omics data. *Frontiers in Immunology*, *15*. Retrieved 2025-11-25, from https://www.frontiersin.org/journals/immunology/articles/10.3389/fimmu.2024.1380386/full doi: 10.3389/fimmu.2024.1380386

Pham, P., Bransteitter, R., Petruska, J., & Goodman, M. F. (2003, July). Processive AID-catalysed cytosine deamination on single-stranded DNA simulates somatic hypermutation. *Nature*, *424*(6944), 103–107. Retrieved 2025-05-15, from https://www.nature.com/articles/nature01760

doi: 10.1038/nature01760

Pike, B. L., Abrams, J., & Nossal, G. J. (1983, March). Clonal anergy: inhibition of antigen-driven proliferation among single B lymphocytes from tolerant animals, and partial breakage of anergy by mitogens. *European Journal of Immunology*, *13*(3), 214–220. doi: 10.1002/eji.1830130307

Piktel, E., Levental, I., Durnaś, B., Janmey, P. A., & Bucki, R. (2018, August). Plasma Gelsolin: Indicator of Inflammation and Its Potential as a Diagnostic Tool and Therapeutic Target. *International Journal of Molecular Sciences*, *19*(9), 2516. Retrieved 2025-09-25, from https://pmc.ncbi.nlm.nih.gov/articles/PMC6164782/ doi: 10.3390/ijms19092516

Pinto, T. N. C., Benard, G., & Fernandes, J. R. (2025). Phenotypic Characterization of B-Lymphocyte Subpopulations in Human Peripheral Blood: A Cost-Effective Seven-Color One-Tube Protocol. In R. Amoriello, C. Ballerini, & A. Mariottini (Eds.), *Immunosenescence: Methods and Protocols* (pp. 15–31). New York, NY: Springer US. Retrieved 2025-11-29, from https://doi.org/10.1007/978-1-0716-4128-6_3 doi: 10.1007/978-1-0716-4128-6_3

Pollard, K. M. (2012, May). Gender differences in autoimmunity associated with exposure to environmental factors. *Journal of Autoimmunity*, *38*(2-3), J177–J186. Retrieved 2025-10-02, from https://pmc.ncbi.nlm.nih.gov/articles/PMC3302961/ doi: 10.1016/j.jaut.2011.11.007

Portugal, S., Obeng-Adjei, N., Moir, S., Crompton, P. D., & Pierce, S. K. (2017, November). Atypical memory B cells in human chronic infectious diseases: An interim report. *Cellular Immunology*, *321*, 18–25. Retrieved 2022-10-19, from https://www.sciencedirect.com/

science/article/pii/S0008874917300990 doi: 10.1016/j.cellimm.2017.07.003

Portugal, S., Tipton, C. M., Sohn, H., Kone, Y., Wang, J., Li, S., ... Crompton, P. D. (2015, May). Malaria-associated atypical memory B cells exhibit markedly reduced B cell receptor signaling and effector function. *eLife*, *4*, e07218. Retrieved 2022-10-10, from https://doi.org/10.7554/eLife.07218 doi: 10.7554/eLife.07218

Pouw, J. N., Olde Nordkamp, M. A. M., van Kempen, T., Concepcion, A. N., van Laar, J. M., van Wijk, F., ... Boes, M. (2022, November). Regulatory T cells in psoriatic arthritis: an IL-17A-producing, Foxp3intCD161 + RORgammat + ICOS + phenotype, that associates with the presence of ADAMTSL5 autoantibodies. *Scientific Reports*, *12*(1), 20675. Retrieved 2025-09-23, from https://www.nature.com/articles/s41598-022-24924-w doi: 10.1038/s41598-022-24924-w

Pugh-Bernard, A. E., Silverman, G. J., Cappione, A. J., Villano, M. E., Ryan, D. H., Insel, R. A., & Sanz, I. (2001, October). Regulation of inherently autoreactive VH4-34 B cells in the maintenance of human B cell tolerance. *The Journal of Clinical Investigation*, *108*(7), 1061–1070. Retrieved 2025-11-28, from https://www.jci.org/articles/view/12462 doi: 10.1172/JCI12462

Punnonen, J., Aversa, G., Cocks, B. G., McKenzie, A. N., Menon, S., Zurawski, G., ... de Vries, J. E. (1993, April). Interleukin 13 induces interleukin 4-independent IgG4 and IgE synthesis and CD23 expression by human B cells. *Proceedings of the National Academy of Sciences of the United States of America*, *90*(8), 3730–3734. Retrieved 2025-11-03, from https://pmc.ncbi.nlm.nih.gov/articles/PMC46375/ doi: 10.1073/pnas.90.8.3730

Punzi, L., Podswiadek, M., Oliviero, F., Lonigro, A., Modesti, V., Ramonda, R., & Todesco, S. (2007). Laboratory findings in psoriatic arthritis. *Reumatismo*, *59 Suppl 1*, 52–55. doi: 10.4081/reumatismo.2007.1s.52

Pène, J., Gauchat, J.-F., Lécart, S., Drouet, E., Guglielmi, P., Boulay, V., ... Yssel, H. (2004, May). Cutting edge: IL-21 is a switch factor for the production of IgG1 and IgG3 by human B cells. *Journal of Immunology (Baltimore, Md.: 1950)*, *172*(9), 5154–5157. doi: 10.4049/jimmunol.172.9.5154

Pène, J., Rousset, F., Brière, F., Chrétien, I., Bonnefoy, J. Y., Spits, H., ... Banchereau, J. (1988, September). IgE production by normal human lymphocytes is induced by interleukin 4 and suppressed by interferons gamma and alpha and prostaglandin E2. *Proceedings of the National Academy of Sciences of the United States of America*, *85*(18), 6880–6884. doi: 10.1073/pnas.85.18.6880

Quách, T. D., Manjarrez-Orduño, N., Adlowitz, D. G., Silver, L., Yang, H., Wei, C., ... Sanz, I. (2011, April). Anergic Responses Characterize a Large Fraction of Human Autoreactive Naive B Cells Expressing Low Levels of Surface IgM. *The Journal of Immunology*, *186*(8), 4640–4648. Retrieved 2022-10-19, from https://www.jimmunol.org/content/186/8/4640 doi: 10.4049/jimmunol.1001946

Ramsköld, D., Parodis, I., Lakshmikanth, T., Sippl, N., Khademi, M., Chen, Y., ... Malmström, V. (2019, February). B cell alterations during BAFF inhibition with belimumab in SLE. *EBioMedicine*, *40*, 517–527. Retrieved 2025-12-01, from https://www.sciencedirect.com/science/article/pii/S2352396418306121 doi: 10.1016/j.ebiom.2018.12.035

Rauber, S., Mohammadian, H., Schmidkonz, C., Atzinger, A., Soare, A., Treutlein, C., ... Ramming, A. (2024, April). CD200+ fibroblasts form

a pro-resolving mesenchymal network in arthritis. *Nature Immunology*, *25*(4), 682–692. Retrieved 2025-09-29, from https://www.nature.com/articles/s41590-024-01774-4 doi: 10.1038/s41590-024-01774-4

Richardson, C., Chida, A. S., Adlowitz, D., Silver, L., Fox, E., Jenks, S. A., ... Sanz, I. (2013, November). Molecular Basis of 9G4 B Cell Autoreactivity in Human Systemic Lupus Erythematosus. *The Journal of Immunology*, *191*(10), 4926–4939. Retrieved 2025-11-25, from https://doi.org/10.4049/jimmunol.1202263 doi: 10.4049/jimmunol.1202263

Rispens, T., & Huijbers, M. G. (2023, April). The unique properties of IgG4 and its roles in health and disease. *Nature Reviews. Immunology*, 1–16. Retrieved 2025-11-03, from https://pmc.ncbi.nlm.nih.gov/articles/PMC10123589/ doi: 10.1038/s41577-023-00871-z

Rivellese, F., Humby, F., Bugatti, S., Fossati-Jimack, L., Rizvi, H., Lucchesi, D., ... Investigators, t. P.-R. (2020). B Cell Synovitis and Clinical Phenotypes in Rheumatoid Arthritis: Relationship to Disease Stages and Drug Exposure. *Arthritis & Rheumatology*, *72*(5), 714–725. Retrieved 2025-11-27, from https://onlinelibrary.wiley.com/doi/abs/10.1002/art.41184 (_eprint: https://acrjournals.onlinelibrary.wiley.com/doi/pdf/10.1002/art.41184) doi: 10.1002/art.41184

Roco, J. A., Mesin, L., Binder, S. C., Nefzger, C., Gonzalez-Figueroa, P., Canete, P. F., ... Vinuesa, C. G. (2019, August). Class Switch Recombination Occurs Infrequently in Germinal Centers. *Immunity*, *51*(2), 337–350.e7. Retrieved 2025-05-25, from https://www.ncbi.nlm.nih.gov/pmc/articles/PMC6914312/ doi: 10.1016/j.immuni.2019.07.001

Rotondo, C., Corrado, A., Cici, D., Berardi, S., & Cantatore, F. P. (2021, Jan-

uary). Anti-cyclic-citrullinated-protein-antibodies in psoriatic arthritis patients: how autoimmune dysregulation could affect clinical characteristics, retention rate of methotrexate monotherapy and first line biotechnological drug survival. A single center retrospective study. *Therapeutic Advances in Chronic Disease*, *12*, 2040622320986722. Retrieved 2025-09-26, from https://doi.org/10.1177/2040622320986722 doi: 10.1177/2040622320986722

Rowland, S. L., Leahy, K. F., Halverson, R., Torres, R. M., & Pelanda, R. (2010, October). BAFF Receptor Signaling Aids the Differentiation of Immature B Cells into Transitional B Cells following Tonic BCR Signaling. *The Journal of Immunology*, *185*(8), 4570–4581. Retrieved 2025-05-21, from https://doi.org/10.4049/jimmunol.1001708 doi: 10.4049/jimmunol.1001708

Rubin, S. J. S., Bloom, M. S., & Robinson, W. H. (2019, May). B cell checkpoints in autoimmune rheumatic diseases. *Nature Reviews Rheumatology*, *15*(5), 303–315. Retrieved 2022-10-19, from https://www.nature.com/articles/s41584-019-0211-0 (Number: 5) doi: 10.1038/s41584-019-0211-0

Saadoun, D., Terrier, B., Bannock, J., Vazquez, T., Massad, C., Kang, I., ... Cacoub, P. (2013, April). Expansion of autoreactive unresponsive CD21-/low B cells in Sjögren's syndrome associated lymphoproliferation. *Arthritis and rheumatism*, *65*(4), 1085. Retrieved 2023-11-21, from https://www.ncbi.nlm.nih.gov/pmc/articles/PMC4479193/ doi: 10.1002/art.37828

Sablé-Fourtassou, R., Cohen, P., Mahr, A., Pagnoux, C., Mouthon, L., Jayne, D., ... French Vasculitis Study Group (2005, November). Antineutrophil cytoplasmic antibodies and the Churg-Strauss syndrome. *Annals of*

Internal Medicine, *143*(9), 632–638. doi: 10.7326/0003-4819-143-9-200511010-00006

Sabouri, Z., Schofield, P., Horikawa, K., Spierings, E., Kipling, D., Randall, K. L., ... Goodnow, C. C. (2014, June). Redemption of autoantibodies on anergic B cells by variable-region glycosylation and mutation away from self-reactivity. *Proceedings of the National Academy of Sciences*, *111*(25), E2567–E2575. Retrieved 2025-11-29, from https://www.pnas.org/doi/10.1073/pnas.1406974111 doi: 10.1073/pnas.1406974111

Samuels, J., Ng, Y.-S., Coupillaud, C., Paget, D., & Meffre, E. (2005, May). Impaired early B cell tolerance in patients with rheumatoid arthritis. *The Journal of Experimental Medicine*, *201*(10), 1659–1667. doi: 10.1084/jem.20042321

Sanders, J.-S. F., Huitma, M. G., Kallenberg, C. G. M., & Stegeman, C. A. (2006, November). Plasma levels of soluble interleukin 2 receptor, soluble CD30, interleukin 10 and B cell activator of the tumour necrosis factor family during follow-up in vasculitis associated with proteinase 3-antineutrophil cytoplasmic antibodies: associations with disease activity and relapse. *Annals of the Rheumatic Diseases*, *65*(11), 1484–1489. doi: 10.1136/ard.2005.046219

Santa Cruz, A., Mendes-Frias, A., Oliveira, A. I., Dias, L., Matos, A. R., Carvalho, A., ... Silvestre, R. (2021). Interleukin-6 Is a Biomarker for the Development of Fatal Severe Acute Respiratory Syndrome Coronavirus 2 Pneumonia. *Frontiers in Immunology*, *12*, 613422. doi: 10.3389/fimmu.2021.613422

Sanz, I., Wei, C., Jenks, S. A., Cashman, K. S., Tipton, C., Woodruff, M. C., ... Lee, F. E.-H. (2019, October). Challenges and Opportunities for Consistent Classification of Human B Cell and Plasma

Cell Populations. *Frontiers in Immunology*, *10*. Retrieved 2025-11-29, from https://www.frontiersin.org/journals/immunology/articles/10.3389/fimmu.2019.02458/full doi: 10.3389/fimmu.2019.02458

Scher, J. U., Sczesnak, A., Longman, R. S., Segata, N., Ubeda, C., Bielski, C., ... Littman, D. R. (2013, November). Expansion of intestinal Prevotella copri correlates with enhanced susceptibility to arthritis. *eLife*, *2*, e01202. Retrieved 2025-09-26, from https://doi.org/10.7554/eLife.01202 doi: 10.7554/eLife.01202

Schickel, J.-N., Glauzy, S., Ng, Y.-S., Chamberlain, N., Massad, C., Isnardi, I., ... Meffre, E. (2017, May). Self-reactive VH4-34–expressing IgG B cells recognize commensal bacteria. *Journal of Experimental Medicine*, *214*(7), 1991–2003. Retrieved 2025-11-29, from https://doi.org/10.1084/jem.20160201 doi: 10.1084/jem.20160201

Sender, R., Weiss, Y., Navon, Y., Milo, I., Azulay, N., Keren, L., ... Milo, R. (2023, October). The total mass, number, and distribution of immune cells in the human body. *Proceedings of the National Academy of Sciences*, *120*(44), e2308511120. Retrieved 2025-05-08, from https://www.pnas.org/doi/10.1073/pnas.2308511120 doi: 10.1073/pnas.2308511120

Shi, X., Jin, L., Dang, E., Chang, T., Feng, Z., Liu, Y., & Wang, G. (2011, December). IL-17A Upregulates Keratin 17 Expression in Keratinocytes through STAT1- and STAT3-Dependent Mechanisms. *Journal of Investigative Dermatology*, *131*(12), 2401–2408. Retrieved 2025-11-28, from https://www.sciencedirect.com/science/article/pii/S0022202X15351083 doi: 10.1038/jid.2011.222

Shimojima, Y., Kishida, D., Ichikawa, T., Takamatsu, R., Nomura, S., &

Sekijima, Y. (2023, July). Features of BAFF and APRIL receptors on circulating B cells in antineutrophil cytoplasmic antibody-associated vasculitis. *Clinical and Experimental Immunology*, *213*(1), 125–137. doi: 10.1093/cei/uxad024

Sieger, N., Fleischer, S. J., Mei, H. E., Reiter, K., Shock, A., Burmester, G. R., ... Dörner, T. (2013). CD22 ligation inhibits downstream B cell receptor signaling and Ca2+ flux upon activation. *Arthritis & Rheumatism*, *65*(3), 770–779. Retrieved 2025-11-23, from https://onlinelibrary.wiley.com/doi/abs/10.1002/art.37818 (_eprint: https://onlinelibrary.wiley.com/doi/pdf/10.1002/art.37818) doi: 10.1002/art.37818

Sims, G. P., Ettinger, R., Shirota, Y., Yarboro, C. H., Illei, G. G., & Lipsky, P. E. (2005, June). Identification and characterization of circulating human transitional B cells. *Blood*, *105*(11), 4390–4398. Retrieved 2025-11-25, from https://doi.org/10.1182/blood-2004-11-4284 doi: 10.1182/blood-2004-11-4284

Slot, L. M., Vergroesen, R. D., Kerkman, P. F., Staudinger, E., Reijm, S., van Dooren, H. J., ... Scherer, H. U. (2021, March). Light chain skewing in autoantibodies and B-cell receptors of the citrullinated antigen-binding B-cell response in rheumatoid arthritis. *PLoS ONE*, *16*(3), e0247847. Retrieved 2022-10-19, from https://www.ncbi.nlm.nih.gov/pmc/articles/PMC8009422/ doi: 10.1371/journal.pone.0247847

Smith, M. J., Ford, B. R., Rihanek, M., Coleman, B. M., Getahun, A., Sarapura, V. D., ... Cambier, J. C. (2019, February). Elevated PTEN expression maintains anergy in human B cells and reveals unexpectedly high repertoire autoreactivity. *JCI Insight*, *4*(3). Retrieved 2025-11-25, from https://insight.jci.org/articles/view/123384 doi:

10.1172/jci.insight.123384

Smolen, J. S., Aletaha, D., Barton, A., Burmester, G. R., Emery, P., Firestein, G. S., ... Yamamoto, K. (2018, February). Rheumatoid arthritis. *Nature Reviews Disease Primers*, *4*(1), 18001. Retrieved 2025-12-01, from https://www.nature.com/articles/nrdp20181 doi: 10.1038/nrdp.2018.1

Sobolewski, P., Walecka, I., & Dopytalska, K. (2017). Nail involvement in psoriatic arthritis. *Reumatologia*, *55*(3), 131–135. Retrieved 2025-11-27, from https://pmc.ncbi.nlm.nih.gov/articles/PMC5534507/ doi: 10.5114/reum.2017.68912

Sokolova, M. V., Schett, G., & Steffen, U. (2022, October). Autoantibodies in Rheumatoid Arthritis: Historical Background and Novel Findings. *Clinical Reviews in Allergy & Immunology*, *63*(2), 138–151. Retrieved 2025-09-24, from https://doi.org/10.1007/s12016-021-08890-1 doi: 10.1007/s12016-021-08890-1

Soomro, M., Stadler, M., Dand, N., Bluett, J., Jadon, D., Jalali-najafabadi, F., ... Barton, A. (2022). Comparative Genetic Analysis of Psoriatic Arthritis and Psoriasis for the Discovery of Genetic Risk Factors and Risk Prediction Modeling. *Arthritis & Rheumatology*, *74*(9), 1535–1543. Retrieved 2025-07-25, from https://onlinelibrary.wiley.com/doi/abs/10.1002/art.42154 (_eprint: https://acrjournals.onlinelibrary.wiley.com/doi/pdf/10.1002/art.42154) doi: 10.1002/art.42154

Specks, U., Fervenza, F. C., McDonald, T. J., & Hogan, M. C. (2001, December). Response of Wegener's granulomatosis to anti-CD20 chimeric monoclonal antibody therapy. *Arthritis and Rheumatism*, *44*(12), 2836–2840. doi: 10.1002/1529-0131(200112)44:12<2836::aid-art471>3.0.co;2-w

Specks, U., Merkel, P. A., Seo, P., Spiera, R., Langford, C. A., Hoffman, G. S., ... Stone, J. H. (2013, August). Efficacy of Remission-Induction Regimens for ANCA-Associated Vasculitis. *New England Journal of Medicine*, *369*(5), 417–427. Retrieved 2025-11-30, from https://www.nejm.org/doi/full/10.1056/NEJMoa1213277 (_eprint: https://www.nejm.org/doi/pdf/10.1056/NEJMoa1213277) doi: 10.1056/NEJMoa1213277

Staniek, J., & Rizzi, M. (2025, March). Signaling Activation and Modulation in Extrafollicular B Cell Responses. *Immunological Reviews*, *330*(1), e70004. Retrieved 2025-11-30, from https://onlinelibrary.wiley.com/doi/10.1111/imr.70004 doi: 10.1111/imr.70004

Stavnezer, J., & Kang, J. (2009, January). The Surprising Discovery That TGFβ Specifically Induces the IgA Class Switch. *The Journal of Immunology*, *182*(1), 5–7. Retrieved 2025-11-03, from https://doi.org/10.4049/jimmunol.182.1.5 doi: 10.4049/jimmunol.182.1.5

Steel, K. J. A., Srenathan, U., Ridley, M., Durham, L. E., Wu, S.-Y., Ryan, S. E., ... Taams, L. S. (2020, March). Polyfunctional, Proinflammatory, Tissue-Resident Memory Phenotype and Function of Synovial Interleukin-17A+CD8+ T Cells in Psoriatic Arthritis. *Arthritis & Rheumatology (Hoboken, N.J.)*, *72*(3), 435–447. doi: 10.1002/art.41156

Stensland, Z. C., Magera, C. A., Broncucia, H., Gomez, B. D., Rios-Guzman, N. M., Wells, K. L., ... Smith, M. J. (2023, May). Identification of an anergic BND cell–derived activated B cell population (BND2) in young-onset type 1 diabetes patients. *The Journal of Experimental Medicine*, *220*(8), e20221604. Retrieved 2025-11-30, from https://pmc.ncbi.nlm.nih.gov/articles/PMC10192302/ doi: 10.1084/jem.20221604

Stohl, W., Hiepe, F., Latinis, K. M., Thomas, M., Scheinberg, M. A., Clarke,

A., ... BLISS-76 Study Group (2012, July). Belimumab reduces autoantibodies, normalizes low complement levels, and reduces select B cell populations in patients with systemic lupus erythematosus. *Arthritis and Rheumatism*, *64*(7), 2328–2337. doi: 10.1002/art.34400

Stone, J. H., Merkel, P. A., Spiera, R., Seo, P., Langford, C. A., Hoffman, G. S., ... Specks, U. (2010, July). Rituximab versus Cyclophosphamide for ANCA-Associated Vasculitis. *New England Journal of Medicine*, *363*(3), 221–232. Retrieved 2025-11-30, from https://www.nejm.org/doi/full/10.1056/NEJMoa0909905 (_eprint: https://www.nejm.org/doi/pdf/10.1056/NEJMoa0909905) doi: 10.1056/NEJMoa0909905

Stuart, P., Nair, R., Tsoi, L., Tejasvi, T., Das, S., Kang, H., ... Elder, J. (2015, December). Genome-wide Association Analysis of Psoriatic Arthritis and Cutaneous Psoriasis Reveals Differences in Their Genetic Architecture. *American Journal of Human Genetics*, *97*(6), 816–836. Retrieved 2022-10-10, from https://www.ncbi.nlm.nih.gov/pmc/articles/PMC4678416/ doi: 10.1016/j.ajhg.2015.10.019

Szodoray, P., Stanford, S. M., Molberg, O., Munthe, L. A., Bottini, N., & Nakken, B. (2016, September). T-helper signals restore B-cell receptor signaling in autoreactive anergic B cells by upregulating CD45 phosphatase activity. *Journal of Allergy and Clinical Immunology*, *138*(3), 839–851.e8. Retrieved 2023-11-20, from https://www.jacionline.org/article/S0091-6749(16)00307-9/fulltext doi: 10.1016/j.jaci.2016.01.035

Taillardet, M., Haffar, G., Mondière, P., Asensio, M.-J., Gheit, H., Burdin, N., ... Genestier, L. (2009, November). The thymus-independent immunity conferred by a pneumococcal polysaccharide is mediated by

long-lived plasma cells. *Blood*, *114*(20), 4432–4440. Retrieved 2025-05-25, from https://doi.org/10.1182/blood-2009-01-200014 doi: 10.1182/blood-2009-01-200014

Tan, M., Hu, J., Xiao, H., Wang, Q., Hu, K., Li, X., ... Kuang, Y. (2023, July). Concurrent onset of skin and joint symptoms correlates with higher psoriatic arthritis disease activity: A single-center retrospective study. *Journal of the American Academy of Dermatology*, *89*(1), 173–175. doi: 10.1016/j.jaad.2023.02.045

Tenazinha, C., Barros, R., Fonseca, J. E., & Vieira-Sousa, E. (2022, July). Histopathology of Psoriatic Arthritis Synovium—A Narrative Review. *Frontiers in Medicine*, *9*. Retrieved 2025-11-27, from https://www.frontiersin.org/journals/medicine/articles/10.3389/fmed.2022.860813/full doi: 10.3389/fmed.2022.860813

Terrier, B., Pagnoux, C., Perrodeau, E., Karras, A., Khouatra, C., Aumaître, O., ... French Vasculitis Study Group (2018, August). Long-term efficacy of remission-maintenance regimens for ANCA-associated vasculitides. *Annals of the Rheumatic Diseases*, *77*(8), 1150–1156. doi: 10.1136/annrheumdis-2017-212768

Thien, M., Phan, T. G., Gardam, S., Amesbury, M., Basten, A., Mackay, F., & Brink, R. (2004, June). Excess BAFF Rescues Self-Reactive B Cells from Peripheral Deletion and Allows Them to Enter Forbidden Follicular and Marginal Zone Niches. *Immunity*, *20*(6), 785–798. Retrieved 2025-11-03, from https://www.sciencedirect.com/science/article/pii/S107476130400144X doi: 10.1016/j.immuni.2004.05.010

Tipton, C. M., Fucile, C. F., Darce, J., Chida, A., Ichikawa, T., Gregoretti, I., ... Sanz, I. (2015, July). Diversity, cellular origin and autoreactivity

of antibody-secreting cell expansions in acute Systemic Lupus Erythematosus. *Nature immunology*, *16*(7), 755–765. Retrieved 2025-11-29, from https://pmc.ncbi.nlm.nih.gov/articles/PMC4512288/ doi: 10.1038/ni.3175

Towler, O. W., Peck, S. H., Kaplan, F. S., & Shore, E. M. (2021, February). Dysregulated BMP signaling through ACVR1 impairs digit joint development in fibrodysplasia ossificans progressiva (FOP). *Developmental Biology*, *470*, 136–146. doi: 10.1016/j.ydbio.2020.11.004

Tzemach, R., Gur, C., Phan, T. S., David, E., Zada, M., Shmueli, M. D., ... Amit, I. (2025, June). Dissection of the immune landscape in psoriatic arthritis defines immunoproteasome up-regulation in treatment resistance. *Science Immunology*, *10*(108), eadu0284. doi: 10.1126/sciimmunol.adu0284

Vallerskog, T., Heimbürger, M., Gunnarsson, I., Zhou, W., Wahren-Herlenius, M., Trollmo, C., & Malmström, V. (2006). Differential effects on BAFF and APRIL levels in rituximab-treated patients with systemic lupus erythematosus and rheumatoid arthritis. *Arthritis Research & Therapy*, *8*(6), R167. doi: 10.1186/ar2076

van Dam, L. S., Dirikgil, E., Bredewold, E. W., Ray, A., Bakker, J. A., van Kooten, C., ... Teng, Y. K. O. (2021, July). PR3-ANCAs predict relapses in ANCA-associated vasculitis patients after rituximab. *Nephrology, Dialysis, Transplantation: Official Publication of the European Dialysis and Transplant Association - European Renal Association*, *36*(8), 1408–1417. doi: 10.1093/ndt/gfaa066

Van Gool, I. C., Kers, J., Bakker, J. A., Rotmans, J. I., Teng, Y. K. O., & Bauer, M. P. (2022). Antineutrophil cytoplasmic antibodies in infective endocarditis: a case report and systematic review of the

literature. *Clinical Rheumatology*, *41*(10), 2949–2960. Retrieved 2025-10-02, from https://pmc.ncbi.nlm.nih.gov/articles/PMC9485185/ doi: 10.1007/s10067-022-06240-w

van Kuijk, A. W. R., Reinders-Blankert, P., Smeets, T. J. M., Dijkmans, B. A. C., & Tak, P. P. (2006, December). Detailed analysis of the cell infiltrate and the expression of mediators of synovial inflammation and joint destruction in the synovium of patients with psoriatic arthritis: implications for treatment. *Annals of the Rheumatic Diseases*, *65*(12), 1551–1557. Retrieved 2025-09-26, from https://www.sciencedirect.com/science/article/pii/S0003496724199451 doi: 10.1136/ard.2005.050963

van Vollenhoven, R. F. (2009, March). Sex differences in rheumatoid arthritis: more than meets the eye... *BMC Medicine*, *7*, 12. Retrieved 2025-10-02, from https://pmc.ncbi.nlm.nih.gov/articles/PMC2670321/ doi: 10.1186/1741-7015-7-12

Vasilopoulos, Y., Gkretsi, V., Armaka, M., Aidinis, V., & Kollias, G. (2007, November). Actin cytoskeleton dynamics linked to synovial fibroblast activation as a novel pathogenic principle in TNF-driven arthritis. *Annals of the Rheumatic Diseases*, *66 Suppl 3*(Suppl 3), iii23–28. doi: 10.1136/ard.2007.079822

Vecellio, M., Hake, V. X., Davidson, C., Carena, M. C., Wordsworth, B. P., & Selmi, C. (2021, January). The IL-17/IL-23 Axis and Its Genetic Contribution to Psoriatic Arthritis. *Frontiers in Immunology*, *11*. Retrieved 2025-12-02, from https://www.frontiersin.org/journals/immunology/articles/10.3389/fimmu.2020.596086/full doi: 10.3389/fimmu.2020.596086

Venkataraman, C., Shankar, G., Sen, G., & Bondada, S. (1999, Au-

gust). Bacterial lipopolysaccharide induced B cell activation is mediated via a phosphatidylinositol 3-kinase dependent signaling pathway. *Immunology Letters*, *69*(2), 233–238. Retrieved 2025-11-26, from https://www.sciencedirect.com/science/article/pii/S0165247899000681 doi: 10.1016/S0165-2478(99)00068-1

Vidarsson, G., Dekkers, G., & Rispens, T. (2014, October). IgG Subclasses and Allotypes: From Structure to Effector Functions. *Frontiers in Immunology*, *5*, 520. Retrieved 2025-11-10, from https://pmc.ncbi.nlm.nih.gov/articles/PMC4202688/ doi: 10.3389/fimmu.2014.00520

Wardemann, H., Yurasov, S., Schaefer, A., Young, J. W., Meffre, E., & Nussenzweig, M. C. (2003, September). Predominant Autoantibody Production by Early Human B Cell Precursors. *Science*, *301*(5638), 1374–1377. Retrieved 2025-05-21, from https://www.science.org/doi/10.1126/science.1086907 doi: 10.1126/science.1086907

Watts, R. A., Mooney, J., Skinner, J., Scott, D. G. I., & Macgregor, A. J. (2012, May). The contrasting epidemiology of granulomatosis with polyangiitis (Wegener's) and microscopic polyangiitis. *Rheumatology (Oxford, England)*, *51*(5), 926–931. doi: 10.1093/rheumatology/ker454

Wei, C., Anolik, J., Cappione, A., Zheng, B., Pugh-Bernard, A., Brooks, J., ... Sanz, I. (2007, May). A New Population of Cells Lacking Expression of CD27 Represents a Notable Component of the B Cell Memory Compartment in Systemic Lupus Erythematosus. *The Journal of Immunology*, *178*(10), 6624–6633. Retrieved 2022-10-10, from https://www.jimmunol.org/content/178/10/6624 doi: 10.4049/jimmunol.178.10.6624

Weisel, N. M., Joachim, S. M., Smita, S., Callahan, D., Elsner, R. A., Conter, L. J., ... Shlomchik, M. J. (2022, January). Surface phenotypes of naive

and memory B cells in mouse and human tissues. *Nature Immunology*, *23*(1), 135–145. Retrieved 2025-11-29, from https://www.nature.com/articles/s41590-021-01078-x doi: 10.1038/s41590-021-01078-x

Weller, S., Sterlin, D., Fadeev, T., Coignard, E., Verge de Los Aires, A., Goetz, C., ... Reynaud, C.-A. (2023, January). T-independent responses to polysaccharides in humans mobilize marginal zone B cells prediversified against gut bacterial antigens. *Science immunology*, *8*(79), eade1413. Retrieved 2025-11-03, from https://europepmc.org/articles/PMC7614366 doi: 10.1126/sciimmunol.ade1413

Weyand, C. M., & Goronzy, J. J. (2003, April). Ectopic germinal center formation in rheumatoid synovitis. *Annals of the New York Academy of Sciences*, *987*, 140–149. doi: 10.1111/j.1749-6632.2003.tb06042.x

Wing, E., Sutherland, C., Miles, K., Gray, D., Goodyear, C. S., Otto, T. D., ... Gray, M. (2023, August). Double-negative-2 B cells are the major synovial plasma cell precursor in rheumatoid arthritis. *Frontiers in Immunology*, *14*. Retrieved 2025-09-27, from https://www.frontiersin.org/journals/immunology/articles/10.3389/fimmu.2023.1241474/full doi: 10.3389/fimmu.2023.1241474

Woodruff, M. C., Ramonell, R. P., Haddad, N. S., Anam, F. A., Rudolph, M. E., Walker, T. A., ... Sanz, I. (2022, November). Dysregulated naive B cells and de novo autoreactivity in severe COVID-19. *Nature*, *611*(7934), 139–147. doi: 10.1038/s41586-022-05273-0

Woodruff, M. C., Ramonell, R. P., Nguyen, D. C., Cashman, K. S., Saini, A. S., Haddad, N. S., ... Sanz, I. (2020, December). Extrafollicular B cell responses correlate with neutralizing antibodies and morbidity in COVID-19. *Nature Immunology*, *21*(12), 1506–1516. Retrieved 2025-

05-25, from https://www.nature.com/articles/s41590-020-00814-z doi: 10.1038/s41590-020-00814-z

Wu, T., Yuan, Y., & Tyring, S. K. (2019, May). Discovery of Autoantibodies Associated with Psoriatic Arthritis. *The Journal of Immunology*, *202*(1_Supplement), 179.2. Retrieved 2025-09-23, from https://doi.org/10.4049/jimmunol.202.Supp.179.2 doi: 10.4049/jimmunol.202.Supp.179.2

Xie, G., Roshandel, D., Sherva, R., Monach, P. A., Lu, E. Y., Kung, T., ... Siminovitch, K. A. (2013). Association of Granulomatosis With Polyangiitis (Wegener's) With HLA–DPB1*04 and SEMA6A Gene Variants: Evidence From Genome-Wide Analysis. *Arthritis & Rheumatism*, *65*(9), 2457–2468. Retrieved 2025-12-01, from https://onlinelibrary.wiley.com/doi/abs/10.1002/art.38036 (_eprint: https://acrjournals.onlinelibrary.wiley.com/doi/pdf/10.1002/art.38036) doi: 10.1002/art.38036

Xu, F., Shen, C., Zhang, S., Liu, Y., Liu, D., Kuang, Y., ... Xiao, Y. (2024, February). Coptisine inhibits aggressive and proliferative actions of fibroblast like synoviocytes and exerts a therapeutic potential for rheumatoid arthritis. *International Immunopharmacology*, *128*, 111433. Retrieved 2025-09-25, from https://www.sciencedirect.com/science/article/pii/S1567576923017605 doi: 10.1016/j.intimp.2023.111433

Xu, K., Tao, T., Jie, J., Lu, X., Li, X., Mehmood, M., ... Liu, Z. (2013, March). Increased importin 13 activity is associated with the pathogenesis of pterygium. *Molecular vision*, *19*, 604–13.

Xu, X., Han, M., Li, T., Sun, W., Wang, D., Fu, B., ... Wei, H. (2020, May). Effective treatment of severe COVID-19 patients with tocilizumab. *Proceedings of the National Academy of Sciences*, *117*(20),

10970–10975. Retrieved 2025-11-30, from https://www.pnas.org/doi/10.1073/pnas.2005615117 doi: 10.1073/pnas.2005615117

Yamada, A., Hikichi, M., Nozawa, T., & Nakagawa, I. (2021, November). FBXO2/SCF ubiquitin ligase complex directs xenophagy through recognizing bacterial surface glycan. *EMBO reports*, *22*(11), e52584. Retrieved 2025-09-25, from https://www.embopress.org/doi/full/10.15252/embr.202152584 doi: 10.15252/embr.202152584

Yang, F., Lu, C., Pan, Q., Zhang, R., Yang, M., Wang, Q., ... Leng, X. (2025, May). 68Ga-FAPI and 18F-NaF PET/CT in psoriatic arthritis: a comparative study. *Rheumatology*, *64*(5), 2575–2582. Retrieved 2025-09-26, from https://doi.org/10.1093/rheumatology/keae577 doi: 10.1093/rheumatology/keae577

Yeo, L., Lom, H., Juarez, M., Snow, M., Buckley, C. D., Filer, A., ... Scheel-Toellner, D. (2015, May). Expression of FcRL4 defines a pro-inflammatory, RANKL-producing B cell subset in rheumatoid arthritis. *Annals of the Rheumatic Diseases*, *74*(5), 928–935. doi: 10.1136/annrheumdis-2013-204116

Yuan, Y., Qiu, J., Lin, Z.-T., Li, W., Haley, C., Mui, U. N., ... Wu, T. (2019). Identification of Novel Autoantibodies Associated With Psoriatic Arthritis. *Arthritis & Rheumatology*, *71*(6), 941–951. Retrieved 2022-06-14, from https://onlinelibrary.wiley.com/doi/abs/10.1002/art.40830 (_eprint: https://onlinelibrary.wiley.com/doi/pdf/10.1002/art.40830) doi: 10.1002/art.40830

Zardin-Moraes, M., Silva, A. L. F. A. d., Saldanha, C., Kohem, C. L., Coates, L. C., Henrique, L. R., ... Chakr, R. M. d. S. (2020, June). Prevalence of Psoriatic Arthritis Patients Achieving Minimal Disease Activity in Real-

world Studies and Randomized Clinical Trials: Systematic Review with Metaanalysis. *The Journal of Rheumatology*, *47*(6), 839–846. Retrieved 2022-10-10, from https://www.jrheum.org/content/47/6/839 doi: 10.3899/jrheum.190677

Zegarra-Ruiz, D. F., Kim, D. V., Norwood, K., Kim, M., Wu, W.-J. H., Saldana-Morales, F. B., ... Diehl, G. E. (2021, June). Thymic development of gut-microbiota-specific T cells. *Nature*, *594*(7863), 413–417. Retrieved 2025-09-26, from https://www.nature.com/articles/s41586-021-03531-1 doi: 10.1038/s41586-021-03531-1

Zhang, W., Zhang, C., Chen, P., Yang, C., Gan, X., Hussain, M., ... Du, H. (2016, December). Circulation autoantibody against Lamin A/C in patients with Sjögren's syndrome. *Oncotarget*, *7*(49), 80252–80261. doi: 10.18632/oncotarget.13256

Zhao, L., Jin, S., Wang, S., Zhang, Z., Wang, X., Chen, Z., ... Wu, H. (2024, August). Tertiary lymphoid structures in diseases: immune mechanisms and therapeutic advances. *Signal Transduction and Targeted Therapy*, *9*(1), 225. Retrieved 2025-12-01, from https://www.nature.com/articles/s41392-024-01947-5 doi: 10.1038/s41392-024-01947-5

Zhao, X., Lin, J., Liu, M., Jiang, D., Zhang, Y., Li, X., ... Gao, Y. (2024, October). Targeting FAP-positive chondrocytes in osteoarthritis: a novel lipid nanoparticle siRNA approach to mitigate cartilage degeneration. *Journal of Nanobiotechnology*, *22*(1), 659. Retrieved 2025-07-25, from https://doi.org/10.1186/s12951-024-02946-y doi: 10.1186/s12951-024-02946-y

Zhao, Y., Odell, E., Choong, L. M., Barone, F., Fields, P., Wilkins, B., ... Spencer, J. (2012, September). Granulomatosis with polyangiitis

involves sustained mucosal inflammation that is rich in B-cell survival factors and autoantigen. *Rheumatology (Oxford, England)*, *51*(9), 1580–1586. doi: 10.1093/rheumatology/kes123

Zhu, J., Shi, X.-F., & Chu, C.-Q. (2020, November). Autoantibodies in psoriatic arthritis: are they of pathogenic relevance? *Chinese Medical Journal*, *133*(24), 2899–2901. doi: 10.1097/CM9.0000000000001228

Zhuang, W., Zhang, Q., Kong, Q., Hui, Y., Shen, J., Zhang, C., ... Ye, Q. (2025). Integrated Single-Cell and Spatial Transcriptomic Analysis Reveals a Pathological Niche Formed by FAP+ Fibroblasts, Immune, and Endothelial Cells in Psoriatic Lesions. *Clinical, Cosmetic and Investigational Dermatology*, *18*, 2323–2340. doi: 10.2147/CCID.S541106

Zikherman, J., Parameswaran, R., & Weiss, A. (2012, September). Endogenous antigen tunes the responsiveness of naive B cells but not T cells. *Nature*, *489*(7414), 160–164. Retrieved 2025-11-25, from https://www.nature.com/articles/nature11311 doi: 10.1038/nature11311

Álvarez Gómez, J. A., Salazar-Camarena, D. C., Román-Fernández, I. V., Ortiz-Lazareno, P. C., Cruz, A., Muñoz-Valle, J. F., ... Palafox-Sánchez, C. A. (2023, August). BAFF system expression in double negative 2, activated naïve and activated memory B cells in systemic lupus erythematosus. *Frontiers in Immunology*, *14*. Retrieved 2025-11-30, from https://www.frontiersin.org/journals/immunology/articles/10.3389/fimmu.2023.1235937/full doi: 10.3389/fimmu.2023.1235937

Çakan, E., Ah Kioon, M. D., Garcia-Carmona, Y., Glauzy, S., Oliver, D., Yamakawa, N., ... Meffre, E. (2023, September). TLR9 ligand sequestration by chemokine CXCL4 negatively affects central B cell tolerance. *Journal of Experimental Medicine*, *220*(12), e20230944.

Retrieved 2025-05-28, from https://doi.org/10.1084/jem.20230944 doi: 10.1084/jem.20230944

Örge, E., Çefle, A., Yazıcı, A., Gürel-Polat, N., & Hulagu, S. (2010, February). The positivity of rheumatoid factor and anti-cyclic citrullinated peptide antibody in nonarthritic patients with chronic hepatitis c infection. *Rheumatology International*, *30*(4), 485–488. Retrieved 2025-10-02, from https://doi.org/10.1007/s00296-009-0997-1 doi: 10.1007/s00296-009-0997-1

A | Appendix Chapter 2

A.1 Primer Probes

A.1.1 Primer probes for RT and BCR amplification

Table A.1: **Probe list for RT reaction of BCR.** An equimolar mixture of all primers was used for the RT reaction of BCR repertoire at a final concentration of 10 µM.

Probe list for RT reaction of BCR	
Ig domain	**Sequence**
IGHA	TGTCCAGCACGCTTCAGGCTNNNNTNNNNTNNNNGAYGACC ACGTTCCCATCT
IGHM	TGTCCAGCACGCTTCAGGCTNNNNTNNNNTNNNNTCGTATC CGACGGGGAATTC
IGHD	TGTCCAGCACGCTTCAGGCTNNNNTNNNNTNNNNGGGCTGT TATCCTTTGGGTG
IGHE	TGTCCAGCACGCTTCAGGCTNNNNTNNNNTNNNNAGAGTCA CGGAGGTGGCATT
IGHG	TGTCCAGCACGCTTCAGGCTNNNNTNNNNTNNNNAGTAGTC CTTGACCAGGCAG

Table A.2: **Probe list for BCR amplification.**

Probe list for BCR amplification		
Name	**Type**	**Sequence**
CNUS	**R**	TGTCCAGCACGCTTCAGGCT
VH1-FR1_F1	**F**	AAGCAGTGGTATCAACGCAGAGTCGCAGGGGC CTCAGTGAAGGTCTCCTGCAAG
VH1-FR1_F2	**F**	AAGCAGTGGTATCAACGCAGAGCTCTGCAGGC CTCAGTGAAGGTCTCCTGCAAG
VH1-FR1_F3	**F**	AAGCAGTGGTATCAACGCAGAGCCTAGGTGGC CTCAGTGAAGGTCTCCTGCAAG

F – forward; R – reverse.

continued on next page

Probe list cont. A.2

Name	Type	Sequence
VH1-FR1_F4	**F**	AAGCAGTGGTATCAACGCAGAGGGATCAAGGC CTCAGTGAAGGTCTCCTGCAAG
VH1-FR1_F5	**F**	AAGCAGTGGTATCAACGCAGAGGCAAGATGGC CTCAGTGAAGGTCTCCTGCAAG
VH1-FR1_F6	**F**	AAGCAGTGGTATCAACGCAGAGATGGAGAGGC CTCAGTGAAGGTCTCCTGCAAG
VH1-FR1_F7	**F**	AAGCAGTGGTATCAACGCAGAGCTCGATGGGC CTCAGTGAAGGTCTCCTGCAAG
VH1-FR1_F8	**F**	AAGCAGTGGTATCAACGCAGAGGCTCGAAGGC CTCAGTGAAGGTCTCCTGCAAG
VH1-FR1_F9	**F**	AAGCAGTGGTATCAACGCAGAGACCAACTGGC CTCAGTGAAGGTCTCCTGCAAG
VH1-FR1_F10	**F**	AAGCAGTGGTATCAACGCAGAGCCGGTACGGC CTCAGTGAAGGTCTCCTGCAAG
VH1-FR1_F11	**F**	AAGCAGTGGTATCAACGCAGAGAACTCCGGGC CTCAGTGAAGGTCTCCTGCAAG
VH1-FR1_F12	**F**	AAGCAGTGGTATCAACGCAGAGTTGAAGTGGC CTCAGTGAAGGTCTCCTGCAAG
VH2-FR1_F1	**F**	AAGCAGTGGTATCAACGCAGAGTCGCAGGGTC TGGTCCTACGCTGGTGAAACCC
VH2-FR1_F2	**F**	AAGCAGTGGTATCAACGCAGAGCTCTGCAGTC TGGTCCTACGCTGGTGAAACCC
VH2-FR1_F3	**F**	AAGCAGTGGTATCAACGCAGAGCCTAGGTGTC TGGTCCTACGCTGGTGAAACCC
VH2-FR1_F4	**F**	AAGCAGTGGTATCAACGCAGAGGGATCAAGTC TGGTCCTACGCTGGTGAAACCC
VH2-FR1_F5	**F**	AAGCAGTGGTATCAACGCAGAGGCAAGATGTC TGGTCCTACGCTGGTGAAACCC

F – forward; R – reverse.

continued on next page

Probe list cont. A.2

Name	Type	Sequence
VH2-FR1_F6	**F**	AAGCAGTGGTATCAACGCAGAGATGGAGAGTC TGGTCCTACGCTGGTGAAACCC
VH2-FR1_F7	**F**	AAGCAGTGGTATCAACGCAGAGCTCGATGGTC TGGTCCTACGCTGGTGAAACCC
VH2-FR1_F8	**F**	AAGCAGTGGTATCAACGCAGAGGCTCGAAGTC TGGTCCTACGCTGGTGAAACCC
VH2-FR1_F9	**F**	AAGCAGTGGTATCAACGCAGAGACCAACTGTC TGGTCCTACGCTGGTGAAACCC
VH2-FR1_F10	**F**	AAGCAGTGGTATCAACGCAGAGCCGGTACGTC TGGTCCTACGCTGGTGAAACCC
VH2-FR1_F11	**F**	AAGCAGTGGTATCAACGCAGAGAACTCCGGTC TGGTCCTACGCTGGTGAAACCC
VH2-FR1_F12	**F**	AAGCAGTGGTATCAACGCAGAGTTGAAGTGTC TGGTCCTACGCTGGTGAAACCC
VH3-FR1_F1	**F**	AAGCAGTGGTATCAACGCAGAGTCGCAGGCTG GGGGGTCCCTGAGACTCTCCTG
VH3-FR1_F2	**F**	AAGCAGTGGTATCAACGCAGAGCTCTGCACTG GGGGGTCCCTGAGACTCTCCTG
VH3-FR1_F3	**F**	AAGCAGTGGTATCAACGCAGAGCCTAGGTCTG GGGGGTCCCTGAGACTCTCCTG
VH3-FR1_F4	**F**	AAGCAGTGGTATCAACGCAGAGGGATCAACTG GGGGGTCCCTGAGACTCTCCTG
VH3-FR1_F5	**F**	AAGCAGTGGTATCAACGCAGAGGCAAGATCTG GGGGGTCCCTGAGACTCTCCTG
VH3-FR1_F6	**F**	AAGCAGTGGTATCAACGCAGAGATGGAGACTG GGGGGTCCCTGAGACTCTCCTG
VH3-FR1_F7	**F**	AAGCAGTGGTATCAACGCAGAGCTCGATGCTG GGGGGTCCCTGAGACTCTCCTG

F – forward; R – reverse.

continued on next page

Probe list cont. A.2

Name	Type	Sequence
VH3-FR1_F8	**F**	AAGCAGTGGTATCAACGCAGAGGCTCGAACTG GGGGGTCCCTGAGACTCTCCTG
VH3-FR1_F9	**F**	AAGCAGTGGTATCAACGCAGAGACCAACTCTG GGGGGTCCCTGAGACTCTCCTG
VH3-FR1_F10	**F**	AAGCAGTGGTATCAACGCAGAGCCGGTACCTG GGGGGTCCCTGAGACTCTCCTG
VH3-FR1_F11	**F**	AAGCAGTGGTATCAACGCAGAGAACTCCGCTG GGGGGTCCCTGAGACTCTCCTG
VH3-FR1_F12	**F**	AAGCAGTGGTATCAACGCAGAGTTGAAGTCTG GGGGGTCCCTGAGACTCTCCTG
VH4-FR1_F1	**F**	AAGCAGTGGTATCAACGCAGAGTCGCAGGCTT CGGAGACCCTGTCCCTCACCTG
VH4-FR1_F2	**F**	AAGCAGTGGTATCAACGCAGAGCTCTGCACTT CGGAGACCCTGTCCCTCACCTG
VH4-FR1_F3	**F**	AAGCAGTGGTATCAACGCAGAGCCTAGGTCTT CGGAGACCCTGTCCCTCACCTG
VH4-FR1_F4	**F**	AAGCAGTGGTATCAACGCAGAGGGATCAACTT CGGAGACCCTGTCCCTCACCTG
VH4-FR1_F5	**F**	AAGCAGTGGTATCAACGCAGAGGCAAGATCTT CGGAGACCCTGTCCCTCACCTG
VH4-FR1_F6	**F**	AAGCAGTGGTATCAACGCAGAGATGGAGACTT CGGAGACCCTGTCCCTCACCTG
VH4-FR1_F7	**F**	AAGCAGTGGTATCAACGCAGAGCTCGATGCTT CGGAGACCCTGTCCCTCACCTG
VH4-FR1_F8	**F**	AAGCAGTGGTATCAACGCAGAGGCTCGAACTT CGGAGACCCTGTCCCTCACCTG
VH4-FR1_F9	**F**	AAGCAGTGGTATCAACGCAGAGACCAACTCTT CGGAGACCCTGTCCCTCACCTG

F – forward; R – reverse.

continued on next page

Probe list cont. A.2

Name	Type	Sequence
VH4-FR1_F10	**F**	AAGCAGTGGTATCAACGCAGAGCCGGTACCTT CGGAGACCCTGTCCCTCACCTG
VH4-FR1_F11	**F**	AAGCAGTGGTATCAACGCAGAGAACTCCGCTT CGGAGACCCTGTCCCTCACCTG
VH4-FR1_F12	**F**	AAGCAGTGGTATCAACGCAGAGTTGAAGTCTT CGGAGACCCTGTCCCTCACCTG
VH5-FR1_F1	**F**	AAGCAGTGGTATCAACGCAGAGTCGCAGGCGG GGAGTCTCTGAAGATCTCCTGT
VH5-FR1_F2	**F**	AAGCAGTGGTATCAACGCAGAGCTCTGCACGG GGAGTCTCTGAAGATCTCCTGT
VH5-FR1_F3	**F**	AAGCAGTGGTATCAACGCAGAGCCTAGGTCGG GGAGTCTCTGAAGATCTCCTGT
VH5-FR1_F4	**F**	AAGCAGTGGTATCAACGCAGAGGGATCAACGG GGAGTCTCTGAAGATCTCCTGT
VH5-FR1_F5	**F**	AAGCAGTGGTATCAACGCAGAGGCAAGATCGG GGAGTCTCTGAAGATCTCCTGT
VH5-FR1_F6	**F**	AAGCAGTGGTATCAACGCAGAGATGGAGACGG GGAGTCTCTGAAGATCTCCTGT
VH5-FR1_F7	**F**	AAGCAGTGGTATCAACGCAGAGCTCGATGCGG GGAGTCTCTGAAGATCTCCTGT
VH5-FR1_F8	**F**	AAGCAGTGGTATCAACGCAGAGGCTCGAACGG GGAGTCTCTGAAGATCTCCTGT
VH6-FR1_F1	**F**	AAGCAGTGGTATCAACGCAGAGTCGCAGGTCG CAGACCCTCTCACTCACCTGTG
VH6-FR1_F2	**F**	AAGCAGTGGTATCAACGCAGAGCTCTGCATCG CAGACCCTCTCACTCACCTGTG
VH6-FR1_F3	**F**	AAGCAGTGGTATCAACGCAGAGCCTAGGTTCG CAGACCCTCTCACTCACCTGTG

F – forward; R – reverse.

continued on next page

Probe list cont. A.2

Name	Type	Sequence
VH6-FR1_F4	**F**	AAGCAGTGGTATCAACGCAGAGGGATCAATCG
		CAGACCCTCTCACTCACCTGTG
VH6-FR1_F5	**F**	AAGCAGTGGTATCAACGCAGAGGCAAGATTCG
		CAGACCCTCTCACTCACCTGTG
VH6-FR1_F6	**F**	AAGCAGTGGTATCAACGCAGAGATGGAGATCG
		CAGACCCTCTCACTCACCTGTG
VH6-FR1_F7	**F**	AAGCAGTGGTATCAACGCAGAGCTCGATGTCG
		CAGACCCTCTCACTCACCTGTG
VH6-FR1_F8	**F**	AAGCAGTGGTATCAACGCAGAGGCTCGAATCG
		CAGACCCTCTCACTCACCTGTG
VH6-FR1_F9	**F**	AAGCAGTGGTATCAACGCAGAGACCAACTTCG
		CAGACCCTCTCACTCACCTGTG
VH6-FR1_F10	**F**	AAGCAGTGGTATCAACGCAGAGCCGGTACTCG
		CAGACCCTCTCACTCACCTGTG
VH6-FR1_F11	**F**	AAGCAGTGGTATCAACGCAGAGAACTCCGTCG
		CAGACCCTCTCACTCACCTGTG
VH6-FR1_F12	**F**	AAGCAGTGGTATCAACGCAGAGTTGAAGTTCG
		CAGACCCTCTCACTCACCTGTG

F – forward; R – reverse.

End of Table

B | Appendix Chapter 3

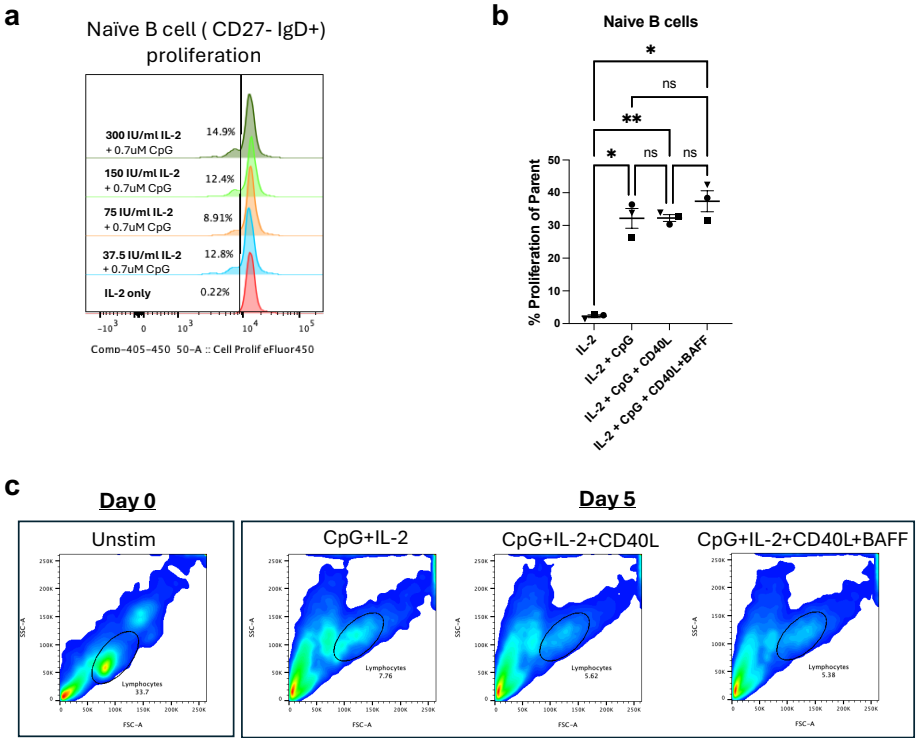

Figure B.1: Additional B cell stimulation conditions tested. a Proliferation frequencies of naïve B cells following 5 days of pan-B cell stimulation with a titration of IL-2 and fixed CpG concentration, representative of one experiment. **b** Proliferation frequencies of naïve B cells following 5 days of naïve B cell enriched stimulation, $n = 3$ independent samples; Bars represent mean with standard error of the mean (SEM); repeated measures ANOVA with Tukey's multiple comparisons post-hoc test. **c** Representative flow cytometry plots ($n = 1$) of frequency of lymphocytes at baseline (Day 0) and following 5 days of stimulations with CpG, IL-2, CD40L or BAFF. $^{*}p < 0.05$; $^{**}p \leq 0.01$; ns - not significant

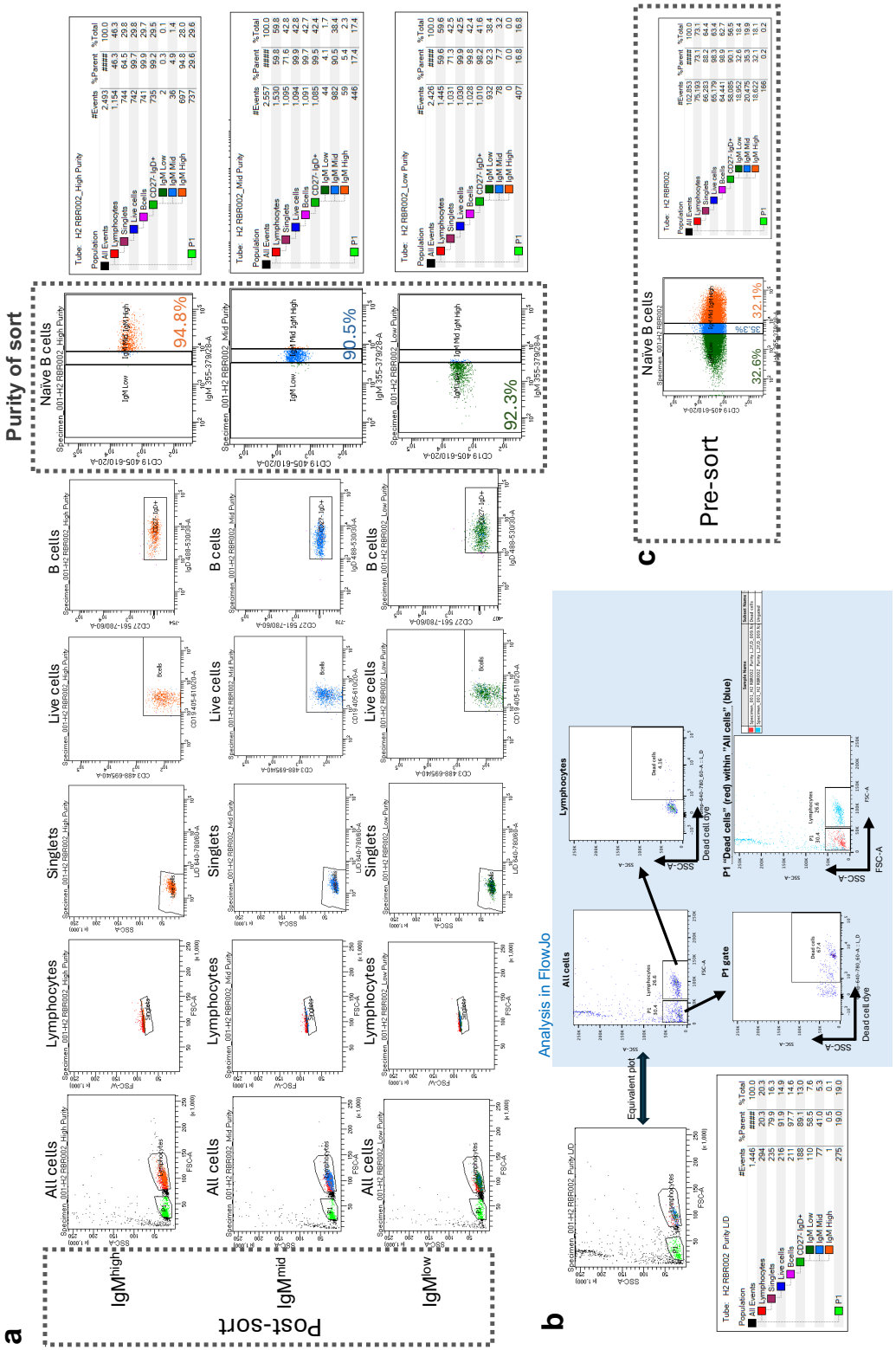

Figure B.2: Purity of FACS-sorted IgM-defined naïve B cell subsets *(see next page)*

Figure B.2 ***(previous page)*****: Purity of FACS-sorted IgM-defined naïve B cell subsets. a**Flow cytometry plots from a representative healthy donor showing the post-FACS-sort purity of IgM^{hi}, IgM^{mid} and IgM^{low} naïve B cell subsets. **b** Flow cytometry plots identifying the 'P1' population (green gate) as dead cells; a mixed aliquot of the previously sorted populations was re-stained with viability dye and re-run on the flow cytometer. The P1 population was viability-dye–positive, confirming that it consists of mostly dead or dying cells during the FACS-sorting process, while the lymphocyte population remained viability-dye– negative.**c** Flow cytometry plot of pre-sort frequencies of IgM^{hi}, IgM^{mid} and IgM^{low} naïve B cell subsets as reference.

The baseline median intensity fluorescence of CD21 in naïve B cells was correlated with the level of IgM expression in healthy donors, but to a lower extent in COVID-19 donors. CD22 did not correlate with IgM in either of the groups (Figure B.3)

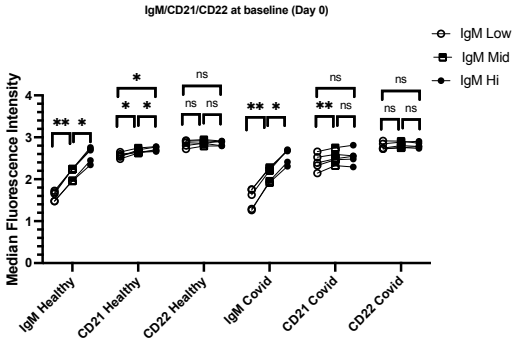

Figure B.3: Baseline CD21 and CD22 MFI in naïve B cells gated on IgM$^{\mathbf{Low}}$, IgM$^{\mathbf{Mid}}$, and IgM$^{\mathbf{Hi}}$ populations. Baseline (day 0) data from the original cohort of donors (healthy $n = 5$ and COVID-19 $n = 5$) was re-analysed. The naïve B cell population was divided into IgM$^{\mathrm{Low}}$, IgM$^{\mathrm{Mid}}$, and IgM$^{\mathrm{Hi}}$ gates equivalent to the FACS-sorting strategy used in subsequent experiments. The graph shows the median fluorescence intensity (MFI) of IgM, CD21 and CD22 for each IgM-defined group. Each dot represents the MFI from one gate within one sample, and the lines connect measurements across the IgM-defined gates for the same donor. Data is logicle-transformed and plotted on linear scale for visualisation. Statistical significance was assessed using two-way repeated-measures ANOVA with Tukey's post-hoc test. $^{*}p < 0.05$; $^{**}p \leq 0.01$; ns - not significant.

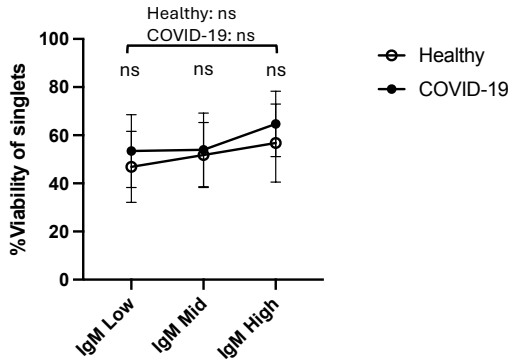

Figure B.4: Viability of IgM FACS-sorted samples after 5 days of stimulation. Summary plot shows the mean cell viability gated on singlets after 5 days of *in vitro* stimulation with CpG + IL-2. Each point corresponds to the mean viability of IgM-sorted samples from $n = 3$ COVID-19 donors and $n = 3$ healthy donors. Statistical differences were tested using two-way repeated-measures ANOVA followed by Tukey's post-hoc test. ns - not significant.

C | Appendix Chapter 4

Table C.1: **Complete summary of mean percentages of BCR isotypes by treatment group and timepoint.** Values represent group means with 95% confidence intervals. BLM - belimumab; PBO - placebo; D1 - day 1; M12 - month 12; M24 - month 24.

Isotype	Timepoint	BLM mean (95% CI)	PBO mean (95% CI)
IGHA1	D1	8.1 (4.2, 12.0)	7.0 (3.4, 10.7)
	M12	7.9 (0.0, 18.5)	4.5 (2.4, 6.5)
	M24	11.3 (0.0, 23.2)	8.4 (1.0, 15.8)
IGHA2	D1	5.5 (3.4, 7.6)	4.7 (2.4, 6.9)
	M12	4.5 (0.0, 9.5)	3.8 (1.8, 5.8)
	M24	4.8 (1.3, 8.3)	8.3 (0.0, 18.4)
IGHD	D1	16.9 (14.3, 19.4)	18.1 (14.8, 21.4)
	M12	18.2 (13.3, 23.1)	19.1 (16.5, 21.6)
	M24	14.4 (8.9, 19.8)	18.1 (10.7, 25.4)
IGHE	D1	0.02 (0.01, 0.03)	0.05 (0.00, 0.10)
	M12	0.02 (0.00, 0.05)	0.04 (0.00, 0.08)
	M24	0.08 (0.00, 0.19)	0.05 (0.01, 0.09)
IGHG1	D1	1.4 (0.8, 2.0)	1.4 (0.3, 2.6)
	M12	1.5 (0.0, 3.1)	1.0 (0.3, 1.7)
	M24	4.2 (0.0, 10.1)	1.4 (0.0, 3.4)
IGHG2	D1	0.9 (0.2, 1.6)	1.4 (0.3, 2.4)
	M12	1.5 (0.0, 4.0)	0.6 (0.1, 1.1)
	M24	1.6 (0.4, 2.8)	2.6 (0.0, 6.3)
IGHG3	D1	0.2 (0.0, 0.3)	0.2 (0.0, 0.5)
	M12	0.3 (0.0, 0.9)	0.1 (0.0, 0.2)
	M24	0.2 (0.0, 0.4)	0.2 (0.0, 0.3)

continued on next page

Table C.1: (continued)

Isotype	Timepoint	BLM mean (95% CI)	PBO mean (95% CI)
IGHG4	D1	0.01 (0.00, 0.01)	0.03 (0.00, 0.05)
	M12	0.02 (0.00, 0.04)	0.01 (0.00, 0.02)
	M24	0.01 (0.00, 0.01)	0.03 (0.0, 0.06)
IGHM	D1	67.0 (62.7, 71.3)	67.1 (62.2, 72.1)
	M12	66.1 (50.4, 81.7)	70.9 (66.8, 74.9)
	M24	63.4 (48.8, 78.1)	60.9 (45.4, 76.4)

End of Table

Table C.2: **Complete summary of mean Vertex and Cluster Gini Indices for all isotypes and timepoints.** Values represent group means with 95% confidence intervals. BLM - Belimumab; PBO - Placebo.

Index	Isotype	Timepoint	BLM mean (95% CI)	PBO mean (95% CI)
Vertex	IGHA1	D1	0.06 (0.05, 0.08)	0.06 (0.02, 0.09)
		M12	0.05 (0.00, 0.10)	0.05 (0.03, 0.08)
		M24	0.08 (0.04, 0.12)	0.05 (0.02, 0.07)
Vertex	IGHA2	D1	0.11 (0.06, 0.16)	0.08 (0.03, 0.12)
		M12	0.07 (0.00, 0.20)	0.09 (0.05, 0.13)
		M24	0.12 (0.07, 0.16)	0.08 (0.04, 0.13)
Vertex	IGHG1	D1	0.02 (0.01, 0.03)	0.01 (0.00, 0.02)
		M12	0.008 (0.00, 0.02)	0.02 (0.00, 0.04)
		M24	0.009 (0.001, 0.02)	0.02 (0.00, 0.06)
Vertex	IGHG2	D1	0.03 (0.02, 0.04)	0.03 (0.00, 0.07)
		M12	0.03 (0.00, 0.06)	0.009 (0.00, 0.02)
		M24	0.02 (0.00, 0.03)	0.005 (0.00, 0.01)

continued on next page

Table C.2: (continued)

Index	Isotype	Timepoint	BLM mean (95% CI)	PBO mean (95% CI)
Vertex	IGHM	D1	0.04 (0.01, 0.06)	0.02 (0.01, 0.04)
		M12	0.04 (0.00, 0.09)	0.01 (0.01, 0.02)
		M24	0.06 (0.00, 0.11)	0.07 (0.00, 0.17)
Vertex	all	D1	0.05 (0.02, 0.07)	0.03 (0.01, 0.05)
		M12	0.05 (0.00, 0.11)	0.02 (0.01, 0.03)
		M24	0.07 (0.01, 0.13)	0.06 (0.00, 0.14)
Cluster	IGHA1	D1	0.16 (0.12, 0.19)	0.15 (0.08, 0.22)
		M12	0.14 (0.01, 0.28)	0.14 (0.10, 0.19)
		M24	0.20 (0.11, 0.28)	0.12 (0.07, 0.18)
Cluster	IGHA2	D1	0.25 (0.17, 0.33)	0.19 (0.11, 0.27)
		M12	0.20 (0.00, 0.48)	0.18 (0.11, 0.26)
		M24	0.24 (0.15, 0.33)	0.21 (0.12, 0.30)
Cluster	IGHG1	D1	0.03 (0.02, 0.05)	0.03 (0.01, 0.06)
		M12	0.02 (0.00, 0.04)	0.04 (0.00, 0.07)
		M24	0.02 (0.01, 0.04)	0.05 (0.01, 0.09)
Cluster	IGHG2	D1	0.07 (0.03, 0.11)	0.06 (0.00, 0.13)
		M12	0.08 (0.00, 0.17)	0.03 (0.01, 0.04)
		M24	0.04 (0.01, 0.07)	0.03 (0.01, 0.05)
Cluster	IGHM	D1	0.07 (0.03, 0.11)	0.05 (0.03, 0.08)
		M12	0.08 (0.00, 0.18)	0.03 (0.02, 0.05)
		M24	0.12 (0.00, 0.23)	0.13 (0.00, 0.31)
Cluster	all	D1	0.11 (0.06, 0.16)	0.08 (0.04, 0.12)
		M12	0.11 (0.00, 0.25)	0.05 (0.03, 0.08)
		M24	0.15 (0.02, 0.29)	0.14 (0.00, 0.30)

End of Table

Table C.3: **Mean % maximum cluster size for all isotypes and timepoints. Values represent group means with 95% confidence intervals.** BLM - Belimumab; PBO - Placebo.

Isotype	Timepoint	BLM mean (95% CI)	PBO mean (95% CI)
IGHA1	D1	2.42 (1.89, 2.95)	2.39 (1.01, 3.78)
	M12	1.29 (0.10, 2.48)	2.08 (1.38, 2.78)
	M24	2.44 (0.88, 3.99)	2.35 (1.76, 2.94)
IGHA2	D1	3.81 (1.33, 6.30)	2.49 (1.24, 3.74)
	M12	1.14 (0.00, 2.50)	2.56 (1.54, 3.59)
	M24	2.82 (1.20, 4.44)	3.34 (2.52, 4.17)
IGHD	D1	0.91 (0.86, 0.96)	0.91 (0.87, 0.95)
	M12	1.31 (0.31, 2.30)	0.93 (0.80, 1.06)
	M24	1.12 (0.62, 1.62)	0.96 (0.80, 1.12)
IGHG1	D1	11.75 (10.73, 12.77)	10.41 (8.38, 12.44)
	M12	10.93 (9.70, 12.16)	10.86 (7.77, 13.95)
	M24	11.03 (10.14, 11.91)	12.44 (8.51, 16.36)
IGHG2	D1	12.22 (9.57, 14.87)	9.74 (5.07, 14.41)
	M12	7.43 (0.86, 14.01)	9.15 (6.32, 11.98)
	M24	8.84 (4.20, 13.49)	9.02 (5.27, 12.77)
IGHG3	D1	6.26 (1.71, 10.81)	8.02 (2.64, 13.40)
	M12	6.03 (0.76, 11.31)	4.92 (0.18, 9.66)
	M24	8.15 (0.66, 15.64)	7.46 (0.00, 16.79)
IGHM	D1	0.47 (0.22, 0.72)	0.39 (0.23, 0.55)
	M12	0.55 (0.00, 1.24)	0.37 (0.07, 0.67)
	M24	0.91 (0.18, 1.64)	0.73 (0.10, 1.37)
all	D1	0.37 (0.20, 0.54)	0.30 (0.17, 0.43)
	M12	0.35 (0.00, 0.77)	0.29 (0.09, 0.49)
	M24	0.82 (0.24, 1.41)	0.50 (0.05, 0.95)

Table C.4: **Mean D5 metric (%) for all isotypes and timepoints.** Values represent group means with 95% confidence intervals. BLM – Belimumab; PBO – Placebo.

Isotype	Timepoint	BLM mean (95% CI)	PBO mean (95% CI)
IGHA1	D1	11.98 (7.04, 16.92)	7.74 (5.45, 10.02)
	M12	12.35 (8.14, 16.57)	8.94 (6.00, 11.88)
	M24	10.12 (5.70, 14.55)	7.91 (5.84, 9.98)
IGHA2	D1	12.15 (8.07, 16.23)	12.95 (9.49, 16.41)
	M12	17.32 (9.36, 25.28)	12.94 (9.06, 16.82)
	M24	12.58 (7.26, 17.89)	13.05 (5.35, 20.74)
IGHD	D1	1.06 (0.58, 1.53)	1.88 (0.00, 4.26)
	M12	1.98 (0.31, 3.65)	1.18 (0.45, 1.92)
	M24	0.83 (0.31, 1.35)	0.57 (0.33, 0.81)
IGHG1	D1	20.52 (15.26, 25.78)	15.44 (10.51, 20.36)
	M12	33.08 (22.11, 44.05)	20.13 (14.96, 25.31)
	M24	16.62 (8.07, 25.18)	14.92 (12.16, 17.69)
IGHG2	D1	28.06 (19.61, 36.51)	19.14 (13.67, 24.62)
	M12	36.87 (15.50, 58.23)	21.79 (14.22, 29.37)
	M24	31.35 (19.48, 43.22)	18.76 (8.08, 29.45)
IGHM	D1	2.83 (1.53, 4.12)	2.25 (1.19, 3.30)
	M12	5.04 (1.32, 8.76)	3.22 (1.20, 5.25)
	M24	2.17 (0.53, 3.81)	1.26 (0.59, 1.94)
all	D1	3.02 (1.19, 4.84)	2.16 (1.17, 3.14)
	M12	3.55 (1.67, 5.44)	2.17 (1.16, 3.19)
	M24	2.87 (0.63, 5.11)	1.36 (0.68, 2.03)

D | Appendix Chapter 5

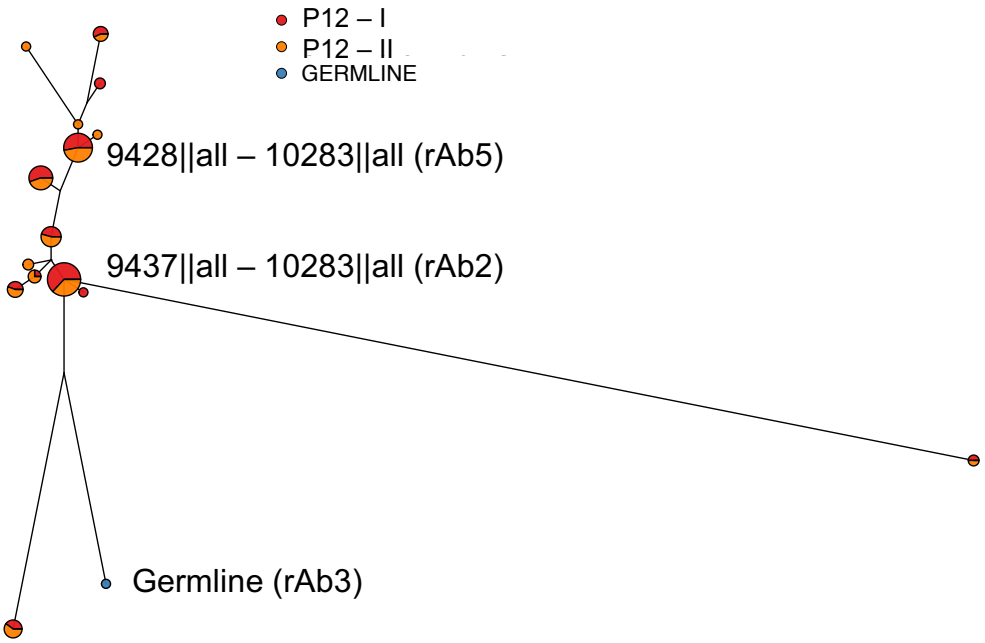

Figure D.1: Graphical B cell lineage tree of clonal members of rAb2, rAb5 and germline revertant sequence (rAb3). Each pie chart represents an identical complementarity-determining region 3 (CDR3) sequence, with pie size proportional to the number of clonal members. The edge length is proportional to the number of nucleotides differences between CDR3 sequences.

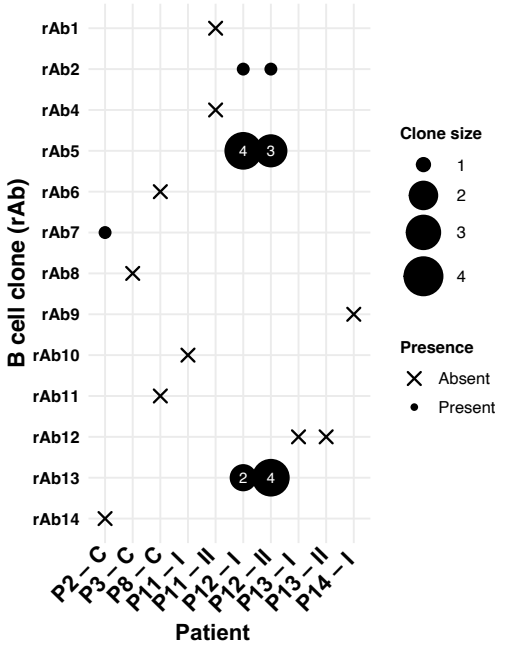

Figure D.2: Presence of selected B cell clones in peripheral blood samples from patients with psoriatic arthritis. The B cell clones shown were the ones produced as recombinant antibodies (rAbs). Clones detected in both peripheral blood and synovial tissue samples are indicated with a dot. Clones absent from peripheral blood but detected in synovial tissue are indicated with an X.

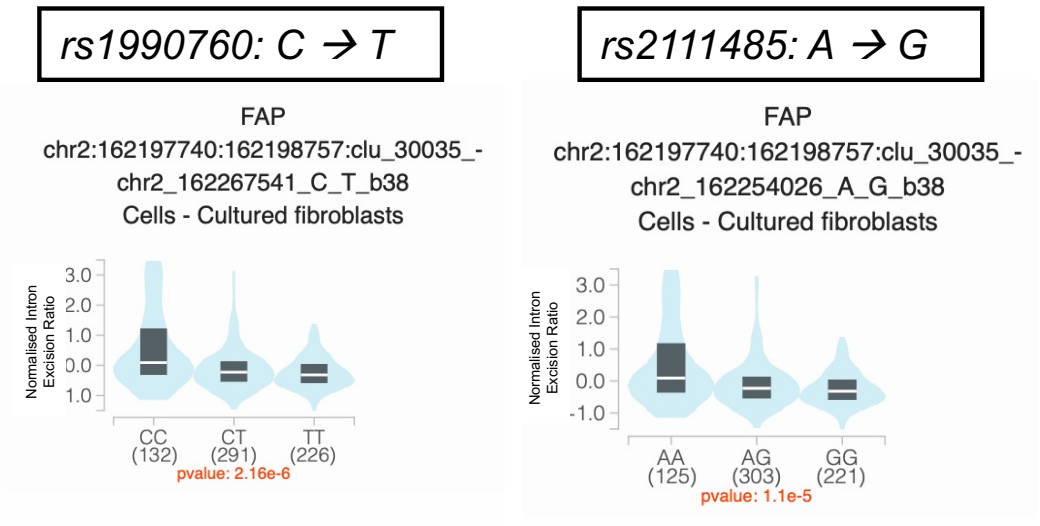

Figure D.3: Genetic variants acting as splicing quantitative trait loci (sQTLs) in fibroblasts. Violin plots show the sQTL effects for variants *rs1990760* and *rs2111485*. Figures adapted from the GTEx v8 portal.